Evidence for prodromal changes in neuronal excitability and neuroinflammation in the CA3 region of the hippocampus in young alpha-synuclein (A30P) transgenic mice and investigation of the effect of intranasal metformin treatment

Ibtisam Al-Musawi

180075405

Thesis submitted for the degree of Doctor of Philosophy at Newcastle University

12 December 2025

Supervisors

Dr Fiona LeBeau

Dr Gavin Clowry

Abstract

The toxic aggregation of the pre-synaptic protein alpha (α)-synuclein is a key feature of several neurodegenerative diseases, including Lewy body dementias (LBDs). Patients with LBDs have progressive cognitive impairment including memory loss and complex visual hallucinations. Recent evidence from patient and rodent models has shown neuronal hyperexcitability and neuroinflammation in most neurodegenerative diseases. Novel research on metformin, a type 2 diabetes drug, has demonstrated anti-inflammatory/neuroprotective properties and can easily penetrate the blood-brain barrier.

I investigated hyperexcitability and neuroinflammatory changes in the hippocampus of young hA30P mice, a transgenic mouse model that over-expresses human mutant alpha-synuclein and tested the effects of metformin treatment on these changes.

Immunofluorescence staining was conducted using sections of the hippocampus from 1-4 months hA30P mice and wild-type (WT) mice as a control. Primary antibodies for neuronal, glial, and neuroinflammatory markers were employed. Proteome cytokine array and label-free mass spectrometry (LF-MS) measurements were made from hippocampal tissue extracts. I also employed intranasal metformin treatment in WT and hA30P mice, followed by immunofluorescence histology.

Immunofluorescence revealed significant differences between WT and hA30P animals in the CA3 region of the hippocampus. An interesting biphasic change in the expression of c-Fos in male hA30P mice was observed with high expression at 1 month, consistent with early onset of hyperexcitability, but lower expression from 2-4 months in male hA30P mice compared to the controls, possibly indicating chronic hyperexcitability. Neuroinflammation was indicated by significant increases in the % area of GFAP, a marker for reactive astrocytes, and the number of Iba-1+ microglia that expressed iNOS immunoreactivity in 1-4 months male hA30P mice compared to WT. A similar increase in %GFAP was observed in female hA30P mice, however, the %Iba-1 area was not different between female WT and hA30P mice. In WT mice aged 2-4 months only 4.6% of Iba-1+ cells co-expressed iNOS. In contrast, in age-matched hA30P mice, 87% of cells co-expressed Iba-1 and iNOS. There was a significant increase in GFAP and Iba-1/iNOS co-expression immunoreactivity in a cohort of 1-

month-old hA30P compared to WT mice. A significant decrease in NeuN positive neurons and perineuronal nets detected with WFA lectin was also observed in the CA3 region of hA30P mice compared to WT at 2-4 months.

The results of LF-MS at 2 months in the hippocampus of male hA30P mice revealed that α-synucleinopathy causes significant changes in the proteome, indicating the effect of overexpressed human mutant α-synuclein. There were 158 significantly upregulated proteins in the hippocampus of hA30P mice involved in neurotransmission, and neuronal activity, such as Tenm1, Wdfy3, Syn, and Lin7, mitochondrial dysfunction such as TOMM6 and Rala, oxidative stress such as Rab-1A, and apoptosis in neurons such as Snrk. At the same time, there were 30 significantly downregulated proteins involved in different biological function e.g. DNA/RNA damage such as Gmpr2, Rps7, and Rbmx. Although there was no direct evidence for neuroinflammation through proteins associated with microglial and astrocytic activation, there were many proteins related to inflammation such as Ddrgk1, Cadps, Syn2, Hspa1l, Hspa2, Hspa5, Hspa8, Lin7a, Lin7b, and Lin7c that showed upregulation in hA30P compared to WT mice.

In a pilot experiment, metformin intranasal treatment significantly reduced the proportion of activated microglia in the CA3 hippocampal region in treated versus vehicle hA30P mice, however, other neuronal and glial markers showed no significant differences.

Overall, my data showed evidence for early network hyperexcitability and neuroinflammation that might contribute to the progression of neurodegenerative changes. Further experiments are needed to explore the therapeutic potential of metformin.

Acknowledgments

I thank God for granting me the opportunity to pursue a PhD in neuroscience since discovering neurodegenerative dementia which triggered my intense curiosity. Glory to God because he predestined the situations and people who assist me in realizing my ambition.

My thanks and gratitude extend to my first supervisor, Dr. Fiona LeBeau, for her continuous help and support throughout my doctoral research and even before I arrived in the UK. She was truly a supporter who offered me a helping hand to stand up and continue many times, thank you from the depths of my heart. I will never forget your great supervision, mentor, and kindness. Thanks to my second supervisor, Dr. Gavin Clowry, for his wise supervision and monitoring of my research. Together you were my only guide to complete my PhD. I learned a lot from both of you, and without your wisdom, patience, and continuous encouragement, I would not have completed the PhD. Your scientific discussions and dialogue were useful, interesting, and fun for me as a student with his teachers. I have very much missed it since I completed my master's degree at Baghdad University 18 years ago.

I want to acknowledge and express my gratitude to Dr. Fiona Oakley, and Dr. Tom Smulders who were on my progress panel, for their advice and assistance. I appreciate their pushing me to defend my work and providing insightful feedback during 3-year panel meetings.

I thank and appreciate all members of LeBeau's research team. I especially mention Dr. Faye McLeod and Dr. David Koss. Their personable morals, and my trust in their scientific Knowledge, made me never hesitate to ask for help or information from them.

I was fortunate to meet many people who are creative in their fields, such as Bethany Dennis. She was not only my budding for my first academic year, but she was my constant reference during whole the 3 years of my study. My thanks to Mark Turnbull, he helped me a lot in my first year. I am lucky that I was his neighbour in the office. He never said to me ‘Say that again’ and directly understood me when I was speaking with him. Somehow, I was easily understanding his nice Geordie accent! Although my skills in English were not good enough at that time.

I am lucky and happy to have had good companionship which mitigated the pressure of studying. The presence of each of my colleagues Lauren Oneill, Anastasia Dimitriou, Ashan Jayasekera, Dr. Lek Srisuwan, and Dr. Daipayan Chowdhury played a big role in creating an atmosphere of comfort and fun during my study period.

Thanks to all the people who helped me to acquire new skills in the laboratory work. I especially mention Ms. Elaine McDermott, who taught me the details of using the microtome. Thanks to Oliver Baddeley who clarified how to analyse the images in the Fiji program. My thanks to Dr. Connie Mackenzie-Gray Scott, and Dr. Elizaveta Olkhova who showed me how to use the microscope appropriately, and for being my favourite friends.

My special thanks to master's students Zhanet Vlaeva, Daisy McAllister, and to graduate students Molly Biles, Sophie Cuthbertson, whom I contributed to the supervisory of their research that related to my work of immunofluorescence staining of 2-4 months hA30P mice.

My great thanks to Mr Pawel Palmowski from Protein and Proteomics Unite for bearing with me and explaining tiny details of how he analysed the raw data resulting from Label-Free Mass Spectrometry by STRING program. Also, I thank Olivia Todd and Dr. Daniel Erskine for teaching me how to use the DAVID database to analyse my proteomics data.

I thank members of the Bio imaging Unit and the Comparative Biology Centre for helping me achieve my PhD project. Thanks to Widad AL-Omairi, Sakinah AL Haddad, Fatima Al-Salem, and Maznah Alhesain who guided me on how to use programs and deal with the university system.

I thank everyone who advised, guided, and provided constructive criticism about my project, such as Dr. Ilona Obara, and Dr. Edward Fielder. I would like to thank all the people who provided me with peace and hope. Facing Dr. Sasha Gartside, and Dr. Adrian Rees in the early mornings, usually with their shiny smile and pure spirits fed me with, positive energy lasting whole the day.

I am currently finishing my doctorial study; I have a feeling of a toddler who just began his journey in the huge neurosciences' jungles. I started my journey with curiosity and passion for learning, and I ended it with even greater curiosity and passion. I hope I will progress with conscience and patience as my father and mother (God bless their souls) taught me.

I would not forget to thank all my supporters and lovers my husband, brothers, sisters, and children for their belief in my abilities and for their continuous assistance. Without their presence in my life, I could not have managed myself to complete my PhD.

Conference Presentations

- **The North-East Postgraduate Student Conference** (Newcastle upon Tyne City, The UK) March 2021, Oral presentation (Investigating the potential neuroprotective effect of inhibition of the mammalian target of rapamycin (mTOR) pathway using both rodent and human models of alpha-synucleinopathy).

- **The International Lowy Body Dementia Conference** (Newcastle upon Tyne City, The UK) June 2021, Live Online Poster Presentations (Evidence for prodromal neuroinflammation in a rodent model of alpha- synucleinopathy).

- **Federation of European Neuroscience Societies Forum** (Paris, France) August 2022, poster participation (Evidence for prodromal neuroinflammation in a rodent model of alpha- synucleinopathy).

- **The North-East Postgraduate Student Conference** (Newcastle upon Tyne City, The UK) October 2022, Poster presentation (Evidence for prodromal neuroinflammation in a rodent model of alpha-synucleinopathy).

- **International Conference on Alzheimer's and Parkinson's disease** (Gothenburg, Sweden) April 2023, poster presentation (Evidence for prodromal neuroinflammation in a rodent model of alpha-synucleinopathy).

- **International British Neuroscience Association Festival of Neuroscience** (Brighton, UK) April 2023, poster presentation (Evidence for prodromal neuroinflammation in a rodent model of alpha-synucleinopathy).

- **Federation of European Neuroscience Societies Forum** (Vienna, Austria) June 2024, poster participation (Evidence for prodromal neuronal hyperexcitability and neuroinflammation in a rodent model of alpha-synucleinopathy (A30P)).

Publications

Some of my work from Chapter 3 and Chapter 4 has been published as first author:

Al-Musawi I, Dennis BH, Clowry GJ and LeBeau FEN (2024). Evidence for prodromal changes in neuronal excitability and neuroinflammation in the hippocampus in young alpha-synuclein (A30P) transgenic mice. Front. Dement. 3:1404841. doi: 10.3389/frdem.2024.1404841

Table of Contents

Abstract 3

Publications 9

Chapter 1 1

Introduction 1

1.1 Neurodegenerative Dementia 0

1.1.1 Alpha-synuclein (α-syn) 1

1.1.2 Dementia with Lewy bodies (DLB) 4

1.1.3 Transgenic mouse models of DLB (hA30P) 5

1.1.5 Hyperexcitability in murine models of AD and DLB 8

1.2 Hippocampus 9

1.2.1 Parvalbumin GABAergic Interneurons 12

1.2.2 Perineuronal nets (PNNs) 14

1.3 Neuroglia 16

1.3.1 Astrocytes 16

1.3.2 Microglia 19

1.3.3 Neuroinflammation 21

1.3.4 Neuroinflammation and Neurodegeneration 22

1.4 Mammalian Target of Rapamycin (mTOR) Pathway: Role in Neurodegeneration 23

1.5 Therapeutic Interventions in Neurodegenerative Diseases 24

1.6 Metformin 26

1.6.1 Metformin and α-synuclein 28

1.6.2 Effect of Metformin in Neurodegenerative Diseases 29

1.7 Nasal Route of Administration to Treat Brain Disease 32

Chapter 2 35

General Methods 35

2.1 Animal provision 35

2.2 Euthanasia and transcardial perfusion of animals with fixative 36

2.3 Slice preparation and ink method for sub-region identification 36

2.4 Immunohistochemistry in free-floating 39

2.5 Imaging and data analysis by the Fiji program 44

2.5.1 Quantification of Human-α-syn Protein Expression 45

2.5.2 Quantification of c-Fos Protein Expression 46

2.5.3 Quantification of Neuron Expression 47

2.5.4 Quantification of PV Interneurons Expression 48
2.5.5 Quantification of Reactive Astrocyte Expression 49
2.5.6 Quantification of Microglia 50
2.5.7 Quantification of iNOS expression with reactive microglia 51
2.6 Statistical analysis 52
Chapter 3 54
3.1 Introduction 54
3.2 Aims 55
3.3 Methods 55
3.4 Results 56
3.4.1. Expression of Human α-syn in the CA3 Region of the Hippocampus of Male 2-4 Month hA30P Mice 56
3.4.2 Decrease in c-Fos+ nuclei/mm^2 in the CA3 Region of the Hippocampus of 2-4 Months Male hA30P Mice 58
3.4.3. Decrease in % area of NeuN in the CA3 Region of the Hippocampus of Male 2-4 Months hA30P Mice 60
3.4.3 Expression of PV Interneurons in the CA3 Region of the Hippocampus of Male 2-4 months hA30P Mice 62
3.4.4 Increase in the Count of PV without PNNs/mm^2 in the CA3 Region of the Hippocampus of Male 2-4 months hA30P Mice 64
3.4.5 Increase in % Area of Reactive Astrocytes in the CA3 Region of the Hippocampus of Male 2-4 Months hA30P Mice 66
3.4.7 Increase in % Area Reactive Astrocytes in the CA3 Region of the Hippocampus of Female 2-4 Months hA30P Mice 69
3.4.8 Increase in % Area Occupied by Microglia, and the Count of Reactive Microglia in the CA3 Region of the Hippocampus of Male 2-4 Months hA30P Mice 72
3.4.9 Increase in % Area Occupied by Microglia in the CA3 Region of the Hippocampus of Female 2-4 Months hA30P Mice 75
3.5 Discussion 78
3.5.1 Human α-syn Expression in the CA3 Region of the Hippocampus 78
3.5.2 Overexpression of Human α-syn Reduced in the % area of NeuN in hA30P mice 80
3.5.3 Changes in PNNs and possibly in PV interneuron function in hA30P mice 81
3.5.4 Decreased c-Fos expression suggests increased chronic neuronal excitability in young hA30P mice 84
3.5.5 Increase in Reactive Astrocytes in the Hippocampus of Male and Female 2-4 Months hA30P Mice 84
3.5.3 Increase in Reactive Microglia in the Hippocampus of Male and Female 2-4 Months hA30P Mice 86
3.6 Conclusion 89
Chapter 4 90

4.1 Introduction 90
4.2 Aims 92
4.3 Methods 92
4.3.1 Intranasal drug delivery 93
4.4 Results 98
4.4.1 Confirmation of Human α-syn Expression in the CA3 Region of the Hippocampus of Male 1-Month hA30P Mice 98
4.4.2 Increase in c-Fos+ nuclei/mm^2 in the CA3 Region of the Hippocampus of 1-Month old male hA30P Mice 100
4.4.2 Increase in Reactive Astrocytes in the CA3 Region of the Hippocampus of 1-month Old Male hA30P Mice 102
4.4.4. Increase in % Area Occupied by Microglia in the CA3 Region of the Hippocampus of Male 1-Month hA30P Mice 105
4.4.5. Increase in the Reactive Microglia in the CA3 Region of the Hippocampus of Male 1-Month hA30P Mice 107
4.4.6. Morphological Changing of Reactive Astrocytes and Microglia of hA30P Mice 109
4.4.7. Intranasal Metformin Treatment Did Not Affect Mouse Body Weight 112
4.4.8. Effect of Metformin in c-Fos in the CA3 Hippocampus of male hA30P Mice 115
4.4.9. Effect of Metformin on Reactive Astrocytes in the Hippocampus of hA30P Mice 117
4.4.10 Effect of Metformin in the Reactive Microglia CA3 Hippocampus of hA30P Mice 119
4.5 Discussion 121
4.5.1 Confirmation of Human α-syn Expression in the CA3 Region of the Hippocampus of Male 1-Month hA30P Mice 122
4.5.2 Increase in c-Fos+ nuclei/mm^2 in the CA3 Region of the Hippocampus of 1-Month Male hA30P Mice 123
4.5.3 Increase in Reactive Astrocytes in the CA3 Region of the Hippocampus of 1-month Male hA30P Mice 124
4.5.4. Increase in Reactive Microglia in the Hippocampus of Male 1-Month hA30P Mice 125
4.5.6 Effect of Metformin on Weight Gain in Male hA30P Mice 127
4.5.7 Effect of Metformin in Reactive Astrocytes in the Hippocampus of Male hA30P Mice 128
4.5.8 Metformin Reduced Reactive Microglial in Male hA30P Mice. 129
4.5.9 Effect of Metformin in c-Fos in the Hippocampus of Male hA30P Mice 130
4.6 Conclusion 132
Chapter 5 133
5.1 Introduction 133
5.2 Aims 136
5.3 Methods 136
5.3.1 Animals 136

5.3.2 Hippocampus Dissection 136
5.3.3 Tissue Lysis Preparation 139
5.3.4 Preparation Standards for Measuring Protein Concentration: 140
5.3.5 Mouse Cytokine Array Panel A 141
5.3.7 LF-MS Proteomics Analysis 144
5.3.8 Proteomic Statistical Analysis 144
5.4 Results 147
5.4.1 Mouse Cytokine Array Panel A Result 147
5.4.2 Label-Free Mass Spectrometry (LF-MS) Proteomics Result 149
5.4.3 Proteomic Analysis of Hippocampal Tissue of hA30P Versus WT Mice Revealed 4165 Unique Proteins 150
5.4.4 STRING Analysis Revealed 7 Distinguished Clusters of Proteins 156
5.4.5 Gene Ontology Reporter DAVID Investigation for the Biological Functions of Significantly Different Proteins 160
5.4.6 The First Function Group of Upregulated Proteins/Genes by Gene Ontology Reporter DAVID for the Biological Functions 161
5.4.7 The Second Biological Function Group of Upregulated Proteins/Genes by Gene Ontology Reporter DAVID for the Biological Functions 163
5.4.8 The Third Biological Function Group of Upregulated Proteins/Genes by Gene Ontology Reporter DAVID for the Biological Functions 167
5.4.9 Down-regulated Proteins/Genes Identified by Gene Ontology Reporter DAVID for the Biological Functions 170
5.4.10 The First Biological Function Group of Downregulated Proteins/Genes by Gene Ontology Reporter DAVID for the Biological Functions 172
5.4.11 The Second Biological Function Group of Downregulated Proteins/Genes by Gene Ontology Reporter DAVID for the Biological Functions 174
5.4.12 The Third Biological Functional Group of Downregulated 177
5.5 Discussion 178
5.5.1 Effect of Overexpression of Human α-syn on Oxidative Stress 185
5.5.2 Effect of Overexpression of Human α-syn on Mitochondrial Outer Membrane 187
5.5.3 Effect of Human α-syn on DNA damage 188
5.6 Conclusion 190
Chapter 6 132
General Discussion 132
6.1 The Main Findings in the Current Thesis 190
6.2 General Discussion 190
6.3 Conclusion 194
6.4 Limitations 194

6.5 Future Work..... 195
Bibliography 198

List of Figures

Chapter 1

Figure 1.1 Human α-syn Protein Structure …….....1

Figure 1.2 Pathological features of LBs…….……...5

Figure 1.3 The strcture of the hippocampus…….……...10

Figure 1.4 The different layers of the Cornus Ammonis and the gyrus dentatus of the Hippocampus.……...11

Figure 1.5 Synaptic connectivity of the hippocampus the trisynaptic circuit……...12

Figure 1.6 Neuroprotective and neurotoxic states of glia ……18

Figure 1.7 Role of glia in neurodegeneration…….…… 20

Figure 1.8 The mTOR pathway controls many cellular functions…….25

Figure 1.9 The *Galega officinalis* is the source of metformin ……..26

Figure 1.10 Chemical structure of metformin……..…27

Figure 1.11 An illustration of metformin's anti-hyperglycaemic action on liver cells.28

Figure 1.12 AMPK and metformin have distinct effects on the phosphorylation of α-syn S129……..……..32

Figure 1.13 An illustration of the physiological systems involved in the delivery of drugs to the brain through the nose……..…….33

Chapter 2

Figure 2.1 Ink method for sub-region identification (horizontal sectioning in the brain of 3-month-old mouse)……38

Figure 2.2 Ink Method for Sub-region Identification (Horizontal sectioning in the brain of 1-month-old mouse). ……..39

Figure 2.3 Ink method for sub-region identification (coronal sectioning in the brain of 2-month-old mouse)……..…….……..40

Figure 2.4 Optimal sections of the intermediate hippocampus…….....40

Figure 2.5 A pipeline of densitometric image analysis steps conducted by the Fiji program for human- α-syn……...45

Figure 2.6 A pipeline of densitometric image analysis steps conducted by the Fiji program for c-Fos……..……...46

Figure 2.7 A pipeline of densitometric image analysis steps conducted by the Fiji program for Neu-N…….……47

Figure 2.8 A pipeline of densitometric image analysis steps conducted by the Fiji program for PV interneurons ……..……48

Figure 2.9 A pipeline of densitometric image analysis steps conducted by the Fiji program for reactive astrocytes ……49

Figure 2.10 A pipeline of densitometric image analysis steps conducted by the Fiji program for microglia……50

Figure 2.11 A pipeline of densitometric image analysis steps conducted by the Fiji program for iNOS in reactive microglia ……...51

Chapter 3

Figure 3.1 Expression of human α-syn in the CA3 Region of the Hippocampus of Male 2-4 Month old hA30P Mice……..……..57

Figure 3.2 Decrease in c-Fos+ nuclei/mm^2 in the CA3 Region of the Hippocampus of Males 2-4 Months hA30P Mice……..….59

Figure 3.3 Decrease in % area of NeuN in the CA3 Region of the Hippocampus of Males 2-4 Months hA30P Mice……..……....61

Figure 3.4 Expression of Parvalbumin Interneurons in the CA3 Region of the Hippocampus of Male 2-4 Months hA30P Mice……..…63

Figure 3.5 Increase in the Count of PV without PNN/mm^2 in the CA3 Region of the Hippocampus of Male 2-4 Months hA30P Mice……..……65

Figure 3.6 Increase in % Area of Reactive Astrocytes in the CA3 Region of the Hippocampus of Male 2-4 Months hA30P Mice……...67

Figure 3.7 Increase in % Area Reactive Astrocytes in the CA3 Region of the Hippocampus of Female 2-4 Months hA30P Mice……..70

Figure 3.8 Increase in % Area Occupied by Microglia and the Count of Active Microglia in the CA3 Region of the Hippocampus of Male 2-4 Months hA30P Mice…….73

Figure 3.9 Increase in % Area Occupied by Microglia in the CA3 Region of the Hippocampus of Female 2-4 Months hA30P Mice……..……76

Chapter 4

Figure 4.1 Acclimatisation and Intranasal Drug Delivery to Mice……..……96

Figure 4.2 Rewarding the Mouse ……..……97

Figure 4.3 Timetable of Metformin Intranasal Delivery to Mice…….……98

Figure 4.4 Expression of Human α-syn in the Hippocampus of Male 1-Month-Old hA30P Mice……99

Figure 4.5 Increase in C-Fos+ nuclei/mm^2 in the CA3 Region of the Hippocampus of Male 1 Month old hA30P Compared to WT Mice……..101

Figure 4.6 Increase in % Area Occupied by Reactive Astrocytes in the CA3 Region of the Hippocampus of 1 Month-old Male hA30P Mice Compared to WT……..103

Figure 4.7 Increase in % Area Occupied by Microglia in the CA3 Region of the Hippocampus of Male 1 Month hA30P Compared to WT Mice……..106

Figure 4.8 Increase in the Count of Reactive Microglia in the CA3 Region of the Hippocampus of Male 1 Month hA30P Compared to WT mice……..108

Figure 4.9 Morphological Changing of Reactive Astrocytes and Microglia in CA3 Region of Hippocampus of hA30P Mice……111

Figure 4.10 Effect of Intranasal Metformin in Body Weight Gain during Treatment……114

Figure 4.11 Effect of Metformin Treatment in c-Fos+ nuclei/mm^2 in the CA3 Region of the Hippocampus of Treated Versus Vehicle Groups of hA30P and WT mice.....116

Figure 4.12 Effect of Metformin Treatment in Reactive Astrocytes in the Hippocampus of Treated Versus Vehicle Groups of hA30P and WT mice…….118

Figure 4.13 Effect of Metformin Treatment in Reactive Microglia in the CA3 Region of the Hippocampus of Treated Versus Vehicle Groups of hA30P and WT mice…….120

Chapter 5

Figure 5.1 Mouse Brain Dissection and Hippocampus Isolation ……....138

Figure 5.2 Quantified of Protein Concentration…….... 141

Figure 5.3 Chem illumination by Densitometric Chemi XRQ and Fiji Program……143

Figure 5.4 LF-MS Proteomics Analysis Steps……..……145

Figure 5.5 Cytokine Array Result……....148

Figure 5.6 Cytokine Array IL-23 Result ……..……..149

Figure 5.7 Scatter Plot Principal Component Analysis (PCA)……....150

Figure 5.8 Venn Diagram of differentially regulated proteins……....151

Figure 5.9 Heat Map Comparison of Protein Expression of Hippocampal Tissue of hA30P Versus WT Mice……....152

Figure 5.10 Volcano Plot of Proteomic Data……153

Figure 5.11 The highest significantly different proteins between hA30P and WT...155

Figure 5.12 STRING Network of Potential Protein Interactions for Upregulation Proteins…….....…157

Figure 5.13 STRING Network of Potential Protein Interactions for Down-Regulated Proteins……158

Figure 5.14 STRING Network of PPI for Significantly Upregulated Proteins in hA30P Compared to WT Mice…….…..159

Figure 5.15 STRING Network of PPI for Significantly Downregulated Proteins in hA30P Compared to WT Mice…….…...160

Figure 5.16 The Output Summary of the Function Annotation Reporter in the DAVID……..…..161

Figure 5.17a Biological Function Group 1 of Functional Annotation Clustering for Biological Function Reporter in the DAVID of Significantly Upregulated Protein in hA30P Compared to WT Mice……..……..……162

Figure 5.17b Biological Function Group 1 of Functional Annotation Clustering for Biological Function Reporter in the DAVID of Significantly Upregulated Protein in hA30P Compared to WT Mice…….…….164

Figure 5.17c Biological Function Group 1 of Functional Annotation Clustering for Biological Function Reporter in the DAVID of Significantly Upregulated Protein in hA30P Compared to WT Mice…….....165

Figure 5.18a Biological Function Group 2 of Functional Annotation Clustering for Biological Function Reporter in the DAVID of Significantly Upregulated Protein in hA30P Compared to WT Mice……..……...166

Figure 5.18b Biological Function Group 2 of Functional Annotation Clustering for Biological Function Reporter in the DAVID of Significantly Upregulated Protein in hA30P Compared to WT Mice……..168

Figure 5.18c Biological Function Group 2 of Functional Annotation Clustering for Biological Function Reporter in the DAVID of Significantly Upregulated Protein in hA30P Compared to WT Mice……..…169

Figure 5.19a Biological Function Group 3 of Functional Annotation Clustering for Biological Function Reporter in the DAVID of Significantly Upregulated Protein in hA30P Compared to WT Mice)……170

Figure 5.19b Biological Function Group 3 of Functional Annotation Clustering for Biological Function Reporter in the DAVID of Significantly Upregulated Protein in hA30P Compared to WT Mice…….171

Figure 5.20 The Output Summary of the Function Annotation Reporter in the DAVID Result of 30 Significantly Downregulation Protein in hA30P compared to WT mice……..……172

Figure 5.21a Biological Function Group 1 of Functional Annotation Clustering for

Biological Function Reporter in the DAVID of Significantly Downregulated Protein in hA30P Compared to WT Mice……..…173

Figure 5.21b Biological Function Group 1 of Functional Annotation Clustering for Biological Function Reporter in the DAVID of Significantly Downregulated Protein in hA30P Compared to WT Mice……..173

Figure 5.22a Biological Function Group 2 of Functional Annotation Clustering for Biological Function Reporter in the DAVID of Significantly Downregulated Protein in hA30P Compared to WT Mice….....174

Figure 5.22b Biological Function Group 2 of Functional Annotation Clustering for Biological Function Reporter in the DAVID of Significantly Downregulated Protein in hA30P Compared to WT Mice……..175

Figure 5.23a Biological Function Group 3 of Functional Annotation Clustering for Biological Function Reporter in the DAVID of 30 Significantly Downregulated Protein in hA30P Compared to WT Mice……..176

Figure 5.23b Biological Function Group 3 of Functional Annotation Clustering for Biological Function Reporter in the DAVID of Significantly Downregulated Protein in hA30P Compared to WT Mice……..……177

List of Tables

Chapter 2

Table 1: Buffers used for the immunoflurescence staining……37
Table 2: Primary antibodies used in IF staining……..…..41-42
Table 3: Secondary antibodies used in IF staining ……43

Chapter 4

Table 4.1: Score Sheet for Used Mice in Metformin Study……113

Chapter 5

Table 5.1: Mouse Cytokines of the Array Panel A……142
Table 5.2: The highest significantly different proteins between hA30P and WT mice……..154

Abbreviations List

A1	Pro-inflammatory astrocytes
A2	Anti-inflammatory astrocytes
A30P	Alanine to proline exchange in position 30
ABPP	Amyloid-beta precursor protein
Abr	Active breakpoint cluster region-related protein
AMP	Adenosine monophosphate
AMPK	Adenosine monophosphate-activated protein kinase
α-syn	Alpha-synuclein
ATP	Adenosine triphosphate
Aβ	Amyloid β-protein
BBB	Blood-brain barrier
BCA	Bicinchoninic assay
BCAA	Branched-chain amino acid
BCAT-1	branched-chain amino acid transferase
BSA	Bovine serum albumin
CA	Cornu Ammonis
CA3	Cornus Ammonis
CB	Calbindin
CBC	Comparative Biology Centre
cGAS	cGAMP synthase
CNS	Central nervous system
DAPI	6-diamide-2-phenylindole
DAVID	Database for Annotation, Visualization, and Integrated Discovery
DDRGK	Domain-containing protein 1
Ddrgk1	DDRGK domain-containing protein 1
DG	Dentate gyrus
DLB	Dementia with Lewy bodies
EC	Entorhinal cortex
ECM	Extracellular matrix
EEG	Electroencephalography
ELISA	enzyme-link immunosorbent assay

eNOS	Endothelial NOS
ETC	Electron transport chain
FDR	False Discovery Rate
GABA	Glutamate gamma amino-butyric acid
GD	Gyrus dentatus
GFAP	Glial fibrillary acidic protein
GMP	Guanosine monophosphate
Gmp2	Guanosine monophosphate reductase 2
GO	Gene Ontology
H	Hilus
HD	Huntington's Disease
HF	Hippocampal fissure
Hspa	Heat shock 70 kDa protein 1-like
Iba-1	Ionized calcium-binding adapter molecule 1
IEG	Immediate early gene
IF	Immunofluorescence
IL-1	Interleukin 1
IL-1β	Proinflammatory cytokines like interleukin 1β
IL-6	Interleukin 6
iNOS	Inducible nitric oxide synthase
IQR	Interquartile range
LBDs	Lewy body dementias
LBs	Lewy bodies
LF-MS	Label-Free mass spectrometry
Lin7	Protein lin-7 homolog B
LPS	Lipopolysaccharides
M1	Proinflammatory microglia
M2	Anti-inflammatory microglia
MIM	Mitochondrial inner membrane
MMP-9	Matrix metalloproteinase 9
MOM	Mitochondrial outer membrane
MS	Multiple sclerosis
MSA	Multiple system atrophy

mtDNA	Mitochondrial deoxyribonucleic acid
mTOR	Mammalian Target of Rapamycin
NAC	Non-amyloid component
NAD+/NADH	Nicotinamide adenine dinucleotide
NALT	Nasopharyngeal lymphoid tissue
NeuN	Neuronal nuclear antigen
nNOS	Neuronal NOS
OXPHOS	Oxidative phosphorylation machinery
OCT1	Organic cation transporter 1
PBS	Phosphate-buffered saline
PCA	Principal Component Analysis
PD	Parkinson’s disease
PDD	Parkinson’s disease dementia
PFA	Paraformaldehyde
PNNs	Perineuronal nets
PNs	Pyramidal neurons
PP2A	Protein phosphatase 2A
PS129	Phosphorylated α-syn serine residue 129
PV	Anti-parvalbumin
Rab-1A	Ras-related protein
Ral	V-ral simian leukemia viral oncogene A
RBD	Rapid eye movement sleep behaviour disorder
Rbmx	RNA binding motif protein, X chromosome
ROC	Receptor-operated ion channels
ROI	Region of interest
ROS	Reactive oxygen species
Rps7	40S ribosomal protein S7
SEM	Standard error of the mean
SG	*Stratum granulare*
SL	*Stratum lucidum*
SLM	*Stratum lacunosum-moleculare*
SNARE	Soluble N-ethylmalemide attachment protein receptor
Snrk	SNF-related serine/threonine-protein kinase

SP	*Stratum pyramidale*
SR	*Stratum radiatum*
SO	*Stratum oriens*
STING	Stimulator of the interferon gene
Syn	Synapsin
SNCA	Synuclein gene
STZ	Streptozotocin
T2D	Type II diabetes
TCA	Citric acid cycle
Tenm1	Teneurin-1
TLR4	Toll-like receptor 4 protein
TNF	Tumour necrosis factor
TNFa	Tumour necrosis factor-alpha
TNF-α	Tumour necrosis factor
TOMM6	Translocase of Outer Mitochondrial Membrane 6
Ubl	Ubiquitin
WAF	Wisteria Floribunda Lectin
Wdfy3	WD repeat and FYVE domain containing 3
WT	Wild type

Chapter 1

Introduction

1.1 Neurodegenerative Dementia

Neurodegenerative disorders, such as the alpha-synucleinopathies are caused by the presence of self-aggregated and insoluble alpha-synuclein (α-syn) protein in both neurons and other cells in the brain (Miller et al., 2022). This protein normally contributes to chemical synaptic neurotransmission through synaptic vesicles, but aggregation and dysfunction of this protein occur in disease. The aggregation and misfolding of α-syn into toxic oligomers and fibrils results in neurodegenerative diseases (Selkoe, 2001). α-synucleinopathy is characterized by abnormal accumulations of α-syn aggregated in Lewy bodies (LBs) and Lewy neurites. The term Lewy body disease (LBD) refers to Parkinson's disease (PD), Parkinson's disease dementia (PDD), and dementia with Lewy bodies (DLB). In advanced disease states, these conditions are associated with neuronal loss and neurodegeneration. Due to the over-diagnosis of PD, and under-diagnosis of DLB, most studies neglect DLB as a field of study so the full prevalence of the condition isn't fully understood (Outeiro et al., 2019).

Dementia is a serious national issue in the UK. There are around 944,000 people with dementia, more than ever before, and the number of people with dementia is expected to grow sharply over the next few decades (Alzheimer's Society, 2024 https://dementiastatistics.org/about-dementia/diagnosis/). In the UK, DLB accounts for approximately 10-15% of patients with dementia (Alzheimer’s Research UK, 2023). The pathological features of DLB are characterized by the aggregation of α-syn protein within neurons and the formation of LBs in the brain stem, limbic systems, and cortical areas. As a result of the loss of nigrostriatal dopaminergic neurons in the substantia nigra caused by LBs and Lewy neurites, dopamine levels are depleted (Schulz-Schaeffer, 2010).

The main clinical features of DLB include progressive cognitive impairment including memory loss, complex visual hallucinations, rapid eye movement sleep behaviour disorder (RBD), and Parkinsonism (Outeiro et al., 2019). McKeith et al. (2017) have reported that there are at least two clinical features above that can contribute to the diagnosis of DLB.

1.1.1 Alpha-synuclein (α-syn)

The α-syn protein is fundamentally unfolded and can interact with various lipid membranes to take on a partly helical shape (Bisaglia et al., 2009). α-syn a highly expressed protein involved in neurotransmission (Selkoe, 2001, McKeith et al., 2017, Mochizuki et al., 2018). While the exact physiological function of α-syn is still unknown, several studies suggest that it interacts with members of the soluble N-ethylmaleimide-sensitive factor attachment protein receptor (SNARE) family to regulate synaptic membrane processes as well as neurotransmitter release (Bellucci et al., 2016).

In dopaminergic neurons, α-syn regulates neurotransmission (Butler et al., 2017) and reduces the recycling rate of vesicles (Jenco et al., 1998). Additionally, α-syn inhibits synaptic vesicle clustering following exocytosis in cultured glutamatergic hippocampal neurons, negatively modulating neurotransmitter release (Nemani et al., 2010). In cultured dopaminergic neurons, α-syn has also been shown to interact with the dopamine transporter to promote neurotransmitter reuptake (Lee et al., 2001), as well as serotonergic neurons, and noradrenergic neurons are also proposed to function by a similar mechanism (Wersinger and Sidhu, 2006).

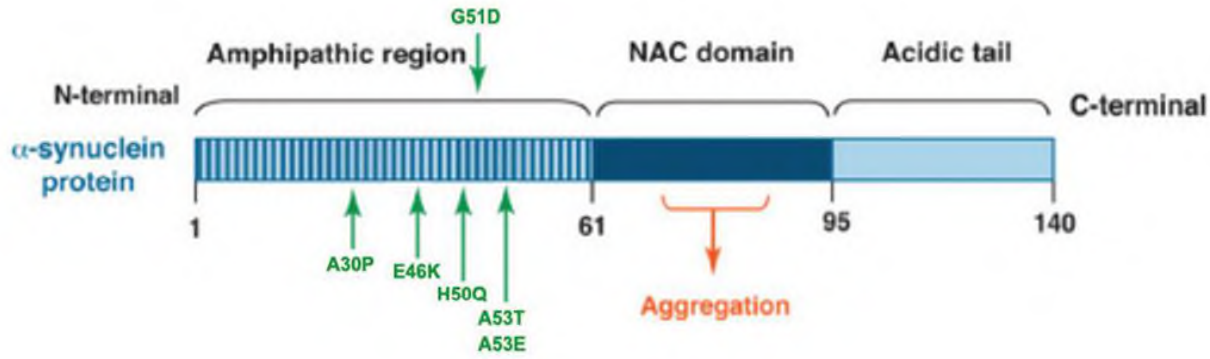

Figure 1.1: Human α-syn Protein Structure. The α-Syn protein can be classified into three regions. The six missense mutations that cause familial PD are located in the amphipathic region of the protein, suggesting that this region functions in an important way (Xu and Chan, 2015). The central hydrophobic region (non-amyloid-component or (NAC) domain) of α-syn is associated with fibril formation (Jethva et al., 2011). Most of the residues in the acidic C-terminal tail are negatively charged and are unfolded (Xu and Chan, 2015).

There has been evidence that mutations in the synuclein (SNCA) gene on chromosome 4 are responsible for the formation of the structures in familial PD

(Meade et al., 2019). The *SNCA* gene encodes a small, soluble 140 amino acid protein, α-syn, which is found throughout the neurons (Fig.1.1) (Norris et al., 2004, Bernal-Conde et al., 2019). The α-syn protein consists of three regions. The C-terminus contains an acid residue-rich region (Bernal-Conde et al., 2019). The highly conserved N-terminal domain encodes for an imperfect 11 amino acid repeat with a consensus motif of KTKEGV, which resembles the lipid-binding domain of apolipoproteins. It enables lipid binding, specifically to negatively charged lipids. This allows for the formation of an alpha helix (Bernal-Conde et al., 2019). Due to its hydrophobic structure, the non-amyloid component (NAC) of proteins allows for oligomerization to occur (Bernal-Conde et al., 2019).

The role of α-syn in PD was first discovered through genetic linkage studies in a few families (Polymeropoulos et al., 1997a). These studies found mutations, gene duplications (Chartier-Harlin et al., 2004), and triplications in the SNCA gene (Byers et al., 2011). Six missense variants in the α-syn gene A30P, A53T, E46K, H50Q, G51D, and A53E have so far been connected to the pathophysiology of PD (Xu and Chan, 2015). When compared to cells expressing wild-type α-syn and control cells, the expression of the mutant isoforms of A53T and A30P increases the cytotoxicity generated by hydrogen peroxide and 1-methyl-4-phenylpyridinium. These mutations impact the response to oxidative stress (Kanda et al., 2000). Furthermore, compared to the wild-type, the A30P, A53T, and H50Q mutations lead to enhanced oligomerisation and fibril formation (Khalaf et al., 2014, Narhi et al., 1999), whereas the G51D and A53T mutations decrease α-syn aggregation (Rutherford et al., 2014, Ghosh et al., 2014). By deactivating the JNK1-Bcl-2 pathway, the E46K mutation impairs macroautophagy (Yan et al., 2014). In genome-wide association studies, a substantial correlation between α-syn and sporadic PD was recently demonstrated (Ramanan and Saykin, 2013, Satake et al., 2009).

Research has identified many mechanisms by which α-syn interacts with neurotransmitters, lipids, carbohydrates, membrane-bound receptors, and other proteins in the brain (Saleh et al., 2015). Although α-syn is a mobile protein, it is mainly found in the axons and presynaptic terminals of neurons in the memory and emotion centres of the brain (Saleh et al., 2015).

α-syn can bind to acidic membranes, and this binding is mediated by amphipathic α-helix in the N-terminal domain. The unfolded cytosolic and membrane-bound states of α-syn are in dynamic equilibrium under physiological conditions (Burré et al., 2014). In contrast, when α-syn acts under pathological conditions, it adopts an abnormal shape of a β–sheet–rich-amyloid conformation, resulting in the formation of fibrils and subsequent deposition of α-syn into LBs (Pineda and Burré, 2017). The α-helical part of the molecule is responsible for the generation of the different types of oligomers, which are currently considered the most toxic. The release pathway for α-syn depends on endosomal integrity (Emmanouilidou et al., 2010, Alvarez-Erviti et al., 2011, Emmanouilidou and Vekrellis, 2016). Exosomes can also release the α-syn. An exosome is a small vesicle with a diameter of 100 nm that transports proteins or RNA between cells (Mutreja and Gamblin, 2017, Jansen et al., 2017). α-syn can enter the extracellular space by active and passive mechanisms, such as leakage through damaged membranes and impairment of cell function. Through interacting with cell membranes and fibrillating, α-syn can accelerate the transporting process (Volles and Lansbury, 2002). α-syn is also believed to cross the cell membrane through pore-like structures such as the voltage-dependent anion channel (Hoogerheide et al., 2017).

The α-syn protein is natively unstructured and cannot form stable secondary structures until bound to phospholipid membranes (Davidson et al., 1998a, Sahay et al., 2015). The α-syn monomers are capable of dynamically forming oligomers, which might aggregate to produce insoluble fibrils (El-Agnaf et al., 1998). It may be possible to promote or prevent α-syn aggregation through post-translational modifications of α-syn (Beyer et al., 2006).

1.1.2 Dementia with Lewy bodies (DLB)

Pathologically, DLB is caused by the aggregation and misfolding of the synaptic protein α-syn. High expression leads to toxic oligomers and fibrils and ultimately forms LBs in neurons, which Frederic Lewy first described in 1912 (McKeith et al., 2017, Selkoe, 2001, Mochizuki et al., 2018). This misfolded α-syn alters the membrane composition, leading to protein aggregation (Hijaz and Volpicelli-Daley, 2020). It eventually leads to the formation of Lewy bodies as the proteins conjugate (Fig.1.2). When LBs accumulate in neurons, they interfere with neurotransmission and cause cognitive dysfunction (Arnaoutoglou et al., 2019).

Both DLB and PDD involve aggregation of α-syn, but they are distinguished by the temporal order in which symptoms appear. In DLB, patients first develop cognitive dysfunction including memory loss, visual hallucinations, and cognitive fluctuations before the onset of motor symptoms. In contrast, in PDD the motor symptoms, which include tremors and the bradykinesia of Parkinson's disease occur first, then a proportion of patients (~ 30%) also progress to develop cognitive dysfunction (McKeith et al., 2017). In general, females are more protected against neurodegenerative disease, possibly due to hormonal mechanisms. A meta-analysis study by Moisan *et al*., 2016 found the male-to-female ratio was 1.48 for the prevalence of PD and 1.49 for its incidence. DLB is more prevalent in males, and sporadic cases generally occur between 50 and 83 years old (McKeith et al., 2004).

Alzheimer's disease (AD) is one of the neurodegenerative diseases that shares common features of aggregation and misfolding of the amyloid beta protein that are normally soluble in physiological conditions (Larson et al., 2012).

Soluble α-syn levels showed a greater correlation to cognitive impairment in AD, in comparison to soluble amyloid beta protein (Aβ) and tau levels (Larson et al., 2012). Cognitive dysfunction may be associated with the misfolding of normal soluble α-syn caused by amyloid deposition, meaning that a build-up of amyloid and synuclein caused the loss of solubility in the intracellular cytosolic proteins (Saleh et al., 2015). It has been demonstrated that cytotoxic species of α-syn form self-aggregating aggregates that spread between cells (Lee et al., 2012), consequently, seeding (Sang et al., 2021) and aggregation perpetuated in a prion-like manner (Vargas et al., 2019, Allen Reish and Standaert, 2015).

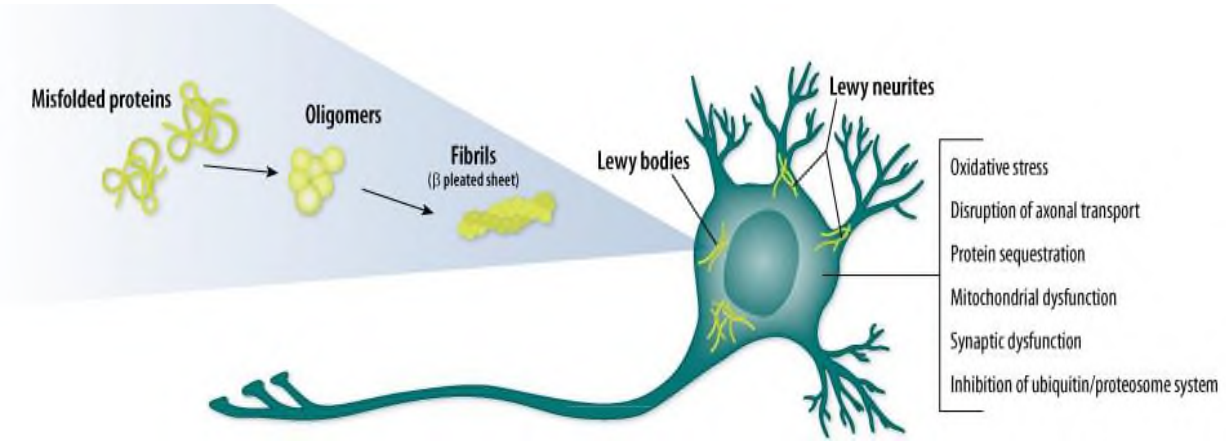

Figure 1.2: Pathological features of LBs. The formation of the LBs goes through different phases starting with initial dust-like particles cross-linked of α-syn to aggregation of ubiquitinated dense filaments ending in the formation of LBs, and finally the degradation and death of the affected neurons (Rietdijk et al., 2017).

1.1.3 Transgenic mouse models of DLB (hA30P)

Although studies involving familial forms of α-synucleinopathy have helped develop our knowledge of α-synucleinopathy pathology, much remains unknown. To study how α-syn contributes to cognitive deficits in α-synucleinopathy, rodent models are frequently used. It is essential to develop transgenic mouse models to study how α-syn might cause the disease. These models allow us to evaluate changes in the brain before permanent damage occurs, allowing interventional treatments to be considered before permanent damage occurs. Hence, we should investigate DLB at the earliest stage of its development before symptoms emerge. A transgenic mouse model allows us to study this stage in greater depth.

There are a variety of rodent models that incorporate a human gene insert, either in wild-type form or with mutations isolated from individuals with familial α-synucleinopathy. The expression of human α-syn in rodents can also be induced by viruses, the injection of preformed fibrils, or the induction of neurodegeneration via toxins (Sommer et al., 2000). The DLB mouse model used in this study is the human mutant mouse (hA30P). A monomeric structure of α-syn is generated by inserting the entire human mutation of the SNCA gene. The A30P missense mutation in the SNCA gene, first described in a patient with familial Parkinson's disease (Krüger et al., 1998), represents a Guanine (G) to Cytosine (C) substitution at nucleotide position 88. As a result, the amino acid position 30 is changed from alanine to proline. Human (hA30P)

transgenic mice were first used to study mutant SNCA gene transport under the Thy-1 promoter (Kahle et al., 2000). Thy-1 protein was originally considered to be expressed in thymocytes-precursor of T cells in the thymus, and cell surface of mature excitatory neurons. However, recent evidence suggests Thy-1 is expressed also in other cell types. It is possible to control the expression of the human SNCA gene inserted in transgenic mice using a variety of promoters, including the Thy-1 promoter like hA30P mice. Kemshead et al. (2002) reported that the Thy-1 promoter is expressed most highly in the striatum and hippocampus, while there were low levels within the substantia nigra (Neumann et al., 2002). hA30P mice express a human mutant form of α-syn from 1 month of after which there is a progressive, age-dependent, increase in pathological human α-syn phosphorylated at serine residue 129 (PS129) (Kahle et al., 2000).

The abnormal α-syn accumulates in neuronal cell bodies when overexpressed, (Kahle et al., 2000). It has been suggested that the hA30P mutation leads to α-syn losing its vesicle-binding properties and altering α-syn's role in neurotransmitter release (Jensen et al., 1998a). Human SNCA gene expression is three-fold higher in Thy-1 A30P mice than expression of the endogenous murine SNCA gene (Kahle et al., 2001). When human α-syn is overexpressed, murine α-syn does not aggregate like the human SNCA gene and its staining pattern remains normal (Kahle et al., 2001). A30P mutation in the SNCA gene may form oligomers at a high rate causing a severe neurodegenerative phenotype due to their accelerated oligomerization rates. The human mutant α-syn causes abnormal interactions with proteins controlling synaptic vesicle trafficking (Dalfó et al., 2004) and reduced membrane bindings, so it competes with mouse α-syn for biding sites but does not function properly (Snead and Eliezer, 2014). By producing phosphatidic acid, phospholipase D2 is believed to contribute to the creation of vesicles at the plasma membrane. Phospholipase D2 translocation to vesicle production sites during high-frequency stimulation may be a crucial step in vesicle recycling (Davidson et al., 1998b). It is believed that the N-terminal region of α-syn, which contains the A53T and A30P alterations, mediates binding to phospholipid membranes. Vesicle recycling may, therefore, be indirectly impacted by mutations in α-syn that change its interaction with and regulation of phospholipase D2 (Jensen et al., 1998b, Jo et al., 2002). At the terminal, the majority of dopamine molecules are typically enclosed in monoaminergic vesicles, where they are shielded from degradation**.** Mutations that impair the ability of α-syn to control phospholipase

D2 activity may result in impaired binding to membrane sites of vesicle recycling, which could ultimately lead to incomplete vesicle recycling. This may contribute to a lack of synaptic vesicles that are available for storing neurotransmitters (Lotharius and Brundin, 2002).

Less dopamine is packaged into vesicles in mice with the A30P mutation was found that this would disrupt the prolonged bursting of dopaminergic neurons (Yavich et al., 2004), although basal neurotransmission is not impacted. Also, the hA30P protein aggregates and is toxic to neurons due to the transformation oligomerization and fibrillation of human α-syn into toxic aggregates of oligomers that then precipitates a cascade of changes, involving mitochondrial dysfunction and oxidative stress which leads to neurodegeneration.

Human α-syn pathology in hA30P mice results in deficits in memory function as determined using the fear conditioning task and Morris water maze, and the mice exhibit increasing motor dysfunction with age after 6 months (Kahle et al., 2000). By 12 months of age, hA30P mice exhibit cognitive dysfunction with impaired memory dysfunction (Freichel et al., 2007) and at 14 months of age, the mice develop motor deficits including rigidity and tremor (Kahle et al., 2000), and by 16 months of age exhibit severe motor dysfunction (Freichel et al., 2007). After that, mice become paralyzed and die prematurely at 17-18 months (Freichel et al., 2007).

There are limited studies about the early cellular changes in young hA30P mice, for the work presented in this thesis, I will be using the hA30P mice at a young age (1-4 months) before the onset of any reported symptoms. The current study aimed to examine changes that occur in young pre-symptomatic mice aged between 1-4 months old compared to the C57BL/6 strain as WT control mice.

1.1.4 Network hyperexcitability in DLB

Although still not widely recognized many neurodegenerative diseases are linked to epilepsy or forms of abnormal cortical excitability. Abnormal epileptiform-like activity or myoclonus has been reported in as many as ~30-50% of patients with AD and DLB (Beagle et al., 2017).

Murine models of AD have been known for some time to exhibit epileptic electroencephalography (EEG) activity and reducing excitability with anti-epileptic drugs has been proven to be successful in restoring cognitive function (Sanchez et al.,

2012). Indeed, there is evidence from studies of patients with both AD and DLB that indicate the presence of hyperexcitability, either in the form of myoclonus or seizures, maybe an early feature of neurodegeneration (Stargardt et al., 2015).

Furthermore, neuronal and/or network hyperexcitability may even worsen the disease progression, thus several studies are investigating possible mechanisms that could reduce this early network hyperexcitability (Vico Varela et al., 2019). To date, there are no effective treatments that can prevent any of the neurodegenerative diseases, so new therapies and treatment strategies are required.

1.1.5 Hyperexcitability in murine models of AD and DLB

As seen in patients with AD the murine models of AD have been known for some time to exhibit epileptic electroencephalography (EEG) activity and reducing excitability with anti-epileptic drugs has proven to be successful in restoring cognitive function (Sanchez et al., 2012). There is a link between abnormal electrical activity causing non-convulsive epileptic discharges and an increase in Aβ levels causing synaptic dysfunction. AD causes epileptiform activity, in part, due to its influence on synapses of neurons (Ghatak et al., 2019, Ghiglieri et al., 2018).

Studies have demonstrated that changes in neuronal physiology result from overexpression of wild-type α-Syn both *in vivo* and *in vitro* (Robson et al., 2018, Tweedy et al., 2021, Stylianou et al., 2020) . According to (Nemani et al., 2010), a threefold increase in human wild-type α-syn expression in the mouse brain reduced neurotransmitter release by preventing synaptic vesicle recycling. Additionally, these transgenic animals showed a selective reduction in particular synaptic vesicle proteins linked to the decreased presynaptic release (Nemani et al., 2010).

LBD rodent models overexpressing human α-syn (either mutant or WT) also exhibit similar excitability changes. Morris et al., 2015, showed that transgenic mice with human wild-type α-syn exhibited interictal spikes and intermittent seizures in the EEG (Morris et al., 2015). Immunohistochemical changes aligned with the functional increased excitability observed. Immunohistochemistry showed mossy fibre sprouting and increased expression of calbindin in the α-syn transgenic mice (Morris et al., 2015, Walker et al., 2002). More recently, (Morris et al., 2015, Peters et al., 2020, Stylianou et al., 2020) have also shown that hyperexcitability may be an early feature of human α-syn pathology in mouse models of DLB.

Furthermore, neuronal and/or network hyperexcitability may even worsen the disease progression, thus several studies are now investigating possible mechanisms that could reduce this early network hyperexcitability (Vico Varela et al., 2019). Previous work in our laboratory demonstrated that the hA30P mice exhibit very early (2-4 months of age) hyperexcitability in the hippocampus (Tweedy et al., 2021) so I focused in my thesis work on this region aiming to investigate the causes of this hyperexcitability, in particular the role neuroinflammation might play in generating abnormal network activity.

1.2 Hippocampus

The hippocampus is a bilateral structure in the temporal lobe of the human and rodent brain. Humans rely on the hippocampus to store and recover declarative memories as well as spatial connections. Memories about facts and events are known as declarative memories e.g. memorizing lines from a play or a speech. The hippocampus plays an essential role in spatial memory and navigation, through the activity of place and grid cells and also in the episodic memory of sequencing the past, present, and future events (Moser et al., 2015, Bear et al., 2020). The hippocampus, including the dentate gyrus (DG), has the shape of a curved tube, which has been compared to a seahorse, and a ram's horn (Cornu Ammonis) (CA). The abbreviation of CA is used in naming the hippocampus subfields CA1, CA2, CA3, and CA4 (Bear et al., 2020) (Fig. 1.3, and 1.4).

The hippocampal subfields CA1, CA2, CA3, and CA4 are defined by a narrowing of the cortex into a single layer of tightly packed pyramidal neurons that curl into a tight U shape. CA4 is embedded in the backward-facing, flexed DG on one border of the "U" (Kosaka et al., 1987). The hippocampus is divided into two parts: anterior and posterior (in primates) or ventral and dorsal (in other animals). Both components are

similar in composition but have diverse tasks and belong to different neural circuits. The dorsal hippocampus is responsible for spatial memory, verbal memory, and conceptual learning; it also contains more place cells than the ventral and intermediate hippocampal areas. The ventral and dorsal hippocampus share similarities with the intermediate hippocampus (Kosaka et al., 1987). The functions of the ventral hippocampus are in fear conditioning and affective processes (Bear et al., 2020).

The dentate gyrus is composed of three layers of cells (or four if the hilus is included) (Bear et al., 2020). The entorhinal cortex (EC) is the primary input of the tri-synaptic (information) circuit to the hippocampus, while CA1 is the primary output, with axons projecting through the perforant pathway to the granule cells of the DG (first synapse). The information is transmitted to CA3 via the mossy fibers (second synapse). CA3 axons, known as Schaffer collaterals, leave the deep section of the cell body, loop up to the apical dendrites, and then extend to CA1 (third synapse). CA1 axons then project back to the EC, closing the circuit.

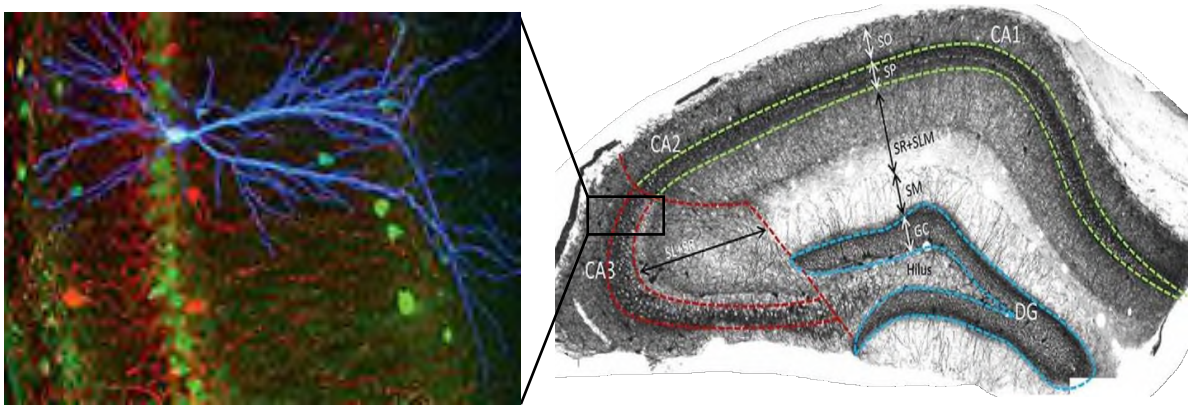

Figure 1.3: The structure of the hippocampus. The right: The hippocampal subfields CA1, CA2, and CA3, and the laminar structure of the hippocampus stratum oriens (SO), stratum pyramidale (SP), and stratum radiatum (SR).The left: The layout of a pyramidale neuron in the pyramidal layer (https://nba.uth.tmc.edu/neuroscience/m/s4/chapter05.html).

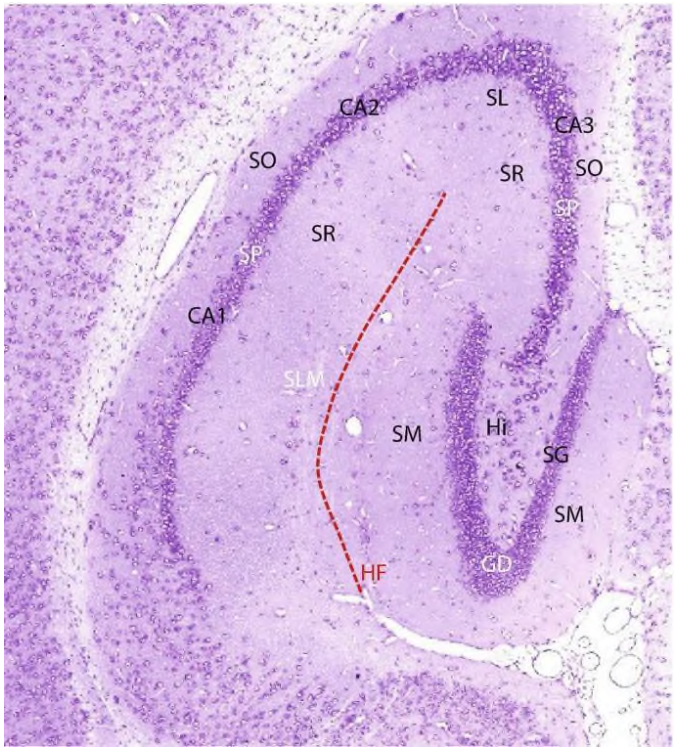

Figure 1.4: The different layers of the Cornus Ammonis and the gyrus dentatus of the Hippocampus. A horizontal cut through the hippocampus formation of a mouse (C57BL/6) reveals the various layers of the gyrus dentatus (**GD**) and Cornus Ammonis (**CA**). *The stratum radiatum* (**SR**) and *lacunosum-moleculare* (**SLM**) come after the *stratum oriens* (**SO**), which is external to internal and contains the axon of pyramidal neurons in the *stratum pyramidale* (**SP**). The CA3 area is the only one where the *stratum lucidum* (**SL**) is found. **DG**: The dendrites of the granule cells of the *stratum granulare* (**SG**) are housed in the *stratum moleculare*. The SG is existed by the mossy fibres, or axon, of the granule cells through the *stratum* multiforme or hilus (Hi) fissure hippocampal (**HF**). **CA** and **GD** contain interneurons in addition to projection neurons, pyramidal cells, and granule cells (Schröder et al., 2020).

Several other connections are crucial to hippocampus function. Aside from the EC, other cortical areas, notably the prefrontal cortex, are served by other output routes. The hypothalamus also receives a major output from hippocampus (Bear et al., 2020). In the current study, I focused on the CA3 region particularly, because it exhibits interictal activity and generates abnormally large gamma oscillations (Le Duigou et al., 2014, Treviño et al., 2007)

.

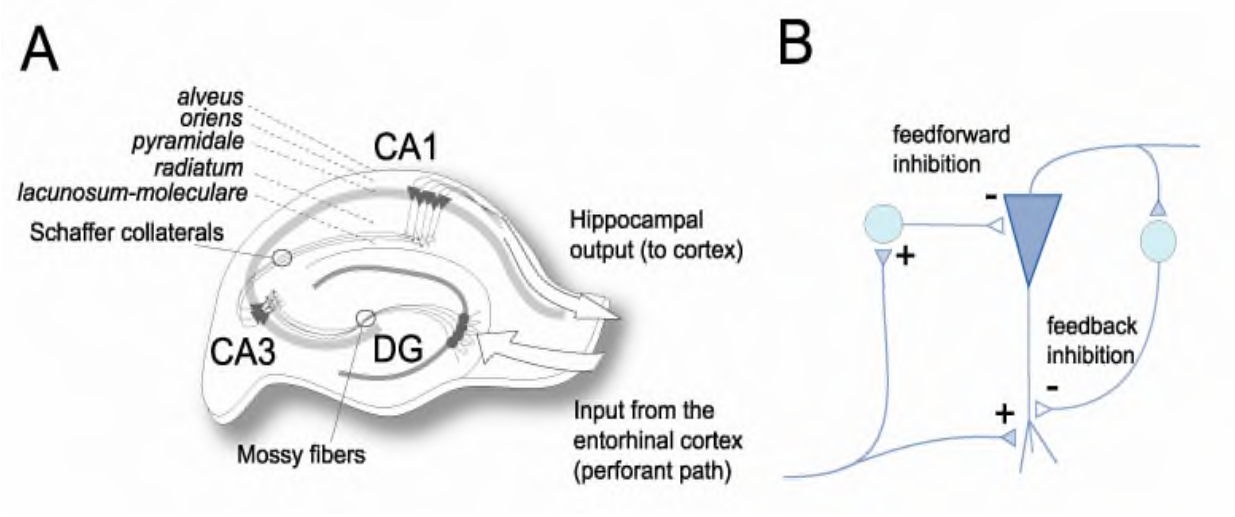

Figure 1.5: Synaptic connectivity of the hippocampus in the trisynaptic circuit. A) The trisynaptic circuit (Bear et al., 2020). **B)** Generation of gamma oscillations depends on the dynamic interplay between fast-spiking inhibitory interneurons and excitatory pyramidal cells. PV interneurons synapse on the cell bodies of excitatory neurons, thus providing inhibition. Glutamatergic neurons, in turn, provide excitatory drive by synapsing on the cell bodies of GABAergic interneurons (Antonoudiou et al., 2020).

1.2.1 Parvalbumin GABAergic Interneurons

Two main populations of neurons exist within the hippocampus. The principal neurons of the CA regions are the glutamatergic pyramidal neurons. They produce glutamic acid, a major excitatory neurotransmitter in the hippocampus, and excitatory pyramidal neurons make up approximately 90% of neurons in the hippocampus (Freund and Buzsáki, 1996). Pyramidal neurons are classified depending on the morphology of the dendritic tree and are found in many areas of the brain including the cerebral cortex, hippocampus, and amygdala (Bear et al., 2020) (Fig.1.3).

The second main neuronal type in the hippocampus is the gamma-aminobutyric acid (GABAergic) interneurons which release the inhibitory transmitter GABA and make up the remaining ~10% of the neurons. GABAergic neurons provide effective inhibition to the pyramidal neurons and other interneurons due to their extensive arbors (Kosaka et al., 1987). Both pyramidal neurons and interneurons are further innervated and modulated by a variety of cholinergic, dopaminergic, serotonergic, and noradrenergic inputs from other brain areas (Avery and Krichmar, 2017).

Different classes of interneurons can be defined by the different expressions of peptides or calcium-binding proteins. Calcium-binding proteins, which are abundant in

the nervous system, can influence the spatial and temporal dynamics of calcium signals (Bjerke et al., 2021). Parvalbumin (PV) and calbindin (CB) are two such proteins that are expressed in essentially non-overlapping clusters of neurons that exhibit fast-spiking and bursting electrophysiological characteristics, respectively (Bjerke et al., 2021). Only around 10–12% of the GABAergic interneurons in the hippocampus are CB+ interneurons, and the *stratum radiatum* contains a large number of CB+ cell bodies (Toth and Freund, 1992). CB interneurons are frequently categorised as *oriens-lacunosum moleculare* cells, bistratified cells, or radial trilaminar cells and have generally innervate the dendrites of pyramidal cells. Although CB interneurons lack the fast-spiking characteristics of most PV+ interneurons, they are essential for inhibition and preserving the equilibrium between excitation and inhibition in the hippocampal network (Puig et al., 2008). PV is expressed in a type of interneuron that is distinguished by fast responses and effective inhibition of surrounding principal neurons (Bjerke et al., 2021) (Fig.1.5B).

The cell bodies of PV interneurons are typically present in or near the *stratum pyramidale* (SP). While PV interneurons primarily innervate pyramidal neurons, it is estimated that 5-15% of synaptic contacts from PV interneurons are to other GABAergic interneurons. A complex network of excitatory and inhibitory connectivity is further enriched by a subset of interneurons that specifically target other interneurons within the hippocampus (Kosaka et al., 1987).

Basket interneurons are the main type of PV interneuron that receive excitatory input from pyramidal neurons and subsequently provide inhibitory feedback to them (Freund and Buzsáki, 1996) (Fig.1.5B). This recurrent inhibition is a basic feedback circuit in the hippocampus that can regulate excitatory responses. The pyramidal neurons produce recurrent excitation, which is a key mechanism in several memory-processing microcircuits (Kosaka et al., 1987).

Appropriate brain function is dependent on networks of inhibitory interneurons and excitatory projection pyramidal neurons that are well-linked and well-organized (Rudy et al., 2011). Inhibitory interneurons influence the activity of pyramidal neurons, which are responsible for transmitting information between neuronal assemblies. Imbalances between these network components can result in brain function abnormalities and neurological diseases such as epilepsy, schizophrenia, and autism spectrum disorder (Jiang et al., 2016).

Glutamatergic neurons and GABAergic interneurons contribute to the generation or regulation of rhythmic network oscillations required for effective signal processing, as well as the commencement and duration of cortical plasticity phases (Bjerke et al., 2021). Inhibitory interneurons are extremely diverse: in rodents, more than 20 unique inhibitory interneuron types have been found in the cerebral cortex and the CA1 area of the hippocampus (Jiang et al., 2016).

Interneurons can also be categorized based on physiological features, such as discharge patterns in response to depolarization (Bear et al., 2020). PV-expressing basket interneurons and some chandelier interneurons have a high rate of spiking. Bouquet (bipolar) interneurons exhibit irregular, adaptive spiking and high input resistance. Neuroglia cells have a slow firing, late spiking firing pattern, as well as slow adaptability (Rudy et al., 2011).

PV inhibitory interneurons appear to be prone to injury in chronic epileptogenic lesions of the neocortex and the hippocampus (Jiang et al., 2016), which is why it was part of my interest in this study.

In this study, I looked at both pyramidal neurons and PV interneurons to understand neuronal hyperexcitability in the CA3 region of the hippocampus in young hA30P. The hippocampus is affected by α-syn pathology in patients with DLB and changes in these regions likely contribute to some of the key features of DLB, including impaired executive function and memory (Robson et al., 2018, Crews et al., 2010).

1.2.2 Perineuronal nets (PNNs)

There is an extracellular matrix (ECM) of proteins surrounding the components of the CNS. GABAergic PV interneurons are particularly enveloped by condensed matrix from these extracellular matrix proteins called perineuronal nets (PNNs). PNNs surround the soma, proximal dendrites, and synapses. Most PV interneurons are surrounded by PNNs in the hippocampus and perirhinal cortex in addition to some hippocampal pyramidal neurons (Fawcett et al., 2022). PNNs regulate plasticity by stabilizing synapses and protecting neurons and their synaptic connections from environmental stress (Cabungcal et al., 2013a). The PNNs also control neuronal plasticity by controlling the formation of new synaptic connections (Reichelt et al., 2019). The relationship between neurons and PNNs is attracting attention as a central mechanism controlling brain plasticity, playing roles as both a regulator of synaptic

plasticity and a protective barrier (Fawcett et al., 2022). PNNs have a delayed developmental trajectory and are key components in the closure of critical periods of heightened neuroplasticity (Fawcett et al., 2019, Miyata and Kitagawa, 2017). In animal models, manipulating PNNs outside this critical window can enhance cognition, suggesting a potentially therapeutic approach for attenuating cognitive decline (Fawcett et al., 2019). However, the crucial role of PNNs in plasticity and protection means that such therapeutic modulation must strike a careful balance: manipulation of PNNs to promote plasticity may have unintended negative consequences resulting from exposure of neurons to neurotoxins (Cabungcal et al., 2013a).

Recent evidence showed that the PNNs play a vital role in memory dysfunction linked to pathological changes. PNNs matrix and neurodegeneration changes are frequently related (Fawcett et al., 2022). Neurons are more susceptible to oxidative stress if the PNNs are damaged. There are also excitatory and inhibitory balance changes, synaptic loss, and synaptic loss all linked with PNNs damage (Wen et al., 2018). Converging evidence indicates that PV interneurons and PNNs are impaired in various neurological disorders. PNNs development and maintenance are necessary for several processes within the CNS, including regulation of GABAergic cell function, protection of neurons from oxidative stress, and closure of developmental critical period plasticity windows. Understanding PNNs' functions may be essential for characterizing the mechanisms of altered cortical excitability observed in neurodegenerative and neurodevelopmental disorders. Indeed, abnormalities of the PNN have been observed in post-mortem brain tissues of patients with schizophrenia and AD. There is impaired development of PNNs and enhanced activity of its key regulator matrix metalloproteinase-9 (MMP-9) in Fragile X syndrome, a common genetic cause of autism. MMP-9, a protease that cleaves ECM, is differentially regulated in several disorders. Despite this, few studies have addressed the interactions between PNNs expression, and neuronal excitability (Wen et al., 2018). In the current thesis, I studied the effect of overexpression of α-syn on the PNNs in the CA3 region hippocampus in young hA30P.

1.3 Neuroglia

We now know that glial cells play an active role in numerous cellular brain functions and are just as important as neurons. Glial cells include astrocytes, microglia, and oligodendrocytes. Neuroglia were so named for their supposed function as the “glue” of the brain holding neurons in place. Neurons and glia are the two primary cell types that make up the CNS. According to some estimates, glial cells, make up 50% of the brain's cells (Azevedo et al., 2009). Glial cells were once believed to play primarily a passive role in sustaining neurons, but mounting evidence points to their involvement in critical homeostatic and developmental processes, and we now know that glial cells play an active role in numerous cellular brain functions and are just as important as neurons (Allen and Lyons, 2018).

1.3.1 Astrocytes

Astrocytes are star-shaped glial cells that make up 20 to 50% of brain volume contiguously connecting the entire CNS by enveloping neuronal synapses, dendrites, cell bodies, and blood vessels with their processes (Sofroniew and Vinters, 2010) (Fig 1.6). From the late 19th century, morphological heterogeneity was identified and astrocytes were classified into two main groups: protoplasmic astrocytes located in the grey matter and fibrous astrocytes in the white matter (Sofroniew and Vinters, 2010) (Pestana et al., 2020). Grey matter protoplasmic astrocytes have revealed most of what we know about astrocyte function and form, whereas white matter fibrous astrocytes have remained relatively unexplored (Mazumder et al., 2022). Protoplasmic astrocytes have been shown to release neurotransmitters such as glutamate and GABA to modulate both excitatory and inhibitory neuronal activity and are closely associated with memory formation due to their role in synaptic remodelling and plasticity (Crotti and Ransohoff, 2016).

The mammalian white matter tracts extensive energy demands compared to the axons, they are metabolically demanding (Ransom and Orkand, 1996, Harris and Attwell, 2012). White matter possesses a relatively limited substrate supply due to a less dense vascular network than gray matter (Moody et al., 1990). In white matter, dense populations of astrocytes supply the main energy sources to axons via lactate

shuttles between neurons and astrocytes (Wender et al., 2000, Pellerin et al., 1998). Axons receive lactate when needed after glucose is taken up from capillaries by astrocyte endfeet and stored as glycogen in astrocytes (Dringen et al., 1993). Whenever ambient glucose alone is insufficient to meet the immediate energy demands, glycogen acts as an energy buffer and converts to lactate (Tekkök et al., 2005, Brown et al., 2003). The lactate becomes demanded fuel than glucose when glucose levels are low or when neuronal activity increases (e.g., firing increases) (Tekkök et al., 2005, Brown et al., 2003).

The role that astrocytes play is diverse and includes the control of neuronal migration during development and functional modulation of mature synapses. These cells play an essential role in brain homeostasis as they are involved in regulating blood flow and maintaining the integrity of the blood-brain barrier (BBB) (MacVicar and Newman, 2015). Additionally, astrocytes control synaptic activity by participating in the tripartite synapse (the sum of the presynaptic membrane, and postsynaptic membrane, and their intimate association with surrounding glia contributes to the generation of activity at the chemical synapse), recycling neurotransmitters, releasing gliotransmitters including glutamate and GABA, buffering extracellular K+ ions, and other processes (Verhoog et al., 2020). The electrical connection between astrocytes, through gap junctions, allows the coordination of responses and aids in the spread of calcium ions throughout the astrocytic network. Astrocytes respond to most neurotransmitters, which evoke an increase in astrocytic intracellular calcium levels and modulation of synaptic transmission within the tripartite synapse (Sofroniew and Vinters, 2010). Furthermore, astrocytes provide metabolic support to neurons through neurovascular coupling (Bear et al., 2020) (Fig 1.7).

Activated astrocytes have recently been classified into two distinct forms (pro- and anti-inflammatory). In response to injury, infection, or disease, non-active (resting) functional astrocytes change to reactive astrocytes state (Favoretto et al., 2023). Pro-inflammatory astrocytes (A1) lose their ability to perform normal physiological functions and secrete neurotoxic factors to remove neurons and synapses. They are characterized by a decrease in ramifications and the length of their processes. The number of pro-inflammatory astrocytes is increased in physiological aging and may therefore infer a vulnerability to neurodegeneration (Crotti and Ransohoff, 2016, Kwon and Koh, 2020). While anti-inflammatory astrocytes (A2) participate in the process of neuroprotection, minimize the damage and repair. They are characterized by an

increase in ramifications and the length of their processes (Crotti and Ransohoff, 2016) (Fig. 1.6 and 1.7).

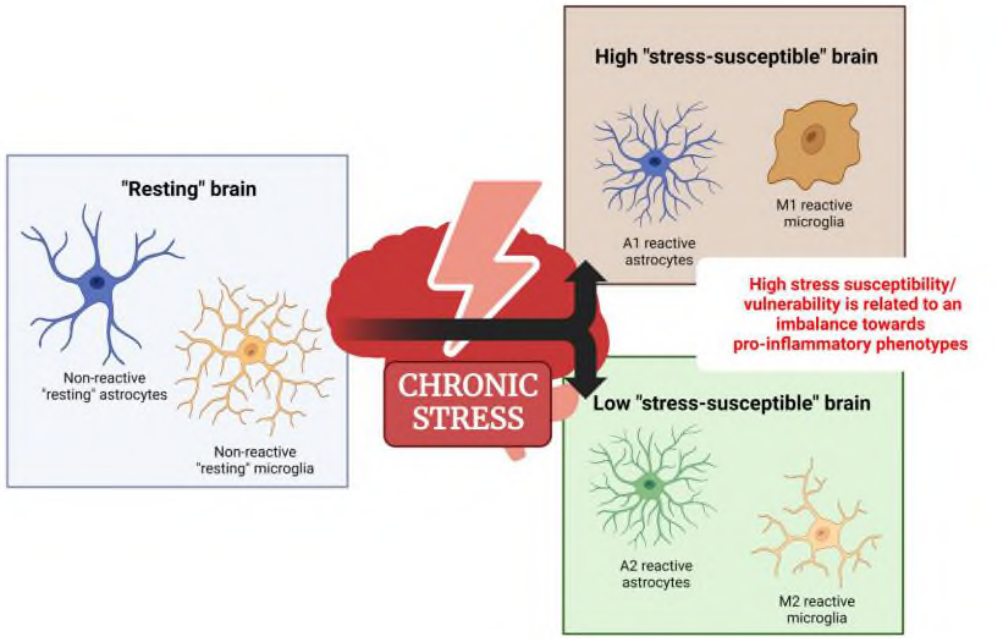

Figure 1.6: Neuroprotective and neurotoxic states of glia. Glial cells' dichotomous functional state under prolonged stress. Stress or noxious stimuli cause astrocytes and microglia to transition from a non-reactive to a reactive functional state. Proinflammatory reactive phenotypic imbalance should be associated with high-stress sensitivity. The anti-inflammatory phenotype is characterized by an increase in ramification and length in the process, and the pro-inflammatory phenotype is characterized by a decrease in ramification and length in the process and an increase in soma size (Favoretto et al., 2023).

While increase in reactive astrocytes typically ends in scar formation, a cascade of changes occurs before this point which are often reversible, including upregulation of glial fibrillary acid protein (GFAP) and vimentin, both intermediate filaments forming the astrocytic cytoskeleton (Sofroniew and Vinters, 2010). Increased expression of GFAP, is a defining characteristic of all reactive astrogliosis types (Anderson et al., 2014, Eddleston and Mucke, 1993). Since elevated GFAP+ levels have been linked to several pathogenic disorders, this protein is now often employed in both clinical and experimental settings as a reliable indicator of reactive astrocytes (Sofroniew and Vinters, 2010). Therefore, I will consider the GFAP as an important histological marker in my study of the early stage of human α-synucleinopathy in hA30P mice.

1.3.2 Microglia

The second major type of glial cell are the microglia. Due to the role of the BBB in excluding the body's immune cells from the brain, the brain's native immune cells are the microglial which act as immune regulators and make up around 10–15% of cells within the brain. The so-called "resting" microglia are incorrectly named, given their active role in the surveillance of their microenvironment, and maintaining homeostasis (Iba et al., 2020, Iba et al., 2023). Non-active (resting) functional microglia are preferentially referred to as ramified surveilling microglia due to their small soma and long processes (Bjerke et al., 2021) (Fig. 1.6, and 1.7). They play a role in synaptic pruning, the removal and fine-tuning of synapses, in network development through phagocytosis. Consequently, microglia are implicated in synaptic plasticity through the phagocytosis of weaker synapses (Favuzzi et al., 2021). In an activated state, microglia produce pro-inflammatory cytokines and chemokines such as in the case of neurodegenerative diseases including α-synucleinopathies (Mavroeidi and Xilouri, 2021, Deyell et al., 2023). Reactive microglia carry out several roles including the release of mediators that activate astrocytes (Zhao et al., 2020) (Favuzzi et al., 2021). Microglia make brief connections with neurons and astrocytes, and it has been shown that following contact neuronal activity is reduced. Potassium (K+) channels on microglia respond to small disturbances in extracellular K+, often caused by damaged or ruptured cells. Microglia may also indirectly modulate neuronal excitability through activation of astrocytes. It is unsurprising therefore that like astrocytes, microglia are implicated in the pathogenesis of epilepsy (Vezzani and Viviani, 2015). Microglia also recognize and respond to immune threats and misfolded proteins. There is growing evidence of neuroinflammation in AD and PD, which may be a result of misfolded proteins inducing microglial reactivity (Zhao et al., 2020). Conversion of microglia from a protective to toxic role can occur because of physiological aging or neurodegenerative disease. Conversion back to the neuroprotective state is promoted by non-steroidal anti-inflammatory drugs (Ajmone-Cat et al., 2010).

Reactive microglia have also been proposed to occupy two distinct states of neurotoxicity (M1) and neuroprotection (M2), marked by the differential release of pro-inflammatory or anti-inflammatory factors, respectively. While both phenotypes of microglia are marked by ionized calcium-binding adapter molecule 1 (Iba-1) upregulation, specific markers can be used to differentiate between each state (Colonna and Butovsky, 2017, Favoretto et al., 2023). The production of pro-inflammatory cytokines and chemokines, such as tumour necrosis factor-alpha (TNFa), interleukin-6 (IL-6), and interleukin-1 (IL-1), which harm neurons, are hallmarks of M1 microglial activation, often referred to as classical activation. M2 microglia in contrast release growth factors, anti-inflammatory cytokines, and pro-survival factors, which encourage the phagocytosis of cellular debris, tissue repair,

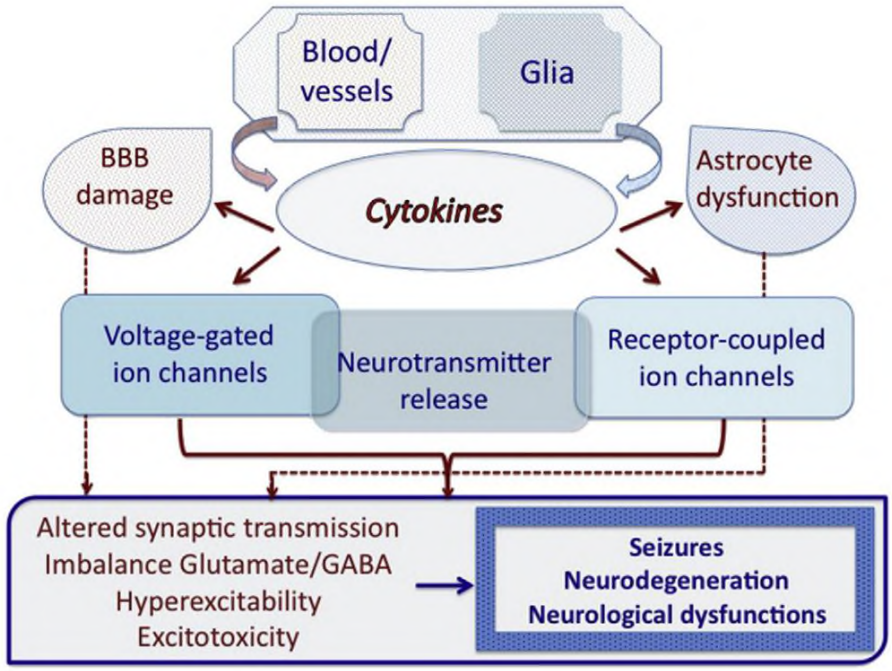

Figure 1.7: Role of glia in neurodegeneration. Schematic representation of the cascade of pathologic events provoked by increased levels of cytokines in the nervous system. Cytokines are synthesized and released by glia (microglia and astrocytes), or imported into nervous tissue by blood immune cells, particularly in pathologic conditions associated with BBB damage. Excessive levels of cytokines can, in turn, promote both glia and BBB dysfunction, with an impact on neuronal cell excitability and viability. Excessive activation of cytokine receptor signaling in neurons may lead to hyperexcitability and excitotoxicity, thereby contributing to neuronal cell loss, neurological deficits, and seizures (Vezzani and Viviani, 2015).

and neuron survival (Colonna and Butovsky, 2017). In this state, the microglia exhibit morphological changes, such as increased soma roundness, and size, increased compactness, and decreased branches (Fixemer et al., 2022, Iba et al., 2020, Iba et al., 2023).

The expression of Iba-1 an adaptor molecule implicated in membrane ruffling, the development of motile cell surface protrusions comprising a meshwork of freshly polymerized actin filaments, is one of the earliest structural changes that may be seen in cells in response to several external stimuli and Iba-1 expression is a defining hallmark of microglia (Sasaki et al., 2008). Iba-1 has been frequently employed as an immunofluorescence marker of microgliosis because it is linked to elevated expression of microglia (Ahmed et al., 2007). Therefore, Iba-1 antibody staining has been conducted in this study.

1.3.3 Neuroinflammation

The term neuroinflammation refers to an inflammatory response originating in the CNS that is caused by the activity of glial cells, such as microglia and astrocytes (Morales et al., 2014). The CNS is protected against damaging stimuli via pathogen clearance and tissue regeneration collectively described as a neuroinflammatory response (Kwon and Koh, 2020). Through the secretion of cytokines, chemokines, reactive oxygen species, and secondary messengers by local CNS cells, endothelial cells, and peripherally derived immune cells, this process includes the production of a cascade of inflammation-inducing mediators (DiSabato et al., 2016).

Research suggests that neurodegenerative disorders create a permanent stimulus that over-activates microglial cells and causes chronic neuroinflammation (Guzman-Martinez et al., 2019). Neuronal dysfunction and cell death are associated with this cycle of chronic neuroinflammation that can lead to cognitive decline (Surendranathan et al., 2015) (Fig. 1.6).

The effects of microglial activation on AD in aged chimpanzees were examined by Edler and colleagues, 2018. Results showed that increasing levels of activated microglia were positively correlated with increasing amyloid plaque volume. This is because activated microglia increase brain cells' production of amyloid, resulting in more plaques and aggravating disease progression (Outeiro et al., 2019). Research has also shown that DLB patients exhibit similar observations following neuroinflammation to those with AD but to a lesser extent. As a consequence, previous findings about AD may apply to DLB (Fixemer et al., 2022).

1.3.4 Neuroinflammation and Neurodegeneration

Neuronal excitability is regulated by the astrocytic network through its critical role in maintaining the concentration of extracellular glutamate at physiologically low levels by clearance of synaptically released glutamate, in addition to buffering extracellular potassium to control neuronal excitability (Bear et al., 2020).

Researchers have previously examined the potential mechanisms behind increased brain hyperexcitability associated with neuroinflammation. It was suggested by Tzour et al, 2016 that microglial activation inhibits Kv7/M channels leading to hyperpolarized neurons. There is evidence that Kv7/M channels are involved in the regulation of neural hyperexcitability in patients with epilepsy (Tzour et al., 2017). Glutamate was released when microglia were activated. Glutamate acts on calcium (Ca2+) of neurons' receptors. Consequently, Kv7/M channels are inhibited, and cortical hyperexcitability is increased (Tzour et al., 2017).

As an alternative explanation for cortical hyperexcitability, over activation of microglia may contribute to synaptic dysfunction in patients with neurodegenerative disorders. The relationship was discussed by Piccioni et al., 2021 in terms of AD. Activating microglia over a prolonged period leads to the production of proinflammatory cytokines like interleukin 1β (IL-1β) TNF-α. Synaptic damage or loss can result from the overproduction of these cytokines since it results in impaired phagocytic capacity of microglia and decreases the release of the neurotrophic factors (Piccioni et al., 2021, Heneka et al., 2015).

Another possible explanation concerning synaptic damage involves microglia engulfing inhibitory synapses in aberrant ways in neurodegeneration. Microglia have been shown to manipulate synaptic transmission by wrapping around inhibitory presynaptic terminals when activated, although there is little research supporting this theory (Andoh et al., 2019). It also supports the idea that neuroinflammation is associated with cortical hyperexcitability.

Therefore, this study depends on activated astrocytes and microglia as the main indicator of neuroinflammation in the model of DLB (hA30P) as markers of neurodegeneration in this transgenic mouse.

1.4 Mammalian Target of Rapamycin (mTOR) Pathway: Role in Neurodegeneration

The pathway that involves the mammalian target of rapamycin (mTOR) controls many cellular functions. mTOR is involved in numerous metabolic and autophagic processes and has been shown to play a role in synaptic plasticity and memory function (Crews et al., 2010). The mTOR pathway is associated with several cellular processes implicated in neurodegeneration including autophagy and is expressed ubiquitously in neuronal and non-neuronal cells (Norwitz and Querfurth, 2020, Wullschleger et al., 2006).

Furthermore, mTOR may play a function in neuroinflammation and has been proven to be neuroprotective in mouse models of AD (Perluigi et al., 2022). The mTOR pathway is considered to be neuroprotective because it promotes protein synthesis, which then enhances synaptogenesis, but it can also impair autophagy leading to neurotoxic protein aggregation (Fig. 1.8) (Norwitz and Querfurth, 2020).

mTOR has also been found to be upregulated in most neurodegenerative conditions including AD (Perluigi et al., 2022) and DLB (Crews et al., 2010). In AD and DLB, mTOR hyperactivation is linked to the accumulation of amyloid-beta and α-syn respectively, within neurons (Caccamo et al., 2010, Norwitz and Querfurth, 2020). Previous studies in human post-mortem tissue have suggested that mTOR was particularly increased in pyramidal neurons that contained α-syn (Crews et al., 2010). mTOR also has a possible role in neuroinflammation and is neuroprotective in rodent models of AD (Sanchez et al., 2012).

The function of mTOR in neurodegenerative disease and epilepsy is of relevance, given the growing recognition that epilepsy, or at least neuronal hyperactivity, maybe early hallmarks of neurodegenerative disease in humans (Zhao et al., 2020). Because of these multiple cellular modulations mTOR activity is now considered to have great potential as a therapeutic intervention aimed at reducing neurodegeneration (Heras-Sandoval et al., 2020).

1.5 Therapeutic Interventions in Neurodegenerative Diseases

In recent years, reducing mTOR activity has gained increasing attention as a potential therapeutic intervention to slow neurodegeneration (Heras-Sandoval et al., 2020). Several compounds are known to act as inhibitors of mTOR including rapamycin, metformin, and everolimus (Thellung et al., 2019).

Recently, pre-clinical studies have shown that inhibition of mTOR using either metformin (type 2 diabetes drug), or rapamycin can mediate a wide range of neuroprotective effects that include reducing oxidative stress, neuroinflammation, and apoptosis. In addition, it protects the BBB (Van Skike et al., 2018, Norwitz and Querfurth, 2020) and mitochondrial integrity (Cao et al., 2019).

mTOR activation promotes, via downstream signalling pathways, increasing protein synthesis but also impairs autophagy leading to mitochondrial dysfunction and protein aggregation (Norwitz and Querfurth, 2020). The WHO reported in 2022 that around 50 million people worldwide suffer from epilepsy and that approximately 5 million new cases are reported every year. Hyperactivated mTOR in both neurodegenerative disease and epilepsy is of particular interest because of the increasing understanding that epilepsy, or at least neuronal hyperactivity, may be early features of neurodegenerative disease (see section 1.1) (Stylianou et al., 2020) (Tweedy et al., 2021). mTOR inhibition has now shown promise as a treatment for epilepsy, with rodent studies showing metformin can ameliorate seizure activity (Ou et al., 2021).

Previous studies have shown that rapamycin is neuroprotective in murine models of AD (Ma et al., 2007, DiTacchio et al., 2015). Notably, rapamycin reduced amyloid-beta and neurofibrillary tangles, and improved cognition in AD models (Caccamo et al., 2010, Spilman et al., 2010). Rapamycin has some side effects, so scientists have looked at other drugs that target mTOR that could have therapeutic intervention in neurodegenerative diseases (Blagosklonny, 2019). There is currently growing interest in metformin as this drug has an mTOR inhibitory effect and is well tolerated in patients (Yang et al., 2017).

In this study, I used metformin treatment to investigate whether it had an anti-inflammatory/neuroprotective effect in hA30P mice.

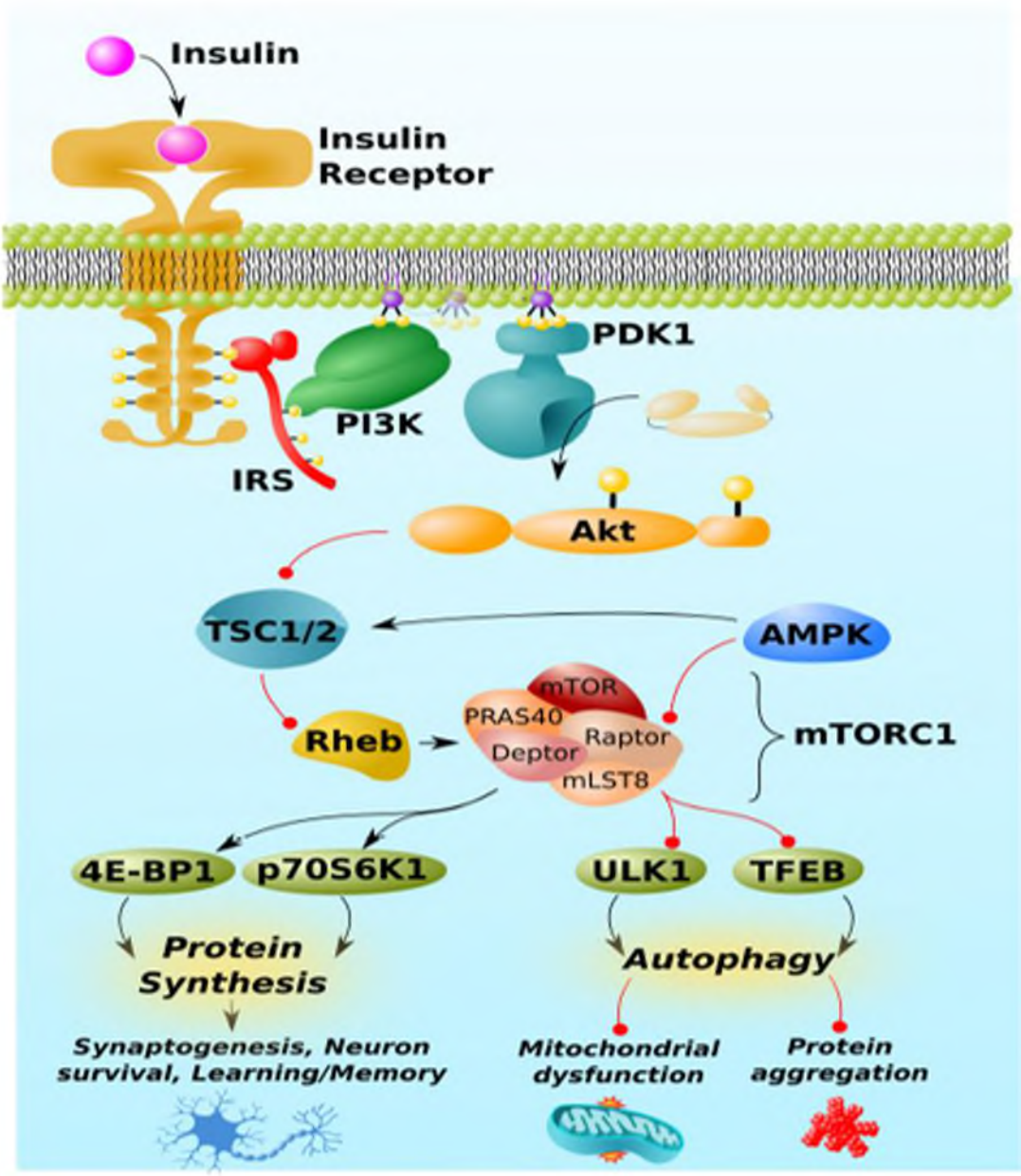

Figure 1.8: The mTOR pathway controls many cellular functions. Several downstream targets of mTOR are involved in autophagy, and the master regulator of lysosomal biogenesis, TFEB defined in full. mTOR activation promotes protein synthesis, including the synthesis of abnormal (cytotoxic) proteins, and synaptogenesis proteins involved in learning, and memory. However, it can also impair autophagy, causing mitochondrial dysfunction and neurotoxic protein accumulation (amyloid-beta, phosphor-tau, α-syn, etc.). Adapted from (Norwitz and Querfurth, 2020).

1.6 Metformin

Metformin basically is a botanical medicine called Galega officinalis. It was used in medieval Europe (Bailey and Day, 2004). This perennial plant grows over two feet high in most tepid regions, including Britain, and has white, purple, or blue flowers (Bailey and Day, 2004) (Fig. 1.9).

According to Palit Palit et al. (1999), the main chemical components of *Galega officinalis* extract are guanidine and glargine. Its hypoglycaemic effect on animals is well documented, but its toxic nature prevented its use in clinical trials. A synthetic biguanide was created by combining two guanidines (Patade and Marita, 2014) (Fig 1.10) that were found to be better tolerated and safer than the plant extract (Patade and Marita, 2014).

Metformin has no obvious side effects if taken as a monotherapy (without combination with other compounds). Metformin's chemical structure is illustrated in (Fig. 10). A French physician, Jean Sterne, synthesized metformin in 1929 and developed it clinically in the 1950s under the name Glucophage ("glucose eater") (Gottlieb and Auld, 1962). Metformin prevents fats, glycogen, and amino acids of the liver from converting into glucose and it enhances the adenosine monophosphate-activated protein kinase (AMPK) enzyme to make the cells more responsive to insulin, and thus normalize blood glucose levels (Imfeld et al., 2012) (Fig. 11).

Figure 1.9: The *Galega officinalis* is the source of metformin. It is also called French lilac. Bailey and Day (2004) describe these plants as being borne as ladders and adorned with short spikes of lilac, pea-like leaves (Bailey and Day, 2004).

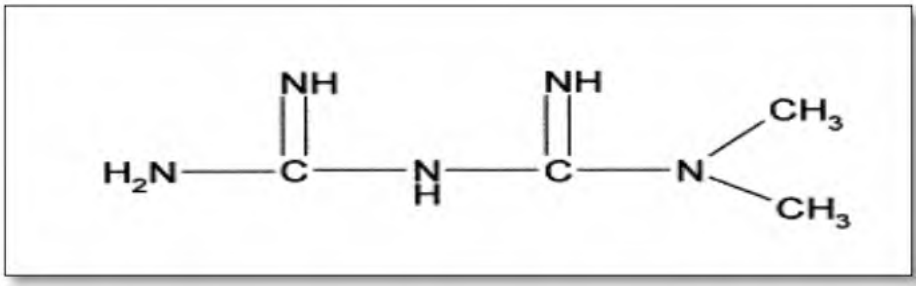

Figure 1.10: Chemical structure of metformin. A hygroscopic, crystalline solid that is white and bitter. C4H11N5 is its molecular formula. The molecule can be dissolved in water freely (Ruggiero-Lopez et al., 1999).

Metformin improves insulin sensitivity and decreases insulin resistance, to avoid metabolic disturbances and serious side effects such as fatal and non-fatal lactic acidosis caused by metformin (Salpeter et al., 2010). Today metformin is the most important compound used in the management of diabetes mellitus (Ruggiero-Lopez et al., 1999). Currently, it is often prescribed for obese or overweight patients, over 40 years of age, with type II diabetes (T2D). The American Diabetes Association and the European Association for the Study of Diabetes currently recommend metformin as the drug of choice when treating type II diabetes (Inzucchi et al., 2015). Since, six decades after the production of metformin, it remains the frequently prescribed oral medicine to treat T2D (Balducci et al., 2010). The number of metformin users in the UK increased from 55.4% to 83.6% from 2000 to 2013 in patients with T2D, (Sharma et al., 2016).

Glucose metabolism correlates with patient cognitive performance (Bohlken et al., 2018). Many studies suggest that individuals with altered insulin signalling, or with T2D, have a higher risk of cognitive decline compared with those who have a healthy metabolism (Carlsson, 2010, Osmanovic Barilar et al., 2015). Considerable research has been conducted into the relationship between the use of antihyperglycemic drugs and dementia risk. Researchers noticed a reduced dementia risk incidence in T2D patients who were using metformin (Hsu et al., 2011, Yang et al., 2019).

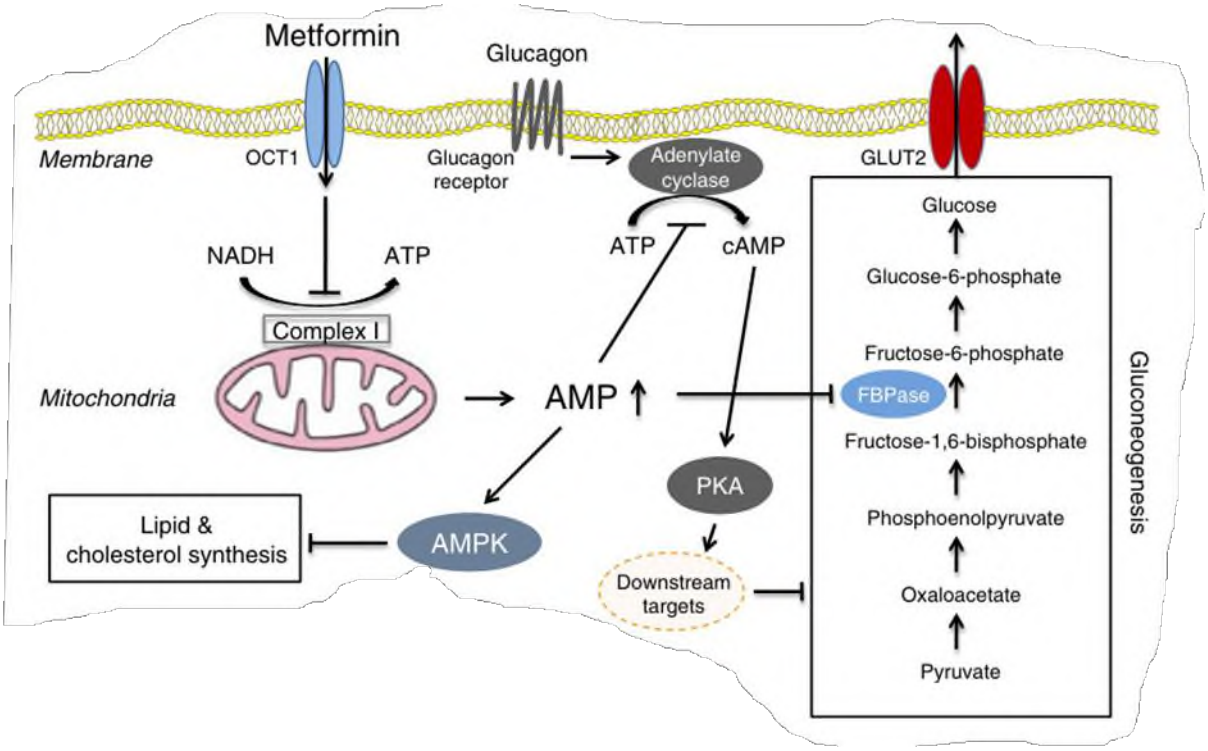

Figure 1.11: An illustration of metformin's anti-hyperglycaemic action on liver cells. Through organic cation transporter 1 (OCT1), metformin is transported from the portal vein into the liver cells (hepatocytes). In the liver cell, metformin inhibits mitochondrial respiration (complex I), resulting in reduced adenosine triphosphate (ATP) production and an increase in AMP levels that inhibit glucose synthesis by directly activating AMPK. By inhibiting the production of cyclic adenosine monophosphate (cAMP), a high AMP concentration is essential for suppressing adenylate cyclase, which in turn decreases the expression of gluconeogenic enzymes such as glucose-6-phosphatase and phosphoenolpyruvate carboxykinase. Based on these results, gluconeogenesis and lipid/cholesterol synthesis are inhibited (Rena et al., 2013).

1.6.1 Metformin and α-synuclein

Interestingly α-syn is upregulated in epilepsy and this was found to be reduced in a rodent model of epilepsy by treatment with metformin (Hussein et al., 2019). It is thought that metformin ameliorates oxidative damage, activates AMPK, inhibits mTOR, reduces apoptosis, and increases phagocytosis which removes abnormal α-syn. These processes lead to reduced seizure activity and improved cognitive function (Han et al., 2016). Several experimental models of epilepsy have been extensively evaluated using metformin, including Lafora disease, progressive myoclonus epilepsy, where metformin treatment delayed the onset of seizures, reduced the duration and frequency of seizures, and helped terminate seizures (Nandini et al., 2019). Recently, metformin was approved for use in patients with Lafora disease (Bisulli et al., 2019).

The metformin neuroprotective effects in PD pathogenesis present a novel promising therapeutic strategy that might improve the current PD and epilepsy

treatments available via inhibiting α-syn phosphorylation by AMPK/mTOR pathway and/or other pathways. In patients with PD, α-syn becomes increasingly phosphorylated at pS129. There are divergent effects of metformin and AMPK on α-syn phosphorylation. α-syn phosphorylation is mediated by multiple kinases, including AMPK. There is evidence that pS129 enhances macro autophagy clearance of aggregated α-syn, but at the same time, it may increase α-syn's toxicity as well. In summary, the pathological role of pS129 in PD is complex and may vary depending on the severity of the disease (Taymans and Baekelandt, 2014). Protein phosphatase 2A (PP2A) inhibits AMPK and dephosphorylates PS129. Therefore, α-syn may contribute to the regulation of AMPK. The potency of metformin's activation of PP2A independent of AMPK is higher than its activation of AMPK, at least *in vitro*, and this promotes dephosphorylation of pS129-α-syn (Curry et al., 2018, Taymans and Baekelandt, 2014).

1.6.2 Effect of Metformin in Neurodegenerative Diseases

Studies showed that metformin treatment reduced the cognitive decline risk among persons with diabetes (Tizazu et al., 2019, Isop et al., 2023). Kim et al. (2021) reported in their longitudinal study of 701,193 Korean patients with diabetes that dual oral therapy with metformin and thiazolidinedione (other anti-diabetic medication), lowered the risk of all types of dementia. Also, metformin improved the activation of AMPK in the prefrontal cortex and hippocampus of high-fat diet mice and enhanced neuronal health markers such as synaptophysin and brain-derived neurotrophic factor (Yang et al., 2019).

There are some contradictory/conflicting results of medical intervention of metformin studies, beyond just differences in treatment parameters and conditions e.g., dosage, duration of treatment, target population, the severity of the case, sex, and the polymorphism or genotype of the patient (Isop et al., 2023).

Although, as outlined above there is a reduced risk of developing AD in long-term users of metformin with diabetes, compared with other antidiabetic drugs (Imfeld et al., 2012),some studies have reported that metformin may also accelerate the pathogenesis of AD. This negative effect of metformin may be mediated by inducing amyloid-beta precursor protein (ABPP) processes and the accumulation of autophagosomes (Son et al., 2016).

Patients with neurological disorders of diverse types have benefited from metformin treatment. mTOR and AMPK signalling pathways are shared in both AD and T2D. This mechanistic link presents a good opportunity to use anti-diabetes drugs for therapeutic or prevention purposes against dementia and cognitive impairment (Karki and Hofmann-Apitius, 2017). However, the mechanisms of action of metformin and its neuroprotective role are still being investigated. In neurons, insulin regulates the metabolism of the Aβ precursor protein, which minimizes the accumulation of Aβ peptides that are pivotal to AD pathogenesis (Chen et al., 2009). Metformin reduces the biochemical changes in the brain of mouse models of AD according to Li et al., 2012 (Li et al., 2012). Metformin is also associated with improved learning, memory, and attention skills in a randomized placebo-controlled crossover study in subjects with mild cognitive impairment (Koenig et al., 2017) and a mouse model of AD (Farr et al., 2019).

Despite a great investment and notable interest from the pharmaceutical industry, no potential drug has been discovered yet that halts cognitive decline and dementia. Metformin could be beneficial in dementia for several reasons. Metformin can facilitate seizure termination and so could reduce the hyperexcitability that might worsen neurodegenerative disease progression (Yang et al., 2017). Although the mechanism of action of metformin in showing neuroprotection and cognitive improvement in models of epilepsy and AD is unclear, its potential to mitigate brain oxidative damage could explain its anti-epileptic effect (Nandini et al., 2019). Numerous pre-clinical studies have shown that, in addition to inhibition of mTOR, metformin could reduce oxidative stress, neuroinflammation, and apoptosis and activate AMPK (Hussein et al., 2019). Modulation of these processes could lead to reduced seizure activity and improved cognitive function in a range of conditions.

Furthermore, metformin has also been shown to improve mitochondrial function and reduce oxidative stress and it has been suggested that reducing the activity of hyperactive mitochondria early in PD could be beneficial (Mor et al., 2020). Metformin inhibits mitochondrial complex I activity (Hur and Lee, 2015). Hawley et al. (2002) attribute this inhibition to metformin-induced activation of AMPK directly. Metformin can partially inhibit mitochondrial complex I activity resulting in a reduction of intracellular adenosine triphosphate (ATP) levels (Zhou et al., 2001) and an increase in adenosine monophosphate (AMP) levels (Fig.1.12), as two molecules of (ADP) are converted into AMP and ATP by adenylate kinase (Dzeja and Terzic, 2009). It may

also help to reduce reactive oxygen species (ROS) by acting on complex I (Peralta et al., 2020).

Glucose utilization and uptake enhancement due to metformin is the reason for the onset delay in neuron-specific Ndufs3, a neuronal deficiency in complex I mouse models (Peralta et al., 2020). Mor et al. (2020) reported that hyperactive mitochondria resulting from dysfunctional-branched chain amino acid (BCAA) metabolism contribute the motor deficits in PD. They also suggested an early reduction of mitochondrial respiration by metformin has efficacious outcomes. Neuronal viability is improved by metformin's role in mitochondrial homeostasis. Neurons normally supply metabolic input to the citric acid cycle (TCA) cycle, a major pathway to produce energy in the mitochondria through the branched-chain amino acid transferase (BCAT-1). TCA cycle gene expression increases with reduced BCAT-1 expression, and steady-state levels of TCA cycle metabolites decrease, possibly due to greater turnover of the TCA cycle (Mor et al., 2020). As a result, mitochondrial respiration increases and reactive oxygen species-mediated damage occurs, resulting in neurodegeneration. Inhibition of complex I may restore mitochondrial homeostasis and viability in response to metformin treatment (Mor et al., 2020).

In addition to neuroprotective effects (Roganovic et al., 2019, Yang et al., 2017) metformin has multifaceted features e.g., rapid ability to cross BBB to reach several brain regions through a safe pharmacokinetic pathway which may exert a therapeutic drug for cognitive decline and dementia of neurodegenerative disorders (Łabuzek et al., 2010b, Takata et al., 2013, Kazkayasi et al., 2022). Overall, evidence of the promising impacts of metformin on neuroprotection/neurogenesis is increasing. Novel studies prove its ability to be beneficial in a wide range of neurological diseases including AD (Wang et al., 2019, Ou et al., 2021), PD (Curry et al., 2018), stroke (Gunn et al., 2018), schizophrenia (Wang et al., 2019), Huntington’s disease (HD) including epilepsy (Sanchis et al., 2019, Ma et al., 2007), and Lafora disease (Bisulli et al., 2019). For this reason, my project is interested in investigating the effect of metformin in the hA30P mice.

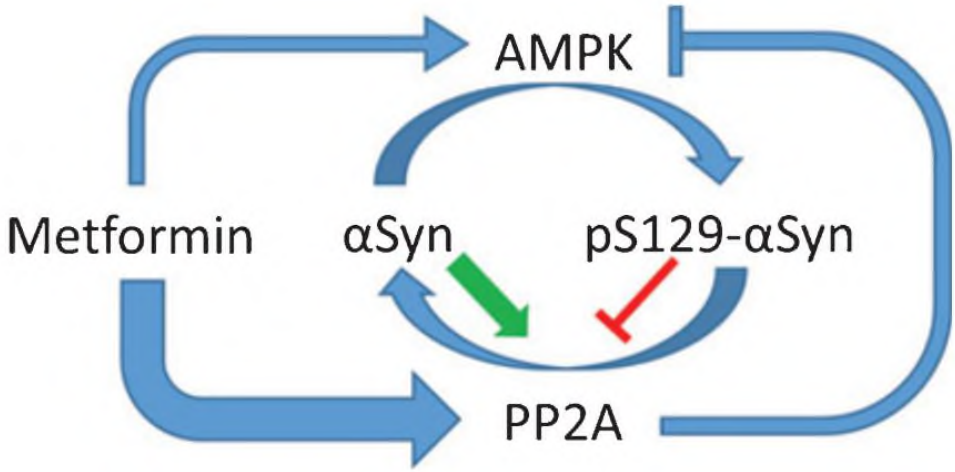

Figure 1.12. AMPK and metformin have distinct effects on the phosphorylation of α-syn S129. PP2A is activated by metformin via AMPK-independent mechanisms, with a greater potency than AMPK, at least in vitro, and, thus, pS129-Syn is dephosphorylated (Curry et al., 2018).

1.7 Nasal Route of Administration to Treat Brain Disease

Many facts have brought researchers' attention to the use of the nasal route of administration to treat brain diseases, such as the nasal route's contribution to causing neurological, neurodegenerative, and cancer diseases due to environmental pollution (Aleya and Uddin, 2020). Some drugs can have difficulty passing through the BBB and, as is the case for metformin, the amount of a drug that can reach the brain is limited due to extensive metabolism and excretion in the systemic circulation which results in an insufficient concentration of the drug that reaches the brain to produce an appropriate therapeutic effect (Pardridge, 2019, Pardridge, 2020).

Nasal delivery of drugs to the brain offers an effective method for preventing and treating brain disorders (Sun et al., 2018). Neurological diseases are effectively controlled by the local delivery of therapeutic drugs to the brain, which reduces the side effects in other tissues. Through the olfactory nerve system, the drug will be delivered noninvasively directly to the brain (Pardridge, 2020) (Fig. 1.13).

In the ethmoid bone, the cribriform plate holds the olfactory bulbs, and sensory neurons are located between the nasal cavity and the brain, which is responsible for directing CSF toward the brain (Sun et al., 2018). In addition, the olfactory neurons are physically connected from the nasal mucosa to the brain so drug delivery through the olfactory region can deliver drugs directly to the brain, without having to go through the systemic circulation (Bahadur et al., 2020). Drugs can be delivered through the

olfactory nerve within 1.5–6 h, and the olfactory epithelial cells within a few minutes (Shield, 2021).

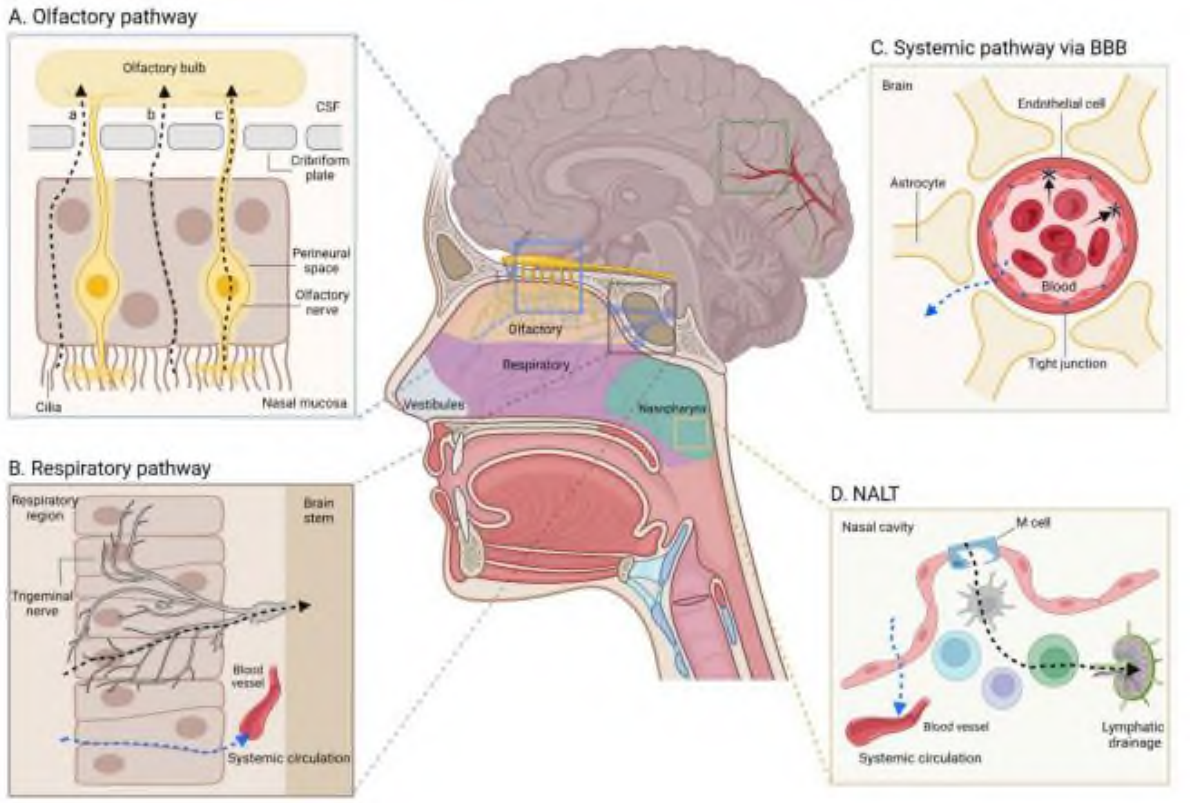

Figure 1.13: An illustration of the physiological systems involved in the delivery of drugs to the brain through the nose. **(A)** Nasal-brain drug delivery may occur through the olfactory pathway. **(B)** The respiratory pathway. **(C)** The systemic pathway through the BBB. **(D)** Through nasopharyngeal lymphoid tissue (NALT). In the nasopharynx, lymphoid tissue is associated with the BBB and the blood-nasopharynx barrier. Olfactory epithelial cells are represented by a and c in A, while olfactory nerve pathways are represented by d. In A, B, and D, black dotted arrows indicate direct routes from the nasal cavity to the brain for drug delivery. Blue dots indicate indirect drug delivery pathways between the nasal cavity and the brain in B–D (Jeong et al., 2023).

Several routes are available for directly delivering drugs into the olfactory region, including:

- Endocytosis and simple diffusion.
- Paracellular methods in intercellular junctions in the olfactory epithelium.
- The intraneuronal pathway in the olfactory nerve.

Naloxone and zolmitriptan are two examples of drugs that can pass through the respiratory epithelium and overcome mucociliary clearance. These drugs can be absorbed into the small blood vessels within the *lamina propria*, where they avoid the first-pass metabolism that occurs with oral agents. However, they still need to pass

through the BBB from the systemic circulation (Ghadiri et al., 2019). Along with a large number of tiny blood arteries, the *lamina propria* of the respiratory epithelium has a high surface area of trigeminal neuron branches, which together provide a significant perineuronal and perivascular channel for medicines to enter the brain (Lochhead and Thorne, 2012, Ross et al., 2004, Thorne et al., 2004, Lochhead et al., 2015).

Thus, the nasal-brain administration route reduces the clinically required doses of drugs while maintaining therapeutic drug concentrations in the brain. Drug absorption rates via the nasal route were like those of intravenous injections (Rejman et al., 2004, Ugwoke et al., 2001, Yates et al., 2002). Generally, there are four applicable formulations for nasal brain delivery. Usually, intranasal solutions are delivered as nasal sprays, but drops can also be used, although the clearance rate from the nasal cavity is faster than that of nasal sprays (Hardy et al., 1985). For example, Diazepam (for sedation and seizure stabilization) is much more bioavailable when administered intranasally than when administered orally or rectally (Hogan et al., 2020).

Although it is still unclear how the nasal-brain pathway exactly works, and there has been insufficient systematization of related information, the nasal-brain route has been proposed as an efficient alternative for drug delivery, and studies have reported continuous success when drugs are delivered through the nasal cavity to the brain (Jeong et al., 2023). So, I decided to use the intranasal route to administer metformin drug to mice in this study to investigate its potential anti-inflammation/neuroprotection role.

Chapter 2

General Methods

2.1 Animal provision

All procedures were performed following the UK Animals (Scientific Procedures) Act 1986 and the EU Directive 2010/63/EU and with the appropriate project license and protocol selection. Same-sex groups of no more than six mice were maintained in 12-hour light/dark cycles with access to food and water *ad libitum*. Whenever possible, animals were not left alone for longer than 24 hours.

(Thy-1)-human h[A30P] α-SYN mice on a C57BL/6 background (henceforth referred to as hA30P mice) were provided by Prof. Philipp Kahle (University of Tübingen, Germany) (K

ahle et al., 2000), and a colony was established at Newcastle University's Comparative Biology Centre (CBC). To refresh every few generations homozygous mice were crossed with C57BL/6 mice bought in from Charles River (Tranent, UK). Immediately following weaning (21 days), the first generation of mice were all heterozygous and were ear-notched and genotyped to obtain a hA30P signal level (Transnetyx, USA). Heterozygous mice from different breeding pairs were then crossed to produce litters containing either wild type, homozygous hA30P, or heterozygous mice. Further genotyping was conducted to determine which mice were homozygous and these were subsequently crossed with hA30P mice from different breeding pairs to establish the hA30P homozygous line. The first litters from each homozygous hA30P line were further genotyped to confirm genotype was correct. Heterozygous mice were used for preliminary immunofluorescence (IF) staining. WT and hA30P lines were maintained separately, with the potential to cross again as needed.

Because I am interested in the characterization of the prodromal stage of α-synucleinopathy in hA30P mice, all mice used in this thesis were between 3 weeks and 4 months of age, with groups at 1 month and 2-4 months being studied. C57BL/6 background mice were bought from outside vendors (Charles River) but were also later established as an in-house WT breeding colony in the CBC at Newcastle University according to ARRIVE guidelines. Male and female mice were used as detailed in subsequent sections.

2.2 Euthanasia and transcardial perfusion of animals with fixative

Mice were first given a small dose of the volatile anaesthetic isoflurane (IsoFlo 100%, Zoetis, UK), which was then followed by the administration of 100 mg/kg of ketamine (Narketan®-10, 100 mg/ml, Vetoquinol, UK) combined with 10 mg/kg of xylazine (Xylacare 20 mg/ml, Animal Care, UK). All major reflexes (eye blinking, pedal withdrawal, righting reflex, and tail withdrawal) were examined to make sure there was no neurological reaction before procedures commenced. When all reflexes were abolished transcardial perfusion was then performed by excising the rib cage through an abdominal incision to access the heart. The left ventricle was punctured with a needle, attached to a 30 ml syringe, and filled with 0.9% NaCl saline while the right atrium was cut to allow blood to flow out of the heart. The flush with solution followed by perfusion with buffered 4% paraformaldehyde (4% PFA) solution **(Thermoscientific, USA)** for transcardial perfusion with fixative. The brain was then removed from the skull, the olfactory bulbs and hindbrain were trimmed off and the brains were stored overnight in 4% PFA solution in the fridge. The following day the 4% PFA solution was replaced with a cryopreservant solution (Table 2.1) until the brain sank (usually after 24 hours). The brains were then frozen and stored at -20°C until use. After brain dissection, each perfusion's effectiveness was evaluated; perfusion was considered successful if there was a movement in the limbs and tail, the body was stiff, and the brain was white and clear of blood.

2.3 Slice preparation and ink method for sub-region identification

Brain sections were prepared by trimming the prefrontal cortex and cerebellum coronally off from the PFA-fixed brain, then cutting the remaining part of the cerebrum down from the midline sagittally into two halves. I spared the left hemisphere and used the posterior part of the right hemisphere which contains the hippocampus. The rest of the cerebrum was returned to the cryopreservant solution (Table 2.1) and kept in the fridge for at least one night before being transferred to the freezer at -20º C.

The posterior part of the hemisphere, containing the hippocampus, was kept in 30% sucrose in 0.1M phosphate buffer saline (PBS) solution (Table 2.1) in the fridge at least overnight before the sectioning process.

Table 2.1: Buffers used for the immunofluorescence staining

Solution	Substances	Concentration
Normal Saline	NaCl	0.87%
1X PBS pH 7.3 at 25º C	NaCl KCl Na_2HPO_4 KH_2KPO_4	137 mM 2.7 mM 10 mM 1.8 mM
Cryopreserving	Glycerol Ethylene 0.3% PBS	30% 30% 20%
Blocking buffer	Donkey serum Triton-X 100 PBS	3% 0.3% 1X

The dorsal, ventral, and intermediate hippocampus share the same morphological shape but have functional and structural distinctions (Bear et al., 2020, Kosaka et al., 1987). To select the correct sections of the region of interest (ROI) which is the CA3 region of the intermediate hippocampus in this study, I designed a method of using ink to identify sub-regions (Fig. 2.1). The ink method depends on using two 24-well plates. In one I collect sections for later IF staining and in the other sections are stained with ink. 35 µm-thick sections were cut horizontally from the posterior part of the hemisphere starting from the ventral side toward the dorsal side, using a freezing stage microtome (Bright Instruments; UK). Four sections were collected in 500 µl of 0.1M PBS for IF in the first well (A1) of the 24-well plate, while the 5th section was put into the first well (A1) of the second 24-well plate for ink staining

which contains 290 µl of 0.1M PBS in every well (Fig. 2.1). This was repeated until the entire ROI of the hippocampus was cut.

After completing the sectioning/collection, I added 10 µl of ink (cartridges blue WH Smith) to every well of the second plate (that means the dilution factor of the ink

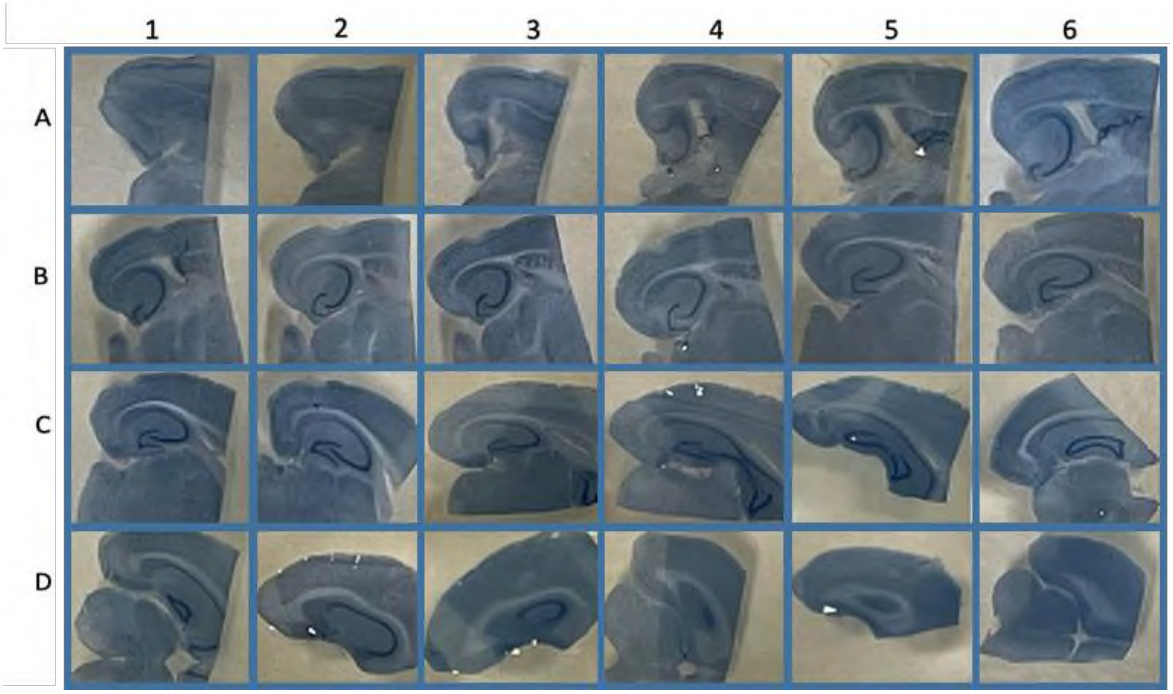

Figure 2.1: Ink Method for Sub-region Identification (Horizontal sectioning of the brain of 3-month-old mouse). The coloured horizontal sections of the hippocampus were in a 24-well plate of diluted ink 1:30 after 5 minutes of shaking. The sectioning started from the ventral to dorsal regions of the hippocampus by collecting 4 sections each time into well A1 the original plate and the fifth section into well A1 of a second ink plate. This was repeated A2-D6 until the whole hippocampus had been sectioned.

was 1:30). The ink plate was then placed on a shaker for at least 5 minutes. Each section becomes coloured with stronger blue staining for the cell-dense regions, such as the pyramidal neurons layer and dentate gyrus, and light blue colour in the rest region of the tissue section. This enabled me to easily visualize the correct hippocampal sections rapidly and easily from the corresponding well plate numbers. This pattern of staining enabled easy recognition of the laminar and sub-regional structure of the hippocampus of ROI to choose from. The ink-coloured sections gave a clear structural view of the tissue section in every well of the inked plate for the corresponding sections in the original well plate. For example, wells B5-C2 in the ink plate in Fig. 2.1 represent the optimal ROI I am interested in (Fig. 2.2, and 2.3), so I used the sections in any sections from these wells (B5-C2) of the original plate for IF staining. I replaced the 0.1M PBS in wells that contain unused optimal ROI sections in

the original plate with 500 µl cryopreservant solution and kept the plate in the freezer at -20º C, until further use.

The ink method provides many sections from each hippocampus and enables the researcher to select the ROI easily. Ultimately it helps to reduce the number of used mice in an experiment and that will be compatible with the 3Rs of the UK Animals (Scientific Procedures) Act 1986 and the EU Directive 2010/63/EU. Furthermore, the ink method for sub-region identification can be used to determine any ROI/sub-ROI of the brain, for example, Fig. 2.3 shows the coronal sectioning of a 3-month-old mouse brain.

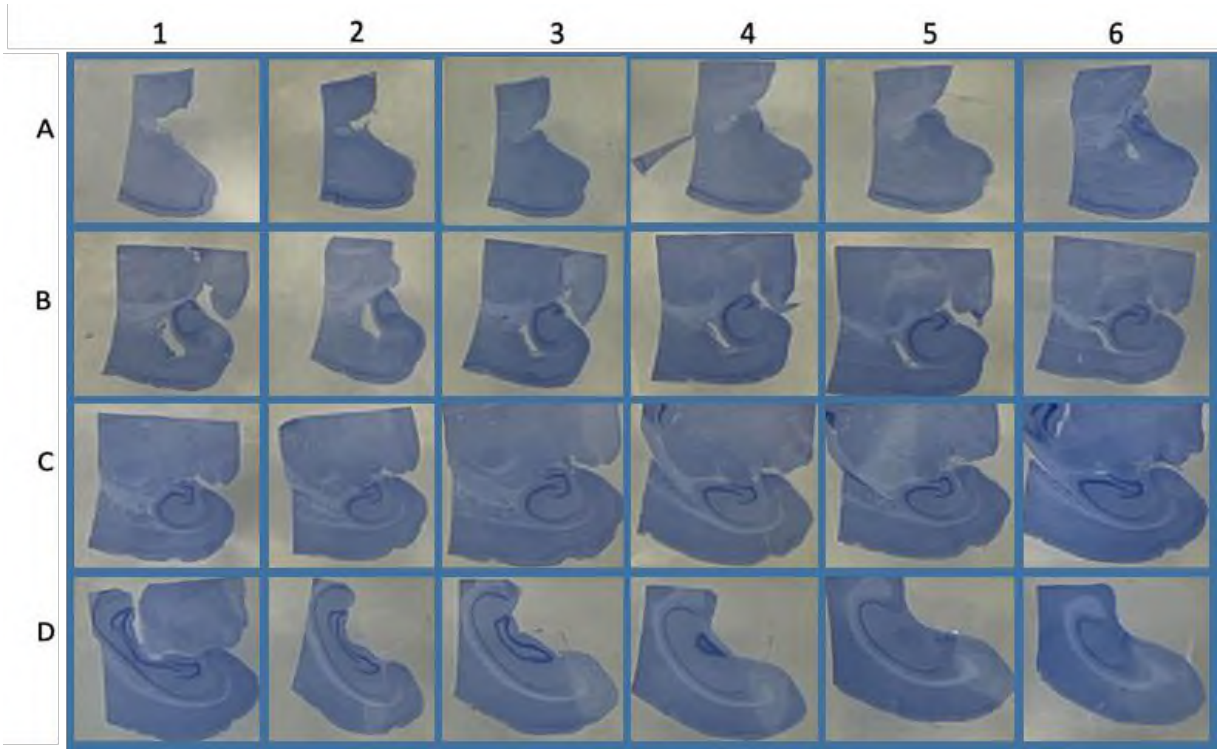

Figure 2.2: Ink Method for Sub-region Identification (Horizontal sectioning in the brain of 1-month-old mouse). The optimal ROI represented by the wells C3-C5 only, because the brain was smaller in the size compared to Fig. 2.1.

2.4 Immunofluorescence in free-floating

After selecting the sections that contained the ROI to stain, three x 10-minute washes in 0.1 M PBS were performed. Sections were then blocked for 3-6 hours at room temperature on a vibrating shaker (mini orbital shaker-Stuart®) using a blocking buffer solution (Table 2.2).

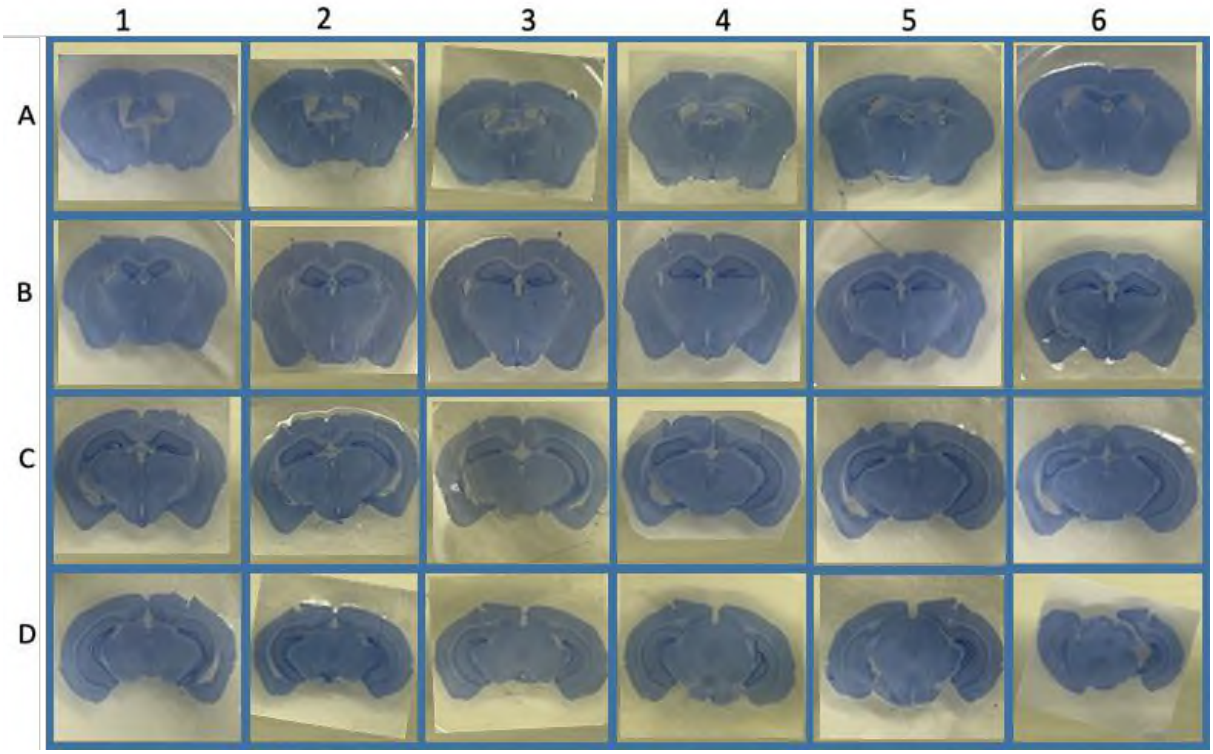

Figure 2.3: Ink Method for Sub-region Identification (Coronal sectioning in the brain of 2-month-old mouse). The coloured coronal sections of the hippocampus were in a 24-well plate of diluted ink (1:30) after 5 minutes of shaking. The sectioning started from the anterior to posterior direction by collecting 3 sections each time starting in well A1.

Depending on the secondary antibodies to be used, donkey serum was added. Because all the secondary antibodies I used in my study were hosted in donkeys. I used normal donkey serum Abcam (cat. No. Normal Donkey Serum ab7475) for the blocking step.

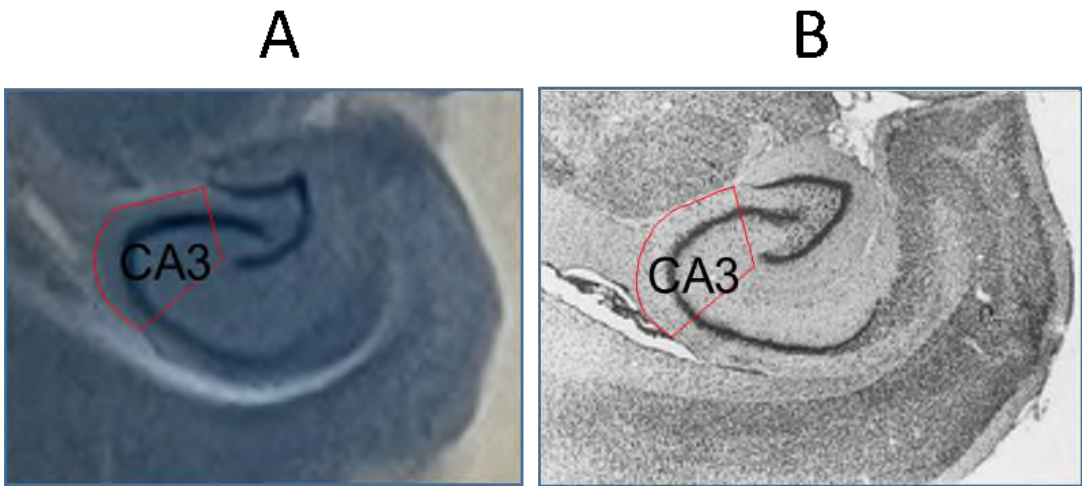

Figure 2.4: Optimal Sections of the Intermediate Hippocampus. A horizontal section in the intermediate hippocampus identified by ink method (A) and corresponding image from the anatomy atlas of mice brain, show CA3 region (B).

For incubating sections in primary antibodies, 0.1 M PBS solution containing 4% serum, and 0.3% Triton X-100 solution was used. The sections were incubated at 4 °C overnight (18–20 hours) on a rotating platform (IKA® ROCKER 3D digital), at no more than 250 rpm, with the blocking buffer from each well-being swapped out for a primary antibody solution (Table 2.2). The following morning, sections were exposed to three 10-minute washes in 0.1 M PBS, followed by the application of the Alexa Fluor-conjugated secondary antibodies corresponding to the immuno-type of the primary antibodies applied (Table 2.3) and a 2-3 hour incubation period at room temperature. To find the suitable concentration of the primary and secondary antibodies, I tested different concentrations (corresponded to positive and negative controls) and compared their images, then chose the lowest concentration that gave the best staining (Table 2.2 and 2.3).

Table 2.2: Primary antibodies used in IF staining

Antibody	Definition	Host	Company code	RRID	Optimal Dilution (v: v)
α-syn	α -synuclein	Rat	Enzo Life Science, Exeter, UK (15G7) ALX-804-258	AB 2050691	1:250
GFAP	Glial fibrillary acidic protein	Rabbit IgG	Dako, Ely, UK Z0334	AB 10013382	1:2000
Iba1	The ionized calcium-binding adapter molecule 1	Goat	Abcam, Cambridge, UK Ab5076	AB 222402	1:2000

Anti-PV	A calcium-binding protein used in a subset of GABAergic interneuron	Mouse	Sigma-Aldrich, USA SAB4200545	AB 23369638	1:1000
NeuN	Neuronal nuclear antigen	Mouse	Abcam, Cambridge, UK ab104224	AB 2732785	1:1000
c-Fos	A surrogate marker to stain immediate early genes (IEGs)	Rabbit	Abcam, Cambridge, UK [EPR21930-238] ab222699	AB 2891049	1:500
WAF	Biotinylated Wisteria Floribunda Lectin	Wisteria floribunda (plant)	Vector Laboratories, UK (B-1355-2)	AB 2077569	1:500
iNOS	Inducible nitric oxide - Inflammation-induced enzyme that produces nitric oxide	Rabbit	Abcam, Cambridge, UK ab283655	AB 3083470	1:200

All the next steps were performed while sections were protected from light to avoid the bleaching of the secondary antibodies. The sections underwent the final three 10-minute washes in 0.1 M PBS and were transferred from the 24-well plate onto gelatine-coated standard glass slides. Once the transferred sections had dried, they

were mounted in Fluoromount-G mounting media with DAPITM (4´, 6-diamide-2-phenylindole) Abcam (catalog. ab104139), which is an aqueous anti-fade mounting medium used to preserve fluorescence when imaging tissues. Its formulation prevents rapid photo-bleaching, and it also contains DAPI to stain the cell nuclei, to quantify cell number and distribution. The sections were then covered with 22 x 50 mm, 0.13-0.17 mm coverslips (avoiding air bubbles). The slides were left at room temperature to dry fully while protected from light and then subsequently stored at 4° C before imaging.

Table 2.3: Secondary antibodies used in IF staining

Secondary Antibody	Manufacturer and Catalog No.	Dilution (v: v)
donkey anti-rabbit IgG, Alexa Fluor 594 nm	ThermoFisher Scientific A-21207	1:1000
donkey anti-goat IgG, Alexa Fluor 488 nm	Abcam Ab150133	1:1000
donkey anti-mouse IgG, Alexa Fluor 488 nm	Invitrogen	1:1000
donkey anti-mouse IgG, Alexa Fluor 568 nm	Invitrogen A10037	1:1000
donkey anti-rat IgG, Alexa Fluor 594 nm	Invitrogen A-21209	1:1000
Texas Red Fluorescein streptavidin, Alexa Fluor 498 nm	VECTOR SA-5006	1:100

2.5 Imaging and data analysis by the Fiji program

In this thesis, all the stained sections were imaged using an upright Nikon Eclipse Ni-E fluorescent microscope equipped with an Andor Zyla 5.2 camera and the Nikon Elements software, except for the images that show the astrocytes and microglia morphology where they were imaged using the Nikon A1 upright laser scanning confocal microscope with Nikon CFI Plan Apo 40x/0.95 NA Air MRD00405 lens, and excited 3 channels with laser lines 405, 488 and 561 nm. The sections were imaged at 10x, 20x, and 100x magnification, keeping exposure settings consistent across filters and conditions. For quantifying iNOS staining with microglia, z-stacks were taken on the Ni-E fluorescent microscope at 20x magnification with a 5 µm step size. For the images that were taken as z-stacks, I compressed only the best four sequenced z-stacks before I started with further analysis. I used the Fiji software program to do a densitometric analysis of the images. Initially, images were cropped to the CA3 hippocampal region using a freehand drawing tool. By converting the images to binary using a threshold value, fluorescence was enhanced, and the noise was reduced.

2.5.1 Quantification of Human-α-syn Protein Expression

The integrated density (Int.Den.) value of fluorescence due to immunoreactivity for human-α-syn reflects the amount of human-α-syn protein expressed in the CA3 region of the hippocampus in WT and hA30P mice sections (ROI) and was analysed using the Fiji program (Fig. 2.5).

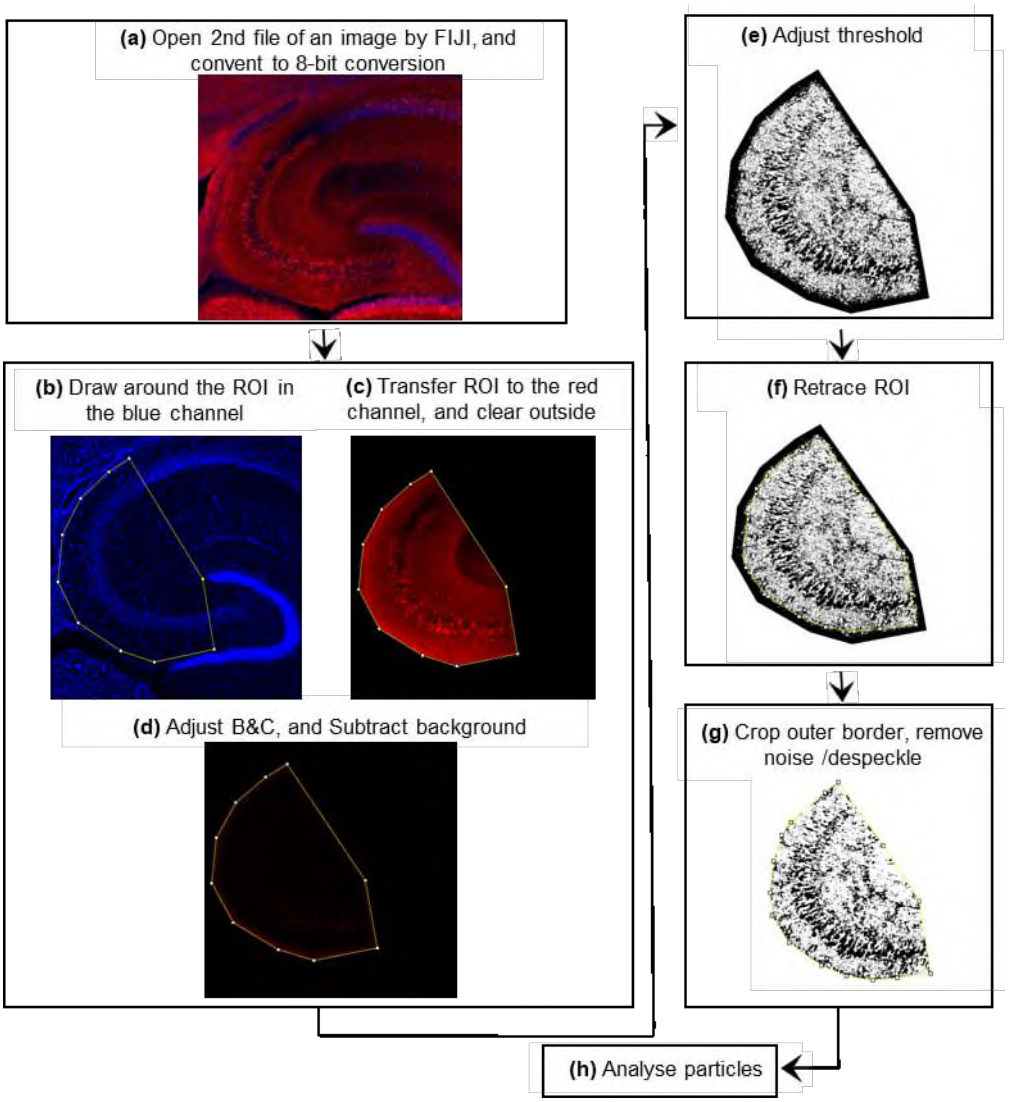

Figure 2.5: A pipeline of densitometric image analysis steps conducted by the Fiji program for human-α-syn. (a) the image was acquired by Nikon NiE fluorescent microscope and the file was opened in Fiji to display all the channels imaged. **(b)** The image was pre-processed, in the blue (DAPI) channel and I defined the ROI of CA3 by drawing the polygon. **(c)** Drawing of the ROI was transferred from the blue to the red channel and cropped. **(d)** Brightness and contrast (B&C) were adjusted, and the background was subtracted (Rolling ball radius). **(e)** The image was then thresholded and converted to a binary (black and white colours) and masked to prepare for analysis. **(f)** The ROI was retraced for post-thresholding processing. **(g)** The outer border was cropped, and then noise / despeckle was removed. **(h)** Set measurement was analyse particles, producing a measurement of the Int.Den. of human-α-syn.

2.5.2 Quantification of c-Fos Protein Expression

To quantify changes in c-Fos expression in ROI in WT and hA30P mice, sections were immunostained for c-Fos. Using Fiji, I counted the nuclei that stained red in the CA3 region of the hippocampus. I use the term c-Fos+ nuclei/mm2 to refer to this counting value, as Fig.6 shows.

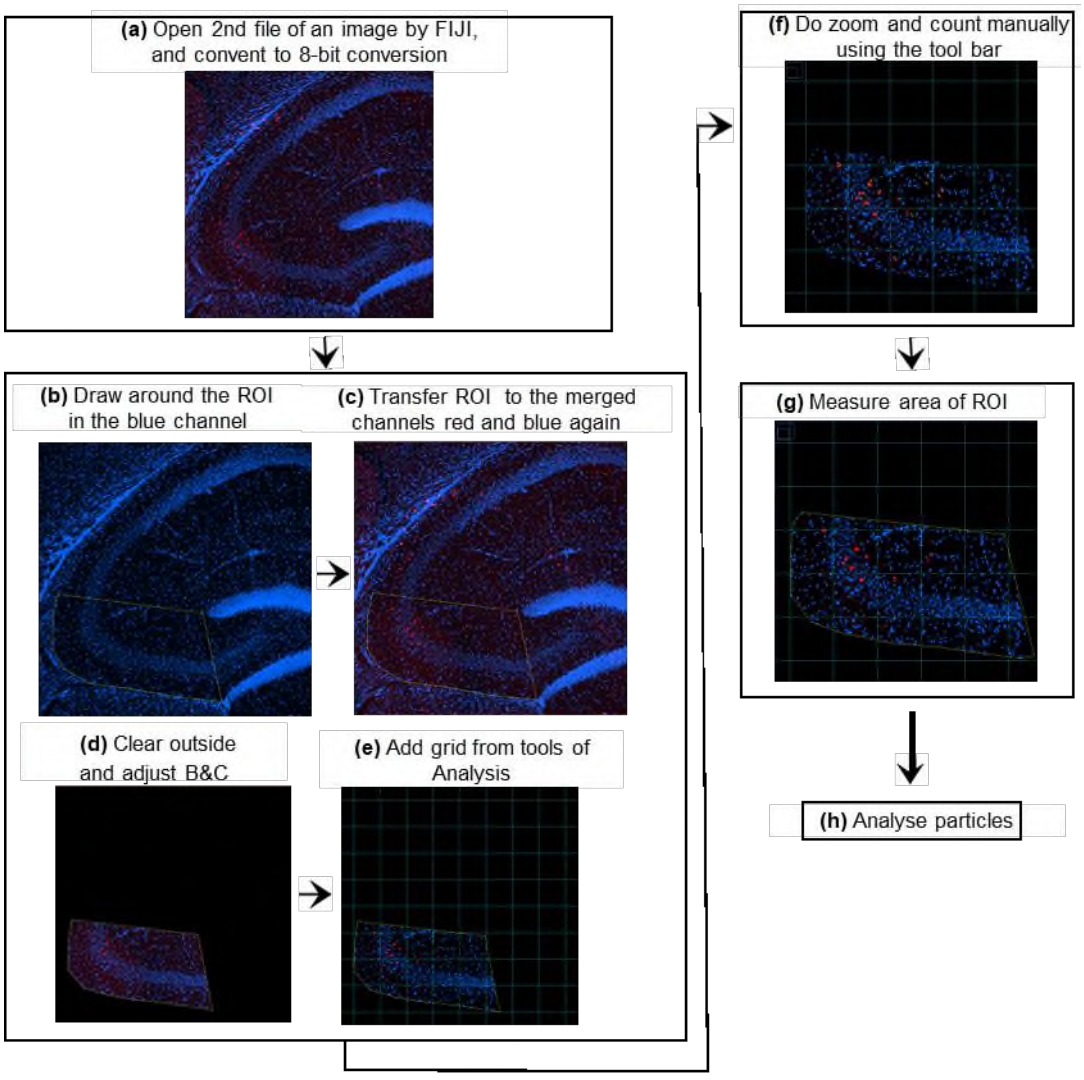

Figure 2.6: A pipeline of densitometric image analysis steps conducted by the Fiji program for c-Fos. (a) The image was acquired by Nikon NiE fluorescent microscope and the file was opened in Fiji to display all channels imaged. **(b)** The image was pre-processed, in the blue (DAPI) channel, and the CA3 was drawn by the polygon. **(c)** The drawing of the ROI was transferred from the blue to the merged channels red and blue again. **(d)** I cropped the outside and adjusted brightness and contrast. **(e)** I added a grid from Tools of Analysis to facilitate manual count. **(f)** I zoomed in and counted manually using the toolbar. **(g)** I measured the area of ROI. **(h)** Then I divided the count of c-Fos+ nuclei by the area of ROI.

2.5.3 Quantification of Neuron Expression

I immunostained neurons for NeuN, and then I quantified the % area occupied by NeuN+ immunofluorescence in the ROI in WT and hA30P mouse sections by the Fiji program as Fig.7 shows.

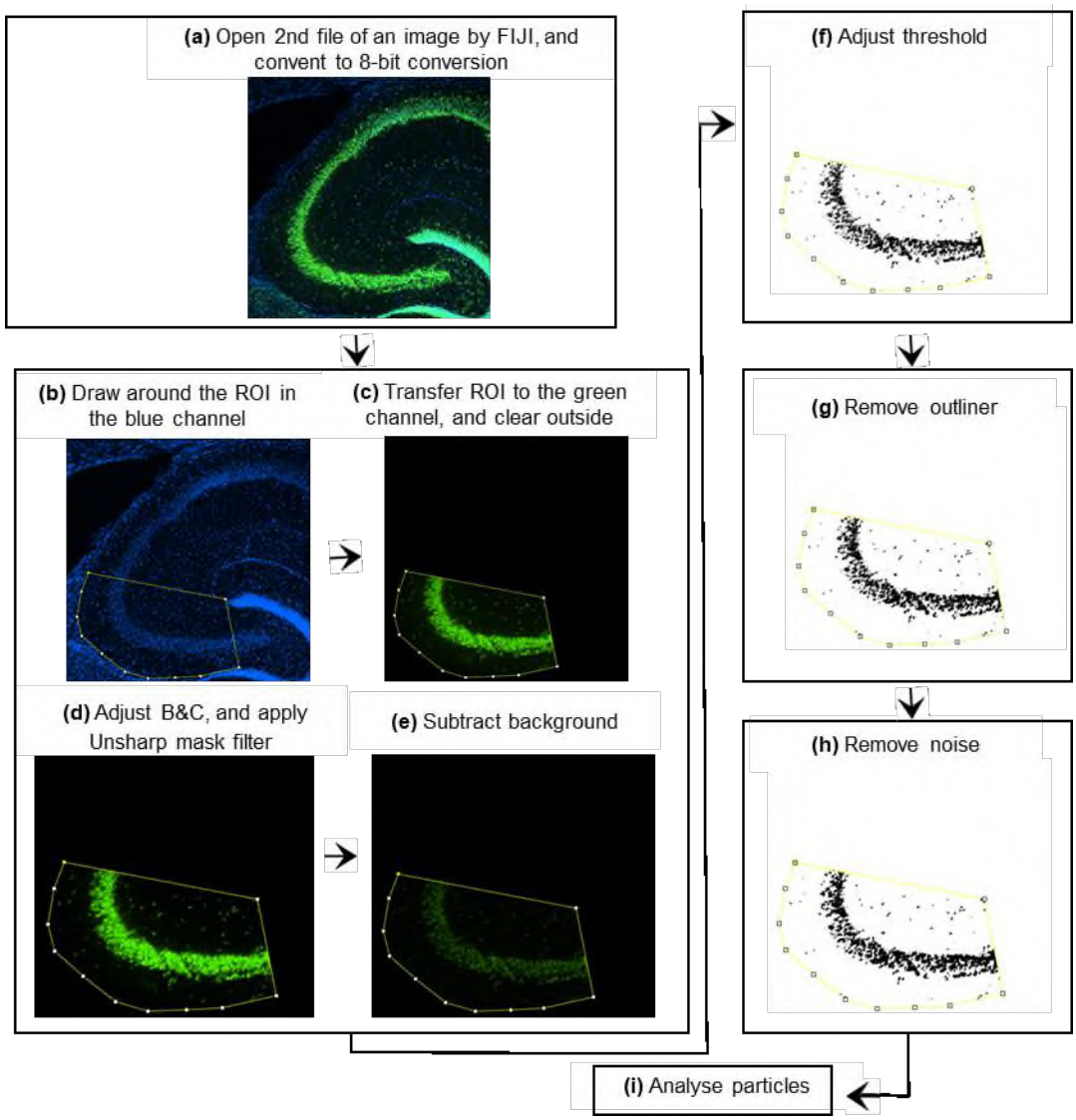

Figure 2.7: A pipeline of densitometric image analysis steps conducted by the Fiji program for Neu-N. (a) The image was acquired by Nikon NiE fluorescent microscope and the file was opened in Fiji to display all channels imaged. **(b)** The image was pre-processed. CA3 was drawn by a polygon in the blue (DAPI) channel drawing. **(c)** The drawing of the ROI was transferred from the blue to the green channel and cropped outside. **(d)** Brightness and contrast were adjusted, and the image was sharpened. **(e)** The background was removed. **(f)** The image was thresholded and converted to a binary mask to prepare for analysis. **(g)** Post-thresholding processing was conducted to remove the outliner. **(h)** I removed the noise and cropped the outer border. **(i)** I set measurements and then analysed particles, producing a measurement of the % area occupied by neurons.

2.5.4 Quantification of PV Interneurons Expression

To quantify changes in PV interneurons expression in the ROI in WT and hA30P mice, sections were immunostained for PV and by using Fiji I measured % the area occupied by PV immunofluorescence including cell bodies and neuropil, as Fig.8 shows.

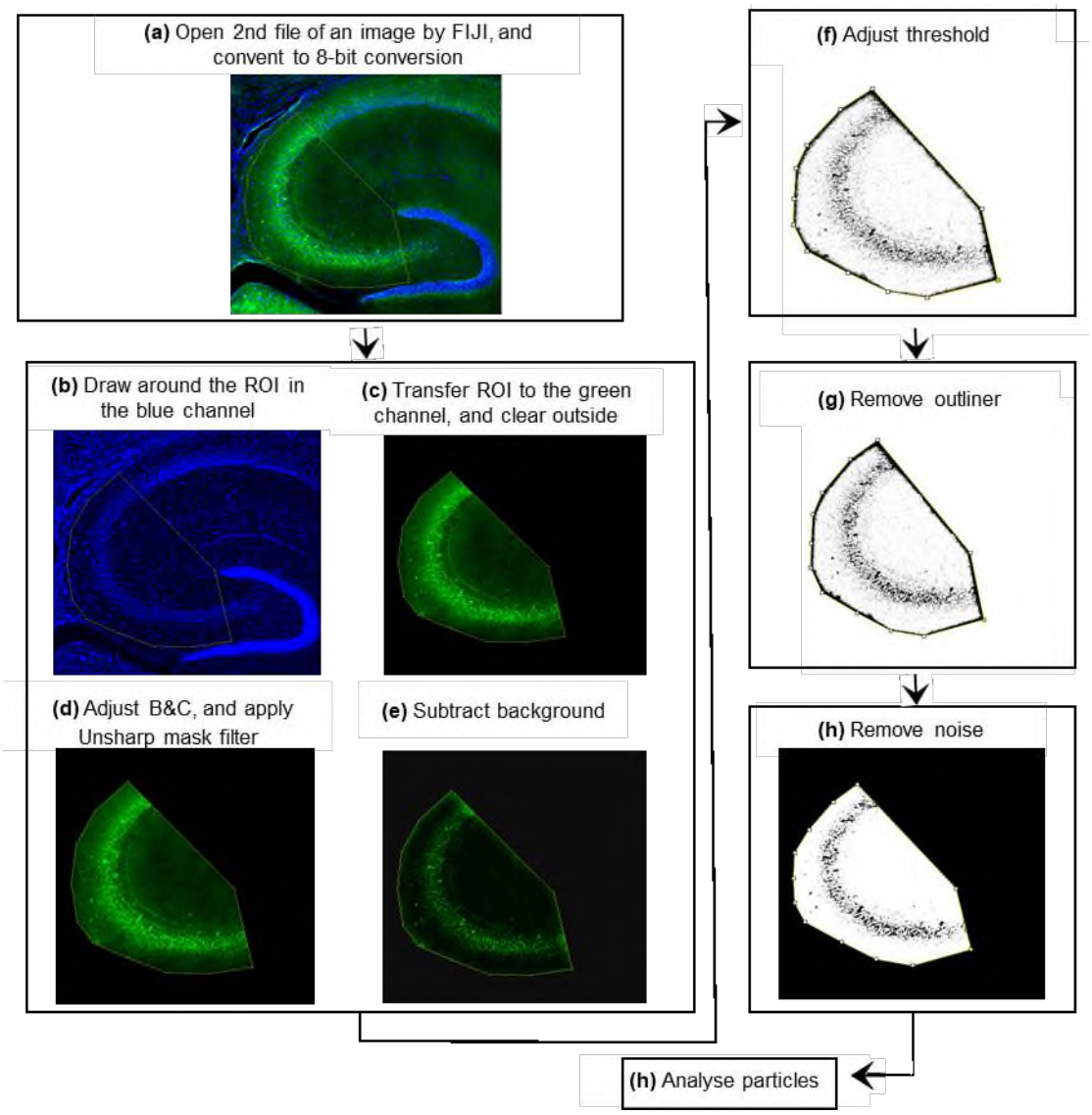

Figure 2.8: A pipeline of densitometric image analysis steps conducted by the Fiji program for PV interneurons. (a) The image was acquired by Nikon NiE fluorescent microscope and the file was opened in Fiji to display all channels imaged. **(b)** The image was pre-processed. The CA3 was drawn by the polygon in the blue (DAPI) channel **(c)** The drawing of the ROI was transferred from the blue to the green channel and cropped outside. **(d)** Brightness and contrast were adjusted, and the image was sharpened. **(e)** The background was removed. **(f)** The image was thresholded and converted to a binary mask to prepare for analysis. **(g)** Post-thresholding processing was conducted to remove the outliner. **(h)** I removed the noise and cropped the outer border. **(i)** I set measurements and then analysed particles to produce the % area occupied by PV.

2.5.5 Quantification of Reactive Astrocyte Expression

To quantify reactive astrocyte expression in the ROI in WT and hA30P mice, sections were immunostained for GFAP. Using Fiji, I measured the % area occupied by reactive astrocytes including cell bodies and processes, as Fig.9 shows.

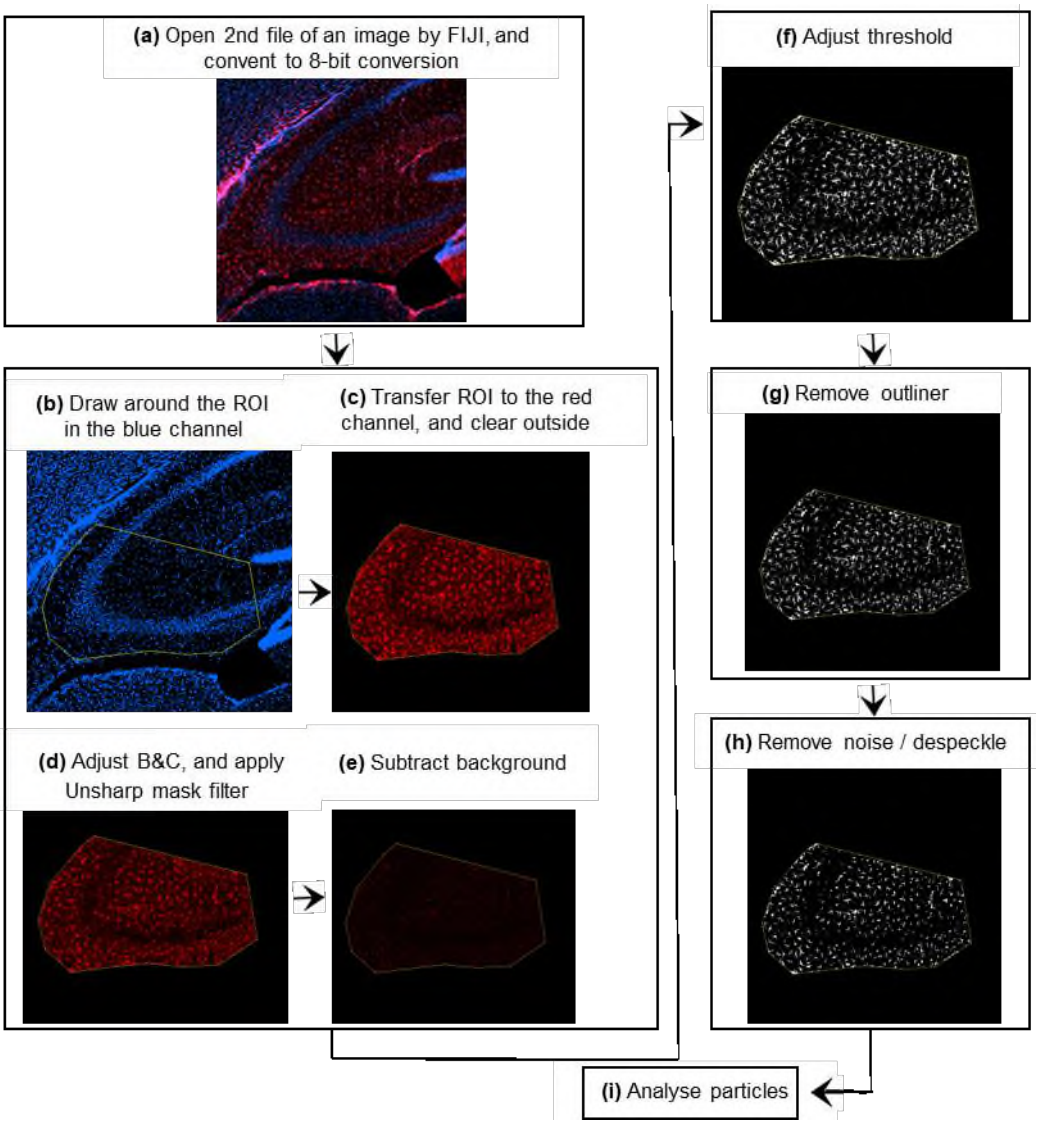

Figure 2.9: A pipeline of densitometric image analysis steps conducted by the Fiji program for reactive astrocytes. (a) Image acquired by Nikon NiE fluorescent microscope and the file is opened in Fiji to display all channels imaged. **(b)** The image is pre-processed, in the blue (DAPI) channel draw CA3 by the polygon. **(c)** The drawing of the ROI has been transferred from the blue to the red channel and cropped outside. **(d)** Brightness and contrast are adjusted, and the image is sharpened. **(e)** The background is removed. **(f)** The image is thresholded and converted to a binary mask to prepare for analysis. **(g)** Post-thresholding processing is conducted to remove the outliner. **(h)** Remove noise and crop the outer border. **(i)** Set measurement then I analysed the particles, producing a measurement of the % area occupied by GFAP.

2.5.6 Quantification of Microglia

I quantified changes in microglia in the ROI in WT and hA30P mice, by immunostaining the sections for Iba-1 and by using Fiji I measured % the area occupied by microglia and their processes, as Fig.10 shows.

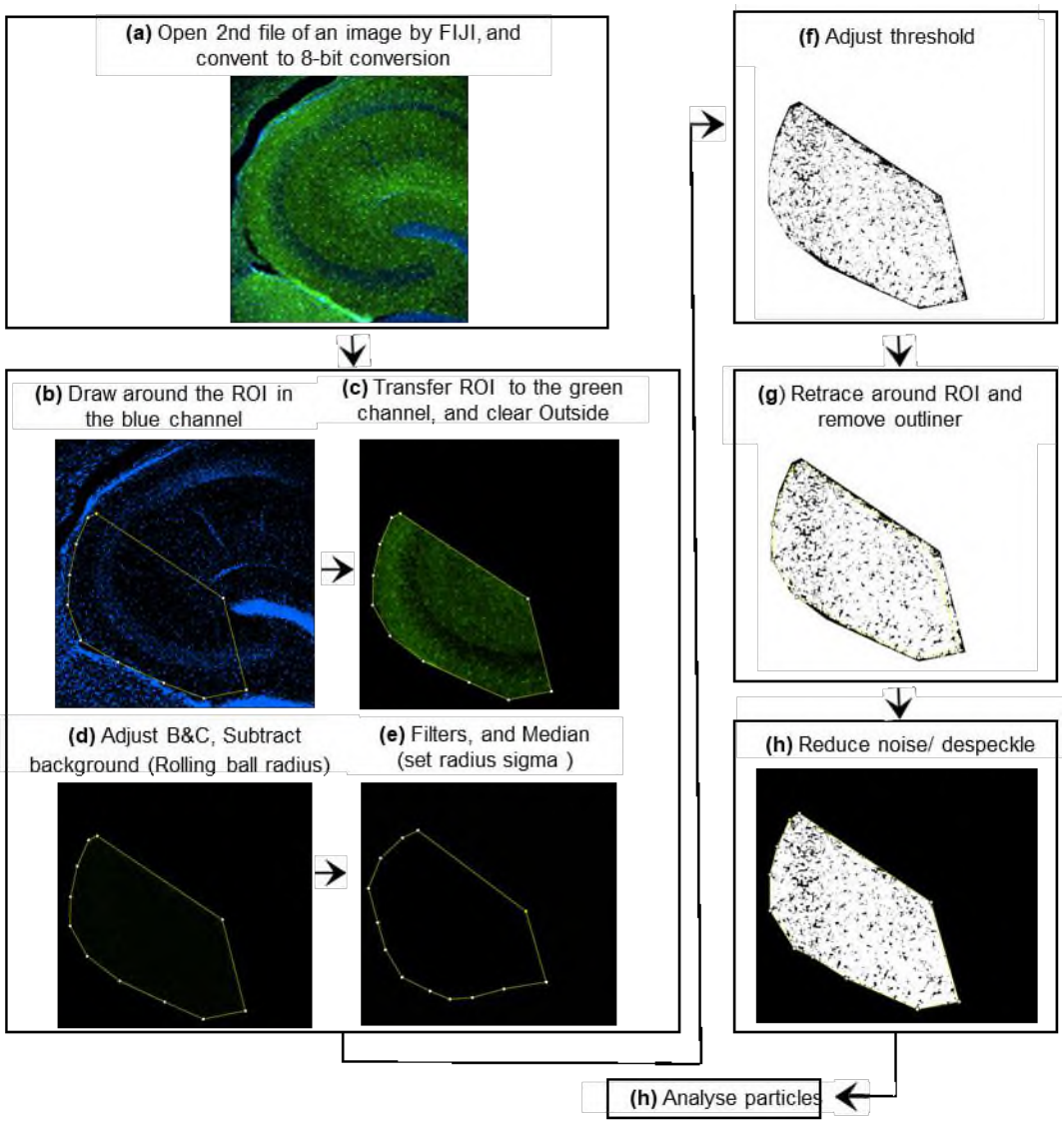

Figure 2.10: A pipeline of densitometric image analysis steps conducted by the Fiji program for microglia. (a) The image was acquired by Nikon NiE fluorescent microscope and the file was opened in Fiji to display all channels imaged. **(b)** The image was pre-processed, and the CA3 was drawn by polygon in the blue (DAPI) channel **(c)** The drawing of the ROI was transferred from the blue to the green channel and cropped outside. **(d)** Brightness, contrast filters, and median (set radius sigma) were adjusted, and **(e)** the background was removed and sliding paraboloid was chosen **(f)** the image was thresholded and converted to a binary mask to prepare for analysis. **(g)** ROI was retraced and the outliner around was removed, then post-thresholding processing was conducted. **(h)** The outer border was cropped. Noise / despeckle was removed and then closed to fill any gaps within cells. **(i)** I set measurements and analysed particles to produce a measurement of the % area occupied by microglia.

2.5.7 Quantification of Iba-1 with iNOS expression

To quantify changes in iNOS protein expression with reactive microglia in ROI in WT and hA30P mice, sections were immunostained for iNOS (red), and ba-1 (green). Using Fiji, I counted Iba-1 with and without iNOS immunoreactivity, as Fig.11 shows.

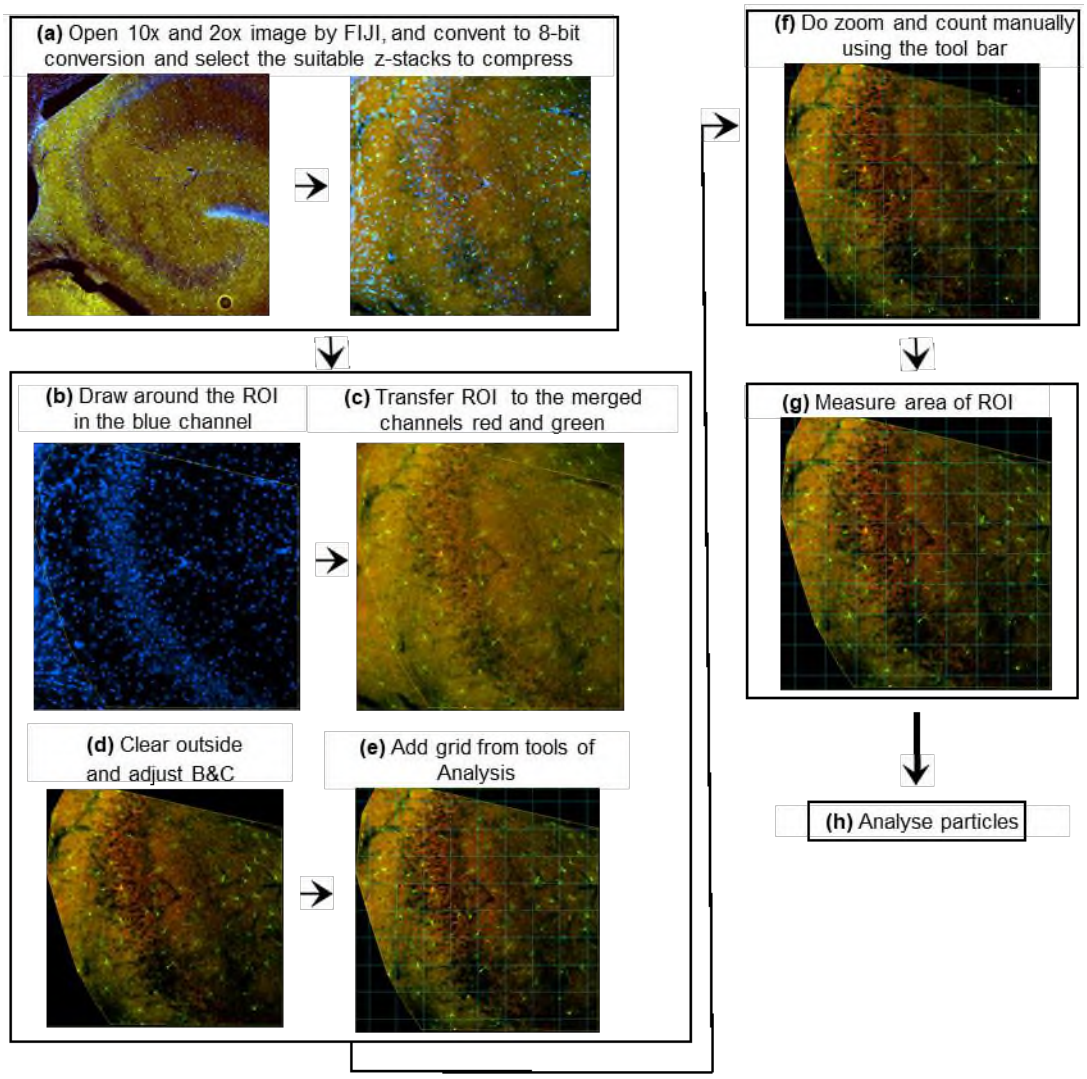

Figure 2.11: A pipeline of densitometric image analysis steps conducted by the Fiji program for iNOS in reactive microglia. (a) The image was acquired by Nikon NiE fluorescent microscope and the file was opened in Fiji to display all channels imaged of 10x and 20x z-stacks and compressed the suitable z-stack. **(b)** The image was pre-processed, and the CA3 was drawn by polygon in the blue (DAPI) channel. **(c)** The drawing of the ROI was transferred from the blue to the merged channels red and green. **(d)** I cropped the outside and then adjusted the brightness and contrast. **(e)** I added a grid from Tools of Analysis to facilitate manual count. **(f)** I zoomed in and counted manually within ROI using the toolbar. **(g)** I measured the area of ROI. **(h)** I divided the count of microglia with and without iNOS manually.

2.6 Statistical analysis

GraphPad Prism Software (Prism 9 USA) was used for the statistical analysis of all data sets. In each figure, the sample sizes are indicated as (n = number of sections/N = number of mice). To see if the data were normally distributed, I first tested for normality using the Shapiro-Wilk test. In the case of data following a normal (Gaussian) distribution, parametric tests were applied. If the distribution of the data in the group did not follow a Gaussian distribution, the data were treated as non-parametric. Bar charts were used to represent parametric data, with mean values and error bars representing the standard error of the mean (SEM). Data for non-parametric analyses were presented as median and interquartile ranges (IQR) and plotted as box plots with individual data values. To evaluate the significant difference between two independent samples, unpaired t-tests were used when data were parametric or a Mann-Whitney rank sum test if non-parametric.

Two-way ANOVA was used when data were parametric or a Kruskal-Wallis test when data were non-parametric to compare the effect of more than two independent variables on one dependent variable. To compare more than two dependent non-parametric variables (laminar distribution), the Friedman test method was used, followed by a Dunns multiple comparison test.

The significance values were reported as *$p < 0.05$ when p is significant, **$p < 0.01$ when p is very significant, and *** $p < 0.001$ when p is extremely significant. Non-significant values were reported as $p > 0.05$.

Chapter 3

Early Neuronal and Neuroinflammatory Changes in the CA3 Region of the Hippocampus of 2-4 Months hA30P Mice

3.1 Introduction

Human mutant α-syn expression is upregulated by 1 month postnatal in hA30P mice and its pathology progresses with age (Schell et al., 2009). Transgenic hA30P mice show declining hippocampal memory function and motor dysfunction by 12-14 months (Kahle et al., 2000, Lindström et al., 2014). Ultimately excess overexpressed mutant human α-syn aggregations cause neuronal cell death in transgenic animals (Watson et al., 2012).

There is evidence from studies of patients with both AD and DLB that indicate the presence of hyperexcitability in the form of myoclonus or seizures (Vicente et al., 2024). More recently, researchers have shown that hippocampal network hyperexcitability may be an early feature of human α-syn pathology in hA30P mice (Stylianou et al., 2020, Tweedy et al., 2021). Thus, hyperexcitability may be an early feature of neurodegeneration (Stargardt et al., 2015).

As discussed in Chapter 1 (section 1.3.2) glial cells are the most abundant and versatile cells in the brain, and they interact with neurons, blood vessels, and themselves to maintain many normal functions of the brain (Colonna and Butovsky, 2017). A vital function of astrocytes is to regulate blood flow and maintain the integrity of the BBB, thereby assisting in brain homeostasis (MacVicar and Newman, 2015, Haim and Rowitch, 2017, Kwon and Koh, 2020). In normal conditions, the astrocytes control synaptic activity by participating in the tripartite synapse and GABA buffering extracellular K+ ions, and other processes (Verhoog et al., 2020). In response to CNS injury, reactive changes in astrocytes' molecular, cellular, and functional profiles occur to minimize tissue damage and repair nearby neurons (Kwon and Koh, 2020).

In human studies of patients with DLB, the correlation between aggregated α-syn and reactive gliosis has been documented (Surendranathan et al., 2015). Neuroinflammation and neuronal hyperexcitability may facilitate cognitive impairment in α-synucleinopathy, where reactive gliosis has been implicated in neurodegeneration and epileptiform activity (Vezzani and Viviani, 2015).

Seizures and other noxious stimuli activate the immediate early gene (IEG) *c-Fos* which leads to transiently increased levels of c-Fos protein in the active cells and many studies have used c-Fos to measure brain activity indirectly (Campeau and Watson, 1997, Campeau et al., 2002). According to current knowledge, the IEG c-Fos appears to be activated in neurons and glial cells (Li et al., 2018). To address whether

the known early hyperexcitability seen in hA30P mice (Tweedy et al., 2021) is associated with neuroinflammation in this chapter, I conducted immunofluorescence (IF) staining on sections from WT and hA30P mice at 2-4 months of age focusing on neuronal and neuroinflammation markers.

3.2 Aims

This chapter aims to understand better neuronal and glial changes at the early stage of a-syn pathology in the CA3 region of the hippocampus hA30P mice and explore evidence of early prodromal or presymptomatic disease-related changes that could be used as potential biomarkers in diagnosis or as therapeutic targets.

3.3 Methods

The methods are outlined in Chapter 2, section 2.2 for anaesthesia, Section 2.3 for tissue preparation, section 2.4 for immunofluorescence staining, and Section 2.5 for imaging and data analysis by the Fiji program.

I stained hippocampal sections using immunofluorescence to confirm human α-syn expression in male 2-4 month hA30P mice. I detected global changes in neuronal activity, changes in neuron population, and the GABAergic parvalbumin interneuron population, in addition to the PNNs by using the antibodies to hα-syn, c-Fos (IEG gene product), neuronal nuclear antigen (NeuN), anti-parvalbumin (PV), as well as Biotinylated Wisteria Floribunda Lectin (WAF) which binds to PNNs (Table 2.2), comparing to age and sex-matched WT mice.

I also investigated whether there are early changes in neuroinflammation in male and female hA30P mice aged 2-4 months compared to age and sex-matched WT mice, by detecting changes in reactive astrocytes using antibodies to GFAP, intermediate filaments forming the cytoskeleton in some astrocytes (Sofroniew and Vinters, 2010). Increased GFAP immunoreactivity represents a change in protein expression and a marker of reactive astrocytes rather than a change in astrocyte number (Serrano-Pozo et al., 2013). Microglia were detected by measuring changes in the ionized calcium-binding adapter molecule 1 (Iba-1) (Hiragi et al., 2018). Anti-inflammatory and pro-inflammatory states of microglia are both marked by Iba-1

upregulation. To detect reactive microglia I co-labelled Iba-1+ cells with antibodies to a specific marker inducible nitric oxide synthase (iNOS) the enzyme that produces nitric oxide (Table 2.2) which is expressed in reactive microglia (Sierra et al., 2014).

The results in this thesis were plotted as an average of the slices (4-7 sections per IF stain) used in each mouse, with at least 3 mice per experimental group (see section chapter 2).

3.4 Results

3.4.1. Expression of Human α-syn in the CA3 Region of the Hippocampus of Male 2-4 Month hA30P Mice

Before investigating changes in neuronal activity and neuroinflammatory modifications, I wanted to confirm that the young hA30P mice showed clear expression of human mutant α-synuclein. I used a group of 2-4 months old male hA30P mice and immunostained for hα-syn (Fig. 3.1).

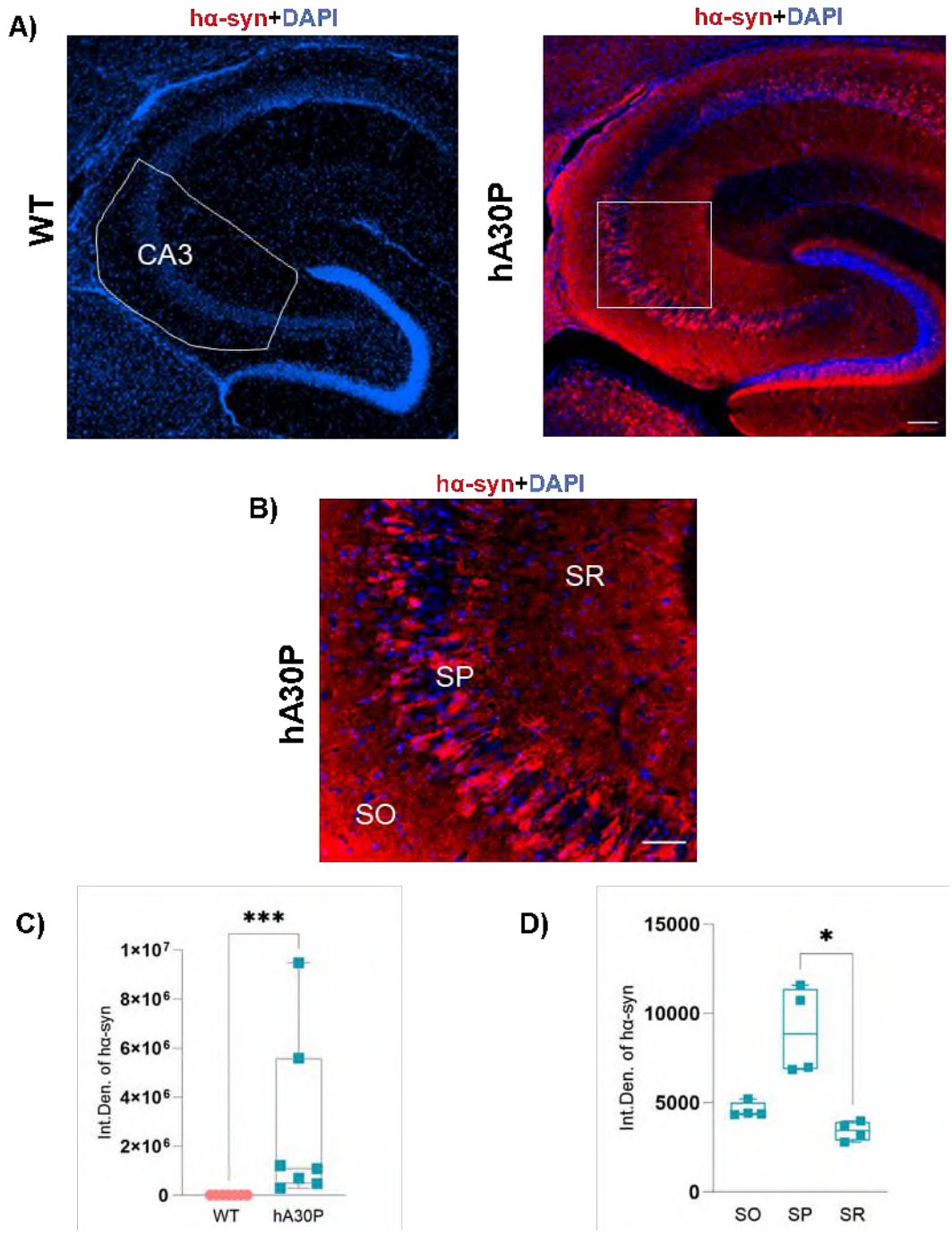

Figure 3.1: Expression of human α-syn in the CA3 Region of the Hippocampus of Male 2-4 Month old hA30P Mice. (A and B) Represent IF images. The hα-syn (red) and the nuclei (blue) (DAPI). Scale bars represent 100 µm A and 50 µm in B. **(A)** High level of human α-syn protein overexpression in the hippocampus of hA30P mice only. **B)** There was a greater expression of hα-syn protein in the deep pyramidal neurons layer, more than in the superficial layer. **(C)** There was a significant increase ***p<0.001 in the integrated density of hα-syn in the CA3 region of the hippocampus of male 2-4 months hA30P mice (N=7) compared to sex and age-matched WT mice (N=7). **(D)** The laminar distribution of the hα-syn in the CA3 region of male 2-4 months hA30P mice (N=4) showed a significant increase *p<0.05 in the SP compared to SR.

As expected, staining for hα-syn confirmed overexpression in the hippocampus only in the hA30P mice (Fig. 3.1A, and B). The expression of human mutant α-syn was clear in the soma of cells in the CA3 region. There was a significantly higher integrated density (Int.Den.) of hα-syn immunofluorescence expressed in the CA3 region of the hA30P mice compared to WT mice. In hA30P median Int.Den. was 1081426, (IQR 471975 – 5585435; n/N = 54 sections/7 mice) versus WT median Int.Den. of 308, (IQR 270 - 333, n/N = 41 sections/7 mice. ***p<0.001; Mann Whitney test) (Fig. 3.1C).

The results also revealed a clear laminar distribution of the expression of the human α-syn in the layers of the hippocampus of the hA30P mice, where *stratum pyramidale* (SP) showed a higher level of human α-syn expression in comparison to *stratum radiatum* (SR) layer (Fig. 3.1A, B and D). There was a significant increase in hα-syn Int. Den. in the SP compared to SR of 2-4 months hA30P mice. In SP median Int. Den. was 8856, (IQR 6885 - 11368, n/N = 12 sections/4 mice) versus SR median Int. Den. of 4392, (IQR 4339 – 5012, n/N = 12 sections/4 mice. *p<0.05; Friedman test). Interestingly, we also found that there was a greater expression of hα-syn in the deep layer of SP compared to the superficial layer in the hippocampus of the hA30P mice (Fig. 3.1B).

3.4.2 Decrease in c-Fos+ nuclei/mm^2 in the CA3 Region of the Hippocampus of 2-4 Months Male hA30P Mice

As outlined above there is evidence in young 2-4 month pre-symptomatic hA30P mice of cortical hyperexcitability due to the pathologic effects of overexpression of human mutant α-syn in their hippocampi (Stylianou et al., 2020, Tweedy et al., 2021). The c-Fos gene belongs to the IEG family of markers that activate following transient increased neuronal activity (Carrion et al., 1999, Lyons and West, 2011), but is also known to be downregulated following chronic activity (Morris et al., 2015). In this staining, I used anti c-Fos antibody as an indirect marker of neuronal activity (Fig. 3.2).

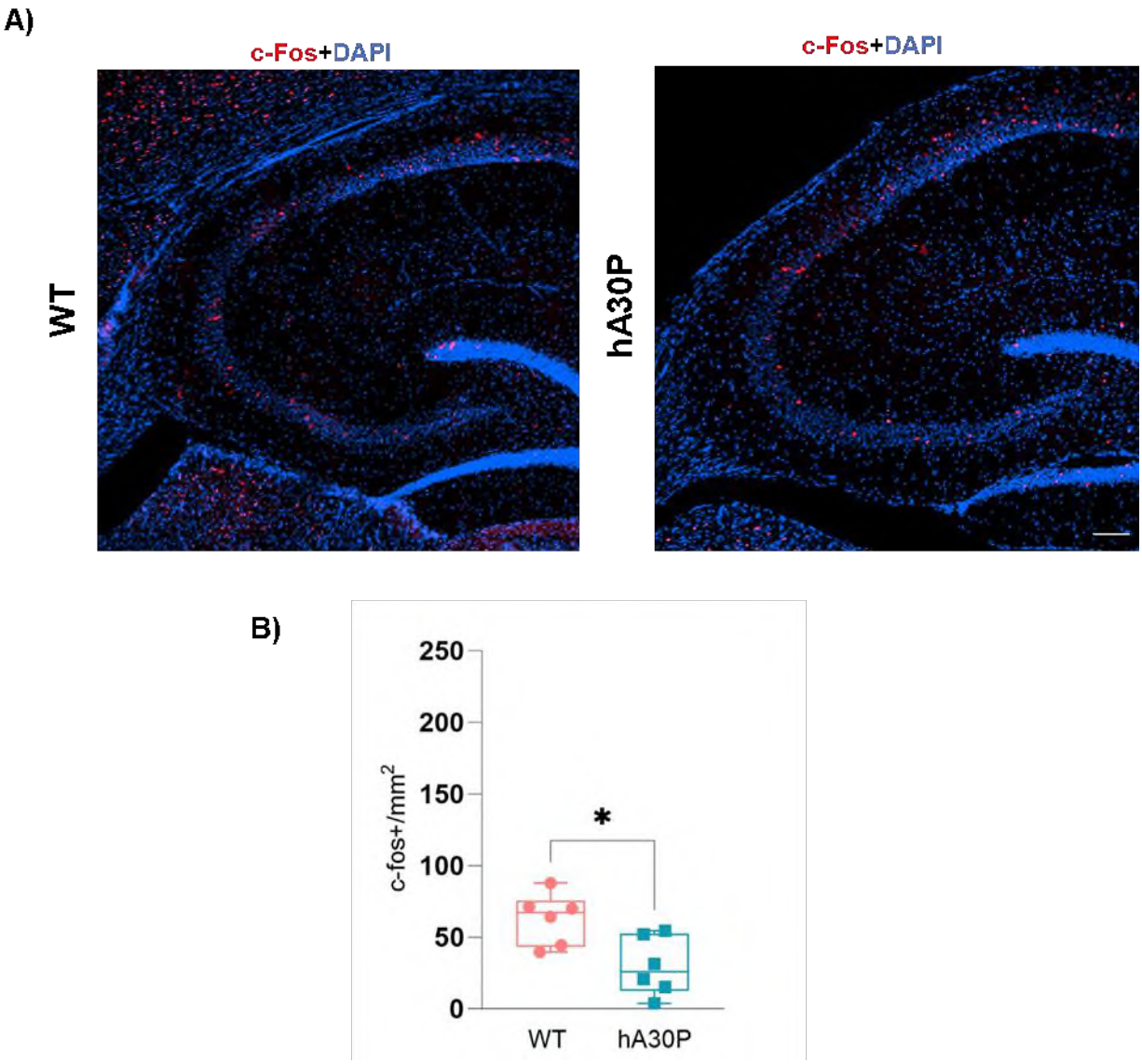

Figure 3.2: Decrease in c-Fos+ nuclei/mm^2 in the CA3 Region of the Hippocampus of Males 2-4 Months hA30P Mice. (A) Representatives IF images. The c-Fos+ protein (red) and the nuclei (blue) (DAPI). Scale bars represent 100 µm. Decrease in c-Fos+ in the hippocampus of hA30P mice compared to WT mice. **(B)** There was a significant decrease *p<0.05 in the count of c-Fos+ nuclei/mm^2 in the CA3 region of the hippocampus of 2-4 months old male hA30P mice (N=6) compared to sex and age-matched WT mice (N=6).

For c-Fos staining, I used a group of male 2-4 months old, hA30P mice and sex and age-matched WT mice. The IF staining result revealed a decrease in nuclei that were c-Fos+ (red dots) in the CA3 region of the hippocampus of hA30P mice compared to the control (Fig. 3.2A, and B). There was a significant decrease in c-Fos+ nuclei/mm^2 present in the CA3 of the hippocampus of hA30P compared to WT mice. In hA30P the median count was 25.9 per section, (IQR 12.50 - 52.59, n/N = 23 sections/6 mice) versus the WT median count of 67.2, (IQR 43.22- 75.53, n/N = 23 sections/6 mice. *$p<0.05$; Mann Whitney test).

This result is consistent with other studies of c-Fos in α-syn transgenic mice with chronic hyperexcitability (Morris et al., 2015, Peters et al., 2020).

3.4.3. Decrease in the % area of NeuN in the CA3 Region of the Hippocampus of Male 2-4 Months hA30P Mice

There is evidence of impaired differentiation and maturation of hippocampal neurons in several AD transgenic mouse models, resulting in neurodegeneration (Krezymon et al., 2013). To investigate if there was a loss in neurons in the hippocampus of young hA30P mice, I used male mice aged 2-4 months old and immunostained for NeuN, co-localised with hα-syn immunofluorescence.

NeuN protein is expressed specifically in nearly all neurons and is used as a biomarker to identify already differentiated neurons (Gusel'Nikova and Korzhevskiy, 2015) (Fig. 3.3).

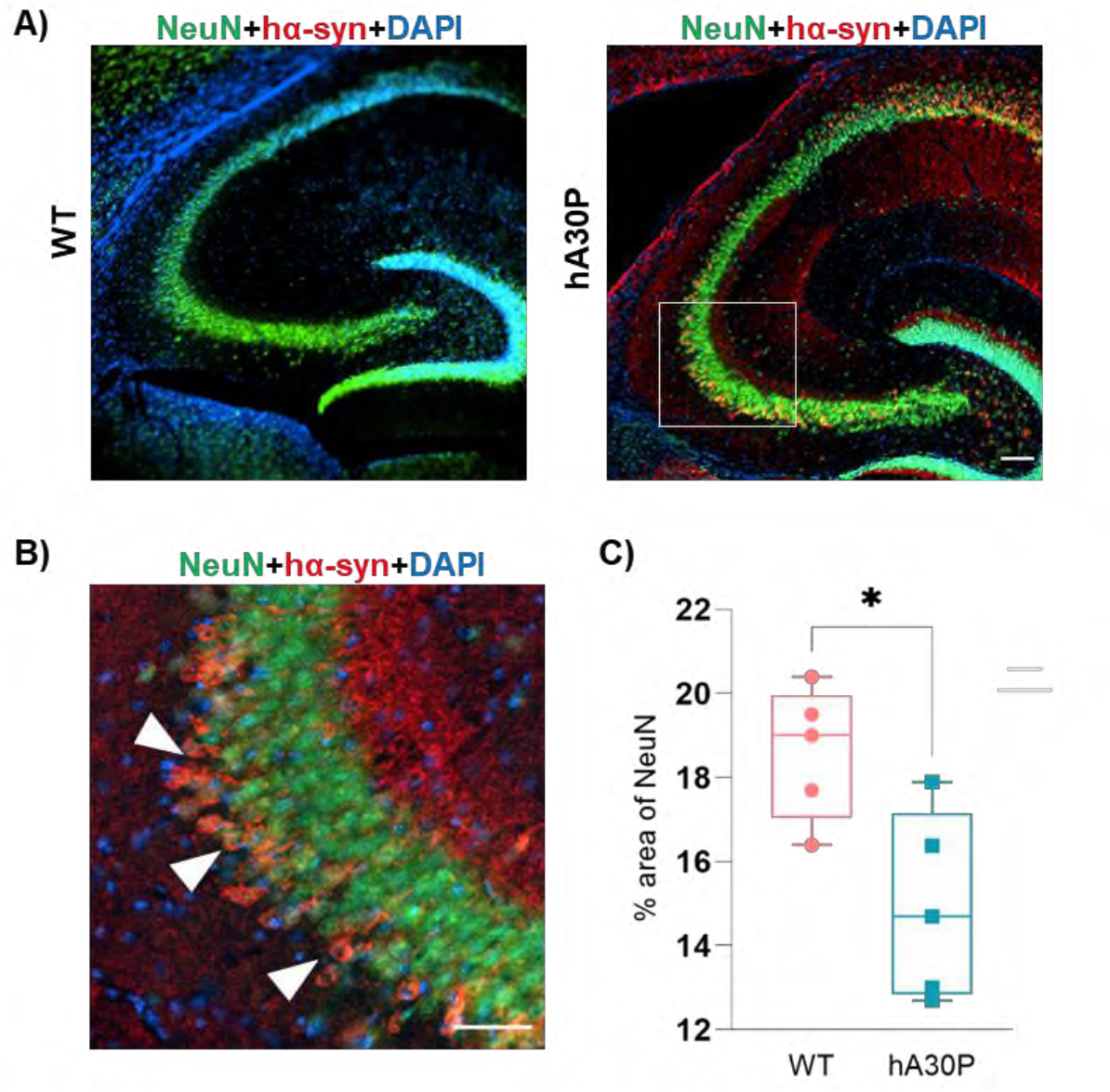

Figure 3.3: Decrease in the % area of NeuN in the CA3 Region of the Hippocampus of Males 2-4 Months hA30P Mice. (A and B) Representative IF images. NeuN neurons (green), hα-syn (red), and the nuclei (blue) (DAPI). Scale bars represent 100 µm in A and 50 µm in B. **(A)** Decrease in % area of expressed NeuN in the CA3 region of the hippocampus of 2-4 months old hA30P mice compared to sex and age-matched WT mice. **(B)** The localization of human α-syn in neurons showed the deep SP contained neurons with higher expression of human α-syn (indicated by white arrows), in comparison to neurons in the superficial layer. **(C)** There was a significant decrease *$p<0.05$ in the % area occupied by NeuN in the CA3 region of the hA30P mice (N=5) compared to WT mice (N=5).

I used a group of 2-4 months old male hA30P mice versus age and sex-matched WT mice as a control group. The results of anti NeuN and hα-syn staining showed a decrease in the expression of NeuN in the CA3 region of the hippocampus of the hA30P mice compared to WT mice (Fig. 3.3A, and C). There was a significant decrease in the % area occupied by NeuN in the CA3 region of the 2-4 months hA30P mice compared to WT mice. In hA30P median % area of a section occupied by anti-NeuN immunostaining was 14.7, (IQR 12.85 -17.14, n/N = 29 sections/5 mice) versus the WT median % area of 19.0%, (IQR 17 - 19.9, n/N = 41 sections/5 mice. *$p<0.05$; Mann Whitney test).

As shown above (section 3.4.1) again the results showed that the deep SP in the hA30P mice had more neurons containing human α-syn compared to neurons in the superficial layer (Fig. 3.3B, orange neurons indicated by white arrows).

3.4.3 Expression of PV Interneurons in the CA3 Region of the Hippocampus of Male 2-4 months hA30P Mice

Imbalances between inhibitory GABAergic interneurons and glutamatergic excitatory pyramidal neurons can result in brain function abnormalities and neurological diseases such as epilepsy, schizophrenia, and autism spectrum disorder, in addition, deficits in PV interneurons occur in AD and DLB in both humans (Xu et al., 2020, Gasiorowska et al., 2021) and rodent models (Tweedy et al., 2021). To investigate whether there were changes in PV interneurons caused by overexpression of human α-syn pathology in the CA3 region of the hippocampus in 2-4 months old male hA30P mice, I conducted IF staining using anti-PV antibodies co-localised with anti-hα-syn immunostaining (Fig. 3.4).

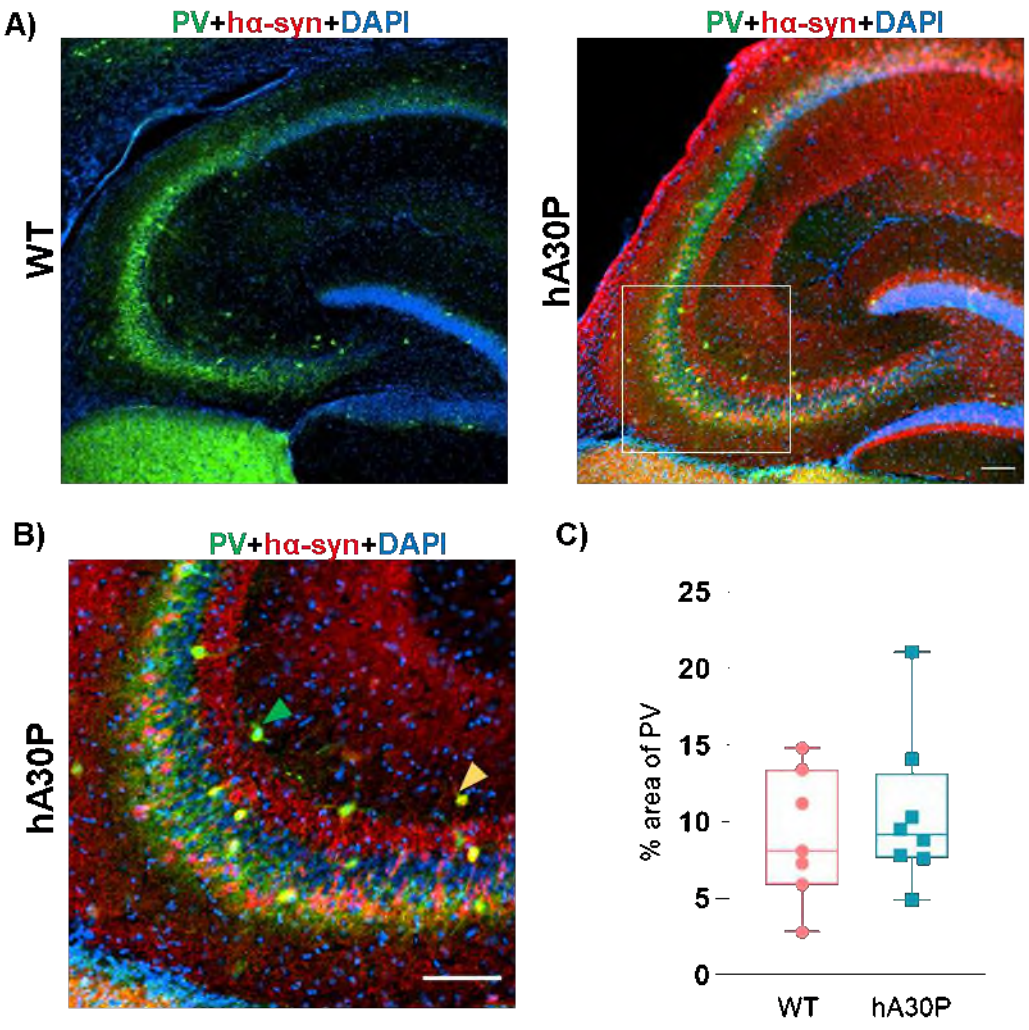

Figure 3.4: Expression of Parvalbumin Interneurons in the CA3 Region of the Hippocampus of Male 2-4 Months hA30P Mice. (A and B) Representative IF images. The PV interneurons without human α-syn (green), the PV interneurons with human α-syn (orange), the hα-syn (red), and the nuclei (blue) (DAPI). Scale bars represent 100 μm in A and 50 μm in B. (A) There was a slightly increasing trend in % area of PV interneurons in the CA3 region of the hippocampus of male 2-4 months old hA30P mice compared to sex and age-matched WT mice. There was overexpression of human α-syn protein only in male 2-4 months old hA30P mice. (B) The localization of hα-syn in the PV interneurons was represented by orange soma of PV interneurons with hα-syn (indicated by orange arrow) and green soma indicating referrer to PV interneurons without human α-syn (indicated by orange arrow). (C) There was no significant difference $p>0.05$ in the % area occupied by PV interneurons in the CA3 region of the hippocampus of male 2-4 months hA30P mice (N=8) compared to WT mice (N=7).

The result of staining with anti-PV and human α-syn antibodies was a small trend towards an increase in the % area occupied by PV in the CA3 region of the hippocampus of the hA30P mice compared to sex and age-matched WT mice (Fig. 3.4A, and C). However, this did not reach statistical significance. In hA30P median % area of PV immunostaining per section was 9.2, (IQR 7.7 – 13.2, n/N = 69 sections/8 mice) versus WT median % area of PV of 8.1, IQR 5.9 - 13.4, n/N = 55 sections/7 WT mice. $p>0.05$; Mann Whitney test).

The immunofluorescence co-labelling of human α-syn with the PV interneurons showed there were a few PV interneuron somas containing hα-syn (indicated by the orange arrow), but most of them were without hα-syn protein (indicated by green arrow) (Fig. 3.4B). However, I did not quantify this further.

3.4.4 Increase in the Count of PV without PNNs/mm^2 in the CA3 Region of the Hippocampus of Male 2-4 months hA30P Mice

Extracellular perineuronal net (PNNs) matrix changes and neurodegeneration are frequently related (Fawcett et al., 2022). The overexpression of hα-syn leads to neuroinflammation in mice (Rannikko et al., 2015) and release of proinflammatory cytokines, reactive oxygen species, and proteinases by reactive microglia can destroy PNNs (Kettenmann et al., 2013). The breakdown of PNNs by cytotoxic proteinases leads to damage to the neurons due to exposure to oxidative stress (Reichelt, 2020). To investigate if the accumulation of hα-syn affects PNNs that surrounded PV interneurons in the hippocampus of male 2-4 months hA30P mice I used biotinylated wisteria floribunda lectin (WAF) binding to identify PNNs, anti-PV antibody to detect PV interneurons, in addition to anti-human α-syn antibody to determine the localization of hα-syn protein within PV interneurons (Fig. 3.5).

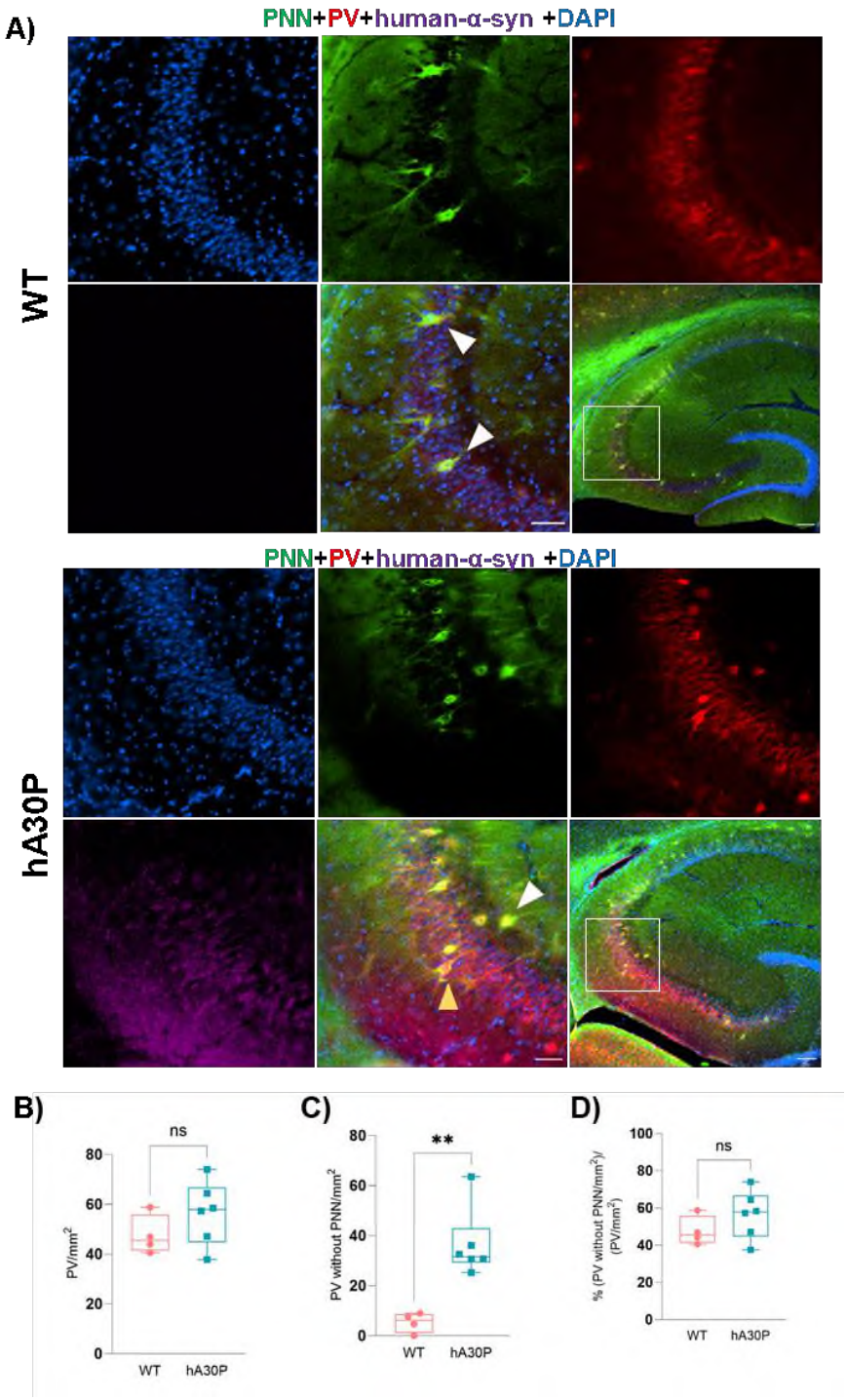

Figure 3.5: Increase in the Count of PV without PNN/mm2 in the CA3 Region of the Hippocampus of Male 2-4 Months hA30P Mice. (A and B) Representative IF images. The PNNs (green), PV interneurons (red), human α-syn (purple), and the nuclei (blue) (DAPI). Scale bars represent 50 µm and 100 µm. **(A)** Increase in the count of PV without PNNs in the CA3 region of the hippocampus of male 2-4 months age of the hA30P mice compared to sex and age-matched WT mice. **(B)** There was no significant difference $p>0.05$ in the total count of PV/mm^2 cells in the CA3 region of the hA30P mice (N=6) compared to WT mice (N=4) **(C)** There was a significant increase $^{**}p<0.01$ in the count of PV without PNNs/mm^2 in the CA3 region of the hA30P mice (N=6) compared to WT mice (N=4) **(D)** There was no significant difference $p>0.05$ in the % of (PV without PNNs/ mm^2)/ (PV/mm^2) in the CA3 region of the hA30P mice (N=6) compared to WT mice(N=4).

The results of IF staining of PV, PNNs, and hα-syn showed there was no statistically significant difference in the total count of PV interneurons in the CA3 region of the hippocampus of the hA30P compared to WT mice (Fig. 3.5A, and B). In hA30P median number of PV/mm^2 per mouse was 57.8, (IQR 44.76 - 66.8, n/N = 12 sections/6 mice) versus WT median PV/mm^2 of 45.4, (IQR 41.41 - 55.85, n/N = 8 sections/4 mice.). However, there was a trend of an increase in PV count in hA30P compared to WT mice, and this result was consistent with the result of a trend to an % area occupied by PV outlined above (Fig. 3.4A, and C).

Interestingly, the result showed the count of PV interneurons not surrounded by the PNNs matrix (indicated by the orange arrow) per mm^2 in the CA3 region of the hA30P mice was significantly greater than in WT mice (Fig. 3.5A, and C). In hA30P median number of PV neurons without PNNs/mm^2 per mouse was 31.6, (IQR 29.2-42.9, n/N = 12 sections/6 mice) versus WT median PV without PNNs/mm^2 of 6.2, (IQR 1.2 – 8.6, n/N = 8 sections/4 mice. **p<0.01; Mann Whitney test).

There was no significant difference in the proportion of the count of PV without PNNs/mm^2 per total count of PV/mm^2 in the CA3 region of the hA30P mice compared to WT mice (Fig. 3.5A, and D). In hA30P the median % (PV without PNNs/ mm^2)/(Total PV/mm^2) was 57.9, (IQR 44.7 – 66.8, n/N = 12 sections/6 mice) versus WT median PV without PNNs/Total PV per mm^2 of 45.5, (IQR 41.5 – 55.9, n/N = 8 sections/4 mice).

3.4.5 Increase in % Area of Reactive Astrocytes in the CA3 Region of the Hippocampus of Male 2-4 Months hA30P Mice

Abnormal expression of aggregated α-syn triggers neuroinflammation by interacting with Toll-like receptor 4 protein (TLR4) expressed on the astrocyte membrane leading to inflammatory responses in humans and mice (Rannikko et al., 2015). In physiological aging, the number of pro-inflammatory astrocytes is increased and may facilitate neurodegeneration (Loveland et al., 2023). To investigate reactive changes that occurred in astrocytes in 2-4 months old hA30P mice due to the pathological effect of overexpression of human mutant α-syn in the hippocampus I first assessed reactive astrocytes by IF staining using anti GFAP antibody in male mice aged 2-4 months (Fig. 3.6).

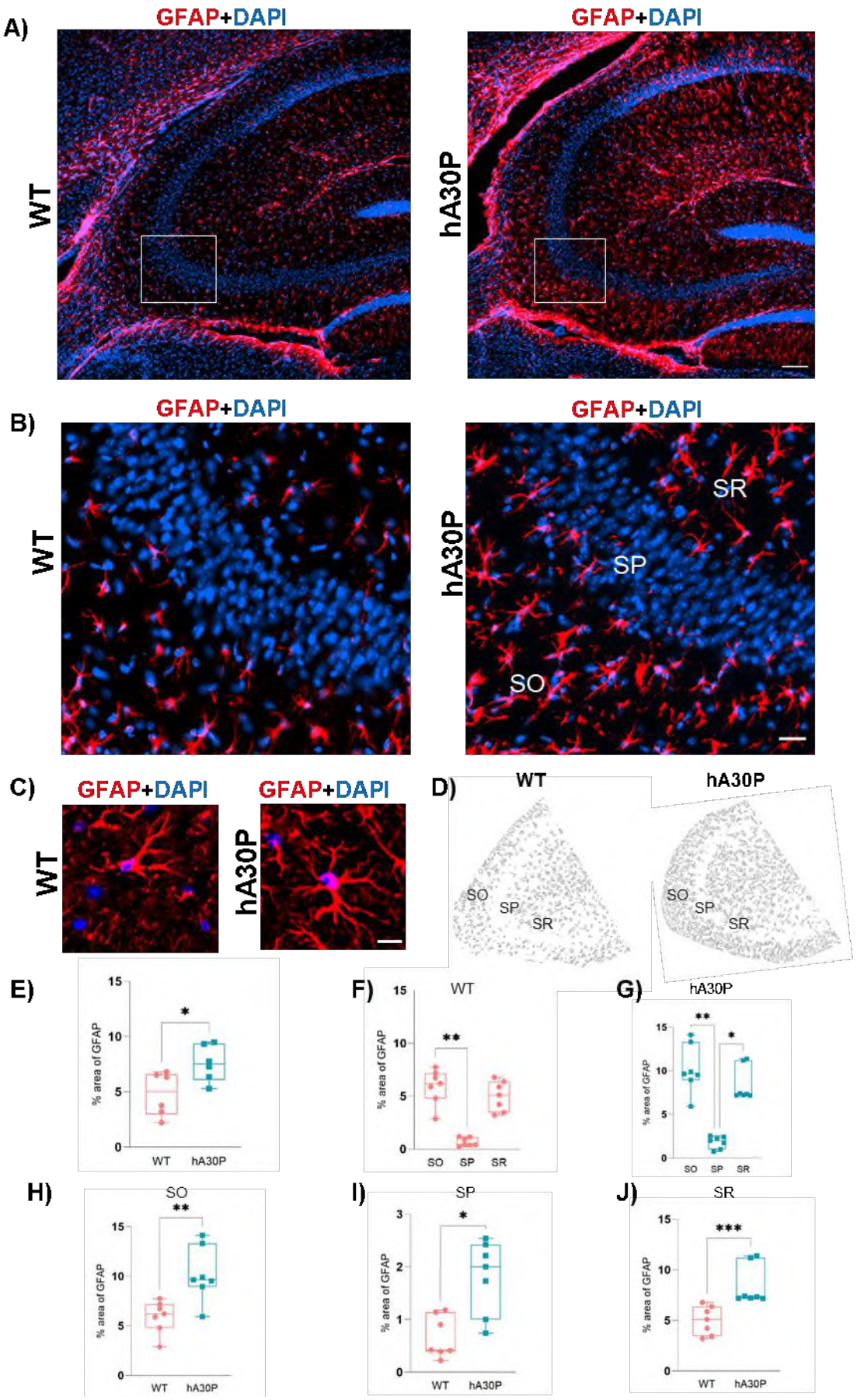
A)
GFAP+DAPI
GFAP+DAPI
WT
hA30P
B)
GFAP+DAPI
GFAP+DAPI
WT
hA30P
SR
SP
SO
C)
GFAP+DAPI
GFAP+DAPI
WT
hA30P
D)
WT
hA30P
SO
SP
SR
SO
SP
SR
E)
% area of GFAP
WT
hA30P
F)
WT
% area of GFAP
SO
SP
SR
G)
hA30P
% area of GFAP
SO
SP
SR
H)
SO
% area of GFAP
WT
hA30P
I)
SP
% area of GFAP
WT
hA30P
J)
SR
% area of GFAP
WT
hA30P

Figure 3.6: Increase in % Area of Reactive Astrocytes in the CA3 Region of the Hippocampus of Male 2-4 Months hA30P Mice. (A, B, and C) Representative IF images. The reactive astrocytes (red) and the nuclei (blue) colour (DAPI). Scale bars represent 100 µm in A, 25 µm in B, and 2 µm in C. **(A)** Increase in reactive astrocytes in the hippocampus of 2-4 months old male hA30P mice compared to sex and age-matched (B) WT mice. **(C)** Morphological changes in reactive astrocytes of hA30P mice compared to WT mice. There was an increase in ramifications and length of the processes in reactive astrocytes compared with normal astrocytes of WT mice. **(D)** Representative Fiji drawing of reactive astrocytes. GFAP+ cells were less localized within the SP layer of the hippocampus in the hA30P and WT male mice. **(E)** There was a significant increase *p<0.05 in the % area of GFAP in hA30P mice (N=6) compared to WT mice (N=6) **(F)** The laminar distribution of GFAP in the WT mice showed a significant increase, **p<0.01 in the % area occupied by GFAP in the SO compared to the SP layer (N=7) **(G)** The laminar distribution of the GFAP of the hA30P mice showed a significant increase **p<0.01 in the % area occupied by GFAP in the SO compared to the SP layer in addition to a significant increase *p<0.05 in the SR compared to SP layer (N=7). Comparing the laminar distribution of the % area of GFAP in the hA30P (N=7) to WT mice (N=7), there was a significant increase **p<0.01 in the SO **(H)**, *p<0.05 in the SP **(I)**, and ***p<0.001 in the SR **(J)**.

The result of staining for GFAP showed a significant increase in the % area occupied by reactive astrocytes in the CA3 region of the hippocampus of the hA30P compared to WT mice (Fig.3.6A, B, and E).

Over the entire CA3 region, there was a significant increase in the % area of GFAP in the hippocampus in male 2-4 months hA30P mice compared to WT mice. In hA30P median % area was 7.5, (IQR 6 – 9.4, n/N = 37 sections/6 mice) versus WT's median % area of 5.1, (IQR 2.9 – 6.6, n/N = 46 sections/6 mice. *p<0.05; Mann Whitney test) (Fig. 3.6E).

The IF staining also showed there was an increase of ramifications and length of the processes of reactive astrocytes of hA30P compared to the WT mice (Fig. 3.6B, and C), although I have not quantified the morphological changes in detail, stereological test is needed to determine these morphological changes.

The drawing of densitometric image analysis by Fiji showed there was an interesting laminar distribution for reactive astrocytes in the hippocampus, where the SP layer showed less reactive astrocytes in comparison to the SO and SR layers in the CA3 region of the hippocampus of both male 2-4 months hA30P and WT mice (Fig. 3.6D).

The laminar distribution of the GFAP in the CA3 region of the hippocampus in 2-4 months male WT mice showed a significant increase in the % area occupied by GFAP only in the SO compared to the SP layer, suggesting there were few astrocytes in the SP layer (Fig. 3.6F). In SO median % area was 6.2, (IQR 4.8 – 7.2, n/N = 23 sections/7 mice) versus SP median % area of 0.4, (IQR 0.39 – 1.2, n/N = 23 sections/7 mice. **p<0.01; Friedman test). The laminar distribution of the GFAP in the CA3 region

of the hippocampus in 2-4 months male hA30P mice also showed laminar differences with again few astrocytes located in the SP. There was a significant increase in the % area occupied by GFAP in the SO compared to the SP layer (Fig. 3.6G). In SO median % area was 9.6, (IQR 8.9 – 13.3, n/N = 27 sections/7 mice) versus SP median % area of 2, (IQR 1 – 2.4, n/N = 27 sections/7 mice. **p<0.01; Friedman test), in addition to a significant increase in the % area occupied by GFAP in the SR compared to the SP layer, in SR median % area was 7.3, (IQR 7.2 – 11.2, n/N = 27 sections/7 mice) versus SP median % area of 2.0, (IQR 1 – 2.4, n/N = 27 sections/7 mice. *p<0.05; Friedman test).

Comparing the hA30P versus WT for each layer there was a significant increase in GFAP in all layers in the hA30P mice. The % area of GFAP in the SO of hA30P was increased compared to WT mice. In hA30P median % area was 9.7, (IQR 8.9 – 13.3, n/N = 27 sections/7 mice) versus WT median % area of 6.2, (IQR 4.8 – 7.2, n/N = 23 sections/7 mice. **p<0.01, Mann Whitney test) (Fig. 3.6H). There was a significant increase in the % area of GFAP in the SP of hA30P compared to WT mice. In hA30P median % area was 2, (IQR 1 – 2.4, n/N = 27 sections/7 mice) versus WT median % area of 0.4, (IQR 0.39 – 1.1, n/N = 23 sections/7 mice. *p<0.05; Mann Whitney test). (Fig. 3.6I). There was a significant increase in the % area of GFAP in the SR of hA30P compared to WT mice. In hA30P median % area was 7.3, (IQR 7.2 – 11.2, n/N = 27 sections/7 mice) versus WT median % area of 5.1, (IQR 3.5 – 6.4, n/N = 23 sections/7 mice. ***p<0.001; Mann Whitney test). (Fig. 3.6J).

3.4.7 Increase in % Area Reactive Astrocytes in the CA3 Region of the Hippocampus of Female 2-4 Months hA30P Mice

There is a 1.5-fold increase in PD prevalence in men compared to women (Moissan, 2016) suggesting that female hormones might slow the progression of the disease in patients. In a PD mouse model, α-syn accumulation was found to be age-dependent, and the degree of astrogliosis and microgliosis was also affected by biological sex with male mice being more severely affected by α-syn toxicity than females (Lamontagne-Proulx et al., 2023). From work in this thesis, I have found changes in neuronal activity and neuroinflammation markers in the CA3 region of the hippocampus of male 2-4 months hA30P mice. To investigate the possible sex

differences in neuroinflammation, I used female 2-4 months hA30P mice and sex and age-matched WT mice and stained with GFAP (Fig. 3.7).

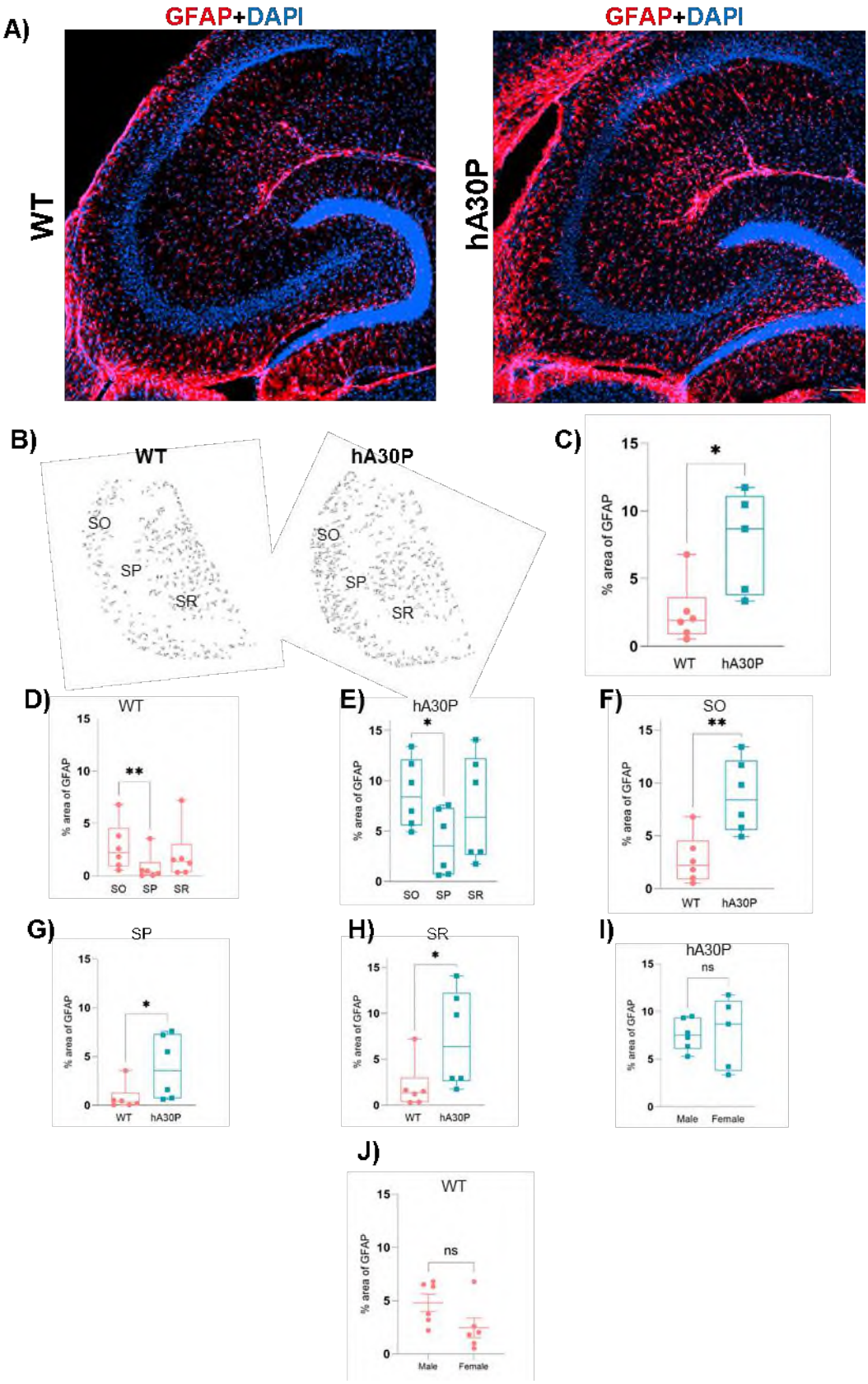

Figure 3.7: Increase in % Area Reactive Astrocytes in the CA3 Region of the Hippocampus of Female 2-4 Months hA30P Mice. (A) Represent IF images. The reactive astrocytes (red) and the nuclei (blue) colour (DAPI). Scale bars represent 100 µm **(A)** High level of reactive astrocyte in the CA3 region of the hippocampus of female 2-4 months old hA30P mice compared to sex and age-matched WT mice. **(B)** Representative Fiji drawing of reactive astrocytes. Astrocytes were less localized within the SP layer in hA30P and WT mice. **(C)** There was a significant increase *p<0.05 in the % area occupied by GFAP in hA30P mice (N=5) compared to WT mice (N=5) **(D)** The laminar distribution of the GFAP female WT mice showed a significant increase **p<0.01 in the % area occupied by GFAP in the SO compared to the SP layer (N=6) **(E)** The laminar distribution of the GFAP in the CA3 region of the hippocampus in female hA30P mice showed a significant increase *p<0.05 in the % area occupied by GFAP in the SO compared to the SP layer (N=6). Comparing the laminar distribution of the % area of GFAP in female hA30P (N=6) to WT mice (N=6), there was a significant increase **p<0.01 in the SO **(F)**, and *p<0.05 in the SP **(G)**, but there was no significant difference in p>0.05 in the SR **(H)**. **(I)** There was no significant difference p>0.05 in the % area occupied by GFAP in male hA30P mice (N=6) compared to female mice (N=5) in the same age. (j) There was no significant difference p>0.05 in the % area occupied by GFAP in male WT mice (N=6) compared to female mice (N=6) in the same age.

The staining with GFAP showed that, as seen in the male mice (Fig. 3.6), we also saw an increase in reactive astrocytes in the hippocampus of females' hA30P mice in comparison to sex and age-matched WT mice (Fig. 3.7A, and C). There was a significantly higher level of % area occupied by GFAP in the CA3 region of females in the hA30P in comparison to WT mice. In hA30P the median % area was 8.7, (IQR 3.8 – 11.1, n/N = 23 sections/5 mice), versus WT median % area of 1.9, (IQR 0.9 – 3.6, n/N = 26 sections/6 mice. *p <0.05; Mann Whitney test).

Like the young male hA30P mice, the results again showed an interesting laminar distribution for the reactive astrocytes in the hippocampus of female 2-4 months hA30P and WT mice, where SO and SR layers showed a high level of GFAP+ astrocytes in comparison to the SP layer (Fig. 3.7B).

The laminar distribution in the CA3 region of 2-4 months female WT mice showed a significant increase in the % area occupied by GFAP in the SO compared to the SP layer. In SO median % area was 2.2, (IQR 0.9 – 4.6, n/N = 26 sections/6 mice) versus SP median % area of 0.3, (IQR 0.04 – 1.3, n/N = 26 sections/6 mice. **p<0.01; Friedman test) (Fig. 3.7D). The laminar distribution of the GFAP female WT mice also showed a significant increase in the % area occupied by GFAP in the SO compared to the SP layer. In SO median % area was 8.4, (IQR 5.6 – 12.1, n/N = 26 sections/6 mice) versus SP median % area of 3.5, (IQR 0.7 – 7.3, n/N = 26 sections/6 mice. *p<0.05; Friedman test) (Fig. 3.7E).

Comparing the changes between hA30P and WT for each laminar I found a significant increase in the % area of GFAP in the SO of females 2-4 months hA30P

compared to WT mice. In hA30P median % area was 8.4, (IQR 5.6 – 12, n/N = 26 sections/6 mice) versus WT median % area of 2.2, (IQR 0.9 – 4.6, n/N = 26 sections/6 mice. **p<0.01; Mann Whitney test). There was a significant increase in the % area occupied by GFAP in the SP layer in hA30P mice compared to WT mice. In hA30P median % area was 3.5, (IQR 0.7 – 7.3, n/N = 26 sections/6 mice) versus WT median % area of 0.3, (IQR 0.04 – 1.3, n/N = 26 sections/6 mice. *p<0.05; Mann Whitney test) (Fig. 3.7G). There was a significant increase in the % area of GFAP in the SR of hA30P mice compared to WT mice. In hA30P median % area was 6.4, (IQR 2.6 – 12.3, n/N = 26 sections/6 mice) versus WT median % area of 1.4, (IQR 0.3 – 3, n/N = 26 sections/6 mice. *p<0.05; Mann Whitney test) (Fig. 3.7H).

In addition, the results showed there was no statistically significant difference in the % area of reactive astrocytes in the CA3 region of the females' hA30P in comparison to males the hA30P mice in the same age. In females median % area was 8.7, (IQR 3.8 – 11.1), n/N = 23 sections/5 mice, versus male median % area of 7.5, (IQR 6 – 9.4, n/N = 26 sections/6 mice.) (Fig. 3.7I).

The results also showed that there was no statistically significant difference in the % area of reactive astrocytes in the CA3 region of the female WT mice in comparison to male hA30P mice of the same age. In female mice median % area was 1.9, (IQR 0.8 – 3.6), n/N = 24 sections/6 mice, versus male median % area of 5.0, (IQR 2.9 – 6.8, n/N = 26 sections/6 mice.) (Fig. 3.7J).

I did notice the values within each cohort of female WT and female hA30P mice at 2-4 months showed considerable variability in the range of % area of GFAP+ astrocytes compared to male WT and hA30P mice at the same age. The % area of in female hA30P ranged from IQR 3.8 – 11.1, versus WT IQR 0.9 – 3.6; while for male was hA30P the range was IQR 6.1 - 9.4, versus WT IQR 2.9 - 6.6.

3.4.8 Increase in % Area Occupied by Microglia, and the Count of Reactive Microglia in the CA3 Region of the Hippocampus of Male 2-4 Months hA30P Mice

The marked changes seen in astrocytes above were because of overexpression of human mutant α-syn in young hA30P mice, thus I also went on to assess whether abnormal α-syn had also induced changes in the expression of reactive microglia (Zhao et al., 2020, Favuzzi et al., 2021). I used the Iba-1 antibody

to quantify microglia. Because both neurotoxic and neuroprotective microglia show an increase in Iba-1 expression, to differentiate between them, I used co-labelling of Iba-1 with the iNOS antibody, an inflammation-induced enzyme that produces nitric oxide and is expressed only in reactive microglia (Dai et al., 2011, Sierra et al., 2014). (Fig. 3.8)

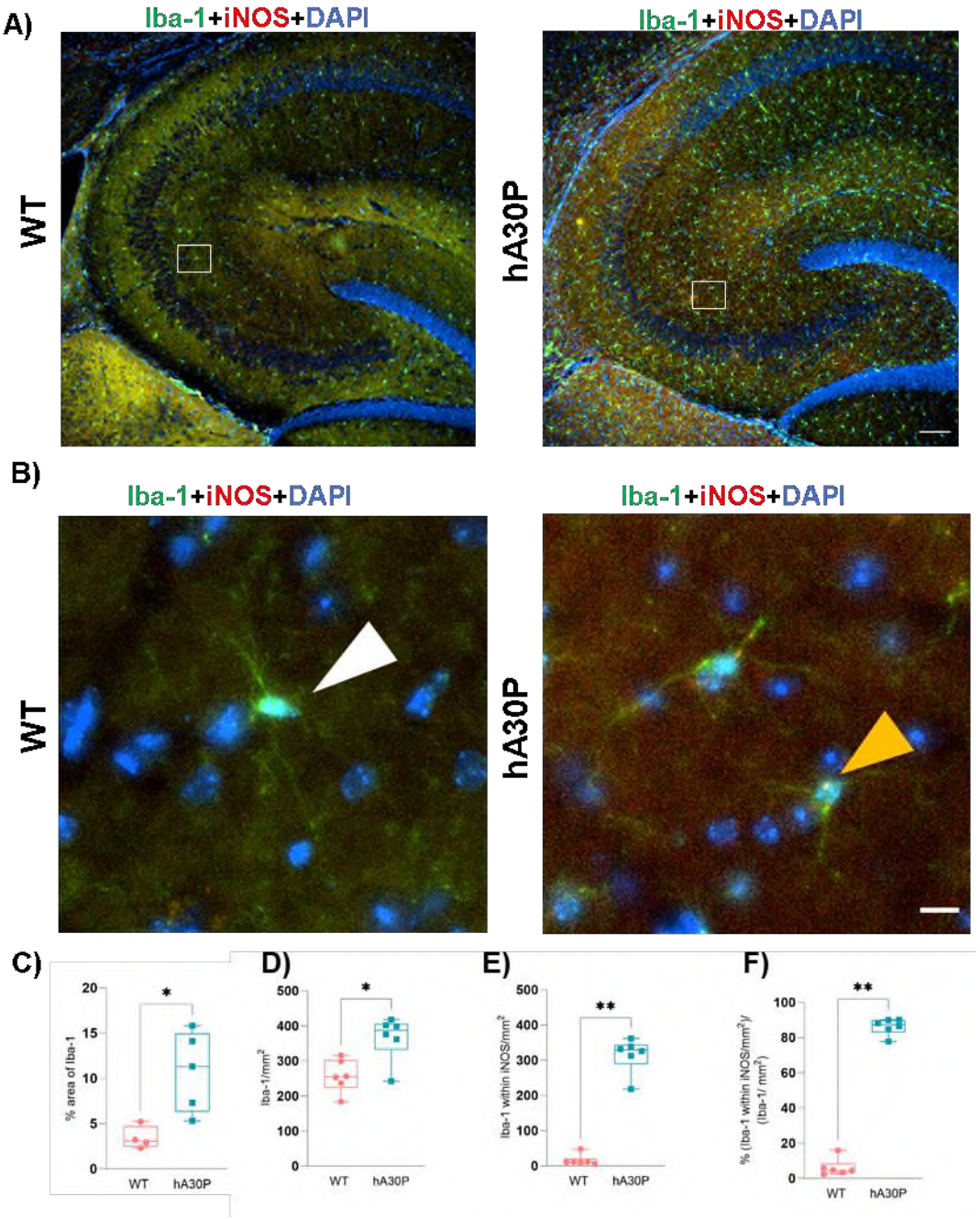

Figure 3.8: Increase in % Area Occupied by Microglia and the Count of Active Microglia in the CA3 Region of the Hippocampus of Male 2-4 Months hA30P Mice. (A and B) Representative IF images. Iba-1 (green), iNOS (red), and the nuclei (blue) (DAPI). Scale bars represent 100 µm in A and 10 µm in B. **(A)** Increase in % area occupied by Iba-1 and increase in total count of Iba-1/mm^2 in the CA3 region of the hippocampus of male 2-4 months old hA30P compared to sex and age-matched WT mice. **(B)** Increase in count of reactive microglia (Iba-1 with iNOS) (indicated by the orange arrow) in the CA3 region of hA30P compared to count of Iba-1 without iNOS (indicated by the white arrow) in WT mice. **(C)** There was a significant increase *p<0.05 in the % area occupied by Iba-1 in the CA3 region of the hA30P mice (N=5) compared to WT mice (N=4). **(D)** There was a significant increase *p<0.05 in the total count of Iba-1/mm^2 in the CA3 region of the male hA30P mice (N=6) compared to WT mice (N=6). **(E)** There was a significant increase **p<0.01 in Iba-1 with iNOS/mm^2 in the CA3 region of the hA30P mice (N=6) compared to WT mice (N=6). **(F)** There was a significant increase **p<0.01 in the % (Iba-1 with iNOS/ mm^2)/ (Iba-1 mm^2) in the CA3 region of the male 2-4 months hA30P mice (N=6) compared to WT mice (N=6).

I used a group of male 2-4 months hA30P mice versus age and sex-matched WT mice as a control group. The results of IF co-staining of Iba-1 and iNOS showed there was a significant increase in the % area occupied by Iba-1 in the CA3 region of the hippocampus in hA30P compared to WT mice. In hA30P mice median % area occupied by Iba-1 was 11.3, (IQR 6.3 – 14.9, n/N = 25 sections/5 mice) versus WT median Iba-1/mm^2 of 3.1, (IQR 2.5 – 4.7, n/N = 20 sections/4 mice. *p<0.05; Mann Whitney test) (Fig. 3.8A, and C). To test whether the increase in the % area was due to an increase in microglial processes, I counted the microglia cell bodies manually with the assistance of Fiji, and the result showed there was also a significant increase in the total count of Iba-1+ cell bodies /mm^2 in the hA30P compared to WT mice (Fig. 3.8A, and D). In hA30P median total count of Iba-1/mm^2 was 387.3, (IQR 332 – 406.1, n/N = 13 sections/6 mice) versus WT median Iba-1/mm^2 of 255, (IQR 223.5 – 303.1, n/N = 12 sections/6 mice. *p<0.05; Mann Whitney test).

The results also revealed a significant increase in the count of reactive microglia (indicated by orange arrow) that co-labelled with iNOS in the hA30P compared to WT mice. The non-reactive microglia were without iNOS co-expression (indicated by white arrows) (Fig. 3.8B and E). In hA30P median Iba-1 with iNOS/mm^2 was 329.1, (IQR 289 – 343.9, n/N = 13 sections/6 mice) versus WT median Iba-1 with iNOS/mm^2 of 11, (IQR 9.4 – 20.5, n/N = 12 sections/6 mice. **p<0.01; Mann Whitney test).

The qualitative assessment also showed there were morphological changes in microglia due to the neuroinflammation. There was an enlargement of soma and a decrease in ramifications and shortening of the processes of microglia (Fig. 3.8B), but I did not quantify these changes. To provide quantitative data on glial morphology stereological analysis may use in future work.

There was also a significant increase in the proportion of co-labelled cells (Iba-1 with iNOS/mm^2)/ (total Iba-1/mm^2) in the hA30P compared to WT mice (Fig. 3.8B, and F). In hA30P median % (Iba-1 with iNOS/mm^2)/ (total Iba-1/mm^2) was 87.4%, (IQR 83.1 – 89.9, n/N = 13 sections/6 mice) versus WT median (Iba-1 with iNOS/mm^2)/ (total Iba-1/mm^2) of 4.6%, (IQR 3.1 – 8.4, n/N = 12 sections/6 mice. **p<0.01; Mann Whitney test). These data demonstrate that most microglia were activated in the hA30P mice as they co-expressed iNOS and Iba1. In contrast in the WT mice, very few microglia exhibited a reactive phenotype.

3.4.9 Increase in % Area Occupied by Microglia in the CA3 Region of the Hippocampus of Female 2-4 Months hA30P Mice

To determine whether there were male versus female differences in the reactive microglia as has been previously reported (Lamontagne-Proulx et al., 2023) I used a group of female 2-4 months old hA30P and WT mice and conducted IF to stain microglia by Iba-1 antibody (Fig. 3.9).

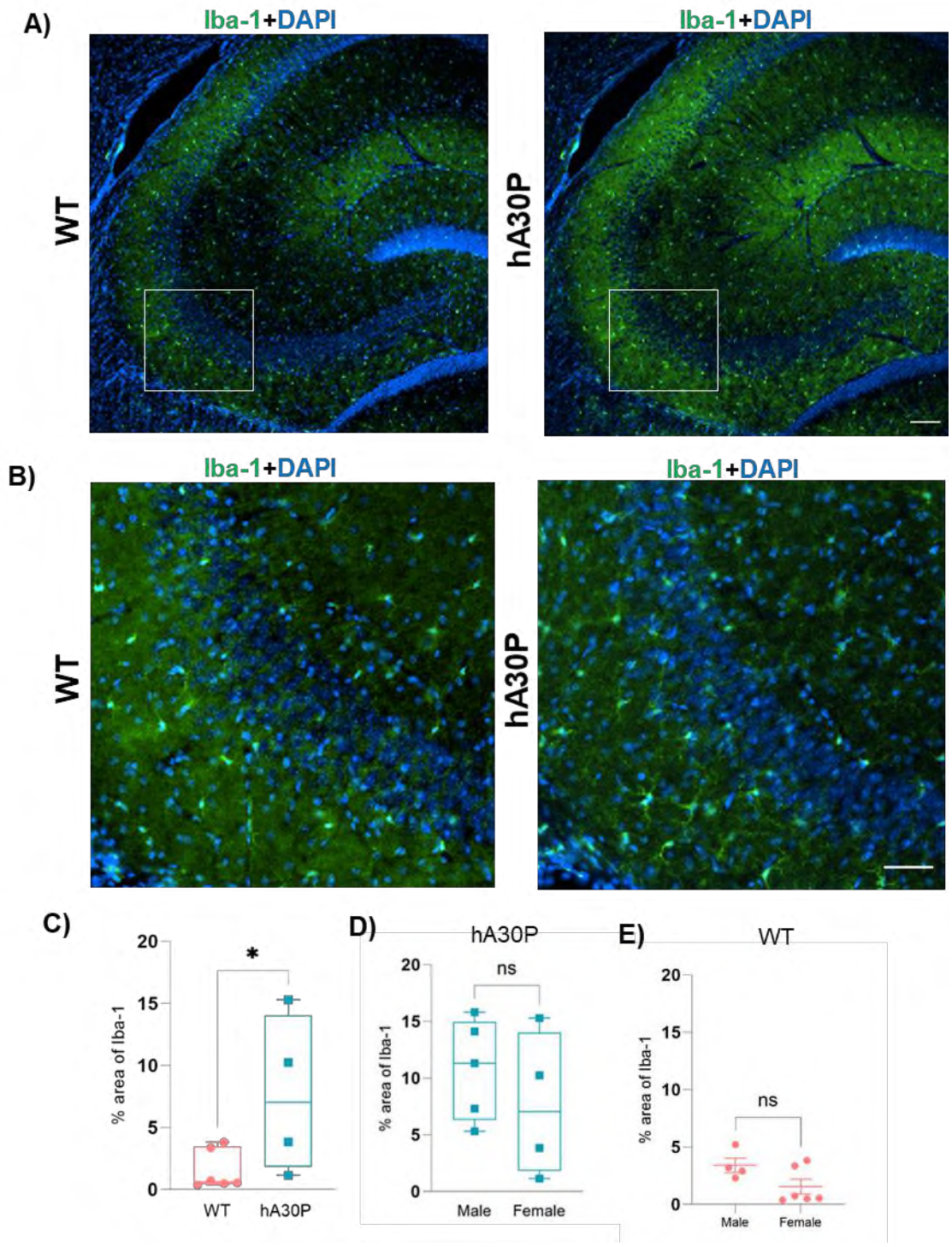

Figure 3.9: Increase in % Area Occupied by Microglia in the CA3 Region of the Hippocampus of Female 2-4 Months hA30P Mice. The microglia (green) and the nuclei (blue) (DAPI). Scale bars represent 100 µm in A and 50 µm in B. **(A, and B)** High level of microglia expression in the hippocampus of females 2-4 months old hA30P mice compared to sex and age-matched WT mice. **(C)** There was a significant increase *p <0.05 in the % area occupied by Iba-1 in the CA3 region of the hippocampus of female hA30P mice (N=4) compared to WT mice (N=6). **(D)** There was no significant difference p >0.05 in the % area occupied by Iba-1 in female hA30P mice (N=4) compared to male hA30P mice (N=5) at the same age. **(E)** There was no significant difference p >0.05 in the % area occupied by Iba-1 in female hA30P mice (N=6) compared to male WT mice (N=4) at the same age.

The staining with Iba-1 confirmed there was also a higher expression of reactive microglia in the CA3 region of the hippocampus of female 2-4 months old hA30P mice in comparison to sex and age-matched WT mice (Fig. 3.9A, B, and C). There was a significant increase in the % area occupied by Iba-1 in the CA3 region of the female hA30P mice. In hA30P median % area was 7, (IQR 1.2 – 14, n/N=16 sections/4) versus the WT median % area of 0.6, (IQR 0.5 – 3.5, n/N = 15 sections/6 mice. *p <0.05; Mann Whitney test).

The qualitative assessment again showed morphological changes in microglia due to neuroinflammation. There was a qualitative increase in ramifications and increase in the length of the processes of microglia in 2 months female hA30P mice compared with WT (Fig. 3.9B), while the reactive microglia in those close to 4 months exerted a decrease in the processes and enlargement in their soma, which may reflect the neuroinflammation severity depending on the hA30P mice age.

However, the results revealed no significant difference in the % area occupied by microglia in the CA3 region of the hippocampus of the female 2-4 months hA30P mice compared to age-matched males (Fig. 3.9D). In female mice median % area was 7, (IQR 1.8 - 14, n/N = 18 sections/4 mice) versus the median % area of 11.3, (IQR 6.3 – 14.9, n/N = 18 sections/5 mice. p>0.05; Mann Whitney test) in male mice.

The results also revealed no significant difference in the % area occupied by microglia in the CA3 region of the hippocampus of the female 2-4 months old WT mice compared to age-matched males (Fig. 3.9E). In female mice median % area was 0.6, (IQR 0.45 – 3.48, n/N = 24 sections/6 mice) versus the median % area of 3.1, (IQR 2.45 – 4.7, n/N = 18 sections/4 mice. p>0.05; Mann Whitney test) in male mice.

However, the values in each cohort of female WT and female hA30P mice at 2-4 months showed considerable variability compared to male mice. The IQR of % area of occupied Iba-1 in female hA30P was 1.8 – 14, versus WT of IQR 0.5 – 3.5, while for male hA30P was IQR 6.3 – 14.9, versus WT of IQR 2.5 – 4.7.

3.5 Discussion

A summary of key findings in Chapter 3 was as follows:

- A significant expression of the hα-syn protein in the CA3 region of the hippocampus of male 2-4 months male hA30P mice, and the expression in the deep layer of the SP was much higher than in the superficial layer.
- A significant decrease in the % area of NeuN IF in the male 2-4 months old hA30P compared to the control.
- A trend to an increase in PV+ interneuron density and % area of PV immunoreactivity in male 2-4 months hA30P mice compared to the control.
- A significant decrease in the count of PV+ neurons without PNNs/mm^2 in male 2-month-old hA30P mice compared to the control.
- A significant down-regulation in c-Fos expression in male 2-4 months old hA30P mice compared to the control.
- A significant increase in GFAP+ reactive astrocytes in both male and female 2-4 months old hA30P compared to WT mice. Interesting laminar distribution of reactive astrocytes across the CA3 layers with few astrocytes present in SP for both male and female 2-4 months of hA30P and WT mice.
- A significant increase in the % area occupied by microglia in both male and female hA30P mice compared to the control, and a significant increase in the count of Iba-1+ iNOS+ microglia in male hA30P compared to the control.

3.5.1 Human α-syn Expression in the CA3 Region of the Hippocampus

The results of human α-syn immunofluorescence staining of the CA3 region of the hippocampus of male 2-4 months hA30P mice showed there was a significant expression of hα-syn protein only in the hA30P mice. This result was expected, and in line with earlier research which showed that hA30P mice start to accumulate pathogenic human α-syn as early as 1 month of age (Schell et al., 2009, Kahle et al., 2000). The hA30P mice have 3 times more expression of human α-syn than endogenous mouse α-syn (Kahle et al., 2000).

Expression of human α-syn reaches a plateau phase at 1 month of age (Kahle et al., 2001), but changes with aging are linked to oligomerization, phosphorylation of serine residue 129 (PS129), and aggregation of α-syn (Kahle et al., 2000, Neumann

et al., 2002, Schell et al., 2009, Ekmark-Lewén et al., 2018). However, I did not stain for pS129, although this would be interesting to do in future studies. In this study, we found that the expression levels of α-syn were variable across mice. This variability in IF of hα-syn levels may reflect differences in the expression of the transgene in different mice or may be due to a problem in staining similar to those encountered in staining human α-syn oligomers in tissue fixed by the PFA procedure. The human α-syn oligomers have been difficult to measure using conventional IF staining techniques because the heteromorphic human α-syn oligomers are difficult to detect *ex vivo* using an anti-hα-syn antibody (Enzo (15G7) ALX-804-258) anti-human α-syn protein. Conformational epitopes of oligomers may be inaccessible or altered on fixed PFA tissue surfaces, hence oligomer pathology could be missed (Behere et al., 2021). To get precise measurements of human α-syn protein, a crucial component, using paraffin-embedded tissue and/or confocal microscope imaging has been suggested, also using another assay to detect the exact concentration of human α-syn protein, like enzyme-linked immunosorbent assay (ELISA) is recommended in future work. However, variability in various measures has been seen previously in hA30P mice (Ekmark-Lewén et al., 2018).

Overexpression of human α-syn under the Thy1 promoter has previously been shown to result in widespread overexpression of the protein in neurons across the brain of hA30P mice (Fernagut et al., 2007). Interestingly, our results showed the expression of the ASYN gene under the Thy1-promoter predominated in the deep layer of the SP in the hippocampus of hA30P mice and was much higher than in the superficial layer. This result was compatible with previous research by Dobbins et al. (2018), who found expression of channelrhodopsin under Thy1 favoured deep-layer CA1 pyramidal neurons (Dobbins et al., 2018). It is becoming increasingly apparent that the hippocampal deep layer pyramidal neurons are distinct from the superficial layer neurons, with physiological differences in connectivity and expression patterns (Slomianka et al., 2011a). This needs to be clarified before α-synucleinopathy changes can be fully explored. In future work, it would be interesting to stain for Thy-1, or human α-syn mRNA, to determine if there are subregional differences in expression within the hippocampal pyramidal neurons layer.

3.5.2 Overexpression of Human α-syn Reduction in % area of NeuN in hA30P mice

Interestingly we found a significant decrease in the % area of NeuN IF in the CA3 region of males 2-4 months old hA30P mice. Although, the reduction in % area of NeuN is not definite marker to reduction in neurons, this result was surprising as we had not expected to see any marked neurons death at this early stage of disease progression. Cognitive dysfunction and motor deficits are not evident in hA30P mice until 12 and 14 months respectively (Kahle et al., 2000). NeuN is extensively used to identify the nuclear protein of neurons in adult vertebrates, there are some limited exceptions, such as photoreceptors in the retina, mitral cells in olfactory bulbs, and Purkinje cells in the cerebellum (Weyer and Schilling, 2003, Wolf et al., 1996), in addition to the neurons in substaintia nigra pars reticulata of gerbil (Kumar and Buckmaster, 2007). However, many studies have reported that NeuN immunoreactivity in neurons is weakened or disappears as a result of various pathological processes (Lind et al., 2005). Staining of neurons and their cytoplasm with NeuN antibody has been observed to disappear completely in the striatum after ischemic damage (Korzhevskii et al., 2009, Kirik et al., 2009). Huntington's disease causes certain neurons in the striatum to cease synthesis of NeuN protein as noted in a human post-mortem brain study of Huntington's patients (Tippett et al., 2007). A decrease in NeuN immunoreactivity in the CA3 region of the hippocampus in mice following brain injury was also reported (Igarashi et al., 2001).

The reduction in % area of neurons at this early age in hA30P mice was not expected. Anti-NeuN antibodies are used to detect neuronal differentiation and assess the functional state of neuron populations in normal and pathological states (Gusel'Nikova and Korzhevskiy, 2015). Although it is more than 20 years since NeuN was first used in immunohistochemical studies on neuronal differentiation in normal and pathological conditions, the mechanisms that contribute to the loss of NeuN immunoreactivity and post-translational modifications of this protein in cells are still unclear (Gusel'Nikova and Korzhevskiy, 2015).

There are several explanations relating to the reduction in % area of NeuN staining. The first case occurs when the NeuN protein is not expressed in a cell or when protein synthesis occurs in a small enough amount that cannot be detected by immunostaining. This case might be behind the reduction in % area of NeuN staining

of young hA30P mice in the current study. The second is that the dephosphorylation of NeuN protein influences the binding ability of epitopes masking the active binding site of antigen and resulting in false negative results and failed antigen-antibody binding (Lind et al., 2005). The third reason for the reduction in NeuN-staining occurrence when the protein translation of NeuN is impaired due to damaged neurons (without affecting their viability). Unal-Cevik et al. (2004) demonstrated that NeuN-staining loss may not always result from neuronal death. The damage in neurons may temporarily suspend the synthesis of this protein by neurons. Neurons that have been exposed to a moderate ischemia model (30 min ischemia) lose NeuN immunoreactivity 6 h after exposure, while still retaining their integrity and nuclei and showing no characteristic signs of death. It has been suggested that NeuN non-immunoreactive neurons are diverse morphologically and do not share a single neurotransmitter system (Sarnat et al., 1998, Kumar and Buckmaster, 2007).

So, my finding of decreased % area of NeuN in the young hA30P mice may suggest that the CA3 region neurons are under stress due to α-syn accumulation, but cell death itself may not have happened yet. Using another marker more specific for death markers such as a caspase 3 marker to detect apoptosis in future work is recommended to distinguish the cause of this loss of % area of NeuN in the hippocampus of young hA30P mice.

The co-staining of NeuN within hα-syn showed that the majority of human α-syn protein was expressed in pyramidal neurons. According to Kemshead et al. 1982, the striatum and hippocampus are the brain regions that express the Thy-1 promoter the most widely (Kemshead et al., 1982).

3.5.3 Changes in PNNs and possibly in PV interneuron function in hA30P mice

PV interneurons are a key component of neuronal oscillations at gamma frequencies (Colgin, 2016, Whittaker et al., 2011) and impairments in PV function play a key role in generating epileptiform activity (Jiang et al., 2016). PV interneurons are also critical for cognitive functions like learning, memory, and planning (Tremblay et al., 2016). In this study, I was interested in quantifying changes in the PV population in hA30P mice because PV interneurons are particularly vulnerable to injury in chronic epileptogenic lesions of the neocortex and hippocampus (Jiang et al., 2016, Zhao et al., 2020). Because PV interneurons have a high energy demand (Kann et al., 2014)

they may be susceptible to hα-syn pathology in the hippocampus of hA30P mice (Olkhova et al., 2024).

The cohort of 2-4 months hA30P mice used in this experiment showed a trend of increase in PV interneurons and their processes in both % area and count/mm^2 in the CA3 region. Previous work also showed there was a trend toward increased numbers of PV interneurons in the CA3 region in 2-4 months male hA30P mice compared to the WT mice (Tweedy et al., 2021). We know the PV interneurons upregulate PV expression in response to increased neuronal activity (Espinoza et al., 2018). At this early stage in the hA30P mice, a trend to increased PV might be a result of increased neuronal activity in PV interneurons as a compensatory attempt to enhance inhibitory feedback of cortical activity (Espinoza et al., 2018).

The PNNs protect PV interneurons against environmental stressors (Reichelt et al., 2019). PNNs have been demonstrated to provide neuroprotection to rodent cortical neurons in dissociated cultures. Miyata et al. 2007, examined the ability of PNNs to protect against the neurotoxic effects of Aβ, an important component of AD plaques (Miyata et al., 2007). They used chondroitinase ABC, an enzyme that is used to degrade chondroitin sulphate proteoglycans, the structural component of PNNs, of neurons in culture. They found that cortical neurons free of PNNs showed significant neurotoxic responses after Aβ1-42 treatment, but neurons associated with PNNs did not reveal neurotoxicity. Using Gclm mice that have genetically impaired antioxidant systems where the modulatory subunit of glutamate cysteine ligase is not expressed (Yang et al., 2021), it has been found that PNNs preferentially surround PV interneurons to protect them against excitotoxicity (Cabungcal et al., 2013b). These results indicate that PNNs may protect neurons from oxidative stress and neurodegeneration. Furthermore, due to their stabilizing effects on neuronal synapses, PNNs around PV interneurons, prevent further plasticity (Chaunsali et al., 2021).

Interestingly in this study, I found a decrease in % area of PNNs in young 2-4 months hA30P mice compared to WT. Previous findings demonstrated that PNN damage might contribute to excitatory-inhibitory imbalance changes, synaptic loss, and increased neuronal susceptibility toward oxidative stress (Wen et al., 2018). The interpretation for the loss of PNNs I observed might be an attempt to increase synaptic plasticity. Research has disputed whether the digestion of PNNs in neurodegenerative diseases is a compensatory mechanism to increase neurons' plasticity and form new

synapses, which would reduce cognitive impairment. Digestion of PNNs by injection of chondroitinase ABC in the hippocampus of two mice models of tauopathy (Tg P301S, and AAV-P301S) resulted in restoring memory to normal levels one week after the injection (Yang et al., 2015). Also, studies in mouse models of AD pathologies demonstrate that removing PNNs enhanced memory (Vegh et al., 2014). Thus, the early decrease in the PNNs we observed in this study might be a compensatory decrease to maintain normal levels of cognitive function. Overall, the trend of an increase in the PV interneurons that was associated with a decrease in PNNs might be due to the insult of human α-syn accumulation.

With more advanced stages of neurodegeneration, there is a reduction in the PV interneuron numbers and depletion in the PNNs reported in some studies. AD and DLB in both human post-mortem tissue (Bernstein et al., 2011) and late-stage disease of rodent models (Zhao et al., 2020) have shown deficits in PV interneurons. With the development of advanced pathology, the degradation of neuroprotective PNNs will likely accelerate degeneration, exacerbate dementia, and lead to advanced cognitive decline (Reichelt, 2020).

Although I did not quantify the exact number of PV interneurons that co-labelled within hα-syn, a small proportion of PV interneurons co-labelled within hα-syn in the CA3 region of hA30P mice. This result was comparable with the previous study by Tweedy et al. 2021, which found 25% of PV interneuron colocalized within human α-syn in the hA30P mice of the same age as the current study (Tweedy et al., 2021). α-syn aggregates are predominantly in excitatory neurons, but it is believed that synaptic interactions with excitatory synapses affect PV inhibitory interneurons indirectly (Ghiglieri et al., 2018, Calabresi et al., 2023), where α-syn could spread extracellularly and be taken up by PV interneurons.

For future work, it is crucial to study the effect of PV and PNNs' role in the neuronal activity changes in different age male and female hA30P mice. The identification of factors linked to neuroinflammation and cortical hyperexcitability will provide direction for therapeutic intervention.

3.5.4 Decreased c-Fos expression suggests increased chronic neuronal excitability in young hA30P mice

The current study showed down-regulation in c-Fos expression in the CA3 region of the hippocampus in hA30P mice of 2-4 months of age. The immediate early genes (IEG) family is considered a marker that activates following neuronal activity (Carrion et al., 1999, Lyons and West, 2011). Seizures and other noxious stimuli have been shown to activate the IEG, such as c-Fos, which leads to increased levels of c-Fos protein in the active cells (Campeau et al., 1997). However, these changes are immediately occurring within minutes. Other studies have shown that chronic activity leads to a decrease in c-Fos expression (Singh et al., 2019, Morris et al., 2015, Torres et al., 2021).

Previous studies in α-syn transgenic mice including mice expressing the A53T mutation (Singh et al., 2019), and wild-type hα-syn mice (Morris et al., 2015, Torres et al., 2021) showed cortical hyperexcitability due to the pathologic effects of overexpression of human α-syn occurred with decreased c-Fos expression. My data in the hA30P mice showing downregulation of c-Fos is, therefore, consistent with chronic hyperexcitability.

However, according to current knowledge, the IEG c-Fos appears to be expressed in glial cells in addition to neurons (Li et al., 2018), So further work is needed to see which cells have the c-Fos to gain a deeper understanding of the relationship between early neuronal hyperexcitability and neuroinflammation.

3.5.5 Increase in Reactive Astrocytes in the Hippocampus of Male and Female 2-4 Months hA30P Mice

Astrocytes, the CNS's most abundant cell population, play an increasingly important role in α-synucleinopathy (Lobsiger and Cleveland, 2007, Di Marco Vieira et al., 2020). The results here showed there was a significant increase in reactive astrocytes in the CA3 region of the hippocampus in both males and females 2-4 months old hA30P compared to WT mice. Research suggests that astrocytes serve as potential eliminators for aggregations of toxic extracellular proteins (Giusti et al., 2024), so they are activated by the presence of α-syn.

Previous human post-mortem studies demonstrated that multiple system atrophy (MSA), Parkinson's disease, and DLB are associated with filamentous synuclein aggregates deposited on astroglia and oligodendrocytes (Kordower et al., 2008). Similar findings were also found, in a human α-syn transgenic mouse model (Lee et al., 2010).

My finding of increased GFAP expression in male and female hA30P mice could be explained by the astrocytes' role in cleaning the parenchymal microenvironment. Lee et al., 2010, found that synuclein released from neuronal cells could be easily endocytosed by astrocytes, causing them to produce glial inclusions and release neuroinflammatory mediators. Upon exposure to neuronal synuclein, astrocytes undergo changes in gene expression that reflect a neuroinflammatory response, including the release of cytokines, chemokines, and adhesion molecules involved in cell migration (Lee et al., 2010). α-syn triggers neuroinflammation by interacting with TLR4 expressed on the astrocyte membrane leading to inflammatory responses (Fellner et al., 2013). My data showed that, even at this early stage of the disease, abnormal mutant human α-syn expression in the hA30P mice is sufficient to trigger an increase in reactive astrocytes.

Qualitative analysis of the IF images revealed an interesting laminar distribution of reactive astrocytes across the CA3 layers with few GFAP+ astrocytes present in SP for both male and female 2-4 months of hA30P and WT mice. The SP showed a significant increase in % area GFAP in male hA30P compared to WT but the same *stratum* did not show a change in female hA30P compared to WT. This result may indicate greater neuroinflammation in male mice compared to female mice (Lamontagne-Proulx et al., 2023). However, no obvious male versus female differences were seen when % area GFAP across the whole CA3 region of hA30P mice was compared control, despite some literature reporting that there are differences between males and females (Yu et al., 2023, Oltra et al., 2023).

The astrocyte reactivity we found in the current study may have contributed to the hyperexcitable hippocampus network state seen in both the hA30P mice (Tweedy et al., 2021), and other transgenic human α-syn lines (Morris et al., 2015, Peters et al., 2020). Because of the changes in the regulation of GABA synthesis and release due to the alteration in the astrocytes' function (Liddelow and Barres, 2017). Along with their homeostatic role, the astrocytes regulate inhibitory neurotransmission through GABA uptake and release (Kilb and Kirischuk, 2022, Andersen et al., 2023), and thus

play an important regulating network excitability. Consistent with this, recent studies have suggested a role for astrocytes in the generation of seizure activity (Chan et al., 2019).

Although I did not quantify the morphological changes that were consistent with reactive astrocytes, an increase in ramification of astrocyte processes was clear in the hippocampus of hA30P compared to WT mice. Overall, the result showed a clear marker of neuroinflammation of increased GFAP indicating that alterations in astrocytes in the hippocampus of hA30P mice occur even at this early age and might be the direct cause of hyperexcitability.

3.5.3 Increase in Reactive Microglia in the Hippocampus of Male and Female 2-4 Months hA30P Mice

The IF results in this chapter reported a significant increase in the % area occupied by microglia in the CA3 region of the hippocampus of both male and female hA30P mice compared to the control, and there was a significant increase in the count of Iba-1+ microglia in male hA30P compared to the control. This result was compatible with previous findings in cell culture of primary microglia (Scheiblich et al., 2021) that demonstrated an increase in microglia in response to aggregated α-syn, which triggered neurodegeneration (Zhang et al., 2005). In the current experiment, it is possible that compromising the BBB can allow toxins and cells (Rana and Musto, 2018) such as invasive macrophages penetrating the hippocampus in hA30P mice. During a mouse brain injury, microglia were demonstrated to play an important role in maintaining BBB integrity (Lou et al., 2016).

Recent studies have shown that microglia can remove and transfer aggregated α-syn load using gap junctions and tunnelling nanotubes from microglia to neighbouring microglial cells (Scheiblich et al., 2021). In PD, microglia play an important role in driving and perpetuating neurodegeneration, although researchers are still unsure how they contribute to neuronal cell death. Impairment in clearance and degradation of α-syn by microglia increased inflammatory profiles and cell death (Scheiblich et al., 2021). However, by degradation via autophagy, microglia have been reported to protect neurons from neuron-released α-syn (Choi et al., 2020). The

correlation between aggregated α-syn and reactive gliosis has been documented increasingly (Çınar et al., 2022).

The extracellular treatment of rodent and human microglia in human neuroblastoma SH-SY5Y cell line culture with aggregated recombinant α-syn has induced various inflammatory responses (Çınar et al., 2022, Klegeris et al., 2008). A further mechanism by which microglia increase α-syn-mediated neurotoxicity depends on NADPH oxidase activation and phagocytosis of α-syn, ultimately leading to neuronal damage (Çınar et al., 2022). Microglial factors including the release of cytokines can also modulate astrocyte responses (Bezzi et al., 2001).

That indicates the increase in reactive microglia that we observed in the current result was in line with the previous studies that have shown that neuroinflammation contributes to neurodegenerative diseases. The abnormal activation of microglia can cause immune dysfunction and the release of neuroinflammatory substances that damage nearby healthy nerve tissue. Neurons gradually degenerate and die over time due to these processes (Zajda et al., 2020, Peña-Bautista et al., 2019). AD, PD, and HD are neurodegenerative diseases characterized by chronic neuroinflammation, driven by persistent abnormal activation of microglia. Neurons and synaptic structures in the brain can be destroyed by prolonged inflammation (Du et al., 2022b). Sustained chronic microglia have been linked to neuronal cell dysfunction, excitability changes in neurons, and neuronal cell death (Vezzani and Viviani, 2015). Also, the current result of an increase in microglia was in line with hyperexcitability in the hippocampus of males at 2-4 months of age of hA30P mice (Tweedy et al., 2021). However, it would be interesting to look at hA30P mice and older age groups and assess changes in both astrocytes and microglia.

Although the current study result showed a trend of decrease in % area of Iba-1 in CA3 of female hA30P compared to male, it did not reach a significant value statistically. This may be due small sample size that was used. This trend for less microglia % area stain in females compared to males might be predicted because previous studies reported that hormones have a role in boosting the immune responses in females (Lamontagne-Proulx et al., 2023).

In response to inflammatory mediators such as lipopolysaccharides (LPS) and cytokines, iNOS is expressed in macrophages, microglia, astrocytes, and other cell types, in addition, two additional isotypes have been recognized: endothelial NOS

(eNOS) that is expressed in endothelial cells, and neuronal NOS (nNOS) that is expressed in neurons (Pacher et al., 2007, Brown and Neher, 2010).

The results of the current study showed there was a significant increase in the count of iNOS co-expression in Iba-1+ cells in addition to a significant increase in the proportion of microglia labelled with iNOS in male hA30P compared to the control. That might indicate the higher neurotoxicity level due to overexpression of human α-syn in the hippocampus of hA30P mice at this early stage of life. The increase in reactive microglia that labelled with iNOS was in agreement with previous studies that found a correlation between iNOS expression in activated microglia and neurodegeneration (Brown and Neher, 2010). TNF-α, IL-1β, and IL-6 have been identified as possible neuroinflammatory mediators in human post-mortem PD brains (Nagatsu et al., 2000, Rajkumar et al., 2020), activated microglia produce iNOS mainly in response to neuroinflammatory factors (Brown and Neher, 2010). Previous research presented evidence that neuronal cell dysfunction and changes in neuronal network excitability are caused by dysregulation of their cytokine manufacture and cellular release of cytokines, or changes in receptor-mediated intracellular pathways in target cells (Vezzani and Viviani, 2015) in human post-mortem brain in the nigrostriatal region (Nagatsu et al., 2000), and in rat microglia culture (Wang et al., 2004).

Recent demonstrated that microglia respond to excitatory glutamate-driven neuronal activity with increased process extension and retraction and decreased motility which can lead to increased network hyperexcitability (Merlini et al., 2021). Healthy microglia could share α-syn burden and mitigate the neuroinflammatory profile (Scheiblich et al., 2021). Meanwhile, cytokines that proinflammatory microglia produce have a role in PNNs degradation, leading to exposure of PV inhibitory interneurons to ROS toxicity (Cabungcal et al., 2013b). PV interneuron damage may increase the network hyperexcitability in the CA3 region of hA30P mice. These, and other studies, suggest microglia are significant regulators of network excitability which will have important implications for elucidating the mechanisms that link network hyperexcitability, neuroinflammation, and neurodegeneration.

Understanding neuroinflammatory changes linked to α-syn is particularly important because PD patients with a pro-inflammatory profile exhibit a faster decline (Kouli et al., 2020).

3.6 Conclusion

The results of this chapter demonstrated that marked gliosis occurred in the young male and female hA30P mice long before the onset of any cognitive or motor deficits that were reported in this mouse line (Kahle et al., 2000, Freichel et al., 2007). The results suggested a close association between early neuronal hyperexcitability and neuroinflammation (Kilb and Kirischuk, 2022, Andersen et al., 2023, Kouli et al., 2020). Chronic hyperexcitability, which we have previously observed in young hA30P mice (Tweedy et al., 2021), was proposed to account for the downregulation of c-Fos seen in hA30P mice aged 2–4 months. I also showed that the changes in c-Fos were coupled with a marked increase in both reactive astrocytes and microglia. The decrease in % area of NeuN observed here in hA30P mice suggested that the neurons were under the stress of overexpressed human mutant α-syn accumulation, even at this early age. The trend of an increase in PV IF expression might indicate a compensatory change in the CA3 region due to hyperexcitability. PV is a calcium buffer, and more active neurons tend to show increased PV expression. The 2-4 months old hA30P showed a decrease in PNNs in the CA3 region, perhaps, because the microglia had switched to a pro-inflammatory state and degraded the PNNs (Wang et al., 2015). Also, the reduction in the PNNs might be due to a compensatory action to enhance the plasticity of the CA3 region of the hippocampus to maintain a normal level of cognition and memory (Yang et al., 2015, Vegh et al., 2014). Principally, the reduction of PNNs in the current study was concurrent with a decrease of c-Fos, a member of the IEG family, that related to memory and learning (Gallo et al., 2018). This chapter revealed obvious neuroinflammation and neuronal changes in the hippocampus of 2-4 months hA30P mice.

Chapter 4

Pilot study investigating anti-neuroinflammatory effects of intranasal Metformin Treatment

4.1 Introduction

Treatment of neurodegenerative dementia is considered a big challenge because of its pathological complexity and the difficulties for pharmacological agents to gain access to the brain. Current methods for diagnosing and treating neurodegenerative diseases are limited. Metformin has been shown to have beneficial effects on neurological diseases (Pérez-Revuelta et al., 2014). Research has shown that metformin readily passes the BBB (Cao et al., 2023, Sanz et al., 2024), although the precise mechanism of metformin transport into the central nervous system remains unclear (McCreight et al., 2016).

Several studies using metformin in human and animal models have shown mitigation of neurodegenerative diseases through anti-inflammatory, antioxidant action, enhancement of BBB function, as well as neuroprotective, and neurogenesis-inducing properties (Isop et al., 2023). These properties make metformin a promising therapeutic choice for the treatment of neurodegenerative disease.

There is evidence linking mTOR signalling to accelerated aging, dysregulation in the mTOR pathway has been shown to promote cancer growth, inflammation, neurological disorders, and T2DM (Dazert and Hall, 2011). Due to the indirect inhibition of mTOR caused by AMPK activation, metformin, an activator of AMPK, has been found to suppress the expression of mTOR (Onken and Driscoll, 2010). As a result of activating AMPK, metformin reduces energy expenditure by inhibiting multiple enzymes involved with ATP synthesis and degradation. Metformin can also enhance mitochondrial biosynthesis, assist autophagy, and maintain cellular health (Ma et al., 2022). Metformin has been shown to lead to a prolonged lifespan and mitigates aging in *C. elegans* (Chen et al., 2017).

The AMPK activation by metformin has an important role in the reduction of protein phosphorylation. Some studies have shown that metformin could inhibit the phosphorylation of α-synuclein (Pérez-Revuelta et al., 2014). However, the impact of metformin on α-syn pathology is not well understood. Interestingly, the induction of autophagy was promoted by pAMPK activation by metformin, which leads to a decrease in α-syn accumulation (Gopar-Cuevas et al., 2023). There was a significant reduction in the accumulation of Aβ, and an improvement in the plaque-associated tau pathology of APP/PS1 mice in the hippocampus and cortex when metformin was

administered (Ou et al., 2018). Metformin also reduced APPc99 and pTau404 expression levels in SAMP8 mice, which is a model for sporadic AD (Farr et al., 2019).

Metformin has been recommended as an additional medication for treating inflammatory and immune-mediated diseases (Pernicova et al., 2020). A dosage of 2550 mg/day for 12 weeks decreases high-sensitive C-reactive protein and decreases tumour necrosis factor (TNF) levels in the blood of individuals with chronic inflammation compared to those treated with glucocorticoid (Pernicova et al., 2020).

Prolonged microglial activation causes chronic neuroinflammation that develops in neurodegenerative diseases and which causes damage to neurons and synapses in the brain (Du et al., 2022a). Evidence shows that metformin can inhibit neuroinflammation. It was observed to reduce cytokine expression and microglia that were activated by lipopolysaccharide in a PD rat model (Tayara et al., 2018). Metformin also mitigates the oxidative damage of neurons and effectively reduces neuroinflammation by suppressing astrocytes and microglia (Isop et al., 2023).

In the hippocampus of mice with APP/PS1, metformin has also been shown to dramatically reduce the concentrations of cytokines TNF-α, interleukin 1 beta (IL-1β), and IL-6 when taken orally (Lu et al., 2020b, Ou et al., 2018). Metformin was found to reduce circulating levels of proinflammatory cytokines in older diabetics after a five-year follow-up study (Tizazu et al., 2019). As a result of the reduction in proinflammatory cytokines, the risk of death was reduced among this population (Tizazu et al., 2019).

BBB dysfunction leads to the increased permeability of pro-inflammatory cytokines contributing to seizure events (Rüber et al., 2018), AD (Anderson et al., 2011), posttraumatic epilepsy (Tomkins et al., 2011), psychiatric disorders, and cognitive impairment in T2D (Serlin et al., 2011). By mitigation of BBB dysfunction in people with diabetes, metformin has been indicated to reduce seizure risk through its anti-inflammatory properties (Liu et al., 2014).

Despite the functions outlined above, and its safe use, recent research reported that patients with diabetes who are treated with metformin show more signs of vitamin B12 insufficiency (Sayedali et al., 2023). To avoid the malabsorption of vitamin B12 that results from the interference of metformin with protein-bounds B12 in the gut (Guéant et al., 2022), the nasal delivery route offers an effective method for preventing and treating brain disorders invasively (Sun et al., 2018) (see Chapter 1 Section 1.7),

especially since metformin could penetrate the BBB (Cao et al., 2022, Sanz et al., 2021).

We, therefore, planned to test metformin treatment given intranasally in a pilot study. I aimed to investigate the potential neuroprotective/anti-neuroinflammation effects of metformin to reduce the neuroinflammatory changes described in Chapter 3 in the hA30P mice. To do this we planned to treat mice for 4 weeks from postnatal day 30 at which point we know α-syn is expressed in the hA30P mice (Kahle et al., 2000). However, before commencing this study we first needed to determine whether neuroinflammation was present and detectable at 1-month of age.

4.2 Aims

This chapter aimed to detect early prodromal disease-related neuronal excitability and neuroinflammatory changes in the CA3 region of the hippocampus of hA30P mice at 1 month of age, compared to age-matched WT mice. I also wanted to determine the feasibility of intranasal metformin treatment to assess the potential neuroprotective/anti-neuroinflammation effects. In particular, I wished to determine whether metformin could reverse the pathological changes that we detected in the CA3 region of the hippocampus of male 2-4-month-old hA30P mice.

4.3 Methods

The methodology of this chapter has two parts.

First: Immunofluorescence staining was conducted to confirm human-α-syn detectable expression in the CA3 ROI of male 1-month-old hA30P mice and to detect if there were changes in neuronal activity, and neuroinflammation markers, compared to age-matched WT mice by using hα-syn, c-Fos, and GFAP and Iba-1 co-labelled with iNOS antibodies, respectively. All related details of mouse anesthesia, brain perfusion with PFA, and immunostaining methodology are as described in Chapter 2, section 2.2 for anaesthesia, section 2.3 for tissue preparation, section 2.4 for Immunofluorescence, and Section 2.5 for Imaging and data analysis by the FIJI program.

Second: Metformin hydrochloride (Cat. No. 2864; Tocris Bioscience, UK) was dissolved in sterile distilled water to prepare in 100 mM solution. Mice were treated with 11.5 mg/kg for 5 days out of seven over 28 days with no treatment at the weekend. In the current study, I used a micropipette to deliver a small drop of the size of 14 µl (split into two rounded; 7 µl, then after 5 min another 7 µl, in purpose to give rest for the mice) that suits the capacity of the nasal cavity of the juvenile mice as the colleagues in the CBC advance. I used the maximum solubility of metformin which is 100 mM concentration. This resulted in only 11.5 mg/kg/day of metformin. I used male 1-month hA30P mice and age and sex-matched WT control mice (Fig. 4.3). The drug and vehicle were at room temperature and the total volume administered was 14 µl split into two rounds of 7 µl each time. After a 5-minute rest, another 7 µl was given, resulting in 14 µl per mouse/day. A score sheet was used to record the health conditions of the mice by observing their coat, breathing, posture, and weight daily (Table 4.1). We used two groups of hA30P mice, the first as a treatment group (N = 3) mice treated with metformin, and the second as a control group (N = 3) treated with vehicle only (sterile distilled water). In addition, we had two groups of WT mice, the first as a treatment group (N = 3) mice treated with metformin, and the second as a control group (N = 3) treated with vehicle only (sterile distilled water).

4.3.1 Intranasal drug delivery

Research on the effects of metformin in different neurodegenerative models showed a wide range of dosages have been used, generally 20-350 mg/kg (Rabiei Poor et al., 2021) to prevent damage to the hippocampus and reduce inflammation. A wide variety of administration routes have also been used in different studies (Isop et al., 2023). An intracerebroventricular injection of streptozotocin induces phosphorylation of insulin receptors in the hippocampus and cerebral cortex of AD mice. According to Kazkayasi et al., 2022 intranasal 200 mg/kg metformin treatment for four weeks significantly reduced the phosphorylation of insulin receptors, consequently increasing the sensitivity of insulin receptors leads to improved learning and memory functions in these mice (Kazkayasi et al., 2022).

This study was conducted using a special intranasal administration method developed by Hanson et al. 2013. The goal of this procedure is to deliver drugs directly to the central nervous system without anaesthesia in mice. This was accomplished by:

- First, acclimatization of the mice to being handled.
- Second, immobilizing the animal's head with a modified scruff grip.
- Third, the drug was administered intranasally with drops administered via a pipette (Fig. 4.1).
- Fourth, the mouse was returned to its cage and rewarded. In my study, I used peanut butter for 3 hours post-dosing which was then removed to avoid the mice gaining too much weight (Fig. 4.2).

After the mice were weaned at the age of 21 days, acclimatization started for 7-10 days (Fig. 4.3) to build up to the handling steps for intranasal drug delivery (Hanson et al., 2013) (Fig. 4.1):

1. I started by placing the mouse in the palm of my hand for two to three minutes, no higher than one foot above the cage's top.
2. After that, I petted the mouse gently from the head to the tail for three minutes in the palm. When doing so the animal will be free to move around and feel safe, and that builds trust in the holder's hands.
3. Using the thumb and pointer finger on the back of the animal's neck after the animal tolerates panic by placing the mouse in the palm for 3 minutes.
4. The next step in acclimation is to hold the mouse by the scruff of its neck for 30 seconds before letting it rest on top of the cage for another 30 seconds.
5. Using the thumb and index finger of the dominant hand, I then held the mouse by its tail to practice the intranasal delivery, by pinning the lower portion of the animal's body to the cage using the middle, ring, and pinkie fingers.
6. After grabbing the bars, I gently stretch the animal out to better grasp the scruff (Fig. 4.1A).
7. In the non-dominate hand, I pinched the mouse firmly behind the neck with the thumb and middle finger (Fig. 4.1B).

8. In the shoulder blades, I make a tent by pulling up the loose skin of the upper back (I avoid pulling up muscles or pressing too hard on the ribcage/spin) (Fig. 4.1C).
9. Then, quickly I place the index finger of the non-dominant hand as close as possible to the mouse's nose while holding back on the skin. The mouse's head should not move vertically or horizontally while the thumb and middle finger were slid into the optimal position (Fig. 4.1D).

The next steps are for performing the intranasal drug delivery. I showed the technician in the CBC the full instructions and video/photos of intranasal delivery for awake mice (Hanson et al., 2013) he/she conducted the following steps:

10. He/she inverted the animal so that the ventral side faced the ceiling, and the neck faced the ground (Fig. 4.1E, and F).
11. Then He/she practiced placing a 45-degree angle micropipette close to the nostrils, once the mouse had become comfortable with the inverted intranasal grip (Fig. 4.1G).
12. As a final step, slowly He/she injected 7 µl of metformin solution /distal water into the tip so that it formed a small droplet (Fig. 4.1H), and He/she made sure the droplet was close enough to the mouse's nostrils for it to inhale. He/she held the mouse in this position for about 15 seconds, before He/she put the animal back in its cage.

13. For positive reinforcement, I gave peanut butter after each acclimation or intranasal dosage session (Fig. 4.2). Before returning an animal to its cage. I also always restored the nest to its original state and changed the gloves between cages to reduce stress (Hanson et al., 2013).

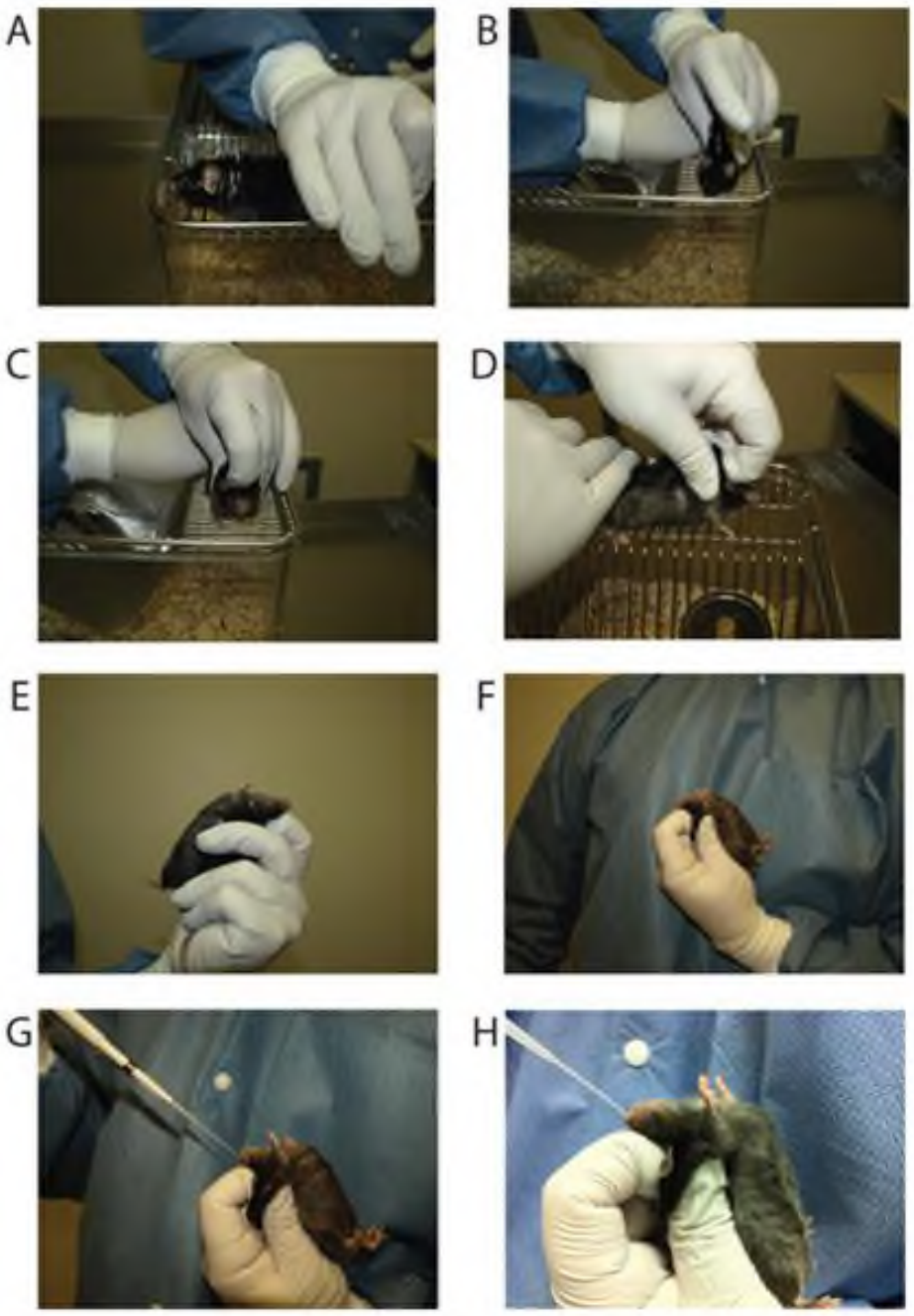

Figure 4.1: Acclimatisation and Intranasal Drug Delivery to Mice. Steps **A** to **F** represent the acclimatization of a mouse, and **G** to **H** are actual delivery. **A)** Holding and petting the mouse for around 2-3 min. **B)** Lightly pinching scruff. **C)** and **D**) Scruff the skin at the neck and shoulder. **E)** Grip for intranasal delivery. **F)** Intranasal gripping and inverting. **G)** Intranasal gripping, inverting, and delivering the drug (metformin solution) or the vehicle (sterile distilled water) to the nares. **H)** Leaving the mouse for 5 min, then intranasal gripping, inverting, and delivering to the second round (Hanson et al., 2013).

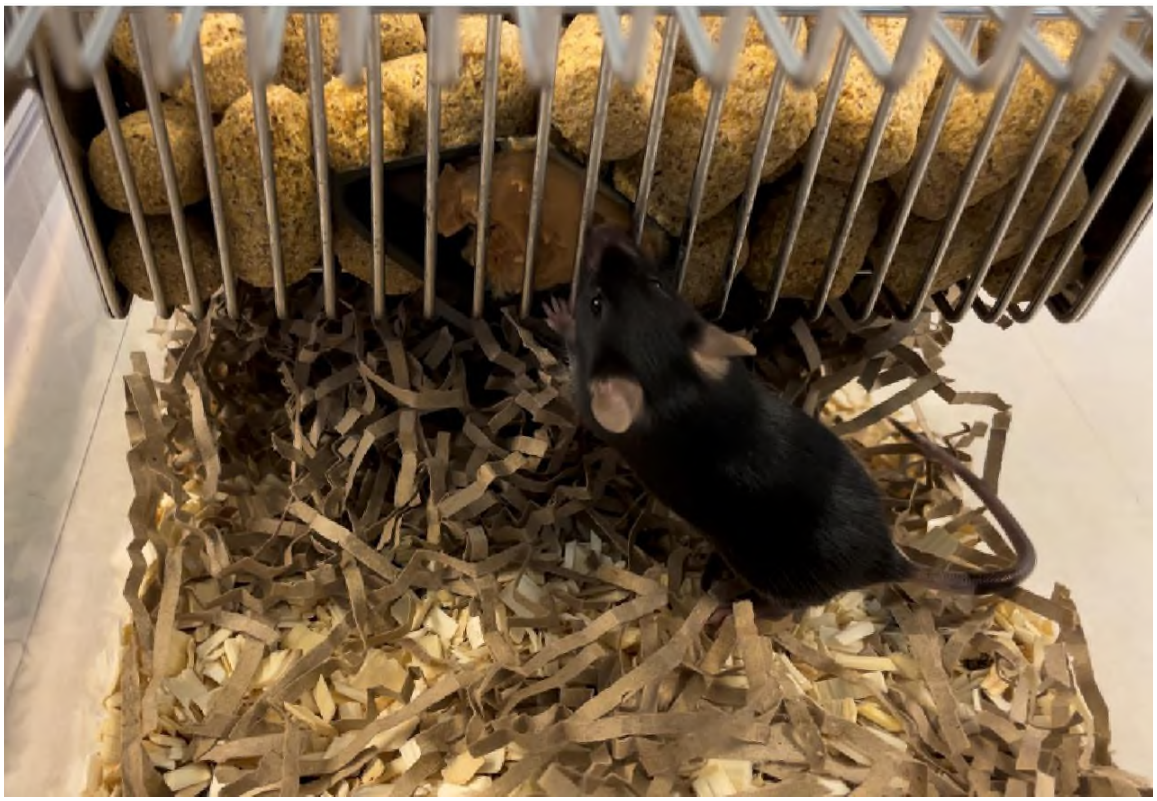

Figure 4.2: Rewarding the Mouse. A mouse was happy after treatment and started eating peanut butter before I closed the lid of the cage.

Intranasal treatment was conducted for 5 days/week for four weeks and animals were checked each day against the checklist (score sheet) (Table 4.1).

At the end of treatment, mice were anesthetized as outlined above for PFA fixation to prepare their brains for immunofluorescence staining to study the effect of the drug on the CA3 region of the hippocampus as outlined above analysed blind the images of IF staining of the metformin study as my supervisor coded the images to avoid unconscious bias while making counts and measurements.

To ensure that the hA30P mice exhibited increased neuronal activity, and neuroinflammation differences in that early stage of 1 month (the age of beginning of the treatment), I carried out immunofluorescence staining on sections hA30P mice 1 month of age before I started with metformin study using the exact the same group of antibodies I planned to use for metformin trail.

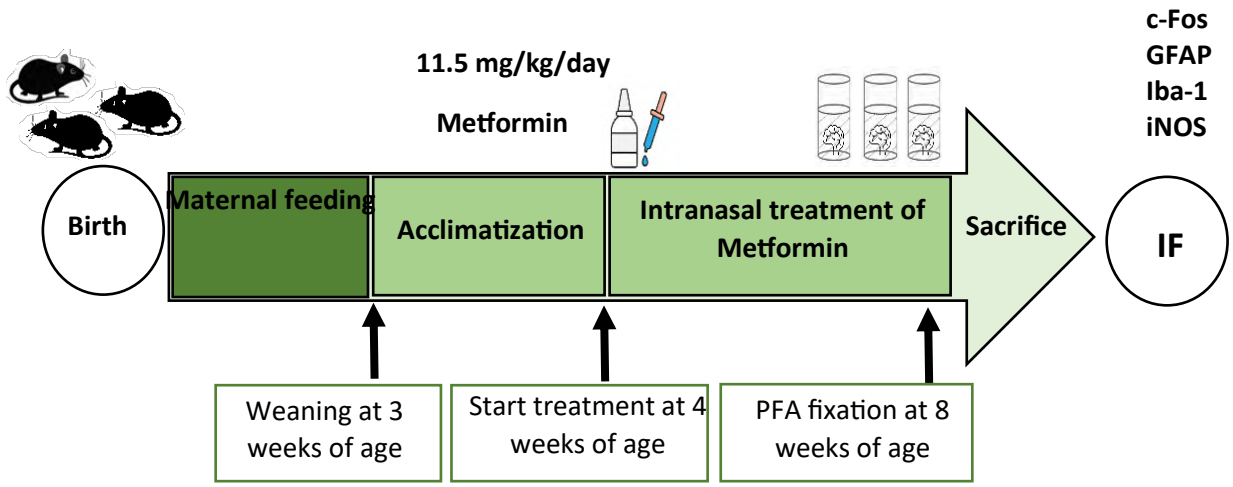

Figure 4.3: Timetable of Metformin Intranasal Delivery to Mice. After weaning, the acclimatization process ran for 10 days, then the intranasal treatment was conducted for four weeks before fixing the mice brains and preparing for immunofluorescence staining.

4.4 Results

In the previous chapter, the results revealed neuronal and neuroinflammatory changes in the CA3 region of the hippocampus in young pre-symptomatic 2-4 months hA30P mice. This chapter aimed to investigate metformin treatment intranasally in 1-month-old hA30P mice, therefore I needed first to confirm that some pathological changes were already present at this very early age.

4.4.1 Confirmation of Human α-syn Expression in the CA3 Region of the Hippocampus of Male 1-Month hA30P Mice

I first used a human α-syn antibody (Table 2.2) in IF staining to confirm if young male 1-month-old pre-symptomatic hA30P mice have detectable overexpression of mutant human α-syn in the hippocampus as previously reported (Schell et al., 2009, Kahle et al., 2000) (Fig. 4.4).

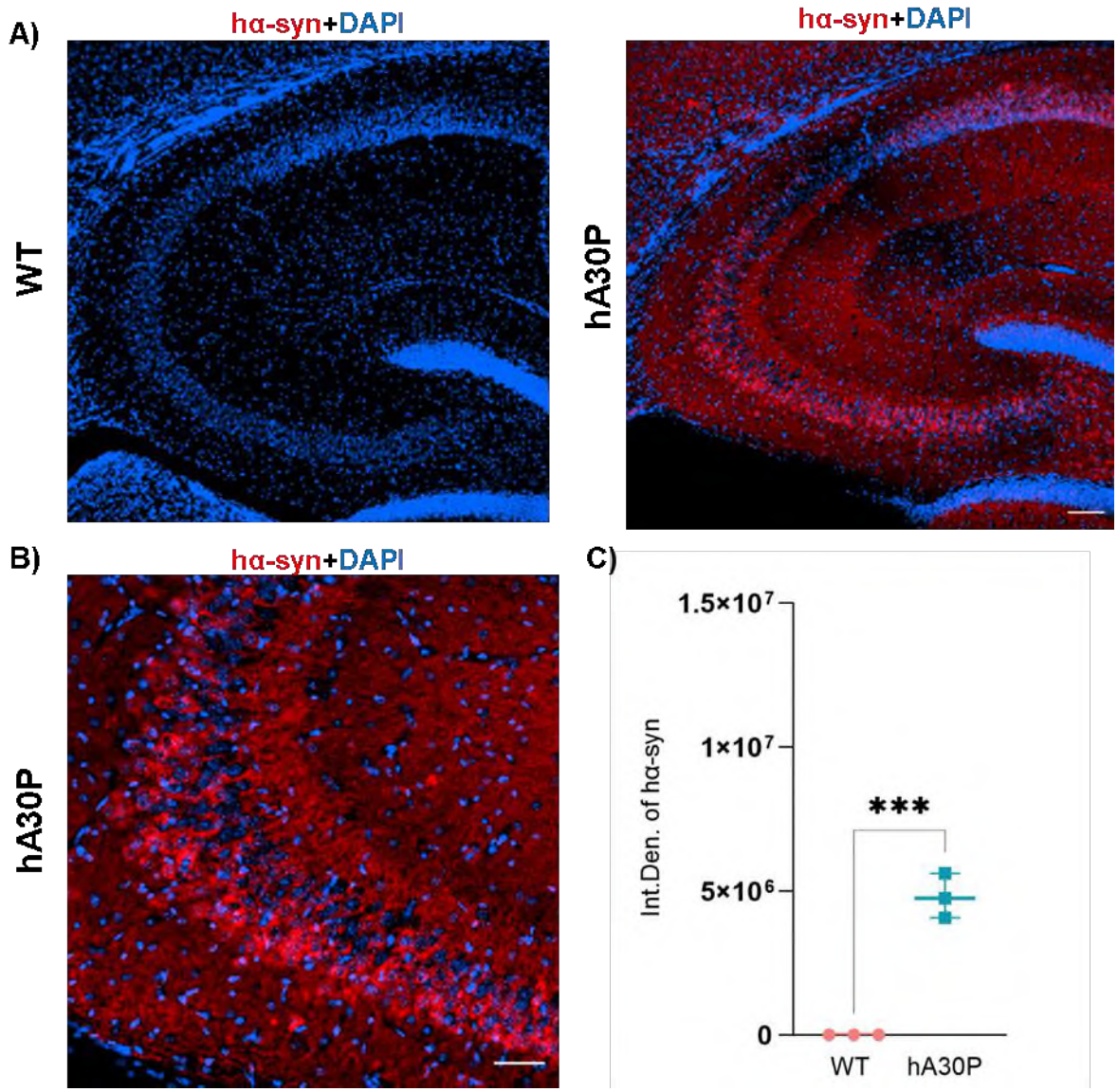

Figure 4.4: Expression of Human α-syn in the Hippocampus of Male 1 Month-old hA30P Mice. (A and B) Represents IF images. The human α-syn (red) and the nuclei (blue) (DAPI). Scale bars represent 100 µm in A and 50 µm in B. **(A)** High level of hα-syn protein overexpression in the hippocampus of 1-month-old male hA30P mice, and no expression in WT mice. **(B)** The deep layer of SP is occupied with human α-syn more than the superficial layer. **(C)** There was a significant increase ***p<0.001 in the integrated density of hα-syn IF in the CA3 region of the hA30P (N=3) compared to WT mice (N=3).

In this experiment, I used a group of male 1-month-old, hA30P versus age and sex-matched WT mice as a control group. IF staining for human α-syn confirmed the overexpression of mutant human α-syn in the hippocampus of the hA30P mice (Fig. 4.4A, and B). There was a significantly higher integrated density detected of human α-syn expressed in the CA3 region of the hA30P mice compared to WT mice. In hA30P mean integrated density was 4746442, (IQR 4074567 – 5611184, n/N = 10 sections/3 mice) versus WT mean integrated density of 235.8, (IQR 233.6 - 275.1, n/N = 9 sections/3 mice. ***$p<0.001$, Unpaired t-test) (Fig. 4.4C).

The results showed there was a clear laminar distribution for the expression of the human α-syn in the layers of the hippocampus of the hA30P mice. However, although I did not calculate the values for the laminar distribution, SP qualitatively showed a higher level of human α-syn expression in the pyramidal cell soma in comparison to SO and SR layers (Fig. 4.4B). Interestingly, as found in 2-4 months hA30P mice (Fig. 3.1C), we also found that there was a greater expression of human α-syn in the deep layer of the SP compared to the superficial layer of the SP in the hippocampus of the hA30P mice.

4.4.2 Increase in c-Fos+ nuclei/mm^2 in the CA3 Region of the Hippocampus of 1 Month old male hA30P Mice

I used the c-Fos antibody (Tables 2.2) for IF staining to indirectly detect the changes in neuronal activity (Carrion et al., 1999, Lyons and West, 2011) in male 1-month-old hA30P mice that may have occurred due to the pathologic effects of expression of mutant human α-syn in the hippocampi at this early age (Fig. 4.5).

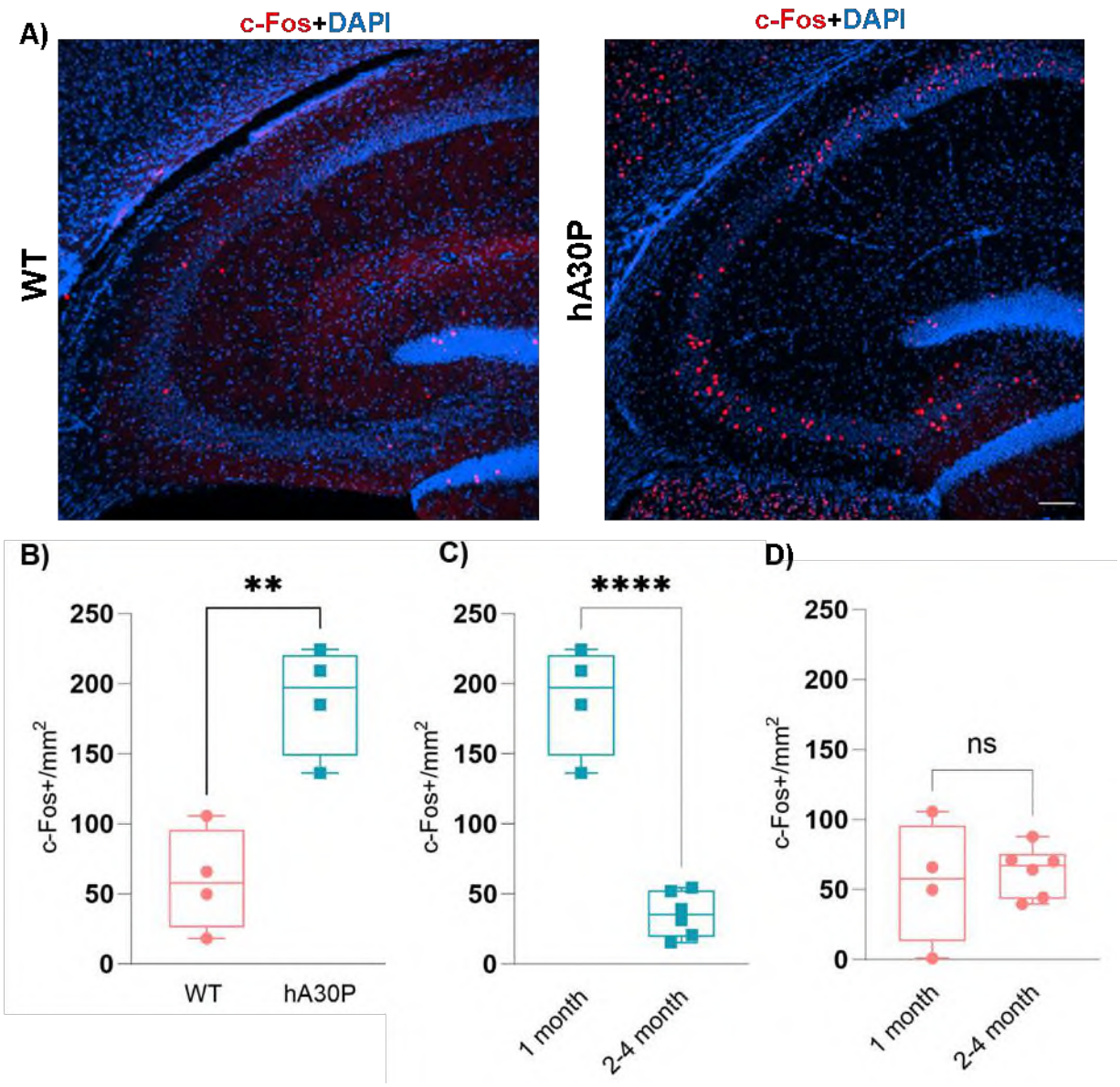

Figure 4.5: Increase in c-Fos+ nuclei/mm^2 in the CA3 Region of the Hippocampus of Male 1 Month hA30P Compared to WT Mice. (A) Representatives IF images. The c-Fos+ protein (red) and the nuclei (blue) (DAPI). Scale bars represent 100 µm. **(A)** Increase in c-Fos+ protein in the CA3 region of the hippocampus of 1-month-old male hA30P mice compared to sex and age-matched WT mice. **(B)** There was a significant increase ** $p<0.01$ in the count of c-Fos+ nuclei/mm^2 in hA30P (N=4) compared to WT mice (N=4). **(C)** There was no significant difference $p>0.05$ in c-Fos+ nuclei/mm^2 in males 2-4 months old (N=6) compared to 1-month WT mice (N=4). **(D)** There was a significant decrease ****$p<0.0001$ in c-Fos+ nuclei/mm^2 in male 2-4 months old hA30P mice (N=6) compared to 1 month age (N=4).

In this IF staining, I used c-Fos antibody in a group of male 1-month-old hA30P mice and sex and age-matched WT mice to detect if there were neuronal changes in the CA3 region of the hippocampus at this early age. Interestingly at 1 month of age the IF staining result revealed a clear increase in the number of nuclei that expressed c-Fos+ protein (red) in the CA3 region of the hippocampus of hA30P mice compared to WT mice (Fig. 4.5A, and B). This was the opposite of the changes observed in hA30P mice aged 2-4 months old when c-Fos was down-regulated (Fig. 3.2A, and B). In hA30P mean c-Fos+ nuclei/mm^2 was 197.2, (IQR 148.6 - 220.6, n/N = 8 sections/4 mice) versus WT mean c-Fos+ nuclei/mm^2 of 57.9, (IQR 26.11 - 95.75, n/N = 8 sections/4 mice. **p<0.01, Unpaired t-test) (Fig. 4.5B). This increase in c-Fos at this early stage could be due to early excitability in juvenile mice, so I went on to compare the results between mice aged 1 and 2-4 months.

The result showed a significant decrease in the count of c-Fos+ nuclei/mm^2 in the CA3 region of the hippocampus of male 2-4 months hA30P mice compared to male 1-month hA30P mice. In 2-4-month-old mean c-Fos+/mm^2 count was 35.31, (IQR 19.33 - 52.59, n/N = 23 sections/6 mice) versus 1-month-old mean c-Fos+/mm^2 of 197.2, (IQR 148.6 - 220.6, n/N = 8 sections/4 mice. ****p<0.0001, Unpaired t-test) (Fig. 3.5C).

In contrast, the result of the comparison of 1-month to 2-4 months of WT mice showed there was no significant difference in the count of c-Fos+ nuclei/mm^2 in the CA3 region of the hippocampus in the two age groups (Fig. 3.5D). In 2 - 4 months old WT mice the mean c-Fos+/mm^2 count was 67.22, (IQR 43.22 - 75.53, n/N = 23 sections/6 mice) versus 1-month mean c-Fos+/mm^2 count of 57.92, (IQR 13.22 - 95.75, n/N = 8 sections/4 mice. p>0.01, Unpaired t-test). These data, therefore, show a biphasic change in c-Fos in hA30P mice, which is increased at one month but decreased by 2-4 months of age compared to the control.

4.4.2 Increase in Reactive Astrocytes in the CA3 Region of the Hippocampus of 1-month Old Male hA30P Mice

The data outlined above show expression of mutant human α-syn and changes in neuronal activity in the CA3 ROI of male 1-month hA30P mice. Therefore, the next aim was to determine whether there was immunohistological evidence of gliosis at this early age. I stained a group of 1-month hA30P male mice and sex and age-matched

WT mice for GFAP antibody (Table 2.2) to detect activated astrocytes (Rannikko et al., 2015, Clarke et al., 2018) (Fig. 4.6).

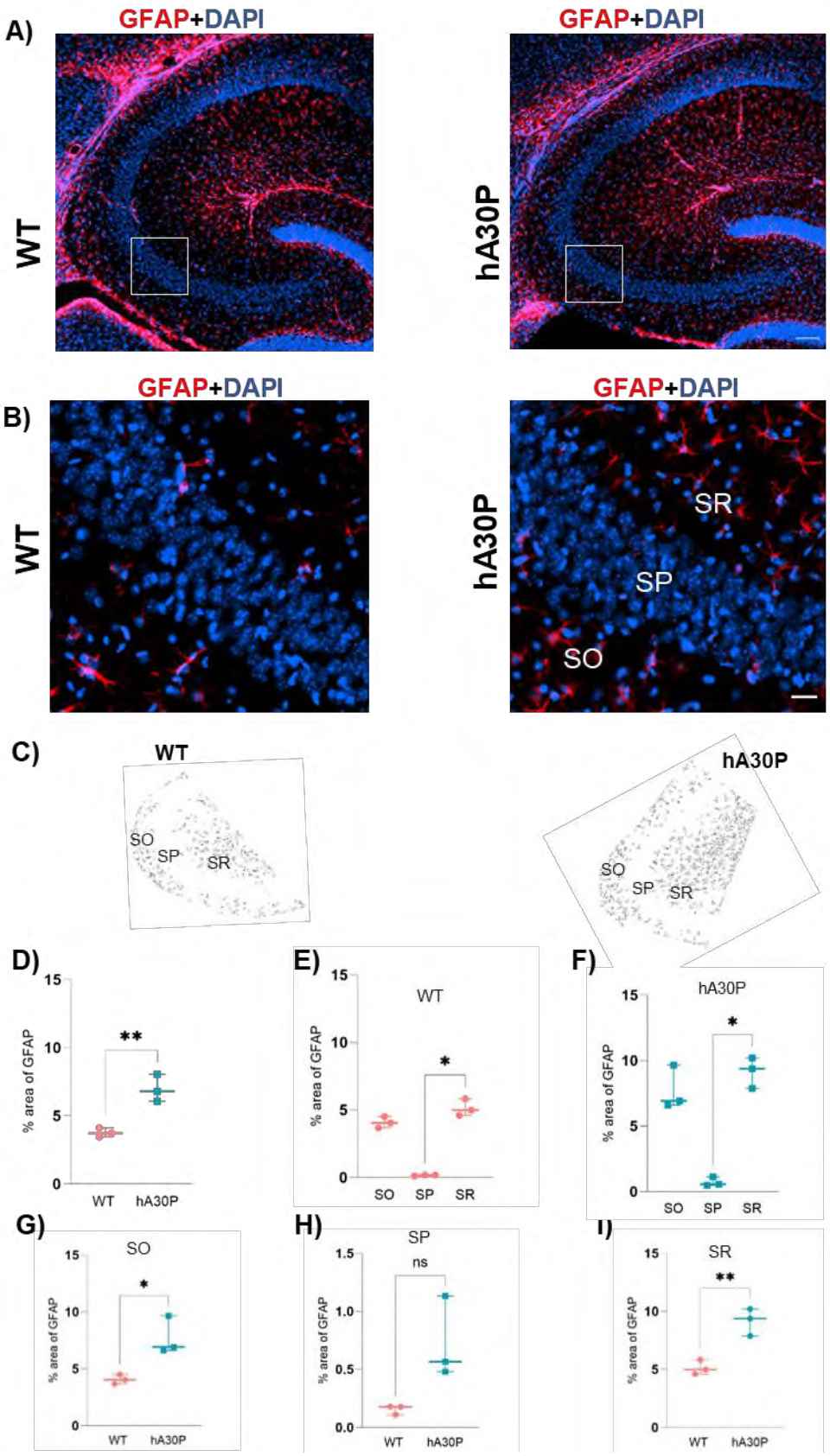

Figure 4.6: Increase in % Area Occupied by Reactive Astrocytes in the CA3 Region of the Hippocampus of 1 Month old Male hA30P Mice Compared to WT. (A, and B) Representative IF images. The reactive astrocytes (red) and the nuclei (blue) colour (DAPI). Scale bars represent 100 µm in A and 25 µm in B. **(A, and B)** Increase in reactive astrocytes in the CA3 region of the hippocampus of 1 month old male hA30P mice compared to WT mice. **(C)** FIJI drawing showing the laminar distribution of GFAP+ cells were less localized within the SP in both the hA30P and WT mice. **(D)** There was a significant increase **p<0.01 in the % area occupied by GFAP in hA30P (N=3) compared to WT mice (N=3). The laminar distribution of the GFAP showed a significant increase *p<0.05 in the % area occupied by GFAP in the SR compared to the SP in both WT mice (N=3). **(E)**, and hA30P mice (N=3). **(F)**. **(G)** There is a significant increase *p<0.05 in the % area occupied by GFAP in the SO in hA30P (N=3) compared to WT mice (N=3). **(H)** There was no significant difference p>0.05 in the % area occupied by GFAP in the SP in hA30P (N=3) compared to WT mice (N=3). **(I)** There was a significant increase **p<0.01 in the % area occupied by GFAP in the SR in hA30P (N=3) compared to WT mice (N=3).

Even at this very young age the result of IF staining with GFAP antibody confirmed high expression of reactive astrocytes in the CA3 region of the hippocampus in hA30P mice compared to the control (Fig. 4.6A, B, and D). There was a significantly higher % area of the CA3 occupied by GFAP immunofluorescence in hA30P mice compared to WT when measured across the whole of the CA3 region. In hA30P mice, the % area occupied by GFAP immunofluorescence had a mean of 6.8% per section (IQR 6.1 – 8.1, n/N = 10 sections/3), versus the WT mean of 3.7, (IQR 3.5 - 4.1, n/N = 12 sections/3. **p<0.01, Unpaired t-test).

Like the male 2-4 months hA30P mice (Chapter 3 Fig. 3.6, and 3.7), the results of the IF images and the FIJI analysis showed there was an interesting laminar distribution for the expression of reactive astrocytes in the layers of the hippocampus where SO and SR layers showed a high level of GFAP expression in comparison to the SP layer (Fig. 4.6B, and C). The laminar distribution of the GFAP in the 1-month male WT mice showed a significant increase in the % area occupied by GFAP only in the SR compared to the SP layer (Fig. 4.6E). In SR mean % area was 4.982, (IQR 4.6 – 5.8, n/N = 12 sections/3 mice) versus SP % area mean of 0.2, (IQR 0.1 – 1.2, n/N = 12 sections/3 mice. *p<0.05; Friedman test) (Fig. 4.6F). The laminar distribution of the GFAP in the hA30P mice also showed a significant increase in the % area occupied by GFAP in the SR compared to the SP. In SR mean % area was 9.4, (IQR 7.8 – 10.2, n/N = 10 sections/3 mice) versus SP mean % area of 0.6, (IQR 0.5 – 1.1, n/N = 10 sections/3 mice. *p<0.05; Friedman test).

When I compared each layer between WT and hA30P mice, there was a significant increase in the % area occupied by reactive astrocytes in the SO layer of the male 1-month hA30P mice in comparison to sex and age-matched WT mice (Fig.

4.6G). In hA30P mean was 6.9, (IQR 6.6 – 9.7, n/N = 10 sections/3 mice) versus WT mean of 4, (IQR 3.8 – 4.5, n/N = 12 sections/3 mice. *p<0.05, Unpaired t-test). However, there were no significant differences in the SP layer in hA30P compared to WT mice (Fig. 4.6H). In hA30P mean was 0.6, (IQR 0.5 – 1.1, n/N = 10 sections/3 mice) versus the WT mean of 0.2, (IQR 0.1 – 0.2, n/N = 12 sections/3 mice. p>0.05, Unpaired t-test). Finally, there was also a significant increase in the % area occupied by reactive astrocytes in the SR layer of hA30P mice compared to WT mice (Fig. 4.6I). In hA30P mean was 9.4, (IQR 7.8 – 10.2, n/N = 10 sections/3 mice) versus WT mean of 4.9, (IQR 4.6 – 5.8, n/N = 12 sections/3 mice. **p<0.001, Unpaired t-test). Overall, these data show that even at 1 month of age there was evidence of increased reactive astrocytes in hA30P mice like that observed in the 2-4 months cohort of mice.

4.4.4. Increase in % Area Occupied by Microglia in the CA3 Region of the Hippocampus of Male 1-Month hA30P Mice

To investigate whether there was a change in microglia due to the pathologic effect of human α-syn (Crotti and Ransohoff, 2016) in the CA3 region of the hippocampus of juvenile males, I used a group of male 1-month hA30P mice and conducted IF staining microglia by Iba-1 antibody (Table 2.2) (Fig. 4.7).

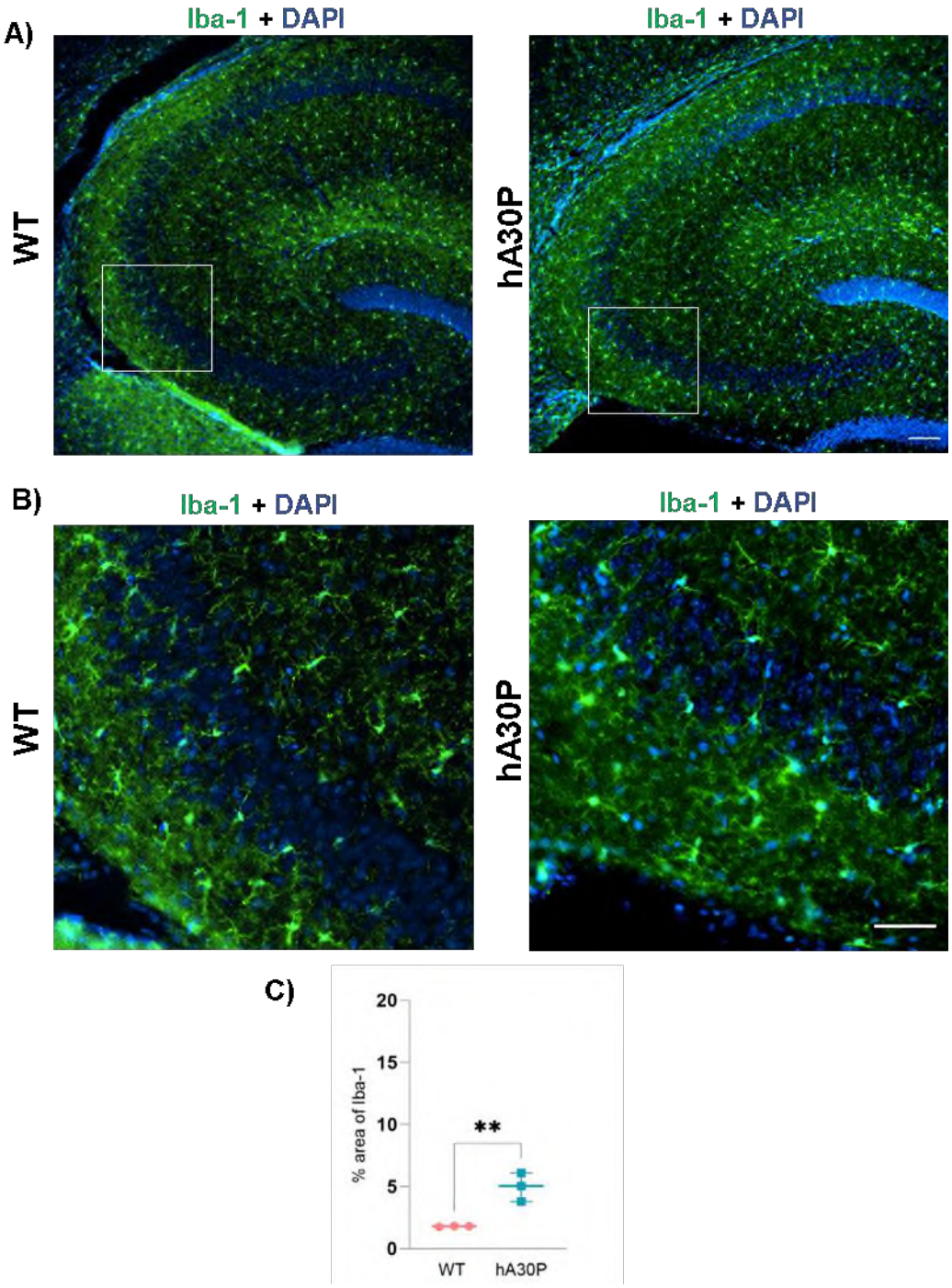

Figure 4.7: Increase in % Area Occupied by Microglia in the CA3 Region of the Hippocampus of Male 1 Month hA30P Compared to WT Mice. The microglia (green) and the nuclei (blue) (DAPI). Scale bars represent 100 µm in A and 50 µm in B. **(A and B)** more microglia with Iba-1 expression in hA30P mice compared to WT mice. **(C)** There was a significant increase **p <0.01 in the % area occupied by Iba-1 in the CA3 region of the hippocampus of hA30P mice (N=3) compared to WT mice (N=3).

The IF staining with Iba-1 antibody showed there was higher expression of microglia in the CA3 region of the hippocampus of male 1-month hA30P mice in comparison to the control mice (Fig. 4.7A, B, and C). There was a significantly higher level of % area occupied by Iba-1 in the hA30P compared to WT mice. In hA30P mean % area occupied by Iba-1 was 5.0, (IQR 3.8 – 6.1, n/N = 10 sections/3 mice) versus WT mean % area of 1.8, (IQR 1.7 – 1.8, n/N = 12 sections/3. **p<0.01, Unpaired t-test).

4.4.5. Increase in the Reactive Microglia in the CA3 Region of the Hippocampus of Male 1-Month hA30P Mice

Neuroinflammation concurrent with brain injury occurs to repair nearby neurons (Crotti and Ransohoff, 2016). I also conducted co-staining of microglia using Iba-1 and iNOS antibodies (Tables 2.2) to differentiate pro-inflammatory from anti-inflammatory microglia because in the pro-inflammatory microglia express iNOS which is the enzyme involved in the inflammation pathway (Dai et al., 2011, Sierra et al., 2014) (Fig. 4.8).

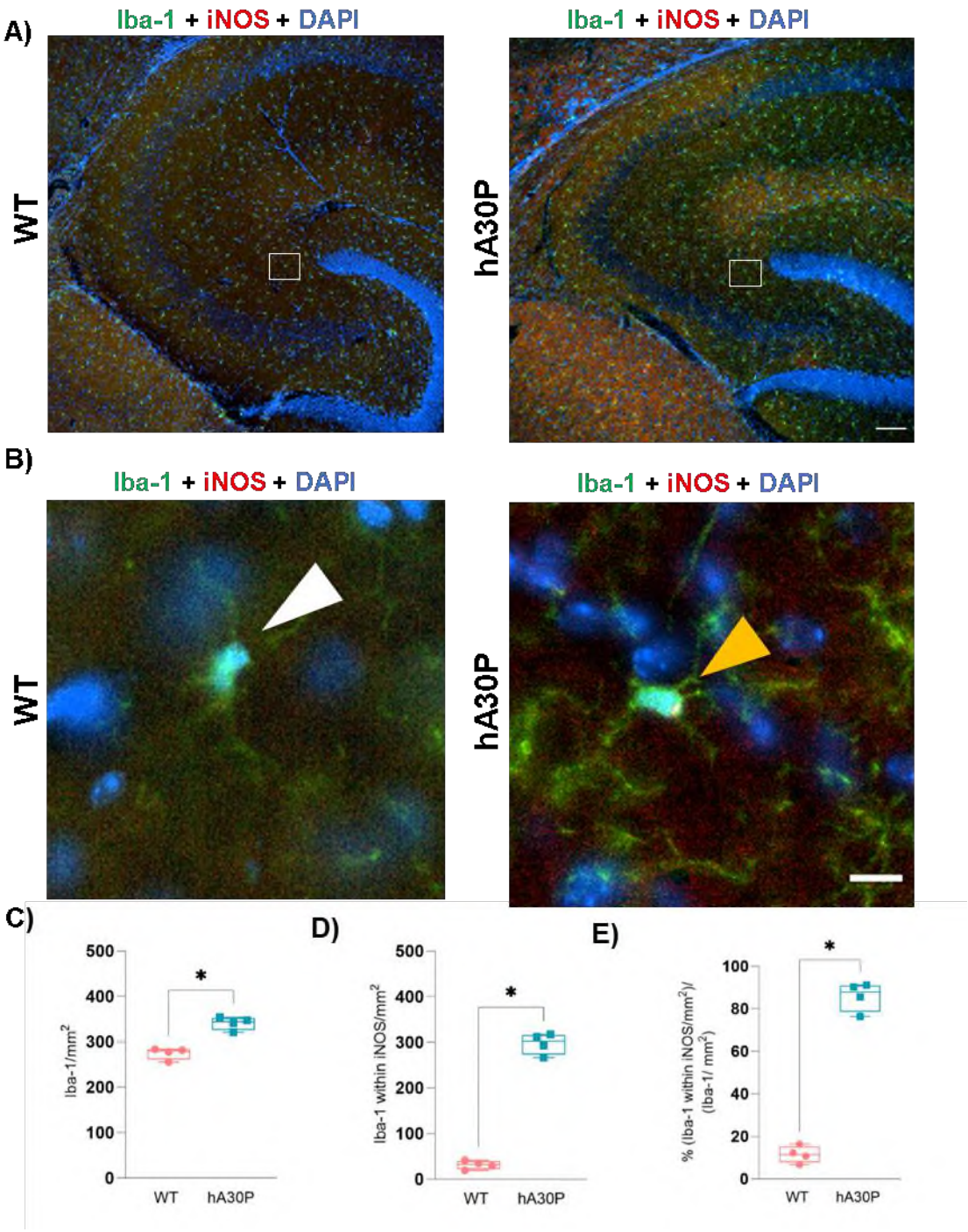

Figure 4.8: Increase in the Count of Reactive Microglia in the CA3 Region of the Hippocampus of Male 1 Month old hA30P Compared to WT mice. (A and B) Representative IF images. Iba-1 (green), iNOS (red), and the nuclei (blue) (DAPI). Scale bars represent 100 µm in A and 10 µm in B. **(A)** Increase in a total count of Iba-1/mm^2 in hA30P compared to WT mice. **(B)** Increase in the Iba-1 microglia with iNOS/mm^2 in hA30P compared to WT mice (the orange arrow points to microglia exhibiting punctate staining for iNOS in the soma). **(C)** There was a significant increase *p<0.05 in the total count of Iba-1/mm^2 in hA30P (N=4) compared to WT mice (N=4). **(D)** There was a significant increase *p<0.05 in the Iba-1 with iNOS/mm^2 in hA30P (N=4) compared to WT mice (N=4). **(E)** There was a significant increase *p<0.05 in % (Iba-1 with iNOS/mm^2)/ (Iba-1/mm^2) in hA30P (N=4) compared to WT mice (N=4).

I used a group of male 1-month-old hA30P mice versus age and sex-matched WT mice as a control group. The results of IF co-staining of Iba-1 and iNOS antibodies showed there was a significant increase in the total count of microglia/mm^2 in the CA3 region of the hippocampus of the hA30P mice compared to WT mice (Fig. 4.8A, and C). In hA30P mice the median count of microglia was 344, (IQR 326.0 – 352.4, n/N = 14 sections/4 mice) versus the WT median count of microglia of 279.7, (IQR 261.1 – 282.9, n/N = 11 sections/4 mice. *p<0.05, Mann Whitney test).

There was also a significant increase in the count of reactive microglia that co-expressed iNOS in the CA3 region of the hippocampus of the hA30P mice compared to WT mice (microglia indicated by white arrow were without iNOS and those with iNOS were indicated by orange arrow) (Fig. 4.8B and D). In hA30P mice the median count of Iba-1 with iNOS/mm^2 positive cells was 302.3, (IQR 273 – 315.9, n/N = 14 sections/4 mice) versus WT median Iba-1 with iNOS/mm^2 of 32.1, (IQR 21.9 – 39.9, n/N = 11 sections/4 mice. *p<0.05, Mann Whitney test).

Also, the result showed a significant increase in the proportion of Iba-1 with iNOS/mm^2)/(Iba-1/mm^2) in hA30P mice compared to WT mice (Fig. 4.8E). In hA30P median % was 87.9, (IQR 78.7 – 90.9, n/N = 14 sections/4 mice) versus WT median % of 11.5, (IQR 7.8 – 15.3, n/N = 11 sections/4 mice. *p<0.05, Mann Whitney unpaired test). Therefore, these data show that even at 1 month of age there was evidence of increased reactive microglia in hA30P mice similar to what was seen in the 2-4 months old hA30P mice.

4.4.6. Morphological Changing of Reactive Astrocytes and Microglia of hA30P Mice

I did not quantify the morphological changes in glial cells that are associated with gliosis and neuroinflammation (Liddelow and Barres, 2017, Torres et al., 2021). However, I did observe some interesting morphological changes occurring in reactive astrocytes and reactive microglia in the CA3 region of the hippocampus of male and female hA30P mice at the different ages (1-month – 4 months) studied in the thesis. Although I selected an age range of mice of 2-4 months as one cohort, I noticed morphological changes between the mice that were closer in age to 2 months compared to those that were close to 4 months of age (Fig. 4.9).

Imaging of the reactive astrocytes and microglia in the CA3 region of the hippocampus of hA30P mice of 1-4 months of age compared to WT mice revealed changes in the morphology in microglia and astrocytes reflecting the severity of neuroinflammation through age (Fig. 4.9A, and B). I also noted that changes in the reactive microglia occurred before the changes in the astrocytes at the same age.

In addition to the increase in the count of microglia in male hA30P at 1 month as outlined above, there was an increase in ramification and length of the processes (white arrow). While the reactive astrocytes still retained normal ramified shape and qualitatively did not look different to those in seen WT mice at this age (blue arrow).

The reactive microglia at 2+ months exhibited an increase in the thickness of their processes, and an enlargement in soma size compared to WT (orange arrow). The reactive astrocytes at the same age showed clear morphological changes with increasing length and ramification of their process, in addition to an increase in the count and crowding toward both boundaries of SP compared to WT mice (green arrow).

The reactive microglia in the hA30P mice for those close to 4 months showed a loss of processes, an enlargement in soma size, and transformation into amoeboid and Jellyfish shapes (red arrow), also they decreased in number. While the reactive astrocytes exhibited increases in their number and length, enlargement in soma, and proximity to the SP (pink arrow).

These changes might indicate an increase in the severity of the neuroinflammation in the CA3 region of hA30P mice, compared to WT, in response to the continuous accumulation of hα-syn and its pathological effects and would be interesting to explore further in future studies.

However, using different analysis program as IMRS instead Fiji, or using stereological tests is recommended in future work as they provided quantification for the dimensions in 3D.

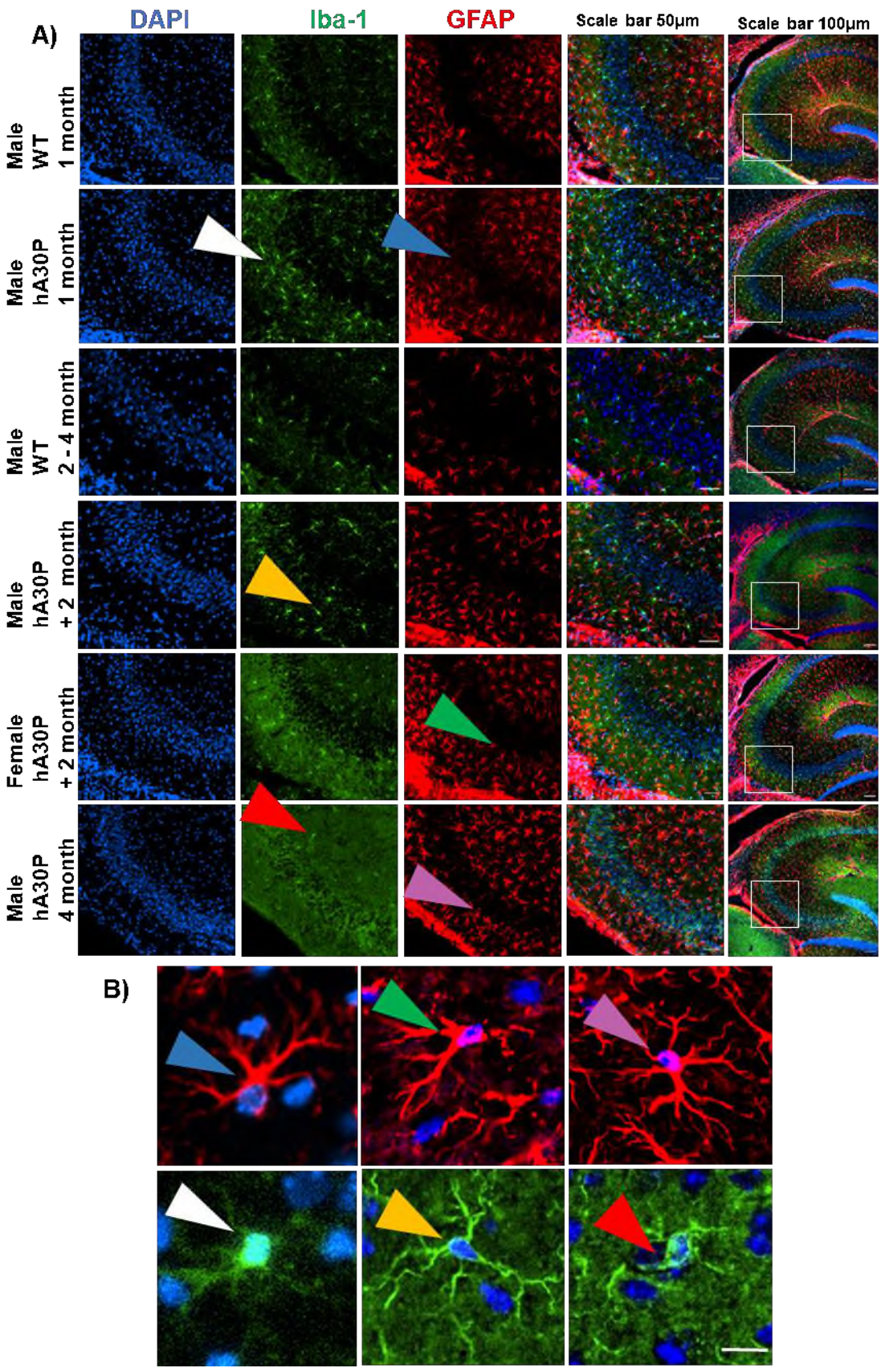
A)
DAPI
Iba-1
GFAP
Scale bar 50µm
Scale bar 100µm
Male WT 1 month
Male hA30P 1 month
Male WT 2 - 4 month
Male hA30P + 2 month
Female hA30P + 2 month
Male hA30P 4 month
B)

Figure 4.9: Morphological Changing of Reactive Astrocytes and Microglia in CA3 Region of Hippocampus of hA30P Mice. Representative IIF images of hippocampi from male and female hA30P mice aged 1-4 months. (DAPI) labelled nuclei with blue, (Iba-1) labelled microglia with green, and (GFAP) labelled reactive astrocytes with red. (**A)** Representative IF image with a scale bar of 50 and 100 µm. (**B)** Represents an expanded view of the microglia and astrocytes indicated by the coloured arrow in A. Microglia started increasing in the count, and morphological changes gradually occurred including an increase in ramification and length of the processes **(white, and orange arrow)** followed by the loss of processes and formation of amoeboid and Jellyfish shapes **(red arrow)** gradually with age. Activation of the astrocyte's response came after the microglia, they gradually increased in the count, ramification, and length of processes **(blue arrow)**, and crowded closer to the SP layer **(green, and pink arrows)**, **(pink arrow)** more, and more depending on the severity/age of hA30P mice.

4.4.7. Intranasal Metformin Treatment Did Not Affect Mouse Body Weight

Benefits of metformin medication for weight loss have been demonstrated in large cohort studies (Yerevanian and Soukas, 2019). Ekmark-Lewen et al., 2018, had previously reported that there was no difference in body weight between hA30P and WT mice at the same age. The average body weight of the mice used in the current study for both hA30P and WT mice was 20 grams at 1 month of age at the start of metformin treatment consistent with other studies (Ekmark-Lewén et al., 2018). To detect the effect of the 11.5 mg/kg/day dosage of intranasal metformin treatment on body weight gain during the four weeks (5 days/week) course of therapy (Fig. 4.10) I weighed the mice daily and recorded that in a score sheet (Table 4.1). I also scored the condition of the coat, breathing, and posture of the mice as indicators of the general health state of the mice under the supervision of the veterinarian at the CBC.

Table 4.1: Score Sheet for Used Mice in Metformin Study

A)

Day	hA30P Vehicle 1				hA30P Vehicle 2				hA30P Vehicle 3				hA30P Metformin 1				hA30P Metformin 2				hA30P Metformin 3			
	coat	breathing	posture	weight	coat	breathing	posture	weight	coat	breathing	posture	weight	coat	breathing	posture	weight	coat	breathing	posture	weight	coat	breathing	posture	weight
1	0	0	0	18.2	0	0	0	17.8	0	0	0	20	0	0	0	17	0	0	0	18	0	0	0	19.3
2	0	0	0	18.9	0	0	0	17.9	0	0	0	21	0	0	0	18	0	0	0	18	0	0	0	19.8
3	0	0	0	18.7	0	0	0	17.9	0	0	0	21	0	0	0	18	0	0	0	19	0	0	0	19.4
4	0	0	0	18.8	0	0	0	17.8	0	0	0	21	0	0	0	18	0	0	0	19	0	0	0	19.5
5	0	0	0	19.1	0	0	0	18.5	0	0	0	21	0	0	0	19	0	0	0	19	0	0	0	19.5
6	0	0	0	19.1	0	0	0	18.5	0	0	0	21	0	0	0	19	0	0	0	19	0	0	0	19.5
7	0	0	0	18.9	0	0	0	18.2	0	0	0	21	0	0	0	18	0	0	0	19	0	0	0	19.5
8	0	0	0	19.7	0	0	0	19.3	0	0	0	21	0	0	0	20	0	0	0	20	0	0	0	20.4
9	0	0	0	20	0	0	0	20	0	0	0	22	0	0	0	20	0	0	0	20	0	0	0	20.5
10	0	0	0	20.2	0	0	0	19.9	0	0	0	22	0	0	0	20	0	0	0	20	0	0	0	20.5
11	0	0	0	20.5	0	0	0	20.2	0	0	0	22	0	0	0	20	0	0	0	20	0	0	0	21.3
12	0	0	0	21	0	0	0	21	0	0	0	22	0	0	0	20	0	0	0	20	0	0	0	21.1
13	0	0	0	20.6	0	0	0	21	0	0	0	22	0	0	0	21	0	0	0	21	0	0	0	21.9
14	0	0	0	21	0	0	0	21.4	0	0	0	22	0	0	0	21	0	0	0	21	0	0	0	21.9
15	0	0	0	21.2	0	0	0	21.3	0	0	0	23	0	0	0	22	0	0	0	21	0	0	0	21.8
16	0	0	0	22	0	0	0	21.8	0	0	0	23	0	0	0	22	0	0	0	21	0	0	0	22.4
17	0	0	0	22.1	0	0	0	22.2	0	0	0	23	0	0	0	22	0	0	0	22	0	0	0	22.4
18	0	0	0	21.9	0	0	0	21.9	0	0	0	23	0	0	0	22	0	0	0	22	0	0	0	22.4
19	0	0	0	21.7	0	0	0	22.4	0	0	0	23	0	0	0	23	0	0	0	22	0	0	0	22.4
20	0	0	0	21.9	0	0	0	22.5	0	0	0	23	0	0	0	23	0	0	0	22	0	0	0	23
21	0	0	0	22.2	0	0	0	23.2	0	0	0	23	0	0	0	23	0	0	0	22	0	0	0	23.5
22	0	0	0	21.3	0	0	0	23.5	0	0	0	24	0	0	0	23	0	0	0	22	0	0	0	23.5
23	0	0	0	22.4	0	0	0	23.3	0	0	0	24	0	0	0	23	0	0	0	22	0	0	0	23.5
24	0	0	0	22	0	0	0	23.5	0	0	0	24	0	0	0	23	0	0	0	22	0	0	0	23.9
25	0	0	0	22.3	0	0	0	23.5	0	0	0	24	0	0	0	23	0	0	0	22	0	0	0	23.9

B)

Day	WT Vehicle 1				WT Vehicle 2				WT Vehicle 3				WT Metformin 1				WT Metformin 2				WT Metformin 3			
	coat	breathing	posture	weight	coat	breathing	posture	weight	coat	breathing	posture	weight	coat	breathing	posture	weight	coat	breathing	posture	weight	coat	breathing	posture	weight
1	0	0	0	18.4	0	0	0	18.2	0	0	0	14	0	0	0	19	0	0	0	17	0	0	0	14.1
2	0	0	0	18.5	0	0	0	18.5	0	0	0	14	0	0	0	19	0	0	0	17	0	0	0	14.2
3	0	0	0	18.6	0	0	0	18.6	0	0	0	14	0	0	0	19	0	0	0	17	0	0	0	15.3
4	0	0	0	20	0	0	0	18.7	0	0	0	15	0	0	0	21	0	0	0	18	0	0	0	16
5	0	0	0	20.5	0	0	0	19.2	0	0	0	16	0	0	0	20	0	0	0	18	0	0	0	16.6
6	0	0	0	20.2	0	0	0	19.9	0	0	0	18	0	0	0	20	0	0	0	19	0	0	0	18.8
7	0	0	0	20.4	0	0	0	21.1	0	0	0	18	0	0	0	20	0	0	0	21	0	0	0	18.6
8	0	0	0	20.5	0	0	0	20	0	0	0	18	0	0	0	21	0	0	0	19	0	0	0	18.2
9	0	0	0	20.7	0	0	0	19.8	0	0	0	19	0	0	0	21	0	0	0	19	0	0	0	19.5
10	0	0	0	20.6	0	0	0	20.1	0	0	0	19	0	0	0	20	0	0	0	20	0	0	0	20.2
11	0	0	0	20.8	0	0	0	21	0	0	0	20	0	0	0	20	0	0	0	21	0	0	0	20.4
12	0	0	0	21.3	0	0	0	21.8	0	0	0	20	0	0	0	20	0	0	0	21	0	0	0	20.4
13	0	0	0	21.2	0	0	0	21.7	0	0	0	21	0	0	0	20	0	0	0	22	0	0	0	21.2
14	0	0	0	21.2	0	0	0	21.4	0	0	0	21	0	0	0	21	0	0	0	21	0	0	0	21.3
15	0	0	0	21.1	0	0	0	21.5	0	0	0	22	0	0	0	21	0	0	0	21	0	0	0	21.9
16	0	0	0	21.3	0	0	0	21.9	0	0	0	22	0	0	0	21	0	0	0	21	0	0	0	22.3
17	0	0	0	22	0	0	0	21.9	0	0	0	23	0	0	0	21	0	0	0	22	0	0	0	23.4
18	0	0	0	21.1	0	0	0	22	0	0	0	23	0	0	0	21	0	0	0	21	0	0	0	23.6
19	0	0	0	22	0	0	0	22	0	0	0	23	0	0	0	21	0	0	0	22	0	0	0	23.3
20	0	0	0	21.5	0	0	0	22.1	0	0	0	22	0	0	0	21	0	0	0	22	0	0	0	23
21	0	0	0	21.9	0	0	0	22.4	0	0	0	24	0	0	0	22	0	0	0	22	0	0	0	23.4
22	0	0	0	22	0	0	0	22.3	0	0	0	24	0	0	0	22	0	0	0	22	0	0	0	23.7
23	0	0	0	22.4	0	0	0	22.4	0	0	0	24	0	0	0	22	0	0	0	22	0	0	0	23.9

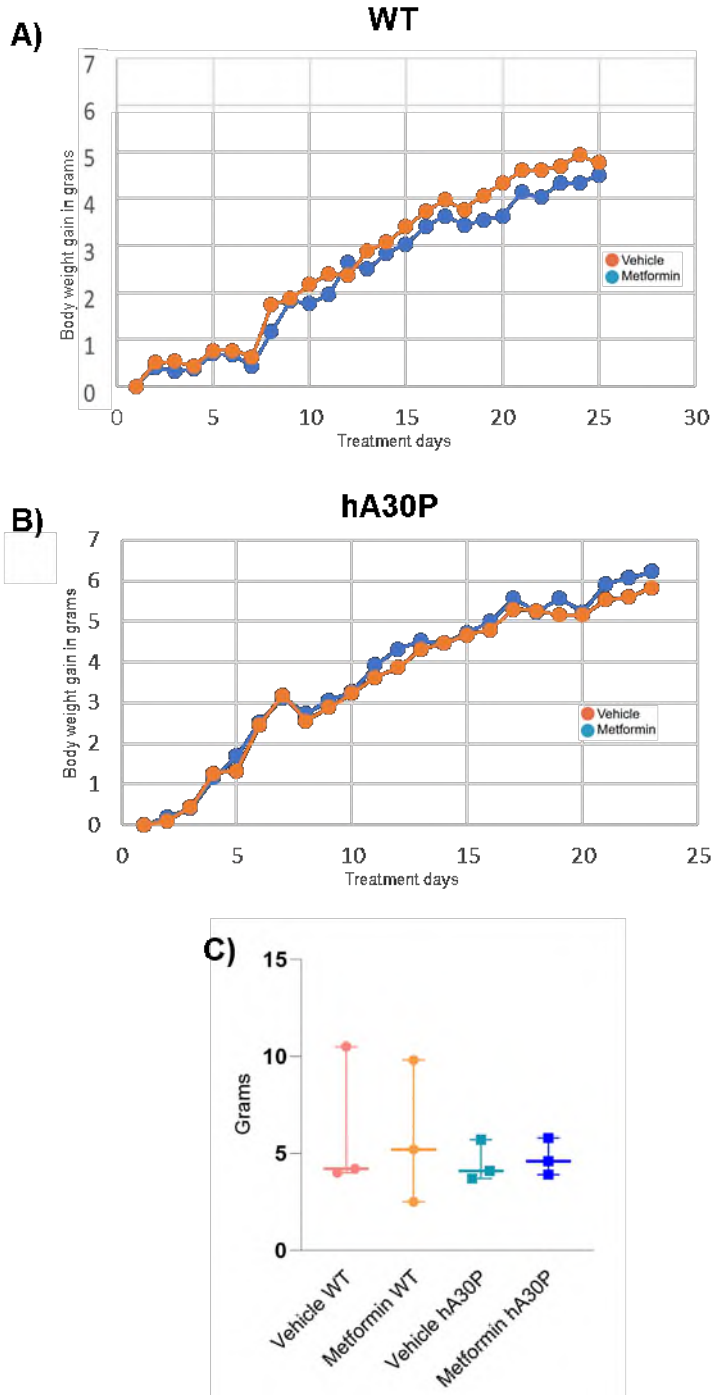

Figure 4.10: Effect of Intranasal Metformin on Weight Gain during Treatment. (A and B) The charts show a normal, gradual increase in body weight of the mice used during the study, **(A)** WT mice (N=3), and **(B)** hA30P mice (N=3). **(C)** There was no significant difference ($p>0.05$) in the body weight gained by animals during the treatment course between treated (N=3) and vehicle (N=3) in both WT and hA30P mice.

The score sheet showed that the mice were tolerant of both the metformin and the intranasal delivery route (Table 4.1). The results showed no significant difference in the body weight gained by animals during the treatment course between metformin-treated and vehicle in both WT and hA30P mice (Fig 4.10A, B, and C). For the metformin-treated hA30P mice median body weight gain was 4.6, (IQR 3.9 – 5.8 mg, N = 3 mice) versus vehicle hA30P median body weight gain of 4.1, (IQR 3.7 – 5.7 mg, N = 3 mice). For the metformin-treated WT mice median body weight gain was 5.2, (IQR 2.5 – 9.8 mg, N = 3 mice) versus vehicle WT median body weight gain of 4.2, (IQR 4 – 10.5 mg, N = 3 mice. $p>0.05$, Ordinary one-way ANOVA).

4.4.8. Effect of Metformin in c-Fos in the CA3 Hippocampus of male hA30P Mice

Studies on metformin have demonstrated neuroprotective effects in various neurological disorders, both in humans and animals (Boccardi et al., 2019, Gantois et al., 2019). Metformin was observed to reduce neuronal degeneration in the hippocampal CA1 region (Fang et al., 2017, Chen et al., 2020).

In view of the biphasic changes in c-Fos expression seen in hA30P mice (Fig. 3.2 and 4.5 IF staining using an anti-c-Fos antibody (Table 2.2) was conducted to detect whether metformin treatment had any effect on network excitability in either WT or hA30P mice (Fig. 4.11).

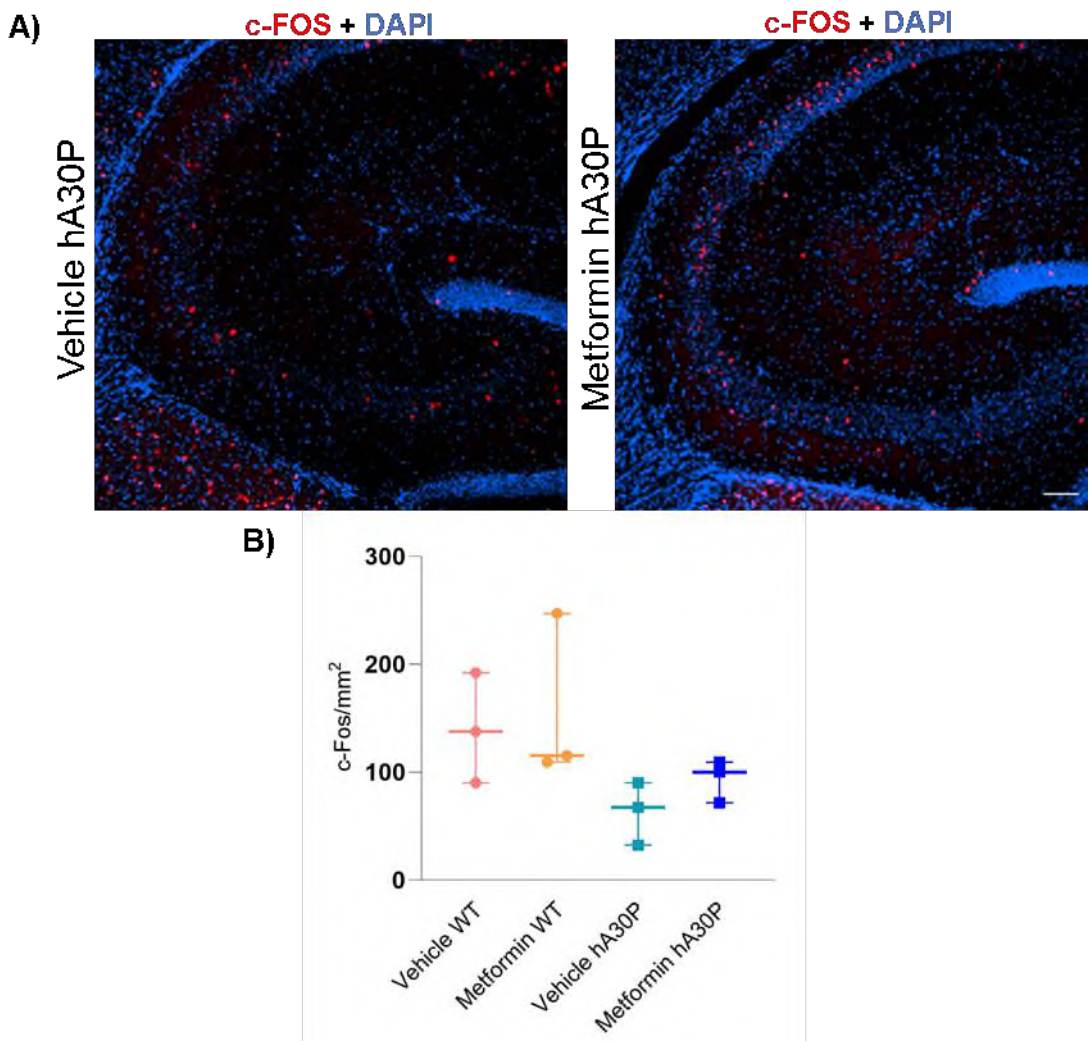

Figure 4.11: Effect of Metformin Treatment in C-Fos+ nuclei/mm^2 in the CA3 Region of the Hippocampus of Treated Versus Vehicle Groups of hA30P and WT mice. (A) Representatives IF images. The c-Fos+ protein (red) and the nuclei (blue) (DAPI). Scale bars represent 100 µm. **(A)** there was no difference in the count of c-Fos+ nuclei in the CA3 region of the vehicle versus treated mice. **(B)** There was no significant difference ($p>0.05$) in the count of c-Fos+ nuclei/mm^2 in treated (N=3) compared to the vehicle (N=3) groups in both hA30P and WT mice

I treated a group of male 1-month-old mice (hA30P and WT) intranasally with metformin 11.5 mg/kg daily for 4 weeks, and I used another group of sex and age-matched mice (hA30P and WT) as control (vehicle) treated with sterile distilled water at room temperature.

Similar to the results, observed in 2-4 months mice (Fig. 3.2), the IF staining with c-Fos antibody of vehicle-treated mice showed that there was a trend towards a decrease in hippocampal c-Fos+ nuclei count in the hA30P compared to WT mice (Fig. 4.11).

The IF result showed there was also a trend to increase in the density of c-Fos+ nuclei in hA30P metformin-treated animals compared to the hA30P vehicle group. However, these changes were not significantly different. (Fig. 4.11A, and B). In metformin-treated hA30P mice the median count of c-Fos+/mm^2 was 100.2, (IQR 71.6 – 109, n/N = 18 sections/3 mice), vehicle hA30P median count of 67.5, (IQR 32.4 – 90.1, n/N = 17 sections/3 mice), and in metformin-treated WT median count of c-Fos+/mm^2 was 115.3, (IQR 109 – 247, n/N = 11 sections/3 mice), vehicle WT median count of 137.6, (IQR 90.1 – 192, n/N = 12 sections/3 mice. $p>0.05$, Ordinary one-way ANOVA).

4.4.9. Effect of Metformin on Reactive Astrocytes in the Hippocampus of hA30P Mice

According to recent data, metformin can modulate chronic neuroinflammation (one of the core pathologies in AD) (Liao et al., 2021). Metformin's neuroprotective effects extend to astrocytes and microglia (Wang et al., 2021). Rabieipoor et al. (2023) reported that metformin therapy reduces astrogliosis in the hippocampus in the sporadic AD mouse model in addition to enhancing cognition. To test whether metformin had an anti-inflammatory effect in this thesis, IF staining using an anti-GFAP antibody (Table 2.2) was conducted in the CA3 region of hA30P mice (Fig. 4.12).

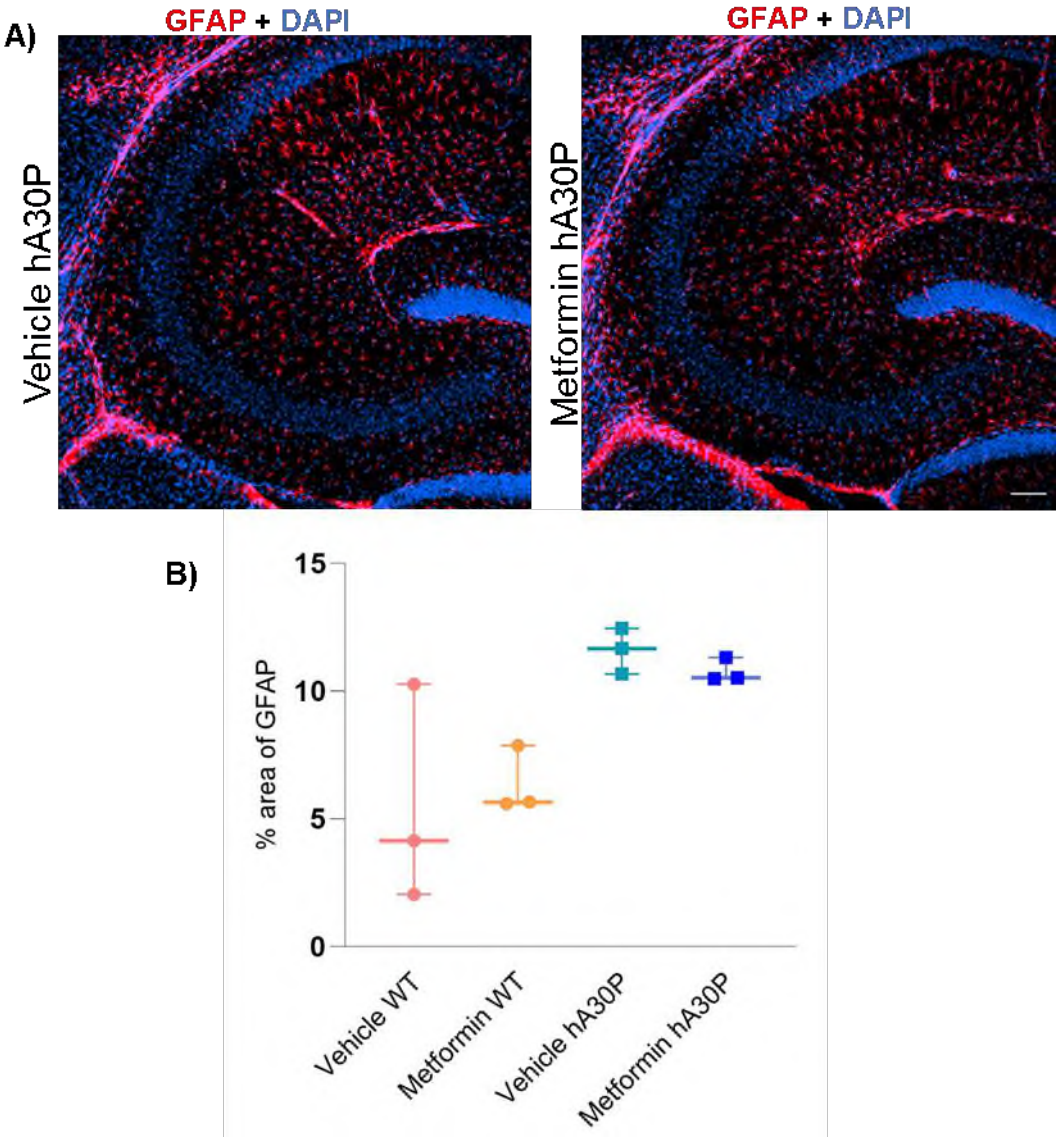

Figure 4.12: Effect of Metformin Treatment in Reactive Astrocytes in the Hippocampus of Treated Versus Vehicle Groups of hA30P and WT mice. (A) Representatives IF images. The GFAP protein (red) and the nuclei (blue) (DAPI). Scale bars represent 100 µm. **(A)** there was no apparent difference in the reactive astrocytes in the CA3 region of vehicle versus treated mice. **(B)** There was no significant difference ($p>0.05$) in the % area occupied by GFAP in treated mice (N=3) compared to the vehicle (N=3) in both hA30P and WT mice.

Again, even though this was only 3 mice, the data very nicely confirms the results shown in Chapter 3 (Fig. 3.6). We found a clear trend to an increase in % area occupied by GFAP+ reactive astrocytes in the CA3 region of the hippocampus of hA30P mice compared to WT mice.

Overall, however, statistical analysis showed no significant differences in % area occupied by reactive astrocytes in the hippocampus between the metformin-treated and vehicle mice in both hA30P and WT mice (Fig. 4.12 A, and B). In metformin-treated hA30P median % area occupied by GFAP immunofluorescence was 10.5, (IQR 10.5 – 11.3, n/N = 12 sections/3 mice), for vehicle hA30P median % area was 11.7, (IQR 10.7 – 12.5, n/N = 12 sections/3 mice), and in metformin-treated WT median % area occupied by GFAP was 5.7, (IQR 5.6 – 7.9, n/N = 12 sections/3 mice), whereas for vehicle WT median % area was 4.1, (IQR 2 – 10.3, n/N = 12 sections/3 mice. $p>0.05$, Kruskal-Wallis test).

4.4.10 Effect of Metformin in the Reactive Microglia CA3 Hippocampus of hA30P Mice

In addition to reducing astrocyte reactivity, metformin therapy inhibits microglial activation, which may reduce neuroinflammation (Wang et al., 2021, Rabieipoor et al., 2023) (Jin et al., 2014). A previous study showed that 200 mg/kg metformin as a daily injection for 2 weeks reduced Iba-1 in the CA3 region of the hippocampus in a sporadic AD mouse model and restored cognition dysfunction (Rabieipoor et al., 2023).

It has been reported via polymerized chain reaction (PCR) analysis that metformin oral drug of 200 mg/kg/day for 8 weeks could massively reduce levels of the mRNA for proinflammatory cytokines such as TNF-α, IL-1B, and IL-6 in the brains of APP/PS1 transgenic AD model, which activate the AMPK pathway in the hippocampus tissue (Lu et al., 2020b). I used IF staining to co-stain Iba-1 with iNOS antibodies (Table 2.2) to detect the potential anti-inflammatory effect of metformin in the current pilot study (Fig. 4.13).

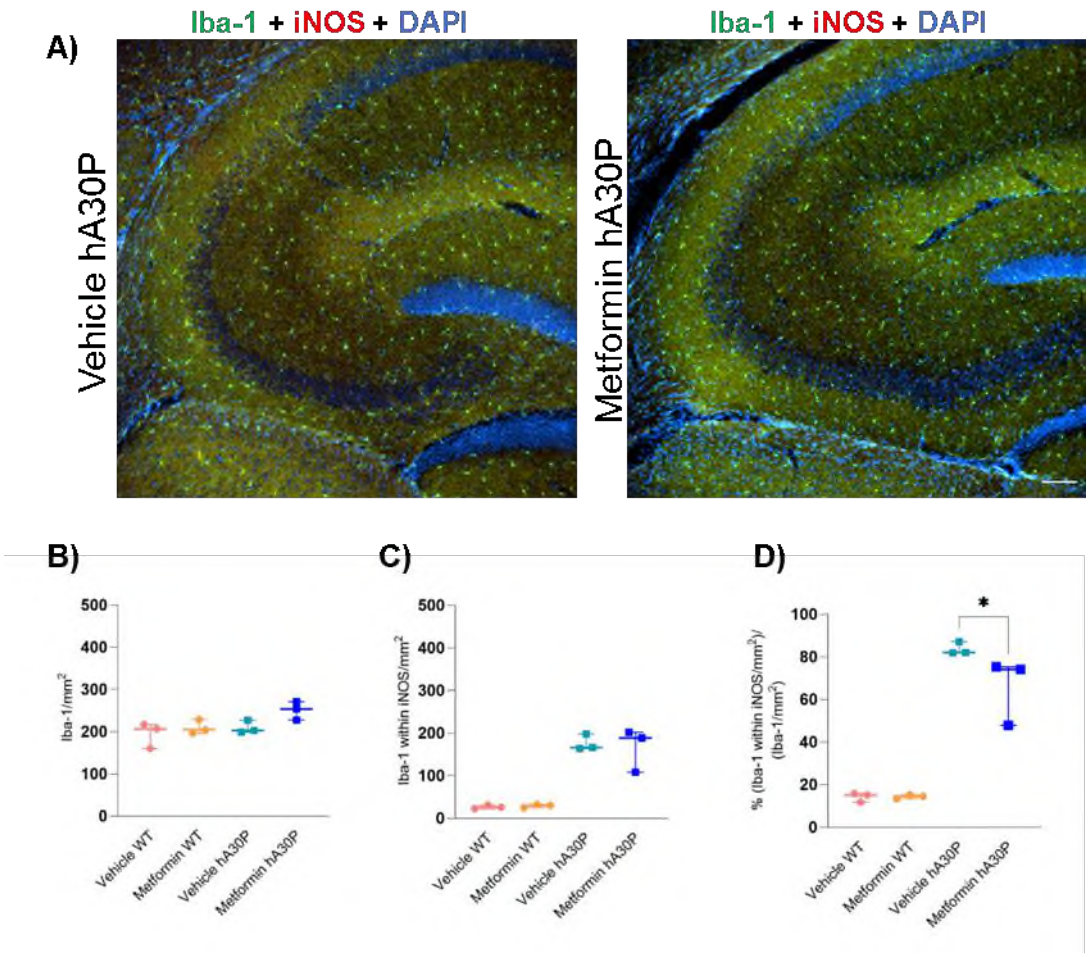

Figure 4.13: Effect of Metformin Treatment in Reactive Microglia in the CA3 Region of the Hippocampus of Treated Versus Vehicle Groups of hA30P and WT mice. (A) Representatives IF images. The Iba-1 (green), iNOS (red), and the nuclei (blue) (DAPI). Scale bars represent 100 µm. **(A)** There was a significant difference in the count of Iba-1 that expressed iNOS/mm^2 in treated mice compared to the vehicle of hA30P mice. **(B)** There was no significant difference ($p>0.05$) in the count of Iba-1 with iNOS/mm^2 in treated (N=3) compared to the vehicle (N=3) of both hA30P and WT mice. **(C)** There is no significant difference ($p>0.05$) in the count of Iba-1 with iNOS/mm^2 in treated mice (N=3) compared to the vehicle (N=3) of both hA30P and WT mice. **(D)** There is a significant decrease (*$p<0.05$) in % (Iba-1 with iNOS/mm^2) / (Iba-1/mm^2) in treated (N=3) compared to the vehicle (N=3) of hA30P mice. There is no significant difference ($p>0.05$) in % (Iba-1 with iNOS/mm^2) / (Iba-1/mm^2) in treated (N=3) compared to vehicle of WT mice (N=3).

The IF of co-staining by Iba-1 with iNOS antibodies showed an increase in the count of Iba-1 with iNOS/mm^2 cells of the CA3 region following treatment in hA30P compared to WT mice like what was observed at one month (See Fig. 4.8)

Also, the IF of co-staining by Iba-1 with iNOS antibodies results revealed that there was no significant difference in the total count of microglia in the CA3 region of the hippocampus between the metformin-treated and vehicle groups in both hA30P and WT mice (Fig. 4.13A, and B). In metformin-treated hA30P median count of Iba-1/mm^2 cells was 253.9, (IQR 227.5 – 271.5, n/N = 12 sections/3 mice), vehicle hA30P the median count was 202.8, (IQR 198.8 – 227.4, n/N = 11 sections/3 mice), and in

metformin-treated WT the median count of Iba-1/mm^2 cells was 204.6, (IQR 196.4 – 229, n/N = 11 sections/3 mice), and vehicle WT the median count was 206.9, (IQR 160.3 – 217.3, n/N = 12 sections/3 mice. p>0.05, Ordinary one-way ANOVA).

No significant difference in the count of reactive microglia (Iba-1+ cells that co-labelled with iNOS) was seen in the hippocampus between the metformin-treated and vehicle groups in both hA30P and WT mice (Fig. 4.13C). In metformin-treated hA30P the median count of cells expressing Iba-1 and iNOS/mm^2 was 188.5, (IQR 108.2 – 201.8, n/N = 12 sections/3 mice), in vehicle-treated hA30P mice the median count was 166.2, (IQR 163.3 – 198, n/N = 11 sections/3 mice). As shown in Chapter 3 the number of reactive microglia co-labelled with iNOS was much lower in the WT mice. In metformin-treated WT the median count of Iba-1 and iNOS/mm^2 was 30.4, (IQR 25 – 32, n/N = 11 sections/3 mice), and in vehicle-treated WT the median count was 26, (IQR 22.7 – 31.6, n/N = 12 sections/3 mice. p>0.05, Ordinary one-way ANOVA).

However, the proportion of reactive microglia/ total microglia per mm^2 in the CA3 of metformin-treated hA30P mice was significantly decreased compared to the vehicle group, while there was no significant difference between metformin-treated WT and vehicle mice (Fig. 4.13D). In metformin-treated hA30P median % (Iba-1 with iNOS/mm^2)/(Iba-1/mm^2) was 74.1, (IQR 47.8 – 75.3, n/N = 12 sections/3 mice), vehicle hA30P median proportion of 82.1, (IQR 81.8 – 87.1, n/N = 11 sections/3 mice. *p<0.05, Ordinary one-way ANOVA), and in metformin-treated WT median % (Iba-1 with iNOS/mm^2)/(Iba-1/mm^2) was 14.6, (IQR 13.4 – 15.3, n/N = 12 sections/3 mice), vehicle WT median proportion of 15.1, (IQR 11.8 – 15.8, n/N = 11 sections/3 mice. p>0.05, Ordinary one-way ANOVA). The result showed the dosage of metformin in the current study did significantly affect the proportion of reactive microglia/ total microglia per mm^2 in the CA3 of metformin-treated hA30P compared to vehicle hA30P mice.

4.5 Discussion

A summary of key findings in Chapter 3 was as follows:

- There is detectable human α-syn protein expression in 1-month hA30P mice.
- A significant increase in c-Fos expression in 1-month hA30P mice compared to the wild type, which was the opposite of the result seen at 2-4 months.

- Like 2-4 months old mice, there was a significant increase in both reactive astrocytes and reactive microglia in 1-month hA30P mice compared to 1-month-old wild-type mice.
- Mice were tolerant to the metformin treatment and did not show any side effects.
- Intranasal metformin treatment of 11.5 mg/kg five days weekly for 4 weeks, did not affect significantly either the % area occupied by GFAP+ reactive astrocytes or the total count of Iba-1 positive microglia/mm^2 in the CA3 region of hA30P mice compared to vehicle-treated controls.
- However, metformin-treated hA30P mice showed a significant reduction in the proportion of iNOS+/Iba-1+ microglia in the hippocampus compared to the vehicle-treated h30AP mice.

4.5.1 Confirmation of Human α-syn Expression in the CA3 Region of the Hippocampus of Male 1-Month hA30P Mice

I started with confirming human α-syn protein expression in the CA3 in the hA30P mice at 1 month of age, before investigating its pathological effect. The IF staining with hα-syn antibody showed an obvious detectable immunofluorescence signal of hα-syn in the hippocampus of hA30P mice only. At the same time, the WT had no hα-syn immunofluorescence reactivity which was evidence of the specificity and efficient detection of the antibody used. In hA30P mice, the human αSYN gene expression is induced during the first postnatal month and remains high throughout life (Neumann et al., 2002, Schell et al., 2009, Ekmark-Lewén et al., 2018). Overexpression of hA30P α-SYN might represent early stages of pathological abnormalities, resulting in pathological accumulations that could finally lead to a PD-like phenotype (Ekmark-Lewén et al., 2018). hA30P mice express human mutant α-syn from 1 month of age, after which there is a progressive, age-dependent, increase in pathological phosphorylated human α-syn serine residue pS129 (Kahle et al., 2000). However, I did not stain for phosphorylated hα-syn in this thesis, but it would be interesting to conduct that in the future, especially at this early age of male and female hA30P mice.

The results of this study showed there was a high level of hα-syn protein overexpression spread across the whole hippocampus of 1-month-old male hA30P

mice compared to WT mice. Again, as outlined in Chapter 3 section 3.4.1, I found a preferential distribution of hα-syn to neurons situated in the deep SP layer of the hippocampus. As discussed in Chapter 3 section 3.5.1 this phenomenon may be explained by the expression of human α-syn protein being controlled by the Thy-1 promoter, as Thy-1 is more prominently expressed in the deep layer of the SP (Dobbins et al., 2018, Slomianka et al., 2011b). Pyramidal cells exhibit heterogeneity in their molecular, morphological, and functional levels corresponding to their preferential location in deep versus superficial SP, within CA3 neurons (Sun et al., 2017) and CA1 neurons (Valero and de la Prida, 2018) in the hippocampus.

Confirmation of a detectable amount of human α-syn in the hippocampus of hA30P mice led us to continue in the investigation of its pathological effects at this early age.

4.5.2 Increase in c-Fos+ nuclei/mm^2 in the CA3 Region of the Hippocampus of 1-Month Male hA30P Mice

To detect the pathological contributions resulting from overexpression of human α-syn in the hippocampus of 1-month-old hA30P. I conducted IF staining with c-Fos, the indirect marker of neuronal activity, before detecting neuroinflammation. Interestingly, in contrast to the results observed at 2-4 months (Chapter 3) where c-Fos expression was decreased, the IF staining at 1 month revealed a clear increase in the number of nuclei containing c-Fos+ protein in the CA3 region of the hippocampus compared to control. This suggests that at the same time as hα-syn expression is evident, there was an early increase in neuronal activity resulting in a transient increase in c-Fos. As we have shown in Chapter 3 when c-Fos was measured at 2-4 months this increase had become a decrease in relative control, likely reflecting the longer period of neuronal excitability.

α-syn protein plays a role in the release of neurotransmitters and the transit of vesicles (Jensen et al., 1998a) and it has been suggested that the hA30P mutation leads to α-syn losing its vesicle-binding properties thus altering α-syn's role in neurotransmitter release (Jensen et al., 1998a). α-syn multimerization restricts the trafficking and recycling of synaptic vesicle neurotransmitters (Wang et al., 2014). The overexpression of α-syn leads to neuroinflammation which might be one cause of the

increased neuronal hyperexcitability (Tzour et al., 2017) in the CA3 region of male hA30P mice at this early age in the current study.

c-Fos expression changes in the hA30P mice were, therefore, found to be biphasic, as the current study showed a transient initial increase in c-Fos in juvenile mice, which may reflect an early increase in neuronal excitability, followed by the later down-regulation following chronic network excitability changes. More recently, it has been shown that in younger mice (2-4 months of age) hippocampal activity is abnormal with increased power of the kainate-evoked gamma frequency oscillations and evidence of epileptic-like activity with interictal discharges, which are not seen in wild-type mice (Tweedy et al., 2021). This biphasic change in the neuronal activity indicated by the change of c-Fos changes in expression that we observed in the current thesis may be due to the progression in the neuroinflammatory state which caused an alteration from hyperexcitability to chronic hyperexcitability in the mice by age from 1 month to 2-4 months.

There is robust evidence demonstrating that c-Fos expression diversely influences the dynamics of networks associated with memory and learning (Gallo et al., 2018). So, our observations may reveal an early change that could contribute to the memory deficits of hA30P mice that occur at around 12 months (Kahle et al., 2000). In future work, it would be interesting to monitor c-Fos expression changes in older males and females in hA30P mice.

4.5.3 Increase in Reactive Astrocytes in the CA3 Region of the Hippocampus of 1-month Male hA30P Mice

The results of this chapter found there were changes in various markers of neuroinflammation in the CA3 region of the hippocampus of the hA30P mice even at the early age of 1 month as represented by the increased levels of reactive astrocytes in hA30P mice compared to sex and age-matched WT mice. As shown in hA30P mice aged 2-4 months, (Chapter 3 section 3.4.8), we also found evidence for increased reactive astrocytes at 1 month. This very early increase in reactive astrocytes may be due to their role in the clearance of α-syn. In addition to astrocytes' role in the homeostasis of the brain, mounting evidence suggests that they are implicated in clearing extracellular aggregated proteins including α-syn via receptor-mediated phagocytosis/pinocytosis (Giusti et al., 2024). TLRs are the potential candidates for

taking up α-syn (Dzamko et al., 2017). As a part of the pattern recognition receptor family, TLRs have been documented as overexpressed in both neurons and glia in PD patients (Dzamko et al., 2017), and in transgenic PD/DLB mouse models overexpressing α-syn (Watson et al., 2012). Despite this, the exact molecular mechanisms of how astrocytes remove misfolded proteins are still unknown (Giusti et al., 2024). Increased IF staining of GFAP antibody is associated with reactive astrogliosis types (Anderson et al., 2014, Eddleston and Mucke, 1993), and my data showed there was a significant increase in % area occupied by reactive astrocytes in the CA3 region in hA30P mice at 1-month of age in comparison with WT mice.

My results again showed a differential laminar distribution of GFAP expressing astrocytes in the hippocampus of 1 month in both hA30P and WT mice, similar to that seen at 2-4 months (Chapter 3) of age where astrocytes were predominantly located in SO and SR, with few observed in SP.

I did, however, notice that in the 2-4 months older group the reactive astrocytes were crowding closer to the SP layer and extending their process gradually in between pyramidal neurons of the SP.

Astrocytes undergo reactive changes in their morphology as well as their molecular, cellular, and functional profiles in response to CNS injury to minimize damage to nearby neurons (Kwon and Koh, 2020). Although I did not quantify the morphological changes in the reactive astrocytes of young hA30P mice, I did notice that at 1-month age (mild neuroinflammation), the astrocytes showed extended processes and increased ramifications. The changes at 2-4 months gradually increase in the ramifications and lengthen the processes until they access the SP. That might reflect the increasing severity of the neuroinflammation in the hippocampus of hA30P mice due to the increase in α-syn with age.

4.5.4. Increase in Reactive Microglia in the Hippocampus of Male 1-Month hA30P Mice

This thesis showed that both the % area of Iba-1+ microglia, and the total count of Iba-1+ microglia were also significantly increased in the CA3 region of the hippocampus in hA30P compared to WT mice at 1 month of age. These two results may reflect an increase in the total count of microglia and/or an increase in their process and ramifications at this early neuroinflammatory stage (Vidal-Itriago et al.,

2022) in the hippocampus of hA30P mice. Activated microglia release reactive oxygen/nitrogen species such as nitric oxide (NO) produced via iNOS (Stykel and Ryan, 2022). The current result was in line with previous studies that showed microglia releasing to iNOS (Loveland et al., 2023) in the CA3 region of hA30P compared mice even at 1 month of age.

Researchers now think that reactive microglia and α-syn aggregates are more relevant than previously thought. Moreover, the progression of α-synucleinopathies may also be influenced by these cells (Tanriöver et al., 2020). It has been shown that the activation of microglia contributes to the spread of α-syn lesions (George et al., 2019, Grozdanov and Danzer, 2018). Recently, microglia have been shown to form tunnelling nanotubes to move aggregated α-syn load to neighbouring microglia for clearance (Scheiblich et al., 2021). In mice overexpressing human wild-type α-syn under a Thy-1 promoter, a previous study also showed that as early as one month there was evidence for activation of the microglia and the maintenance of immunological responses to α-syn overexpression (Watson et al., 2012).

Although I did not quantify the morphological changes in reactive microglia, I observed some differences between WT and hA30P mice as microglia exhibited increased ramification of processes in hA30P mice. Alterations in microglia morphology might indicate the transformation of microglia from a surveilling/silent state to activated microglia due to acute or chronic stress phase, followed by an active/ phagocytic state in response to neuroinflammation severity. This result was compatible with previous research (Edler et al., 2018, Vidal-Itriago et al., 2022). Also, the observation of morphological changes in reactive microglia that occurred before those of astrocytes in the CA3 region of hA30P mice in the current study confirmed previous studies that reported that the reactive microglia showed an increase in number and changed shape earlier than astrocytes (Bantle et al., 2021). However, there is a possibility that dysfunction of the BBB caused an increase in the penetration of peripheral macrophages (that are also labelled with Iba-1) (Laurent et al., 2017) in the CA3 region of hA30P mice in the current study.

It would be worth studying the morphological changes of the microglia at different disease stages of male and female hA30P mice in the future. The current study used Iba-1 which stains all microglia types that are present in brain parenchyma and the peripheral microglia as well, in addition to the use of iNOS which is produced in many cells other than reactive microglia. Using antibodies specific to the

differentiation of microglia from other macrophages, such as antibodies against trans-membrane protein 119 (Tmem119) would be important in the future. Tmem119 is a highly expressed unique gene on the surface of the microglia cell (Bennett et al., 2016). Also, it would be interesting to conduct differential quantification for the microglia in the different layers of the hippocampus as I did for astrocytes, although qualitatively microglia appeared to be more uniform in their distribution.

4.5.6 Effect of Metformin on Weight Gain in Male hA30P Mice

Evidence of the promising impact of metformin on neuroprotection/neurogenesis is increasing day by day. Novel clinical studies prove metformin's ability to protect against the adverse effects of neurological diseases including AD (Liao et al., 2021). In the brains of PD patients, metformin lessens neuronal damage (Lu et al., 2020a). Metformin reverses schizophrenia in a rat model (Wang et al., 2019). Metformin intake enhances the condition of Huntington's disease (HD) patients (Hervás et al., 2017) by improving the cognitive status. Also, it helps Lafora disease patients (Bisulli et al., 2019) by possible reduction of seizure frequency and enhancing general clinical improvement of patients.

I, therefore, wanted to conduct a pilot study to determine the potential for metformin treatment to reverse the neuroinflammatory changes we have seen in the hA30P mice. I first demonstrated that handling, and daily nasal administration of metformin did not affect the mice using a daily score sheet. In addition, I showed in the current study, that the metformin treatment regime did not affect the weight of the mice compared to the vehicle-treated groups.

The dosage in the current study was low compared to the previous study by Kazkayasi et al., 2022 when they used a volume of 28 µl intranasally with a dosage of 200 mg/kg/day for their mice (Kazkayasi et al., 2022). This dose of metformin seems rather improbable as it is impossible to dissolve metformin at that concentration (Tocris Bioscience, UK). The authors may have used a suspension of metformin, but they did not mention that in their published paper, nor did they respond to our inquiry via email. However, the dosage of 11.5 mg/kg that I used was not low compared with the dosage of 20 mg/kg used by Fang et al., 2017 to effectively reduce CA1 region damage in a neonatal hypoxic-ischemic rat model (Fang et al., 2017). Fang and his colleagues

used a single dose of subcutaneous 20 mg/kg metformin and reported that 24 hours after HI damage, metformin administration significantly reduced brain oedema and infarct sizes. Metformin's neuroprotective and anti-neuroinflammation effects were linked to a reduction in microglia, astrocytes, cytokines, and neuronal apoptosis, in addition to enhanced integrity of the BBB (Fang et al., 2017).

4.5.7 Effect of Metformin in Reactive Astrocytes in the Hippocampus of Male hA30P Mice

In general, the result of IF showed that metformin did not affect the increase in GFAP we have previously observed in Chapter 2. I treated only three hA30P mice with metformin, and the results were variable among these small groups as one mouse showed a great reduction of the GFAP in the CA3, and that might be indication of actual penetration of metformin to the hippocampus in the brain and had some effect. Another mouse showed a slight decrease in GFAP expression, but the third mouse showed a negative effect of metformin treatment where it exhibited an increase of % area occupied by GFAP compared to the vehicle-treated group. This is in contrast to another study in a sporadic AD mice model (C57BL/6 mice treated with STZ) a 200 mg/kg dosage of metformin injected intra-peritoneal for two weeks resulted in a reduction of astrocyte reactivity and microglial activation in the hippocampus of 5-6 months old mice (Rabieipoor et al., 2023). The difference in the results of our study might be due to the much lower dose of metformin that I used (keeping in mind that STZ used in medical research to produce an animal model for hyperglycemia and Alzheimer's in a large dose) but it has been shown that a single 20 mg/kg dose of subcutaneously metformin treatment did inhibit TLR4/NFκB signalling, which in turn reduces activated astrocytes and microglia and neuronal apoptosis in the CA1 region of the hippocampus, (Fang et al., 2017). Therefore, we hypothesized that metformin might be able to reduce the increase in reactive astrocytes seen in the hA30P mice. Our data, however, do not show a marked change in GFAP expression following metformin treatment, although it is possible that with a greater number of animals, we might have seen a statistically significant reduction in GFAP. Another reason we did not see a significant reduction in reactive astrocytes in the current study may be due the two-day gap in treatment over the weekends.

It is worth trying to treat mice for continuous days without gaps in future studies and also possibly twice daily injections while keeping the same concentration of metformin and the same route of administration.

4.5.8 Metformin Reduced Reactive Microglial in Male hA30P Mice

Immunofluorescence results of the current study showed there was no significant difference in the total count of Iba-1/mm^2 in the CA3 region of the hippocampus of metformin-treated male hA30P mice, nor the count of reactive microglia/mm^2 compared to vehicle mice. However, interestingly the proportion of the number of microglia that co-expressed iNOS was significantly reduced in the metformin-treated hA30P mice compared to vehicle mice. These data, therefore, suggest that metformin treatment in the hA30P mice was able to significantly reduce the number of reactive microglia seen in the CA3 region. This reduction in reactive microglia was compatible with many other studies' findings that used metformin as an anti-inflammatory drug (Liu et al., 2014, Lu et al., 2020b, Ou et al., 2018, Tizazu et al., 2019). For examples:

Metformin can suppress the activation of microglia in a mouse model of PD (Ryu et al., 2020). Chemokines and cytokines enzymes such as iNOS, IL-6, IL-1β, and TNF-α are involved in neonatal cerebral inflammation after neonatal hypoxic-ischemic brain injury (Vezzani and Viviani, 2015). Genes transcription of these pro-inflammatory enzymes is influenced by the activation of nuclear factor kappa-light-chain-enhancer of activated B cells (NF-κB) (Nijboer et al., 2009). Oral administration of 50 mg/kg metformin for four weeks suppressed activation of microglia and reduced levels of proinflammatory cytokines (TNF- and IL-1) in a mice model of PD (Ryu et al., 2020).

Jing et al. (2018) investigated how metformin reduced chronic low-grade inflammation in high-fat-diet-fed C57/6J male mice. Jing and his team used ELISA, and flow cytometry, for the markers CD11c and MCP-1 in adipose tissue. Metformin (300 mg/kg/d) administered orally for 7 weeks could turn microglia of the M2 pro-inflammatory state into an anti-inflammatory M1 type phenotype via elevated levels of the anti-inflammatory cytokine interleukin-10 (IL-6) and TNF-α in serum, in addition to a reduction in CD11c and MCP-1 compared with control cells. They demonstrated that the modulation of macrophage polarization to an anti-inflammatory, M2 phenotype was partly due to the activation of AMPK signalling (Jing et al., 2018).

Studies showed that nuclear factor (NF) protects the brain by regulating the dephosphorylation of the Tau protein (Docrat et al., 2021). Metformin has been shown to inhibit NF-κB in various cell types and reduce their production of proinflammatory cytokines (Du et al., 2022a) and in male Sprague–Dawley rats (Zhu et al., 2015). All these anti-inflammatory actions of metformin could have contributed to the reduction in the number of iNOS labelled microglia that I saw in this study following treatment.

4.5.9 Effect of Metformin in c-Fos in the Hippocampus of Male hA30P Mice

This study showed that metformin did not significantly alter the c-Fos expression in treated mice compared to vehicle mice in both the WT and hA30P mice. However, there was a trend to increase c-Fos in metformin-treated mice compared to the vehicle group, which may indicate there was possibly an action to reduce neuronal hyperexcitability. Earlier, we showed that c-Fos expression changes are biphasic, there was an early increase in c-Fos which indicated a neuronal hyperexcitability, followed by down-regulation in c-Fos which indicated a chronic hyperexcitability excitability changes. The trend of increase in c-Fos in metformin-treated hA30P mice might be due to its effect of mitigating neuroinflammation by the treatment of metformin (Liu et al., 2014, Lu et al., 2020a, Ou et al., 2018, Tizazu et al., 2019), as the following sections will show.

Also, the trend of increase in c-Fos in treated hA3P mice might be due to its ability to regulate releasing of glutamate in the synapsis and attenuate hyperexcitability. mTOR is increased in neurological disorders (Zhao et al., 2020, Norwitz and Querfurth, 2020). Although the mechanisms of action of metformin are not completely known, by activating the AMPK pathway, metformin suppresses the mTOR signalling which has been shown to regulate many crucial cellular activities (DiTacchio et al., 2015). Metformin has also been shown to regulate glutamate release at presynaptic terminals, and the effect occurs independently of AMPK (Chen et al., 2020). In addition, it has a role in alleviating pain related to diabetic neuropathy through attenuating hyperexcitability in sensory neurons (Ma et al., 2015). By intraperitoneal injection of STZ in rats Ma et al., 2015, demonstrated that metformin can mitigate diabetes-induced hyperalgesia and allodynia, which might be associated with its anti-oxidative properties through the AMPK pathway (Ma et al., 2015). So, they suggested it as an effective drug for abnormal sensations in painful diabetic neuropathy but

indirectly this suggests that metformin may be able to alter neuronal activity levels and thus could impact c-Fos expression.

Our findings in the current thesis were in line with the above findings. Using more specific antibodies and a larger group size of mice might find more supportive evidence for the role of metformin in ameliorating α-synucleinopathy.

For future work it is recommended to use micro-dialysis, or liquid chromatography-tandem mass spectrometry to determine the concentration of drugs in specific tissue.

However, I found that there was some variation among the metformin-treated hA30P mice (N=3) used in the current study, which may be due to different responses toward the delivery route of the intranasal method. Foo et al. 2007, stated that the variation in respiration rate and administration angle caused inter-individual and/or inter-trial variability in intranasal delivery to the brain. Effectiveness-wise, intranasal injection of a solution or administration as a spray will undoubtedly have the advantage of delivering the drug to the brain, avoiding the first-pass effect, and providing a quick effect; however, the device plume angle and administration angle were major factors affecting nasal deposition efficiency in the case of nasal administration using nasal spray (Foo et al., 2007).

Overall, the metformin pilot study conducted during this thesis work had some limitation factors, such as dosage and duration of treatment. The small group size was a limitation statistically because when the sample is larger in size and random in choice, it becomes more representative of the population and stronger statistically.

Despite the tolerance for mice towards metformin and the delivery route in this experiment, there were some issues. I could summarize them as the following:

Using an intranasal delivery route for the first time in the CBC of Newcastle University and applying the 3Rs to get a valuable statistically accepted result was a big challenge. Therefore, we chose to use a small number of mice to conduct this pilot study. Also, using a small drop of 14 µl/day only of metformin solution with a concentration of 100 mM (the maximum solubility) was suitable for the small nasal cavity of the juvenile mice. It is possible giving a repeat dose (twice/day) will give better results in future work. Skipping the weekend days without treatment may also have affected the treatment regime as the drug presumably reduces to a low concentration during these days. All these factors might negatively affect our results in this thesis.

Also, it will be beneficial to use more accurate detection methods like PCR, real-time PCR, Western blot consecutive, and proteomic analysis to measure markers at a molecular level difference such as enzymes, chemokines, and cytokines between treated and vehicle mice.

4.6 Conclusion

This chapter's findings showed that the young 1-month male hA30P mice showed a detectable overexpression of human mutant α-syn accumulation by IF staining and exerted gliosis well in advance of any known motor or cognitive abnormalities even at this early age (Kahle et al., 2000, Freichel et al., 2007). The current results suggested a close association between early neuronal hyperexcitability and neuroinflammation (Kilb and Kirischuk, 2022, Andersen et al., 2023, Kouli et al., 2020). Hyperexcitability, which we have previously observed in young hA30P mice (Tweedy et al., 2021), was proposed to count for the upregulation of c-Fos seen in young hA30P mice. The result showed that 1-month hA30P mice experienced an increase in c-Fos that was coupled with a marked increase in both reactive astrocytes and microglia. Depending on morphological changes in microglia in the CA3 region of 1, 2-4 months hA30P mice, my observation showed a transition of microglia from an M2 anti-inflammatory state to M1 to a pro-inflammatory state, although I did not quantify these changes. This chapter revealed obvious neuroinflammation and neuronal changes in the hippocampus of 1-month hA30P mice.

Intranasal metformin treatment was tolerated well by the mice and did not show observable side effects. However, the dosage of 11.5 mg/kg for five days weekly for 4 week regime, did not affect significantly both of % area occupied by reactive astrocytes or the total count of microglia/mm^2 in the CA3 region of hA30P mice compared to the vehicle. However, metformin-treated mice showed a significant reduction of iNOS expression in the microglia of the hippocampus compared to the vehicle. This result was compatible with many previous studies, which demonstrated the neuroprotective and anti-inflammatory role of metformin.

Chapter 5

Proteome Cytokine Array and Proteomics Analysis of the Hippocampus of Male 2 Months hA30P and WT Mice

5.1 Introduction

The data reported in Chapters 3, and 4 showed changes in various neuroinflammatory markers in the young pre-symptomatic hA30P mice. In this chapter, I aimed to investigate the role of neuroinflammation further and explore other potential pathways that might be modulated by human mutant α-syn in the hA30P mice. I therefore decided to explore other possible pathways using the proteome cytokine array Kit, and Label-free mass spectrometry (LF-MS) Proteomics to detect possible effects of α-synucleinopathy in 2-month age hA30P mice.

I predicted that several other pathways might show altered levels of expression in hA30P resulting from abnormal α-syn expression. Autophagy is one pathway that is essential for neuronal homeostasis, primarily as a housekeeping mechanism to prevent protein aggregates, including α-syn, and defective organelles from accumulating. Balanced, bidirectional trafficking of intracellular constituents between distal neurites and the cell soma is required for neuronal homeostasis (Gunn et al., 2018). Autophagosomes and endosomes that fuse in the distal axon of neurons must be retrogradely transported to the soma to fuse with lysosomes where their contents are degraded (Crews et al., 2010). Thus, modest alterations in autophagosome formation, maturation, or trafficking would be expected to have disastrous consequences for autophagic flux and neuronal homeostasis, because aggregated protein accumulation in the brain is frequent in various neurodegenerative disorders (Gunn et al., 2018). Recent research suggests that increasing autophagy in mouse models of neurodegenerative diseases can reduce disease protein accumulation, protect against toxicity associated with protein aggregation, and have potential therapeutic benefits (Heras-Sandoval et al., 2020). Thus, I was interested to see if changes in the expression of proteins involved in autophagy were evident in 2-month-old hA30P mice.

Aggregations of α-syn lead to a multitude of other harmful intracellular effects, such as an increase in oxidative stress, disruption of axonal transport, degradation of the ubiquitin-proteosome machinery, impaired mitochondrial function, and synaptic dysfunction (Irwin et al., 2013, Hsu et al., 2000, Scott et al., 2010).

Other changes that might be relevant and occurring in young hA30P mice include potential changes in mitochondria. Mitochondria are exceptionally well-

positioned to play a critical role in neuronal cell survival because they are key regulators of energy production in the neurons (Thellung et al., 2019). They are responsible for the production of the energy molecule ATP, and endogenous ROS, in addition to homeostasis of intracellular calcium ions, and programmed cell death (apoptosis) (Thellung et al., 2019). Mitochondria appear to be particularly vulnerable to physiological aging because they experience the most extreme age-related changes, including structural degeneration such as swelling and cristae loss, partial or total disintegration of the mitochondrial inner membrane (MIM), decreased respiration, and loss of ATP production (Turrens and Boveris, 1980). Furthermore, brain cells rely heavily on mitochondrial oxidative phosphorylation machinery (OXPHOS), which includes respiratory complexes (Graziotto et al., 2012).

Evidence has accumulated indicating that mitochondria may also be prone to selective destruction by mitophagy, the process of collecting and degrading damaged mitochondria by lysosomes. Mitophagy is essential for the removal of defective mitochondria and mutant mitochondrial deoxyribonucleic acid DNA (mtDNA) since DNA repair in mitochondria is significantly less robust than in the nucleus (Larsen et al., 2005). There have been numerous instances where mitochondria have been localized within autophagosomes (Koopman et al., 2010).

Both α-syn misfolding/aggregation and mitochondrial dysfunctions have been studied extensively about neuronal degeneration in PD (Exner et al., 2012) (Bose and Beal, 2016). The mitochondria involve mitochondrial complex I of the nicotinamide adenine dinucleotide (NAD+)/NADH is considered an integral element of the OXPHOS (Thellung et al., 2019). Complex I (NADH-ubiquinone oxidoreductase) is the first complex in the electron transport chain (ETC) and catalyses the electron transfer from NADH oxidation to ubiquinone. This electron transport is linked to the pumping of protons across the IMM, which contributes to the electrochemical gradient required for ATP production via Complex V or ATP synthase (Wirth et al., 2016, Koopman et al., 2010). Interfering of abnormal α-syn in mitochondria's function and structure has been widely reported (Zhu et al., 2016). A plethora of evidence suggests that the aetiology and progression of PD might be related to impaired autophagy clearance and mitochondrial dysfunctions. These dysfunctions include bioenergetics and calcium handling defects, and there is evidence showing that α-syn contributed to the physiological and pathological impairment of mitochondria (Zhu et al., 2016). Some mitochondrial processes, including cytochrome c release, calcium homeostasis, and

ATP production, are directly affected by α-syn (Zhu et al., 2016). It has been shown that cellular α-syn can selectively localize to mitochondrial sub-compartments upon specific stimuli, suggesting novel mechanisms by which α-syn can act. Thus, I expected that I might see changes in the expression levels of proteins associated with mitochondrial function in the hA30P mice.

Recent research showed there is a specific innate immune pathway that helps to prevent viral and bacterial infections by recognizing fragments of DNA in cells (Liu et al., 2021). A toxin operating on cyclic guanosine monophosphate (GMP) – ATP (cGAMP) synthase (cGAS) can activate the protein stimulator of the interferon gene (STING) when DNA fragments bind to it (Liu et al., 2021). In addition to recognizing fragments of self-DNA arising from released mitochondrial DNA or damaged genomic DNA, cGAS also recognizes DNA derived from invading pathogens (Liu et al., 2021).

There is mounting evidence demonstrating that mitochondrial dysfunction develops before the onset of symptoms in PD (Thellung et al., 2019). Thus, it is possible that mitochondrial dysfunction could be a very early change in the hA30P mice as suggested by Tweedy et al 2021 (Tweedy et al., 2021). The cGAS/STING pathway also plays a role in the brain's response to pathological aggregation of α-syn (Hinkle et al., 2022). Furthermore, in primary mixed glial and human postmortem tissue cultures for PD, misfolded α-syn may also cause genomic DNA damage to microglia, which triggers cGAS/STING-driven neuroinflammation and is a key mechanism of neurodegeneration (Hinkle et al., 2022). Multiple system atrophy (MSA) is also associated with the activation of STING by α-synucleinopathy. According to recent studies in human postmortem MSA tissue, astrocytes were found to be activated by STING (Inoue et al., 2021). Also, enhanced mitochondrial oxidative stress and DNA damage have been seen in transgenic mice overexpressing human wildtype α-syn (Bender et al., 2013). We, therefore, hypothesized that proteomic analysis of the hippocampus of young hA30P mice may shed light on α-syn-induced changes in autophagy, mitochondria, and oxidative stress pathways.

5.2 Aims

The principal aims of this chapter were to measure inflammatory activity via quantification of Chemokine and Cytokine expression, and look at other pathways induced by overexpression of α-syn in the hippocampus of male 2-month-old hA30P mice compared to age and sex-matched WT mice, by using two methods:

1- Proteome cytokine array Kit
2- LF-MS Proteomics.

Detection and quantification of the consequences of aggregation of α-syn protein in prodromal stages of diseases is important for understanding pathophysiological events that may lead to developing better diagnostic tools and/or therapies.

5.3 Methods

5.3.1 Animals

WT (C57BL/6) mice were bought from outside vendors (Charles River) and used as controls. The hA30P was an in-house breeding colony in the CBC facility at Newcastle University housed according to ARRIVE guidelines. In this chapter, I used 5 male 2-month-old hA30P mice and another 5 sex and age-matched WT mice. For each mouse, one hippocampus lysate was used in the proteome cytokine array, and the other hippocampus went to LF-MS proteomics analysis. For analysis of the hippocampus fresh brain tissue, I sacrificed mice by Schedule 1, a humane killing regulated procedure under ASPA. I used the dislocation of the neck method, and then I isolated the hippocampus in the following steps.

5.3.2 Hippocampus Dissection

I carried out the protocol approved by the veterinary office of Zurich (https://www.youtube.com/watch?v=XUbIOG1Euf4), with minor modifications. A cold surface was needed to preserve brain tissue during the dissection, so a pre-chilled metal cleaned plate was used in addition to the usual dissecting tools. The dissection process steps are illustrated in Figure 5.1, as the following steps:

1- Using schedule 1, the neck was dislocated. The brains were then isolated from the skull and rinsed with cold PBS to remove excess blood from the brain. The brain was then placed on the cold plate on the ventral side. Blotting paper, moistened with PBS, and placed on the cold dissection surface beforehand prevented the brain from sliding too much.
2- The prefrontal cortex was trimmed off by cutting the brain coronally from the middle and stored separately. Then the following steps were used to dissect the hippocampi (Fig. 5.1 images 1-5) (I modified only step-in image 3, by cutting the brain coronally instead of sagittally to spare the prefrontal cortex as a whole unit).
3- A cut along the groove of the inter-hemispheric fissure with a scalpel blade perpendicular to the plate was done. Then the two halves of the brain were gently pulled apart. The brain half was then oriented with the lateral side upward. Fresh tissue allowed us to distinguish different brain parts based on their colour differences (Fig. 5.1 images 6-7).
4- The posterior parts of the brain were removed by cutting along the border of the cerebral cortex. Then the remaining tissue was flipped so that the medial side faced upwards (Fig. 5.1 images 6-7).
5- The hippocampus medial surface tissue was isolated by inserting the tip of one spatula underneath the corpus callosum and gently pulling out the thalamus, septum, and underlying stratum, removing this block of tissue using the other spatula (Fig. 5.1 images 8-9).
6- The banana-shaped hippocampus was easy to recognize at this stage. The hippocampus was removed carefully by placing the tip of the spatula under the ventral part of the hippocampus, rolling it out, and separating it from the cortex so there was no damage to the hippocampus (Fig. 5.1 images 10-12). Any remaining pieces of cortex were cut away since the cortex appears different in colour from the hippocampus. Immediately the isolated hippocampus was transferred to a labelled Eppendorf tube with liquid nitrogen for two minutes,

before being frozen at -96° C until use. The same steps were followed with the second half of the brain.

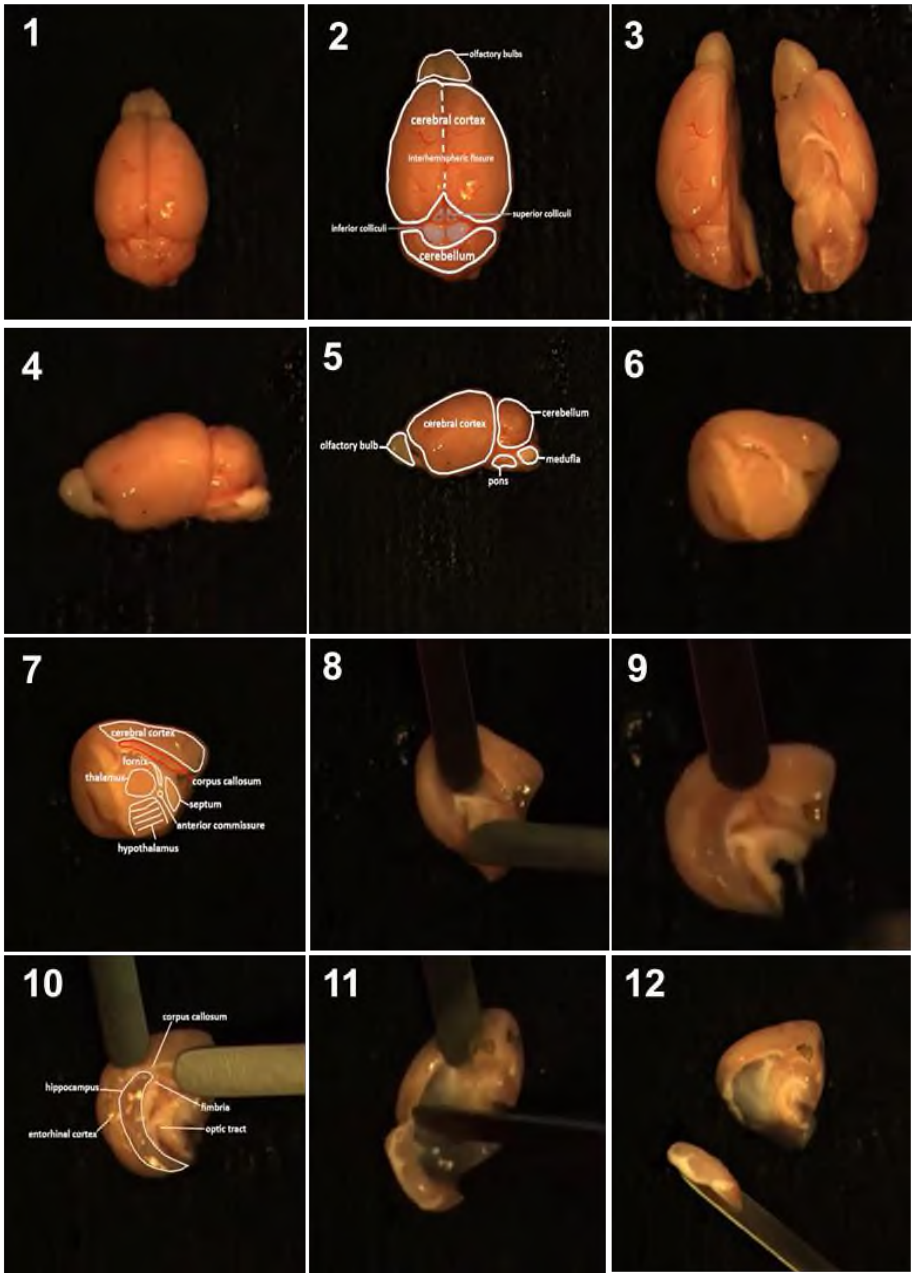

Figure 5.1: Mouse Brain Dissection and Hippocampus Isolation. Images **1-5** show that the hippocampus was removed from the skull and rinsed by cold PBS. Images **6-7** show the prefrontal cortex, and the cerebellum were trimmed and the tissue was cut sagittally from the interhemispheric fissure. Images **8-9** show the gentle pulling out of the thalamus, septum, and underlying stratum, removing this block of tissue using the other spatula. Image **10** shows that the banana-shaped hippocampus was easy to see at this step. Images **11-12** show that the rolling of the spatula separated the hippocampus from the cortex. (https://www.youtube.com/watch?v=XUbIOG1Euf4).

5.3.3 **Tissue Lysis Preparation**

After isolating the hippocampi, one hippocampus was used to prepare lysate for cytokine array work. Cytokine Proteome ProfilerTM Array (Mouse Cytokine Array Panel A) was purchased from biotechne^{R} R&D SYSTEMS. The average weight of the hippocampus in mice aged 2 months was ~15 mg. Based on previous research using the same kit, 100 µg for mouse hippocampal lysate was processed following the manufacturer's instructions (Scuderi et al., 2018, Beggiato et al., 2020). That means a 1:15 dilution would be sufficient for the homogenization of the hippocampus because it is expected to contain protein > 10 µg/µL. The resulting yield provided protein concentration > 10 µg/µL would be enough protein required for the reaction of antibody-antigen of the membrane due to the kit (Scuderi et al., 2018, Beggiato et al., 2020). WT mice would be expected to contain no, or low, cytokines concentrations therefore I used 1000 µg per membrane to avoid a weak signal. In summary, lysate of one hippocampus homogenized in 1 ml BPS should be sufficient to give a reaction in the array.

To avoid degradation of the proteins in the samples/solution during the preparation of the lysate I used cold solutions and an ice bath as recommended. The following steps explain the tissue homogenization for the Mouse Cytokine Array Panel A kit material and procedure:

1. 200 ml of ice-cold PBS was prepared.
2. 10 ml of 1X PBS with 1 complete mini protease inhibitor cocktail tablet was vortexed.
3. Homogenization of hippocampal tissue with 1X PBS at 1:15 (w: v) was achieved by adding 1% Triton-X 100 (approximately 3 µl) followed by a protease inhibitor cocktail (150 µl per hippocampus). Then quick vertexing and passing the tissue multiple times through 1000 µl and 200 µl tips of the insulin syringe needle was the easiest way to accomplish hippocampus tissue homogenization.
4. Lysate was then frozen at -70° C for at least 2 hours, then thawing the tissue was an essential step to complete lysis of the tissue.
5. The samples were then centrifuged at 10,000xg for 5 minutes at 4°C to split the debris from the supernatant.

6. The Bicinchoninic assay (BCA), a colorimetric test based on copper that is used to quantify the protein, was performed to determine the protein concentration of the used samples.

5.3.4 Preparation Standards for Measuring Protein Concentration:

To determine the protein concentration in the hippocampal lysate, the BCA method depending on the following steps:

1. To prepare the solution, 100 mg of bovine serum albumin (BSA) powder was dissolved in an amount of PBS 1X, resulting in a 10 mg/ml concentration at the end of the procedure.
2. To prepare 1000 µg/ml, 1 ml of the solution above was diluted with 9 ml of PBS 1X. 8 Eppendorf tubes of BSA 1000, 800, 600, 400,200, 100, 50, and 0.0 µg/ml were prepared.
3. 190 µl of A+B (50:1) standards were added to the first and second columns of a 96 well-plate (usually prepared by mixing 4900 µl of A+B and 100 µl of A+B) standards to the third and fourth columns, two for the WT lysis and two for the hA30P lysis, followed by the addition of 10 µl of 0.0 g/ml standard concentrations as duplicates to A1 and A2. Then, 10 µl each of 50 g/ml standard concentration was added to B1 and B2. A duplicate of 10 µl at 100 g/ml standard concentration was added in C1 and C2. A duplicate of 10 µl at 1000 g/ml standard concentration was also added in C1. From the WT lysis, 10 µl was added to A3 and A4. From the hA30P lysis, 10 µl was added to B3 and B4. It was important to avoid air bubbles when mixing each addition. 96 well-plate standards were diluted 1:50 (1 µl tissue lysis + 49 µl 1X PBS) before use.
4. The plate was left at room temperature for 30 minutes.
5. To quantify hippocampus protein concentration. I measured the absorbance by a spectrophotometer for the whole 96 well-plate and plotted the absorbance reading (Fig 5.2).

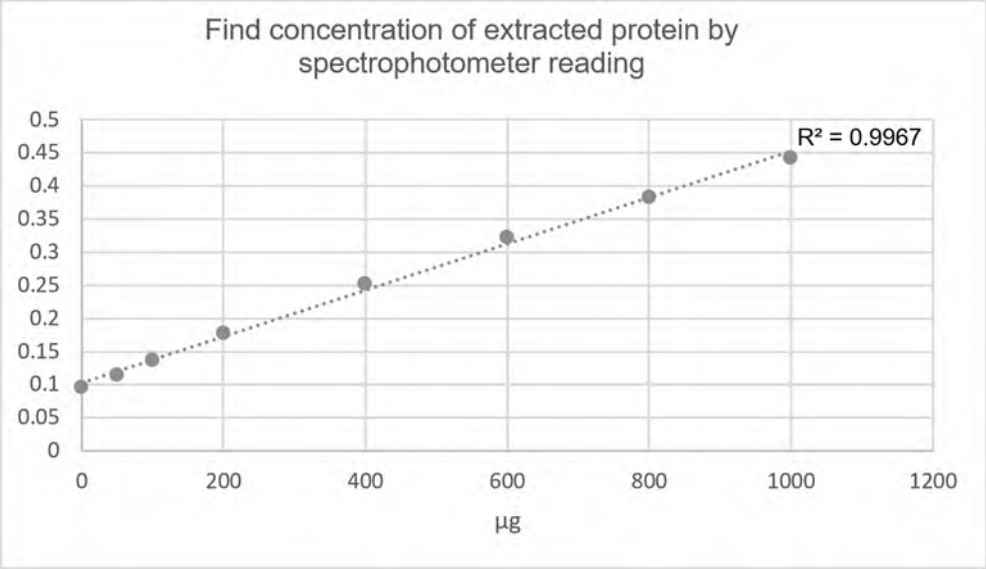

Figure 5.2: Quantification of Protein Concentration. The plot shows the relationship between absorbance reading in a spectrophotometer at 562 nm wavelength and the concentration of extracted protein from hippocampal tissue lysate on the Bicinchoninic assay.

5.3.5 Mouse Cytokine Array Panel A

To measure cytokines and chemokines levels in the hippocampus lysate, a commercial kit available from biotechne^{R} R&D SYSTEMS (Abingdon UK), Proteome Profiler^{TM} Array (Mouse Cytokine Array Panel A) with Catalog Number (ARY006) was used by applying the manufacturer's instructions.

Mouse Cytokine Array Panel A differentiates cytokines levels between samples by detection simultaneously. Without performing numerous immunoassays, it is possible to determine relative levels of expression for 40 mouse cytokines with detection antibodies listed in the kit leaflet's appendix (Table 5.1).

Proteome Profiler Mouse Cytokine Array Kit, Panel A uses a sandwich immunoassay on nitrocellulose membranes that have been spotted with capture antibodies in duplicate.

The procedure of the kit involved three main steps:

Step 1: The samples were diluted and mixed with a cocktail of biotinylated detection antibodies.

Step 2: The sample-antibody mixture was placed on the Mouse Cytokine Array membranes for incubation. Membrane-immobilized captured antibodies (spotted in duplicate) were bonded to any cytokine/detection antibody complex present.

Step 3: After a wash to remove unbound material, Streptavidin-HRP, and chemiluminescent detection reagents were added sequentially. Chemiluminescent detection reagents were used to visualize captured proteins. There was a proportional increase in light production at each spot based on the amount of cytokine bound. There is a video showing the procedure at https://www.youtube.com/watch?v=1lt1f_-Elwg.

Table 5.1: Mouse Cytokines of the Array Panel A

Target	Target
BLC	IL-16
C5/C5a	IL-17
G-CSF	IL-23
GM-CSF	IL-27
I-309	IP-10
Eotaxin	I-TAC
sICAM-1	KC
IFN-ϒ	M-CSF
IL-1α	JE
Il1β	MCP-5
IL-1ra	MIG
IL-2	MIP-1α
IL-3	MIP1β
IL-4	MIP-2
IL-5	RANTES
IL-6	SDF-1
IL-7	TARC
IL-10	TIMP-1
IL-13	TNF-α
IL-12 p70	TREM-1

Figure 5.3: Chem illumination by Densitometric Chemi XRQ and FIJI Program. The top panel and bottom panel represented an image of a nitrocellulose membrane treated with WT protein lysate at the top and with hA30P protein lysate at the bottom.

Based on an analysis of the average grey value (0–255) for each spot on the array, the relative expression of each cytokine was calculated. Starting with the positive (reference) spots, and ending with the negative (blank) spots, (a signal generated from a clear area on the array, or a negative control spot was used as a background value). The pixel density signal values for each spot were analysed by FIJI and recorded in a spreadsheet file in Microsoft Excel to manipulate each spot of the array using a template (Fig. 5.3, and Table 5.1). The average signal (pixel density) of each pair of duplicate spots was calculated. Then, the following formula was used to determine the relative signal intensity for each spot on the array:

$$\text{Relative intensity} = \frac{\text{(Measured gray value} - \text{average gray value of negative control)/ average gray value of positive control)}}{100}$$

5.3.7 LF-MS Proteomics Analysis

In this analysis, the hippocampi from the opposite hemisphere of the mice used in the cytokine array above were used. The labelled frozen hippocampi of WT and hA30P mice were sent off to the Protein and Proteomics unit at Newcastle University, where their proteomic analysis protocol was applied.

In summary, the LF-MS process included the homogenization of hippocampus tissue, after that the extracted protein was alkylated and acidified by S-trap cartridges. Then, it was digested with trypsin enzyme. The resulting peptide samples were injected in Exploris 480 via Thermo Scientific liquid chromatography-mass spectrometry (LC-MS) instrument. The peptides were separated using UltiMate 3000 RSLCnano HPLC (Tyanova et al., 2016) (Fig. 5.4).

5.3.8 Proteomic Statistical Analysis

An alignment was performed between the raw proteomic data (peptide sequence intensity) acquired from the Protein and Proteomics Unit and the known sequences of proteins via MaxQuant v2.0.3.0 program. Peptides that aligned with less than at least two unique peptide hits were discarded. Averages of the five most sequence-intense peptides related to a given protein indicated the abundance of that protein. Excel was used to log2 transform and normalize the data for both hA30P cases (N = 5) and WT cases (N = 5). To control the unequal loading during peptide injection in the LC-MS instrument, the medians of each data set of a protein were equalized and adjusted by using the subtract function in the Perseus program for normalization. The analysis excludes peptides that are not present in 100% of all used hippocampal lysate peptides of hA30P or WT mice.

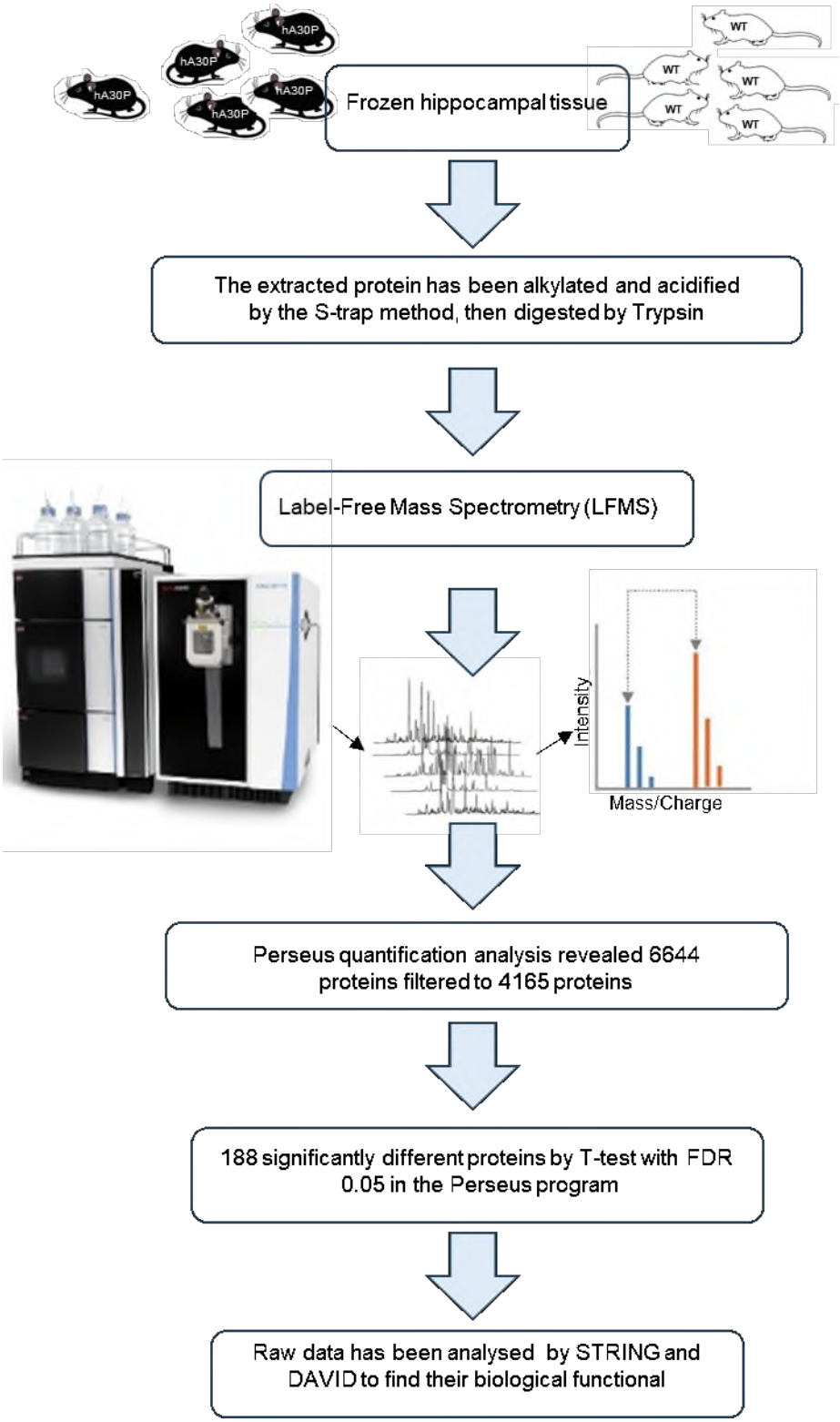

Figure 5.4: LF-MS Proteomics Analysis Steps

A report of the results was generated to include protein groups. I received the report from the Protein and Proteomics Unit and conducted further processing in Perseus (version 1.6.15.0). Then the data were pooled to compare hA30P cases versus WT cases. According to the normal distribution of the data, the values are imputed in the Perseus program. The confidence cut-off representative of the False Discovery Rate (FDR) was applied to the search result file on both peptide and protein levels. The FDR was estimated in Perseus using a two-sample t-test, and permutation-based algorithm. The FDR is a statistical term to adjust the p-value of multiple comparisons, calculated as follows: false positives/false positives plus true positives. When the cutoff of FDR is smaller, more emphasis is placed on changes that result from the statistical calculation. So, that I depended on FDR = 0.05. The s0 is used to minimize the coefficient of variation. The s0 adjusts the relative importance of the p-value of a t-test and the difference between medians. When s0 equals 0 only the p-value matters, but also at non-zero s0 the difference of medians plays a role. The data of the current study that presented Perseus with a threshold of s0 = 0.1 is close enough to zero to make the p-value matter more.

After the FDR analysis, those proteins that were significantly elevated or downregulated (in hA30P hippocampi compared to WT) were submitted to the Gene Ontology Reporter Database for Annotation, Visualization, and Integrated Discovery (DAVID) website (https://david.ncifcrf.gov/tools.jsp) (Dennis et al., 2003, Huang et al., 2007). The analysis was performed to identify biological processes enriched above the background group (all hA30P data were detected with significance thresholds of FDR<0.05, and s0 = 0.1). In addition, STRING, a database for evidenced and predicted interaction among proteins, (1.6.15.0) (https://string-db.org/) was used to visualize interactions between proteins in upregulated and downregulated groups. Network enrichment values were calculated using the full background proteomic set. STRING produces a network of potential protein interactions (PPI) between proteins in a network, where each node in the network represents a protein, and the thickness of the edges (lines connecting nodes) corresponds to the strength of the confidence of the protein interactions. The strength of the interaction score in STRING indicates the confidence of how much this database judges a particular interaction as true depending on the available knowledge from previous research findings. In Prism 9.0 (GraphPad Software, USA), scatter plot analysis was performed using a non-parametric Mann-Whitney test with a significance threshold of p<0.05. Then, I

analysed some proteins/genes that had a more significant difference by further bioinformatics tools available in GeneCards (https://www.genecards.org/).

5.4 ***Results***

5.4.1 Mouse Cytokine Array Panel a Result

The results obtained using the commercial cytokine array (Fig 5.3) were variable, although, I got a reliable protein concentration for every hippocampal lysate, and precisely followed the manufacturer's instructions. I kept all the steps of the experiment constant and used the same lysate of WT and the same lysate of hA30P. Overall, I conducted three different runs to try to obtain consistent results. The different runs were as follows:

The cytokine array kit had 4 nitrocellulose membranes with sequenced printed numbers as codes for labelling. For example, a kit had numbers B1017, B1018, B1019, and B1020. For the 1st experiment, I used WT lysate for the 1st membrane (odd number) and hA30P lysate for the 2nd membrane (even number). The result of pixel densitometry showed that most cytokine values were greater in the hA30P compared to WT mice. In the 2nd experiment, I used the membranes with an even number for WT and those with an odd number for hA30P lysate which gave a completely opposite result.

Finally, in the 3rd experiment, I repeated the experiment using only one hA30P hippocampus lysate sample. Surprisingly, the result showed different pixel densitometry in the two treated membranes (Fig. 5.5). When we contacted the manufacturer company, they suggested that the densitometry measures in my experiment were perhaps too low and therefore under the detection threshold for the array.

When I analysed the data, each experimental run gave statistically significant differences (Fig. 5.6). For example, interleukin 23 (IL-23) was significantly increased in hA30P mice in Experiment 1 but significantly decreased in Experiment 2 compared to WT. Then in Experiment 3 with the same lysate the hA30P sample was significantly different from itself (Fig 5.6).

Figure 5.5: Cytokine Array Result. I got variable results by using the same protein lysate for the three experiments**. A)** Cytokine Array Experiment 1 showed a significant increase in IL-23 in the hippocampus of hA30P compared to WT mice. **B)** Experiment 2, showed an opposite result, although the same lysate of experiment 1 was used. **C)** By using the same protein lysate of only hA30P of experiment 1, the result showed there was a significant difference between the nitrocellulose membranes.

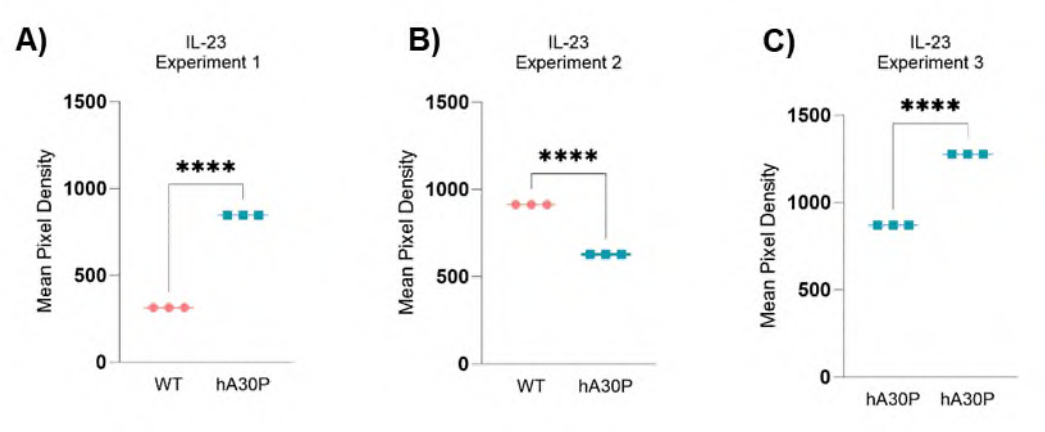

Figure 5.6: Cytokine Array IL-23 Result. I got variable results by using the same protein lysate for the three experiments**. A)** Cytokine Array Experiment 1 showed a significant increase in IL-23 in the hippocampus of hA30P compared to WT mice. **B)** Experiment 2, showed an opposite result, although the same lysate of experiment 1 was used. **C)** By using the same protein lysate of a hA30P mouse of experiment 1, the result showed there was a significant difference between the nitrocellulose membranes.

In view of the variability in the above cytokine array experiments, I went on to conduct a proteomic analysis of young WT versus hA30P hippocampus.

5.4.2 Label-Free Mass Spectrometry (LF-MS) Proteomics Result

In this experiment, I used 5 male 2-month-old hA30P mice bred in-house, and another 5 sex and age-matched WT bought in from an external provider on different dates. The scatter plot of principal component analysis (PCA) in this attempt illustrated that there was a difference between hA30P and WT hippocampal protein content (proteomics), but while the hA30P group seemed to be consistent, the WT mice showed a considerable spread of data. In this case, the result did not identify many proteins that were significantly different between the experimental groups. To solve this situation, we ran a new LF-MS experiment keeping the same hA30P mice hippocampal tissue samples but a new group of WT group that had also been bred in-house in the CBC of Newcastle University. This time the PCA resulted in clearly separated groups between WT and hA30P mice (Fig. 5.7).

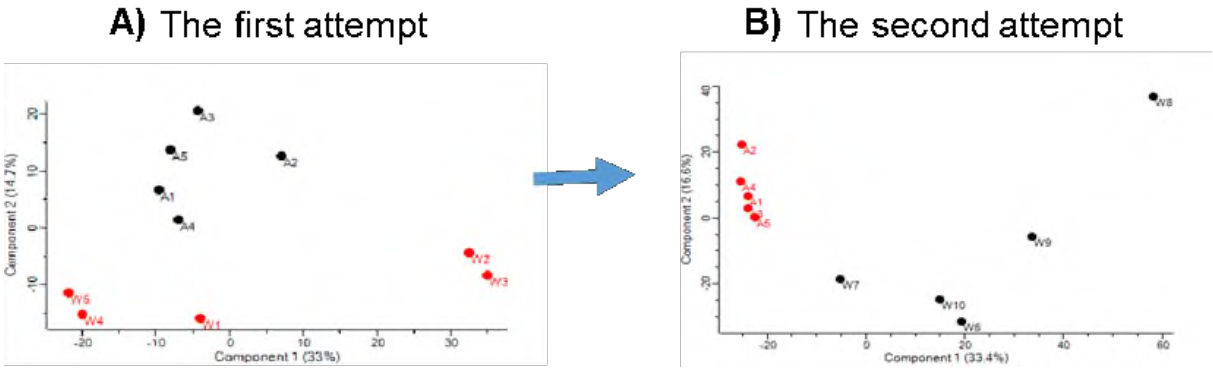

Figure 5.7: Scatter Plot Principal Component Analysis (PCA). A) Represented the first experiment of LF-MS using hA30P mice that had been bred in the CBC, and WT mice that had been bought from the external provider at different dates. The result showed there was an interaction between the two groups, but the data were not very well separated. **B)** Represented the second experiment of LF-MS using hA30P and WT mice had been bred in the CBC, the result showed there was a good separation in their protein content between the different genotypes.

5.4.3 Proteomic Analysis of Hippocampal Tissue of hA30P Versus WT Mice Revealed 4165 Unique Proteins

LF-MS quantification for the proteome resulted in 6644 proteins filtered to 4165 proteins when excluding those with only 1 peptide detected, and subsequent proteomic analysis revealed there were 4165 unique protein elements (FDR = 0.05, and s0 = 0.1 threshold) identified in the samples. The number of significantly elevated proteins was 158 in the hippocampus of hA30P (N = 5) versus control of WT mice (N = 5), while there were 30 proteins reported as being significantly reduced (Fig. 5.8).

The data plotted as a hierarchal clustering (heat map platform) analysis of differential gene expression with upregulated proteins in red, and downregulated proteins in green (Fig. 5.9).

Bioinformatics and Evolutionary Genomics

Input files:

List names	number of elements	number of unique elements
proteins	4268	4165
significant down regulated	24	24
significant up-regulated	139	138
Overall number of unique elements		4165

Image result:

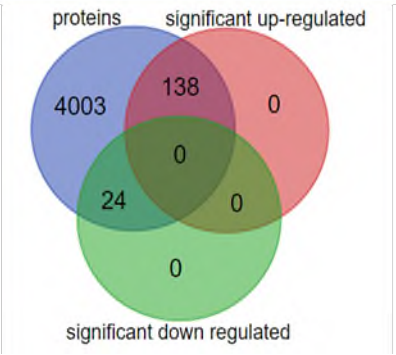

Figure 5.8: Venn diagram of differentially regulated proteins. Although LF-MS revealed 158 significant up-regulated proteins and 30 significant down-regulated proteins in the hippocampus of hA30P (N = 5) versus control of WT mice (N = 5). The Venn diagram revealed there was a significant elevation of 138 proteins and there were 24 reported as being significantly reduced. The rest of the proteins were not identified.

Proteomics analysis of LF-MS was then visualized via a volcano plot generated by Perseus (Fig. 5.10). The protein which was the highest p-value in the plot was the SNCA showing that this protein showed the greatest upregulated protein that was quantified in hA30P compared to WT mice and help validate the remainder of our findings.

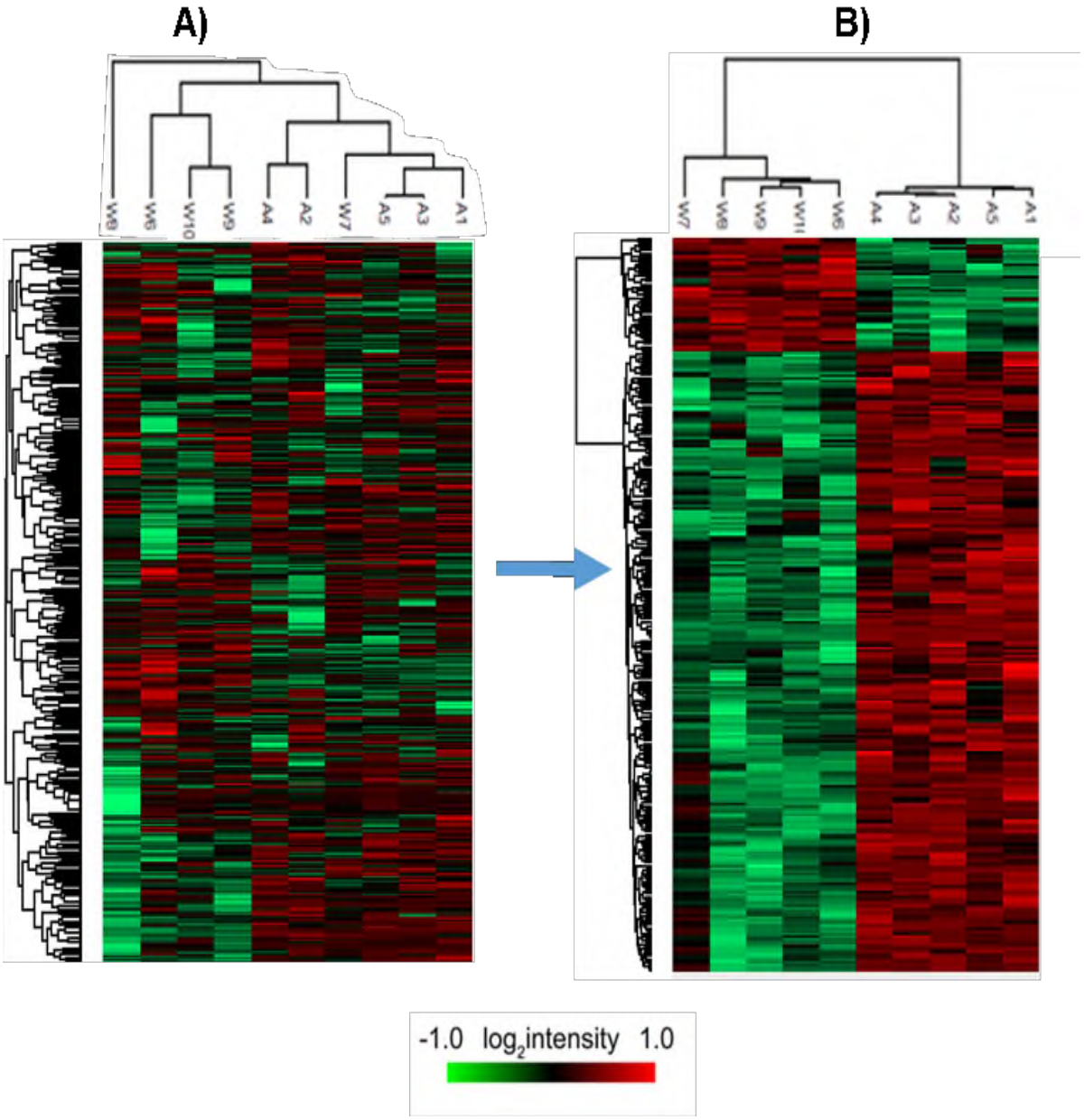

Figure 5.9: Heat Map Comparison of Protein Expression of Hippocampal Tissue of hA30P Versus WT Mice. The hierarchal clustering analysis illustrated expression levels of individual proteins in total lysates acquired from both WT (N=5 mice) and hA30P (N=5 mice) hippocampi tissue. Upregulated proteins were in red, and downregulated were in green colour.

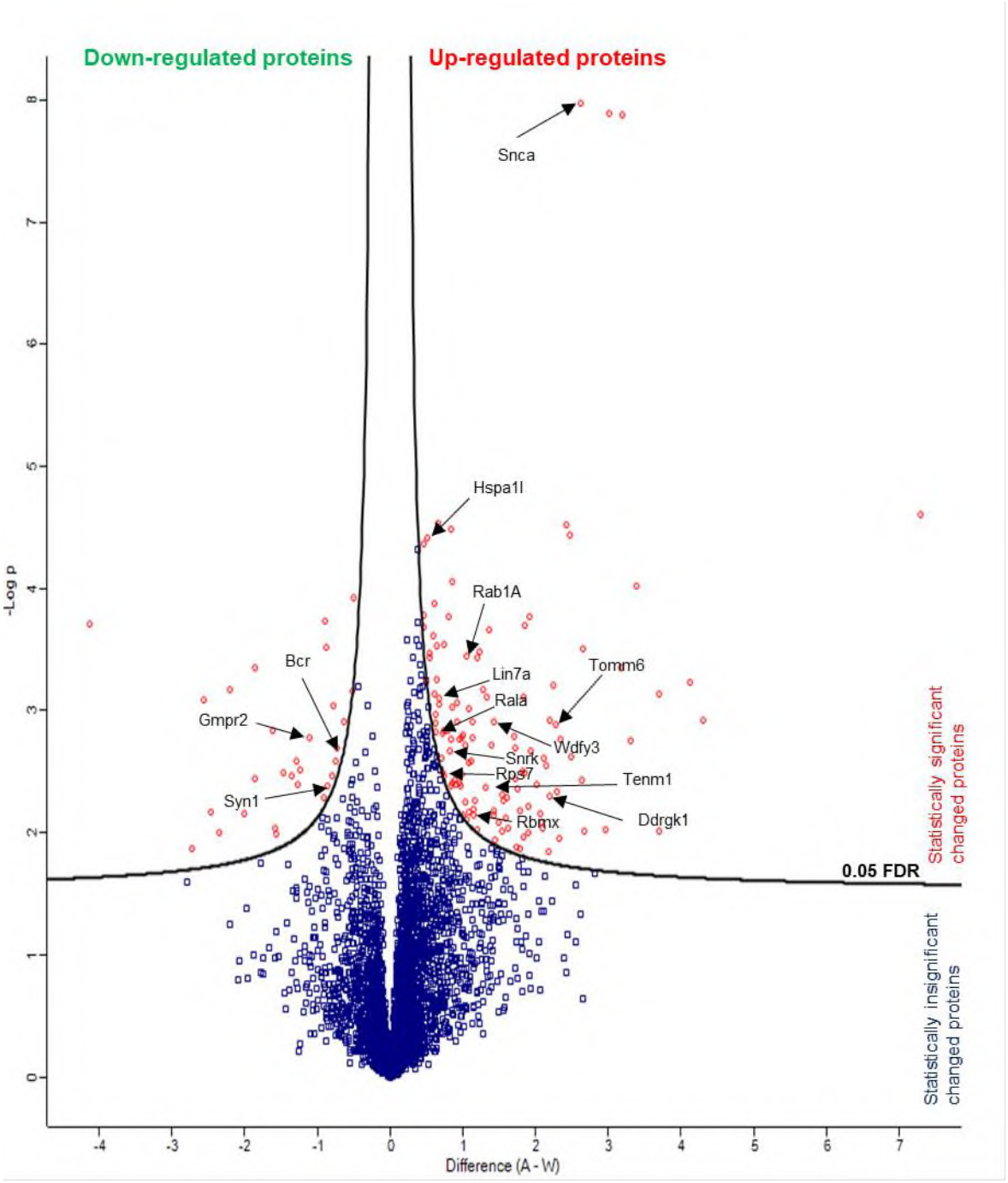

Figure 5.10: Volcano Plot of Proteomic Data. The Y-axis is –Log 2 of P-VALUE, and X- the axis is Log 2 of Fold Change for difference between hA30P-WT (A-W), and threshold of 0.05 FDR (false discovery rate). Proteins that have significant differences are highlighted in red, and non-significant differences are in blue. LM-FS and subsequent proteomic functional analysis revealed the significant elevation of 158 proteins and there were 30 reported as being significantly reduced in the hippocampus of hA30P (N = 5) versus control of WT mice (N = 5).

The 158 proteins that were significantly different in hA30P compared to WT mice are indicated in Perseus. The proteins that were unchanged are indicated in blue. The upregulated proteins are on the right side of the volcano plot, and the down-regulated are on the left side (Difference = hA30P-WT; A-W). I summarized the top 15 proteins that were significantly different based on the highest fold change, between WT and hA30P mice, in Table 5.2.

Table 5.2: The highest significantly different proteins/genes between hA30P and WT mice

Gene ID	Protein Description	Fold Enrichment	Term of Functional Role	p-value of t-test
Wdfy3	WD repeat and FYVE domain containing 3	4.8 upregulated	Glycosyltransferase	p<0.05
Tenm1	Teneurin-1	4.6 upregulated	Stress response	p<0.01
Hspa1l; Hspa2; Hspa5; Hspa8	Heat shock 70 kDa protein 1-like	4.6 upregulated	Autophagy	p<0.01
Rab1A	Ras-related protein Rab-1A	2.9 upregulated	Stress response	p<0.01
Rala	v-ral simian leukemia viral oncogene A	2.8 upregulated	Exocytosis	p<0.01
Lin7a;Lin7b;Lin7c	Protein lin-7 homolog B	2.8 upregulated	Exocytosis	p<0.01
Rps7	40S ribosomal protein S7	2.4 upregulated	Ribosomal protein	p<0.01
Tomm6	Mitochondrial import receptor subunit TOM6 homolog	2.3 upregulated	Mitochondrial outer membrane	p<0.01
Rbmx	RNA binding motif protein, X chromosome	1.9 upregulated	Ribonucleoprotien	p<0.01
Snrk	SNF-related serine/threonine-protein kinase	1.2 upregulated	Nucleus	p<0.01
Ddrgk1	DDRGK domain-containing protein 1	1.9 upregulated	Autophagy	p<0.01
Snca; Sncb	α-synuclein	1.2 upregulated	Nucleus **and cytoplasm**	p<0.01
Gmpr2	guanosine monophosphate reductase 2	131.2 downregulated	Purine metabolism	p<0.01
Abr	Active breakpoint cluster region-related protein	6.2 downregulated	Guanine-nucleotide releasing factor	p<0.01
Syn1; Syn2; Syn3	Synapsin	3.5 downregulated	Synapse	p<0.05

The 15 most significantly different proteins depending on fold changes between hippocampal proteomics of hA30P and WT mice are shown in Fig. 5.11.

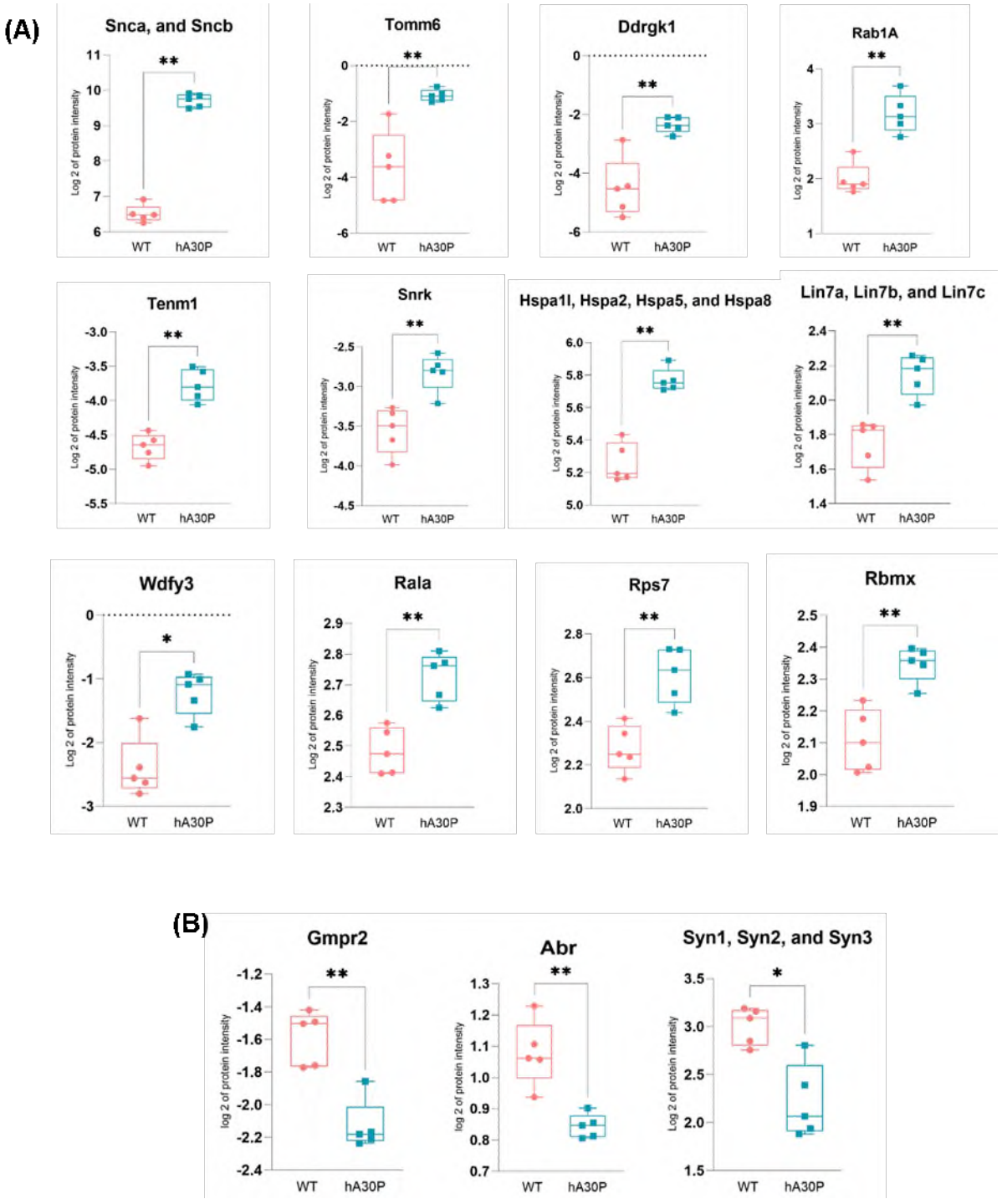

Figure 5.11: The 15 highest significantly different proteins between hA30P and WT (A) Represented GraphPad Prism plots for the highest upregulated genes. **(B)** Represented GraphPad Prism plots for the highest downregulated genes.

Interestingly, nearly all the above proteins that were upregulated in the hA30P mice are associated with autophagy, mitochondrial functions, stress response, or exocytosis. All of these are pathways one might predict would be impacted by α-syn overexpression in hA30P mice.

5.4.4 STRING Analysis Revealed 7 Distinguished Clusters of Proteins

To make the protein data results easier to visualize and to analyse the interactions between the significantly different proteins, I went on to conduct STRING analysis.

The result of the STRING PPI network of the significant difference proteomics of hA30P compared to WT mice showed there were 7 distinguishable protein clusters: 5 clusters contained upregulated proteins (Fig. 5.12) and 2 clusters contained downregulated proteins (Fig. 5.13). All these clusters had significantly more interactions in the network than would be expected by chance. In other words, the proteins interact with one another more often than would be expected if the same size and kind of proteins were randomly chosen from the genome. Biologically, such enrichment indicates at least a partial relationship among the proteins in the cluster. The result showed that all the proteins formed strong potential protein interaction networks that were represented by high PPI (Fig. 5.14, and 5.15).

The STRING proteomics data for 158 significantly elevated proteins suggested there were 5 clusters (Fig. 5.12, and 5.14) which were as follows:

1. Cluster 1 G-Protein Activity had 28 proteins.
2. Cluster 2 Cytoplasmic Translation had 22 proteins.
3. Cluster 3 mRNA Splice Site Selection had 14 proteins.
4. Cluster 4 Proteasome Degradation had 9 proteins.
5. Cluster 5 (not defined) had 2 proteins.

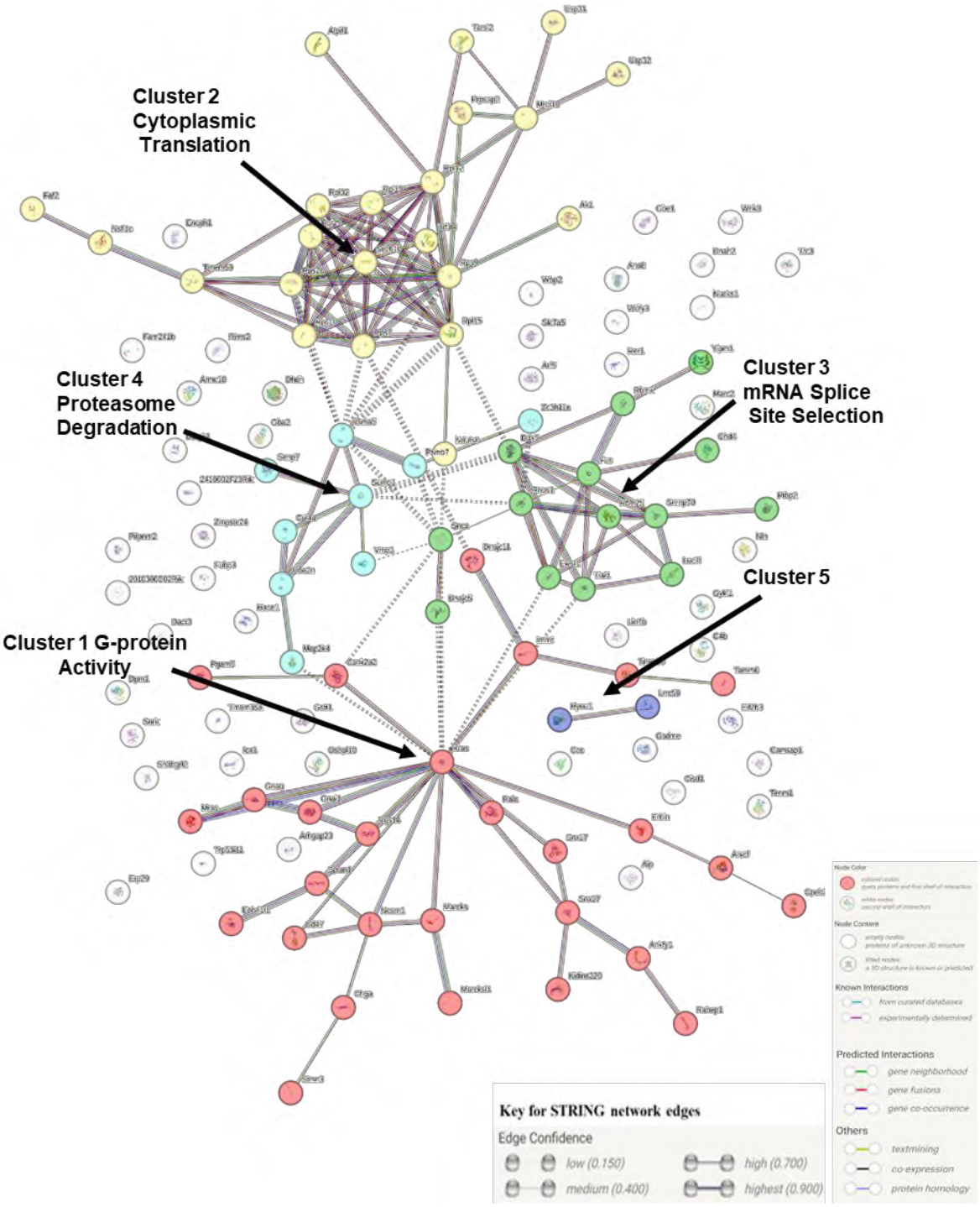

Figure 5.12: STRING Network of Potential Protein Interactions for Upregulation Proteins. Each node represents a protein, with the thickness of the network edge (line connecting nodes) representing the confidence of protein interaction with a minimum required interaction score of 0.4 medium confidence. LF-MS revealed significantly higher protein interaction networks compared to expect for 5 clusters of significantly elevated proteins.

While the STRING proteomics data for 30 significantly down-regulated proteins suggested there were 2 clusters (Fig. 5.13, and 5.15).

1. Cluster 1 (not defined) had 3 proteins.
2. Cluster 2 (not defined) had 2 proteins

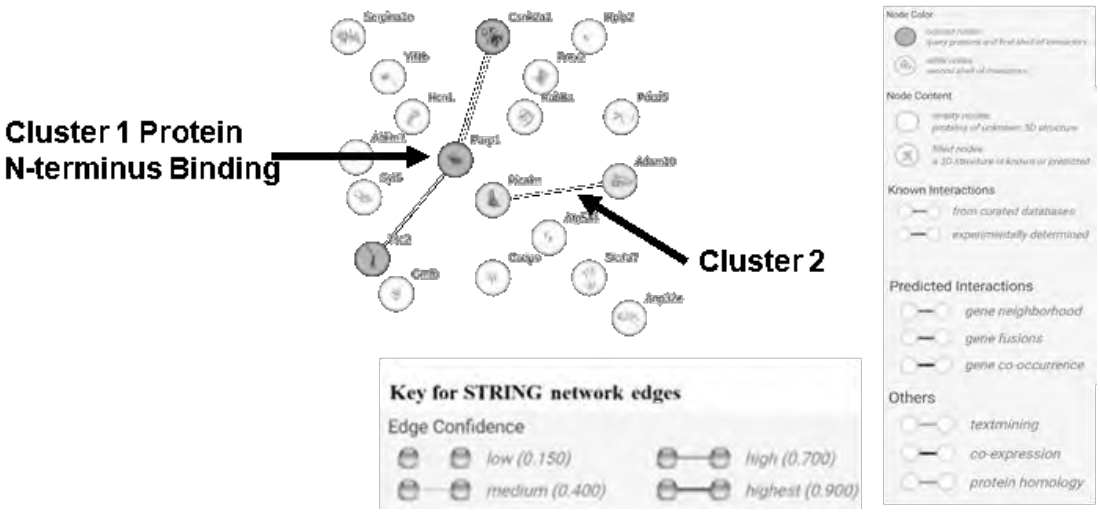

Figure 5.13: STRING Network of Potential Protein Interactions for Down-Regulated Proteins. Each node represents a protein, with the thickness of the network edge (line connecting nodes) representing the confidence of protein interaction with a minimum required interaction score of 0.4 medium confidence. LF-MS revealed 2 clusters of significantly downregulated proteins.

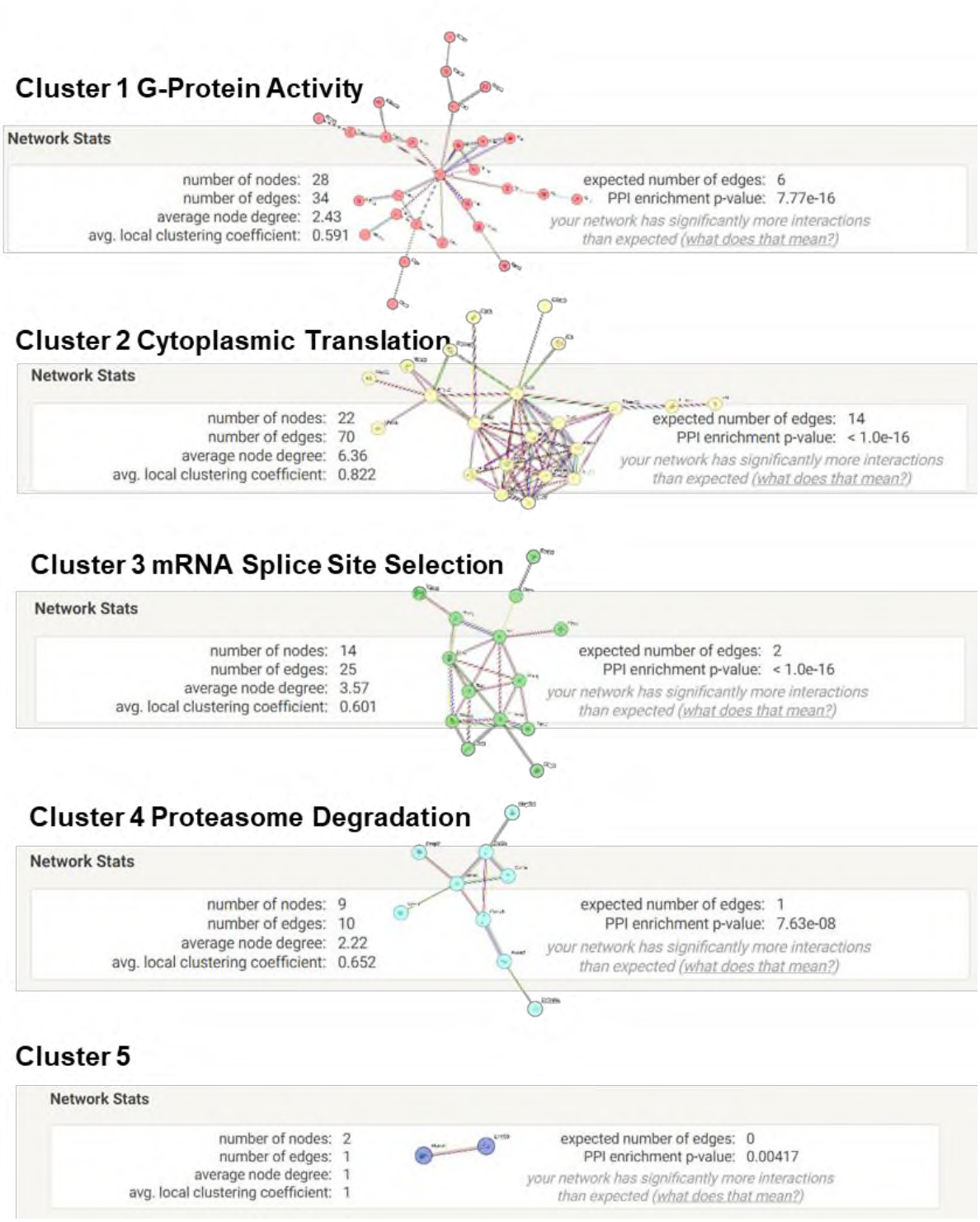

Figure 5.14: STRING Network of PPI for Significantly Upregulated Proteins in hA30P Compared to WT Mice. STRING network of PPI displayed 5 clusters due to upregulated proteins with their number of nodes, number of edges, expected number of edges, PPI enrichment p-value, average node degree, and average clustering coefficient in addition to their visual net. All 5 clusters had significant interactions more than expected.

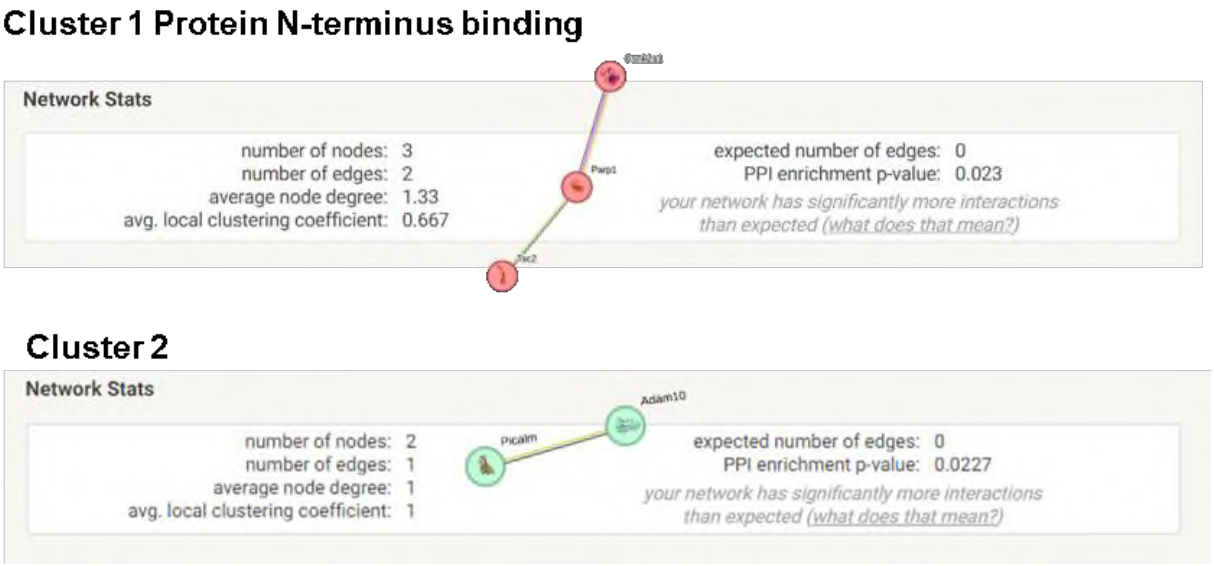

Figure 5.15: STRING Network of PPI for Significantly Downregulated Proteins in hA30P Compared to WT Mice. STRING network of PPI displayed 2 clusters of downregulated proteins with their number of nodes, number of edges, expected number of edges, PPI enrichment p-value, average node degree, and average clustering coefficient in addition to their visual net.

5.4.5 Gene Ontology Reporter DAVID Investigation for the Biological Functions of Significantly Different Proteins

To explore the potential biological function of the significantly different proteins between the hippocampus of hA30P and WT mice obtained from the proteomics test, the Gene Ontology (GO) reporter, DAVID was used.

Upregulated proteins and down-regulated proteins were analysed separately. The 158 elevated proteins were entered as a 'Gene List' in DAVID, along with a background protein list that included the 4165 proteins that were detected in the comparison of hippocampi of hA30P mice (N=5) versus 5 WT mice (N=5). Based on this, three biological functionally distinct groups were represented in (Figs. 16, 17, 18, and 19).

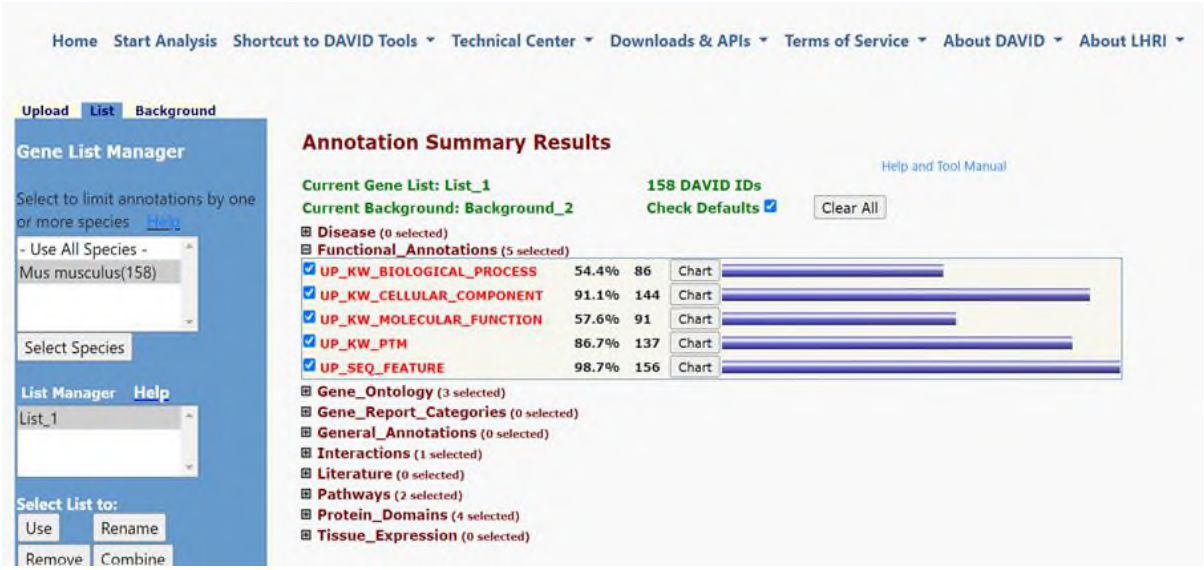

Figure 5.16: The Output Summary of the Function Annotation Reporter in the DAVID. The data input resulted in 158 Significantly Upregulation Proteins in hA30P Compared to WT mice. The result revealed that 3 main charts depending on biological function groups in hA30P compared to WT mice (background) have been inputted.

5.4.6 The First Function Group of Upregulated Proteins/Genes by Gene Ontology Reporter DAVID for the Biological Functions

The first functional group of upregulated proteins in the gene ontology reporter DAVID identified consisted of 6 groups of proteins that related to the following cellular functions (Fig. (Fig 5.17 a-c).

1. **Stress Response** with enrichment 4.6-fold above the background and contained 7 genes (Fig. 5.17b).

2. **Autophagy** with enrichment 2.9-fold above the background and contained 7 genes (Fig. 5.17b).

3. **mRNA splicing** with enrichment 2.1-fold above the background and contained 10 genes (Fig. 5.17b).

4. **Ubiquitin (Ubl) Conjugation Pathway** with enrichment 1.9-fold above the background and contained 11 genes (Fig. 5.17c).

5. **mRNA processing** was expressed with enrichment 1.8-fold above the background and contained 10 genes (Fig. 5.17c).

6. **Exocytosis** with enrichment 2.8-fold above the background and contained 5 genes (Fig. 5.17c).

The first functional group of upregulated proteins almost overlapped with the groups identified in the STRING analysis, which included upregulated G protein activity from cluster 1, and mRNA splice site selection, from cluster 3 (Fig. 5.12, and 5.14)

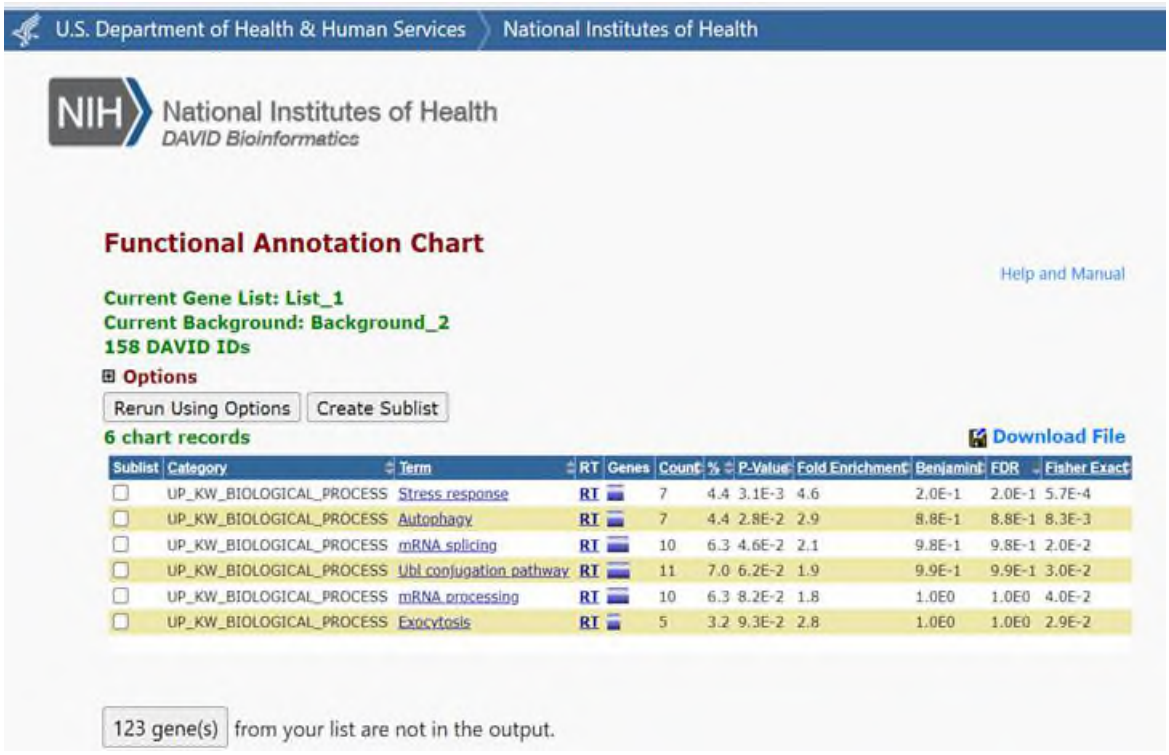

Sublist	Category	Term	RT	Genes	Count	%	P-Value	Fold Enrichment	Benjamini	FDR	Fisher Exact
☐	UP_KW_BIOLOGICAL_PROCESS	Stress response	RT		7	4.4	3.1E-3	4.6	2.0E-1	2.0E-1	5.7E-4
☐	UP_KW_BIOLOGICAL_PROCESS	Autophagy	RT		7	4.4	2.8E-2	2.9	8.8E-1	8.8E-1	8.3E-3
☐	UP_KW_BIOLOGICAL_PROCESS	mRNA splicing	RT		10	6.3	4.6E-2	2.1	9.8E-1	9.8E-1	2.0E-2
☐	UP_KW_BIOLOGICAL_PROCESS	Ubl conjugation pathway	RT		11	7.0	6.2E-2	1.9	9.9E-1	9.9E-1	3.0E-2
☐	UP_KW_BIOLOGICAL_PROCESS	mRNA processing	RT		10	6.3	8.2E-2	1.8	1.0E0	1.0E0	4.0E-2
☐	UP_KW_BIOLOGICAL_PROCESS	Exocytosis	RT		5	3.2	9.3E-2	2.8	1.0E0	1.0E0	2.9E-2

Figure 5.17a: Function Group 1 of Functional Annotation Clustering for Biological Function Reporter in the DAVID of Significantly Upregulated Protein in hA30P Compared to WT Mice. The result revealed that there were 6 terms involved proteins that related to Stress Response, Autophagy, and mRNA splicing Exocytosis, Ubl conjugation pathway, and Exocytosis were expressed proteins in hA30P compared to WT mice (background).

5.4.7 The Second Biological Function Group of Upregulated Proteins/Genes by Gene Ontology Reporter DAVID for the Biological Functions

The second function group of upregulated proteins in the gene ontology reporter DAVID consisted of 3 groups of proteins that related to the following cellular functions (Fig. 5.18a-c):

1. **Mitochondrial Outer Membrane (MOM)** with enrichment 2.3-fold above the background and contained 16 genes (Fig. 5.18b).
2. **Golgi Apparatus** with enrichment 1.6-fold above the background and contained 50 genes (Fig. 5.18b).
3. **Nucleus** with enrichment 1.2-fold above the background and contained 7 genes (Fig. 5.18c).

(A)

158 DAVID IDs
7 record(s)

1) Stress Response

OFFICIAL_GENE_SYMBOL	GENE NAME
Hspa1l	heat shock protein 1-like(Hspa1l)
Hspa2	heat shock protein 2(Hspa2)
Hspa8	heat shock protein 8(Hspa8)
Hyou1	hypoxia up-regulated 1(Hyou1)
Map2k4	mitogen-activated protein kinase kinase 4(Map2k4)
Sumo1	small ubiquitin-like modifier 1(Sumo1)
Tenm1	teneurin transmembrane protein 1(Tenm1)

(B)

158 DAVID IDs
7 record(s)

2) Autophagy

OFFICIAL_GENE_SYMBOL	GENE NAME
Rab1A	RAB1A, member RAS oncogene family(Rab1a)
Rab1b	RAB1B, member RAS oncogene family(Rab1b)
Wdfy3	WD repeat and FYVE domain containing 3(Wdfy3)
Hspa8	heat shock protein 8(Hspa8)
Map1lc3a	microtubule-associated protein 1 light chain 3 alpha(Map1lc3a)
Map1lc3b	microtubule-associated protein 1 light chain 3 beta(Map1lc3b)
Vmp1	vacuole membrane protein 1(Vmp1)

(C)

158 DAVID IDs
10 record(s)

3) mRNA splicing

OFFICIAL_GENE_SYMBOL	GENE NAME
Ddx17	DEAD box helicase 17(Ddx17)
Ddx5	DEAD box helicase 5(Ddx5)
Rbm25	RNA binding motif protein 25(Rbm25)
Rbmx	RNA binding motif protein, X chromosome(Rbmx)
Rnps1	RNA binding protein with serine rich domain 1(Rnps1)
Arvcf	armadillo repeat gene deleted in velocardiofacial syndrome(Arvcf)
Hspa8	heat shock protein 8(Hspa8)
Ptbp2	polypyrimidine tract binding protein 2(Ptbp2)
Srpk1	serine/arginine-rich protein specific kinase 1(Srpk1)
Srpk2	serine/arginine-rich protein specific kinase 2(Srpk2)

Figure 5.17b: Biological Function Group 1 of Functional Annotation Clustering for Biological Function Reporter in the DAVID of Significantly Upregulated Protein in hA30P Compared to WT Mice. Three terms involved proteins that related to **(A)** Stress response, **(B)** Autophagy, and **(C)** mRNA splicing with enrichment of 4.6, 2.9, and 2.8-fold respectively, above the background in hA30P compared to WT mice (background).

(D)

158 DAVID IDs
11 record(s)

4) Ubl conjugation pathway

OFFICIAL_GENE_SYMBOL	GENE NAME
Ddrgk1	DDRGK domain containing 1(Ddrgk1)
Hace1	HECT domain and ankyrin repeat containing, E3 ubiquitin protein ligase 1(Hace1)
Senp7	SUMO1/sentrin specific peptidase 7(Senp7)
Cul4a	cullin 4A(Cul4a)
Map1lc3a	microtubule-associated protein 1 light chain 3 alpha(Map1lc3a)
Map1lc3b	microtubule-associated protein 1 light chain 3 beta(Map1lc3b)
Sumo1	small ubiquitin-like modifier 1(Sumo1)
Ttc3	tetratricopeptide repeat domain 3(Ttc3)
Usp31	ubiquitin specific peptidase 31(Usp31)
Usp32	ubiquitin specific peptidase 32(Usp32)
Ube2n	ubiquitin-conjugating enzyme E2N(Ube2n)

(E)

158 DAVID IDs
10 record(s)

5) mRNA processing

OFFICIAL_GENE_SYMBOL	GENE NAME
Ddx17	DEAD box helicase 17(Ddx17)
Ddx5	DEAD box helicase 5(Ddx5)
Rbm25	RNA binding motif protein 25(Rbm25)
Rbmx	RNA binding motif protein, X chromosome(Rbmx)
Rnps1	RNA binding protein with serine rich domain 1(Rnps1)
Arvcf	armadillo repeat gene deleted in velocardiofacial syndrome(Arvcf)
Hspa8	heat shock protein 8(Hspa8)
Ptbp2	polypyrimidine tract binding protein 2(Ptbp2)
Srpk1	serine/arginine-rich protein specific kinase 1(Srpk1)
Srpk2	serine/arginine-rich protein specific kinase 2(Srpk2)

(F)

158 DAVID IDs
5 record(s)

6) Exocytosis

OFFICIAL_GENE_SYMBOL	GENE NAME
Lin7a	lin-7 homolog A, crumbs cell polarity complex component(Lin7a)
Lin7b	lin-7 homolog B, crumbs cell polarity complex component(Lin7b)
Lin7c	lin-7 homolog C, crumbs cell polarity complex component(Lin7c)
Rims2	regulating synaptic membrane exocytosis 2(Rims2)
Rala	v-ral simian leukemia viral oncogene A (ras related)(Rala)

Figure 5.17c: Biological Function Group 1 of Functional Annotation Clustering for Biological Function Reporter in the DAVID of Significantly Upregulated Protein in hA30P Compared to WT Mice. Three terms involved proteins that related to **(D)** Exocytosis, **(E)** Ubl conjugation pathway, and **(F)** Exocytosis with enrichment of 2.8, 1.9, and 1.8-fold respectively, above in hA30P compared to WT mice (background).

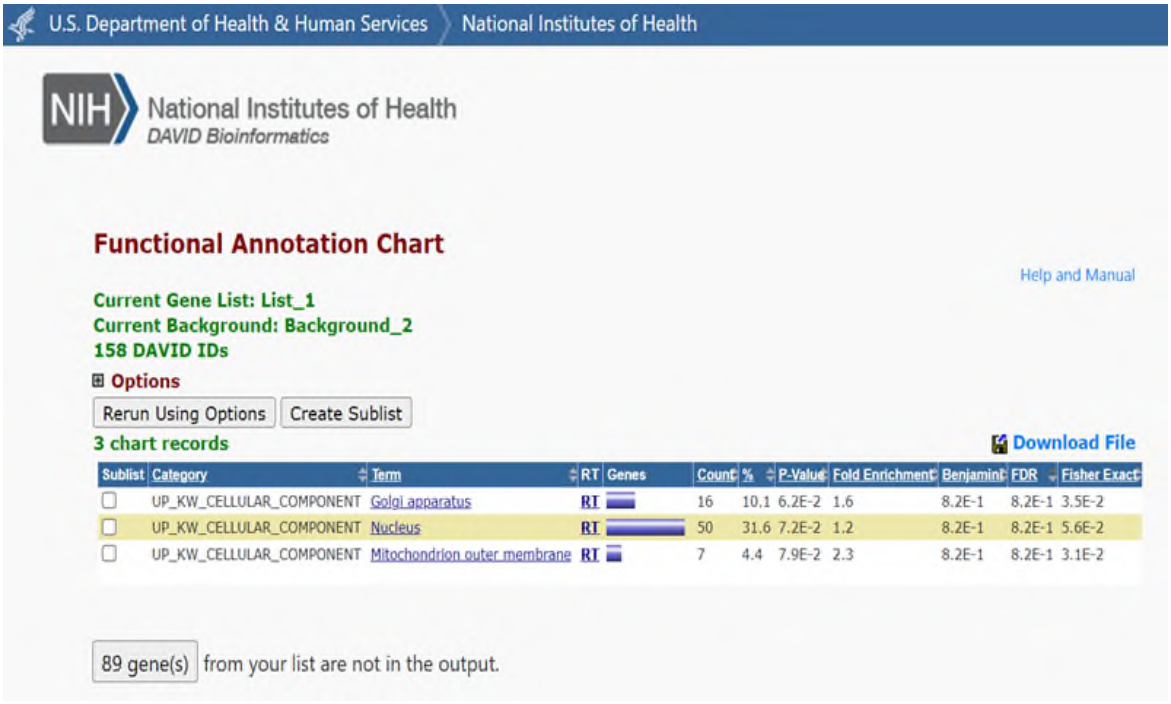

Figure 5.18a: Biological Function Group 2 of Functional Annotation Clustering for Biological Function Reporter in the DAVID of Significantly Upregulated Protein in hA30P Compared to WT Mice). The result revealed that three terms involved proteins related to the Golgi apparatus, the Mitochondrial outer membrane, and the Nucleus were expressed in hA30P compared to WT mice (background).

This chart almost represented Cluster 2 from upregulated proteins of Cytoplasmic translation that have been identified from STRING analysis (Fig.5.12, and 14).

5.4.8 The Third Biological Function Group of Upregulated Proteins/Genes by Gene Ontology Reporter DAVID for the Biological Functions

The third functional group of upregulated proteins in the gene ontology reporter DAVID identified consisted of 3 groups of proteins that related to the following cellular functions (Fig. 5.19a, and b):

1. **Ribosomal Protein** with enrichment 2.4-fold above the background and contained 10 genes (Fig. 5.19b).
2. **Ribonucleoprotein** with enrichment 7.6-fold above the background and contained 12 genes (Fig. 5.19b).
3. **Glycosyltransferase** with enrichment 2.5-fold above the background and contained 4 genes (Fig. 5.19b).

(A)

158 DAVID IDs
16 record(s)

1) Golgi apparatus

OFFICIAL_GENE_SYMBOL	GENE NAME
Arf1	ADP-ribosylation factor 1(Arf1)
Arf2	ADP-ribosylation factor 2(Arf2)
Arf4	ADP-ribosylation factor 4(Arf4)
Arf5	ADP-ribosylation factor 5(Arf5)
Hace1	HECT domain and ankyrin repeat containing, E3 ubiquitin protein ligase 1(Hace1)
Kras	Kirsten rat sarcoma viral oncogene homolog(Kras)
Nsfl1c	NSFL1 (p97) cofactor (p47)(Nsfl1c)
Rab1A	RAB1A, member RAS oncogene family(Rab1a)
Gba2	glucosidase beta 2(Gba2)
Gnaq	guanine nucleotide binding protein, alpha q polypeptide(Gnaq)
Ica1	islet cell autoantigen 1(Ica1)
Rer1	retention in endoplasmic reticulum sorting receptor 1(Rer1)
Snx1	sorting nexin 1(Snx1)
Stmn3	stathmin-like 3(Stmn3)
Ttc3	tetratricopeptide repeat domain 3(Ttc3)
Usp32	ubiquitin specific peptidase 32(Usp32)

(B)

158 DAVID IDs
7 record(s)

2) Mitochondrial outer membrane

OFFICIAL_GENE_SYMBOL	GENE NAME
Cisd1	CDGSH iron sulfur domain 1(Cisd1)
Dnajc11	DnaJ heat shock protein family (Hsp40) member C11(Dnajc11)
Armc10	armadillo repeat containing 10(Armc10)
Gykl1	glycerol kinase-like 1(Gykl1)
Mtarc2	mitochondrial amidoxime reducing component 2(Mtarc2)
Pgam5	phosphoglycerate mutase family member 5(Pgam5)
Tomm6	translocase of outer mitochondrial membrane 6(Tomm6)

Figure 5.18b: Biological Function Group 2 of Functional Annotation Clustering for Biological Function Reporter in the DAVID of Significantly Upregulated Protein in hA30P Compared to WT Mice. The 2 terms involved proteins that related to **(A)** Golgi apparatus, and **(B)** Mitochondrial outer membrane with enrichment of 1.6, and 2.3-fold respectively above the background in hA30P compared to WT mice (background).

This biological function group almost represents Cluster 5 of upregulated proteins of proteasome degradation that resulted from STRING analysis (Fig.5.12, and 14).

(C)

158 DAVID IDs
50 record(s)

3) Nucleus

OFFICIAL_GENE_SYMBOL	GENE NAME
Ddx17	DEAD box helicase 17(Ddx17)
Ddx5	DEAD box helicase 5(Ddx5)
Erbin	Erbb2 interacting protein(Erbin)
Ewsr1	Ewing sarcoma breakpoint region 1(Ewsr1)
Gnai1	G protein subunit alpha i1(Gnai1)
Hdgfl2	HDGF like 2(Hdgfl2)
Hdgfl3	HDGF like 3(Hdgfl3)
Nsfl1c	NSFL1 (p97) cofactor (p47)(Nsfl1c)
Psip1	PC4 and SFRS1 interacting protein 1(Psip1)
Rbm25	RNA binding motif protein 25(Rbm25)
Rbmx	RNA binding motif protein, X chromosome(Rbmx)
Rnps1	RNA binding protein with serine rich domain 1(Rnps1)
Sh3bgrl2	SH3 domain binding glutamic acid-rich protein like 2(Sh3bgrl2)
Snrk	SNF related kinase(Snrk)
Tial1	Tia1 cytotoxic granule-associated RNA binding protein-like 1(Tial1)
Wdfy3	WD repeat and FYVE domain containing 3(Wdfy3)
Wbp2	WW domain binding protein 2(Wbp2)
Ylpm1	YLP motif containing 1(Ylpm1)
Arvcf	armadillo repeat gene deleted in velocardiofacial syndrome(Arvcf)
Csnk2a2	casein kinase 2, alpha prime polypeptide(Csnk2a2)
Chd4	chromodomain helicase DNA binding protein 4(Chd4)
Cyfip2	cytoplasmic FMR1 interacting protein 2(Cyfip2)
Enoph1	enolase-phosphatase 1(Enoph1)
Fubp3	far upstream element (FUSE) binding protein 3(Fubp3)
Fus	fused in sarcoma(Fus)
Gstt1	glutathione S-transferase, theta 1(Gstt1)
Gnaq	guanine nucleotide binding protein, alpha q polypeptide(Gnaq)
Hspa8	heat shock protein 8(Hspa8)
Hdgf	heparin binding growth factor(Hdgf)
Lrrc59	leucine rich repeat containing 59(Lrrc59)
Map2k4	mitogen-activated protein kinase kinase 4(Map2k4)
Nucks1	nuclear casein kinase and cyclin-dependent kinase substrate 1(Nucks1)
Ptbp2	polypyrimidine tract binding protein 2(Ptbp2)
Psmb7	proteasome (prosome, macropain) subunit, beta type 7(Psmb7)
Psma5	proteasome subunit alpha 5(Psma5)
Rps10	ribosomal protein S10(Rps10)
Rps28	ribosomal protein S28(Rps28)
Rps7	ribosomal protein S7(Rps7)
Rps9	ribosomal protein S9(Rps9)
Srpk1	serine/arginine-rich protein specific kinase 1(Srpk1)
Srpk2	serine/arginine-rich protein specific kinase 2(Srpk2)
Snrnp70	small nuclear ribonucleoprotein 70 (U1)(Snrnp70)
Sumo1	small ubiquitin-like modifier 1(Sumo1)
Snca	synuclein, alpha(Snca)
Tenm1	teneurin transmembrane protein 1(Tenm1)
Ttc3	tetratricopeptide repeat domain 3(Ttc3)
Tars3	threonyl-tRNA synthetase 3(Tars3)
Usp32	ubiquitin specific peptidase 32(Usp32)
Ube2n	ubiquitin-conjugating enzyme E2N(Ube2n)
Zmpste24	zinc metallopeptidase, STE24(Zmpste24)

Figure 5.18c: Biological Function Group 2 of Functional Annotation Clustering for Biological Function Reporter in the DAVID of Significantly Upregulated Protein in hA30P Compared to WT Mice. The term involved proteins related to **(C)** Nucleus with enrichment 1.2-fold above the background in hA30P compared to WT mice (background).

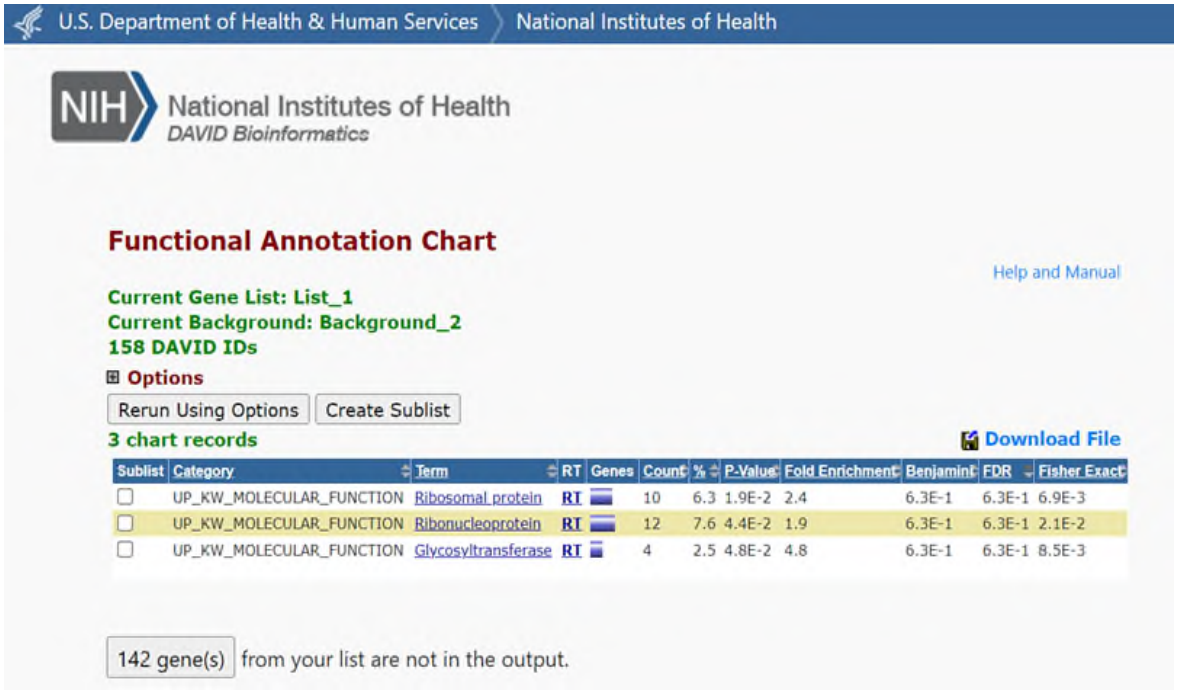

Figure 5.19a: Biological Function Group 3 of Functional Annotation Clustering for Biological Function Reporter in the DAVID of Significantly Upregulated Protein in hA30P Compared to WT Mice). The result revealed that three terms involved proteins related to Ribosomal Protein, Ribonucleoprotein, and Glycosyltransferase expressed in hA30P compared to WT mice (background).

5.4.9 Down-regulated Proteins/Genes Identified by Gene Ontology Reporter DAVID for the Biological Functions

The 30 downregulated proteins were entered as a 'Gene List' in DAVID, along with a background protein list that included the 4165 proteins that were detected in the comparison of 5 hippocampi of hA30P mice versus 5 WT mice. Based on this, three different biological function groups were found (Figs. 20, 21, 22, and 23).

(A)

158 DAVID IDs
10 record(s)

1) Ribosomal protein

OFFICIAL_GENE_SYMBOL	GENE NAME
Mrpl19	mitochondrial ribosomal protein L19(Mrpl19)
Rpl12	ribosomal protein L12(Rpl12)
Rpl13	ribosomal protein L13(Rpl13)
Rpl15	ribosomal protein L15(Rpl15)
Rpl29	ribosomal protein L29(Rpl29)
Rpl32	ribosomal protein L32(Rpl32)
Rps10	ribosomal protein S10(Rps10)
Rps28	ribosomal protein S28(Rps28)
Rps7	ribosomal protein S7(Rps7)
Rps9	ribosomal protein S9(Rps9)

(B)

158 DAVID IDs
12 record(s)

2) Ribonucleoprotien

OFFICIAL_GENE_SYMBOL	GENE NAME
Rbmx	RNA binding motif protein, X chromosome(Rbmx)
Mrpl19	mitochondrial ribosomal protein L19(Mrpl19)
Rpl12	ribosomal protein L12(Rpl12)
Rpl13	ribosomal protein L13(Rpl13)
Rpl15	ribosomal protein L15(Rpl15)
Rpl29	ribosomal protein L29(Rpl29)
Rpl32	ribosomal protein L32(Rpl32)
Rps10	ribosomal protein S10(Rps10)
Rps28	ribosomal protein S28(Rps28)
Rps7	ribosomal protein S7(Rps7)
Rps9	ribosomal protein S9(Rps9)
Snrnp70	small nuclear ribonucleoprotein 70 (U1)(Snrnp70)

(C)

158 DAVID IDs
4 record(s)

3) Glycosyltransferase

OFFICIAL_GENE_SYMBOL	GENE NAME
Gbe1	1,4-alpha-glucan branching enzyme 1(Gbe1)
Wdfy3	WD repeat and FYVE domain containing 3(Wdfy3)
Dpm1	dolichyl-phosphate mannosyltransferase subunit 1, catalytic(Dpm1)
Gba2	glucosidase beta 2(Gba2)

Figure 5.19b: Biological Function Group 3 of Functional Annotation Clustering for Biological Function Reporter in the DAVID of Significantly Upregulated Protein in hA30P Compared to WT Mice. The 3 terms involved proteins that related to **(A)** Ribosomal Protein, **(B)** Ribonucleoprotein, and **(C)** Glycosyltransferase with enrichment of 2.4, 7.6, and 2.5-fold respectively above in hA30P compared to WT mice (background).

5.4.10 The First Biological Function Group of Downregulated Proteins/Genes by Gene Ontology Reporter DAVID for the Biological Functions

The first functional group of downregulated proteins in the gene ontology reporter DAVID identified consisted of 2 groups of proteins that related to the following cellular functions (Fig. 5.21a, and b):

1. **Purine Metabolism** with enrichment 6.2-fold above the background and contained 2 genes (Fig. 5.21b).
2. **Cell Shape** with enrichment 6.2-fold above the background and contained 2 genes (Fig. 5.21b).

This biological function group almost represented downregulated proteins of Cluster 1 of Protein N-terminus binding that resulted from STRING analysis (Fig.5.13, and 15).

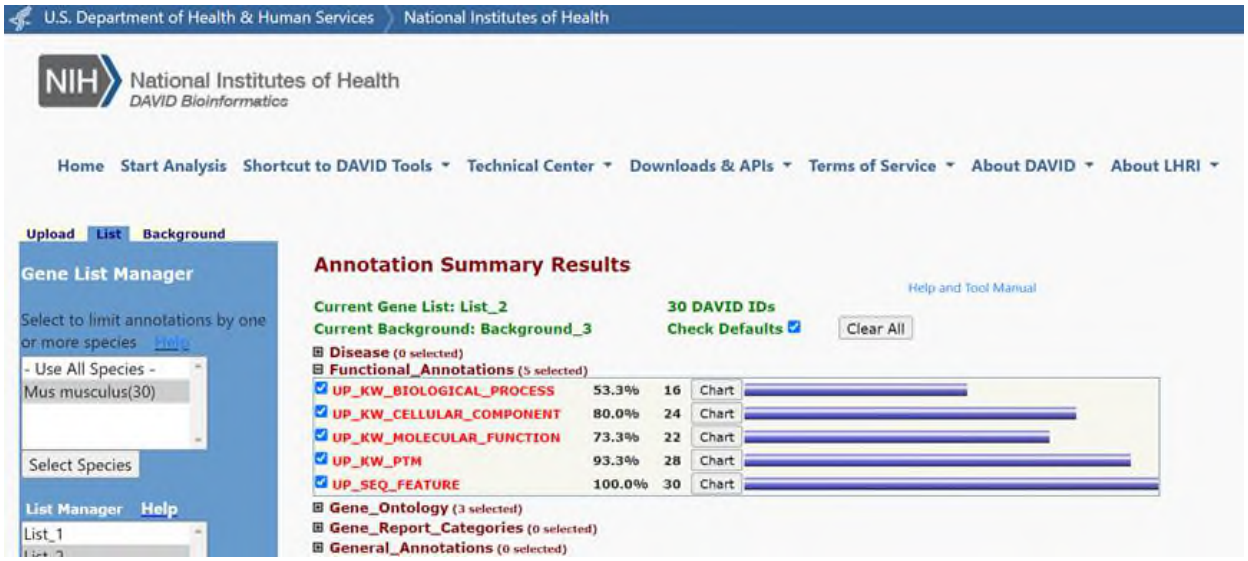

Figure 5.20: The Output Summary of the Function Annotation Reporter in the DAVID Result of 30 Significantly Downregulation Protein in hA30P compared to WT mice. The result revealed that 3 main biological function groups in hA30P compared to WT mice (background) have been inputted.

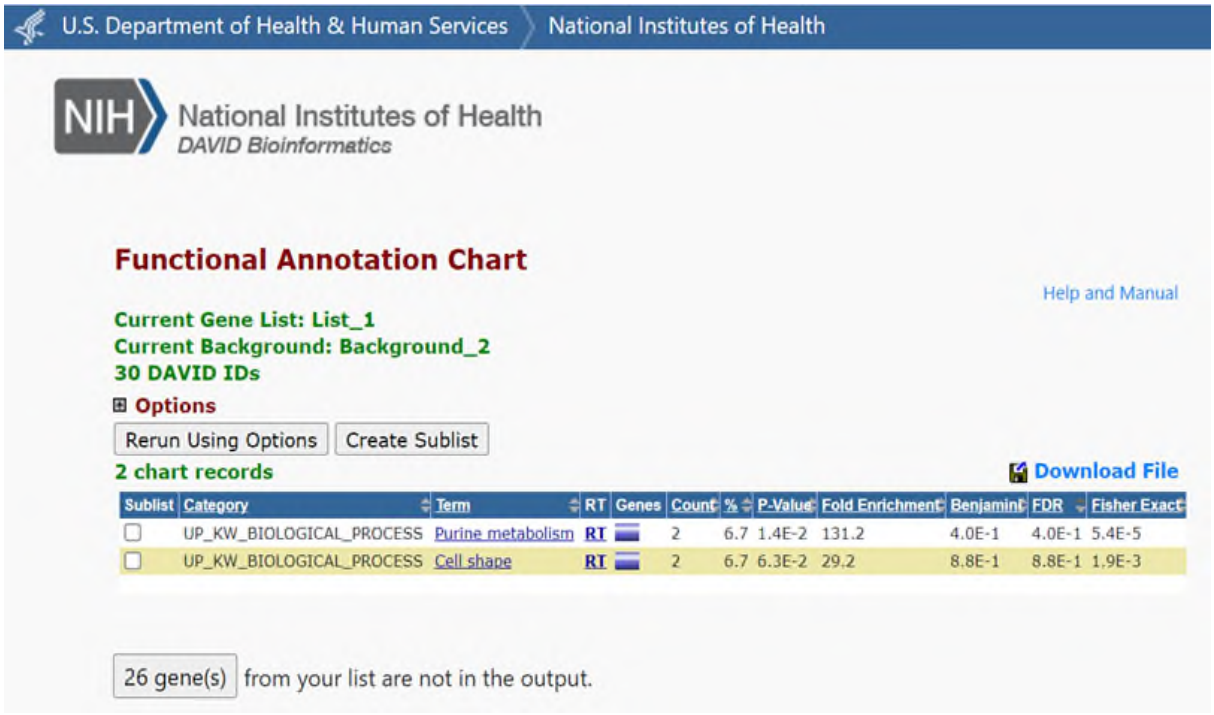

Figure 5.21a: Biological Function Group 1 of Functional Annotation Clustering for Biological Function Reporter in the DAVID of Significantly Downregulated Protein in hA30P Compared to WT Mice. The result revealed that 2 terms of involved proteins related to Purine metabolism, and Cell shape in hA30P compared to WT mice (background).

(A)

30 DAVID IDs
2 record(s)

1) Purine metabolism

OFFICIAL_GENE_SYMBOL	GENE NAME
Gmpr2	guanosine monophosphate reductase 2(Gmpr2)
Gmpr	guanosine monophosphate reductase(Gmpr)

(B)

30 DAVID IDs
2 record(s)

2) Cell shape

OFFICIAL_GENE_SYMBOL	GENE NAME
Myh10	myosin, heavy polypeptide 10, non-muscle(Myh10)
Myh9	myosin, heavy polypeptide 9, non-muscle(Myh9)

Figure 5.21b: Biological Function Group 1 of Functional Annotation Clustering for Biological Function Reporter in the DAVID of Significantly Downregulated Protein in hA30P Compared to WT Mice. The 2 terms involved proteins that related to **(A)** Purine metabolism, and **(B)** Cell shape, both with enrichment of 6.7-fold above the background in hA30P compared to WT mice (background).

5.4.11 The Second Biological Function Group of Downregulated Proteins/Genes by Gene Ontology Reporter DAVID for the Biological Functions

The second functional group of downregulated proteins in the gene ontology reporter DAVID identified consisted of 4 groups of proteins that related to the following cellular functions (Fig. 5.22a, and b):

1- **Cytoplasmic Vesicle** with enrichment 4.4-fold above the background and contained 8 genes (Fig. 5.22b).
2- **Synapse** with enrichment 3.5-fold above the background and contained 7 genes (Fig. 5.22b).
3. **Golgi Apparatus** with enrichment 3.0-fold above the background and contained 8 genes (Fig. 5.22b).
4. **Cell Projection** with enrichment 2.9-fold above the background and contained 5 genes (Fig. 5.21b).

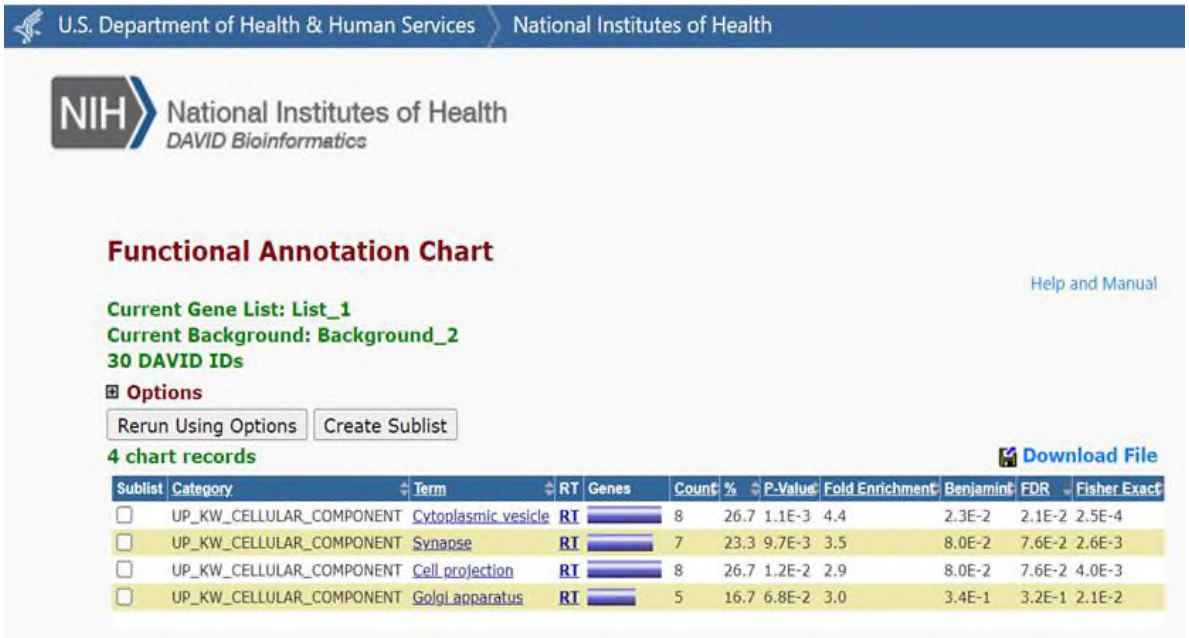

Sublist	Category	Term	RT	Genes	Count	%	P-Value	Fold Enrichment	Benjamini	FDR	Fisher Exact
☐	UP_KW_CELLULAR_COMPONENT	Cytoplasmic vesicle	RT		8	26.7	1.1E-3	4.4	2.3E-2	2.1E-2	2.5E-4
☐	UP_KW_CELLULAR_COMPONENT	Synapse	RT		7	23.3	9.7E-3	3.5	8.0E-2	7.6E-2	2.6E-3
☐	UP_KW_CELLULAR_COMPONENT	Cell projection	RT		8	26.7	1.2E-2	2.9	8.0E-2	7.6E-2	4.0E-3
☐	UP_KW_CELLULAR_COMPONENT	Golgi apparatus	RT		5	16.7	6.8E-2	3.0	3.4E-1	3.2E-1	2.1E-2

Figure 5.22a: Biological Function Group 2 of Functional Annotation Clustering for Biological Function Reporter in the DAVID of Significantly Downregulated Protein in hA30P Compared to WT Mice. The result revealed that 4 terms of involved proteins related to Cytoplasmic vesicle, Synapse, Golgi apparatus, and Cell projection were expressed with 4.4, 3.5, 3.0, and 2.9-fold enrichment respectively in hA30P compared to WT mice (background).

Gene Report	Official Gene Symbol	Gene Name
A) Cytoplasmic vesicle	Cadps	Ca2+-dependent secretion activator (Cadps)
	Rab8a	RAB8A, member RAS oncogene family(Rab8a)
	Adam10	a disintegrin and metallopeptidase domain 10(Adam10)
	Myh9	myosin, heavy polypeptide 9, non-muscle(Myh9)
	Picalm	phosphatidylinositol binding clathrin assembly protein (Picalm)
	Syn1	synapsin I(Syn1)
	Syn3	synapsin III(Syn3)
	Syt5	synaptotagmin V(Syt5)
B) Synapse	Bcr	BCR activator of RhoGEF and GTPase (Bcr)
	Cadps	Ca2+-dependent secretion activator (Cadps)
	Abr	active BCR-related gene (Abr)
	Syn1	synapsin I(Syn1)
	Syn2	synapsin II(Syn2)
	Syn3	synapsin III(Syn3)
	Syt5	synaptotagmin V(Syt5)
C) Cell projection	Bcr	BCR activator of RhoGEF and GTPase (Bcr)
	Elavl4	ELAV like RNA binding protein 4(Elavl4)
	Rab8a	RAB8A, member RAS oncogene family (Rab8a)
	Adam10	a disintegrin and metallopeptidase domain 10 (Adam10)
	Abr	active BCR-related gene (Abr)
	Myh10	myosin, heavy polypeptide 10, non-muscle(Myh10)
	Slc4a7	solute carrier family 4, sodium bicarbonate cotransporter, member 7(Slc4a7)
	Syn1	synapsin I(Syn1)
D) Golgi apparatus	Rab8a	RAB8A, member RAS oncogene family(Rab8a)
	Yif1b	Yip1 interacting factor homolog B (S. cerevisiae) (Yif1b)
	Adam10	a disintegrin and metallopeptidase domain 10 (Adam10)
	Picalm	phosphatidylinositol binding clathrin assembly protein (Picalm)
	Syn1	synapsin I(Syn1)

Figure 5.22b: Biological Function Group 2 of Functional Annotation Clustering for Biological Function Reporter in the DAVID of Significantly Downregulated Protein in hA30P Compared to WT Mice. The 4 terms involved proteins that related to **(A)** Cytoplasmic vesicle, **(B)** Synapse, **(C)** Cell projection, and **(D)** Golgi apparatus with enrichment of 4.4, 3.5, 2.9, and 3.0-fold respectively above the background in hA30P compared to WT mice (background).

Figure 5.23a: Biological Function Group 3 of Functional Annotation Clustering for Biological Function Reporter in the DAVID of 30 Significantly Downregulated Protein in hA30P Compared to WT Mice. The result revealed that there was 1 term of involved proteins that related to Guanine-nucleotide releasing factor was expressed with 6.2-fold enrichment in hA30P compared to WT mice (background).

5.4.12 The Third Biological Functional Group of Downregulated Proteins/Genes by Gene Ontology Reporter DAVID for the Biological Functions

The third functional group of downregulated proteins in the gene ontology reporter DAVID identified consisted of 1 group of proteins that related to the following cellular functions (Fig. 5.23a, and b):

1- **Guanine-Nucleotide Releasing Factor** with enrichment 6.2-fold above the background and contained 3 genes (Fig. 5.22b).

Gene Report	Official Gene Symbol	Gene Name
Guanine-nucleotide releasing factor	Bcr	BCR activator of RhoGEF and GTPase(Bcr)
	Abr	active BCR-related gene(Abr)
	Prex2	phosphatidylinositol-3,4,5-trisphosphate-dependent Rac exchange factor 2(Prex2)

Figure 5.23b: Biological Function Group 3 of Functional Annotation Clustering for Biological Function Reporter in the DAVID of Significantly Downregulated Protein in hA30P Compared to WT Mice. The term involved proteins that related to Guanine-nucleotide releasing factor with enrichment of 6.2-fold above in hA30P compared to WT mice (background).

5.5 Discussion

A summary of key findings in Chapter 5 was as follows:

- LF-MS illustrated that there was a clear difference in protein expression levels between the hippocampus of 2 months hA30P compared to control mice.
- LF-MS quantification for the proteome resulted in 6644 different proteins filtered to 4165.
- The significantly elevated proteins were 158 in the hippocampus of hA30P (N = 5) versus control of WT mice (N = 5), while there were 30 proteins reported as being significantly downregulated in hA30P mice.
- The highest twelve significantly different upregulated proteins between hA30P and WT mice depending on fold changes were Wdfy3, Tenm1, Hspa1l; Hspa2; Hspa5; Hspa8, Rab1A, Rala, Lin7a; Lin7b; Lin7c, Rps7, TOMM6, Rbmx, Snrk, Ddrgk1, and Snca; Sncb.
- Terms of the functional role of these upregulated proteins are related to glycosyltransferase, stress response, autophagy, exocytosis, ribosomal protein, MOM, ribonucleoproteins, and nucleus.
- The highest three significantly different downregulated proteins/genes between hA30P and WT mice depending on fold changes were Gmpr2, Abr, and Syn1; Syn2; Syn3.
- The role of the functional term of these downregulated proteins is related to purine metabolism, guanine-nucleotide releasing factor, and synapse.

We did not feel the cytokine array Kit was detecting accurately so that data of cytokine array will not be discussed further.

Each of the terms and clusters that resulted from the LF-MS data involved many proteins. I summarised the 15 most significantly different proteins between hippocampal proteomics of hA30P and WT mice depending on fold changes as the following and have considered their significance to the hA30P mouse model and the other data discussed in this thesis.

The highest significantly upregulated protein:

- **α-synuclein (α-syn) SNCA:** As expected α-syn was the most upregulated protein in hA30P compared to WT mice. This was expected because the hA30P mice have an inserted and expressed mutant SNCA gene for human α-syn (Kahle et al., 2000), in addition to the murine α-syn that is present in both control and hA30P mice. In normal conditions α-syn plays a role in synaptic activity e.g., regulation of the trafficking of synaptic vesicles and release of neurotransmitters. α-syn monomers also enhance vesicle priming during synaptic vesicle exocytosis. In neurons and glial cells, the SNARE proteins are crucial for neurotransmitter release as well as other processes (Han et al., 2017). α-syn has a role in exocytosis fusion pores fusion and dilation and is important to maintain normal SNARE-complex during aging (Burré et al., 2010, Burré et al., 2014). Specifically, α-syn has a role in the regulation of dopamine neurotransmission via association with dopamine (Polymeropoulos et al., 1997b, Burré et al., 2010, Burré et al., 2014). The overexpression of α-syn leads to α-synucleinopathy in LBD patients and mouse models of LBD as hA30P mice. The fact that the α-syn protein showed the most significantly altered protein expression in the hA30P was a confirmation of the LF-MS data.

- **WD repeats and FYVE domain containing 3 (Wdfy3)**: Involved in the creation of cytoplasmic ubiquitin-containing inclusions and their autophagic degradation (Orosco et al., 2014, Dragich et al., 2016). Crucial for the development of major forebrain commissures as well as axonal tract creation throughout the brain and spinal cord (Dragich et al., 2016). Plays a role in the brain cells' capacity to react to guidance cues signals (Dragich et al., 2016). An increase in Wdfy3 in the current study would agree with the activation of defense mechanisms in the hippocampus to remove excess α-syn via the autophagy process.

- **Teneurin-1 (Tenm1):** Regulates the establishment of proper neuroplasticity and neural development in the limbic system (Wang et al., 2005). In the hippocampus and amygdala, Tenmn1 facilitates a rapid reorganization of actin- and tubulin-based cytoskeleton elements (Wang et al., 2005, Al Chawaf et al.,

2007). Tenm1 is considered a bioactive neuroprotective peptide because it induces brain-derived neurotrophic factor-transcription inhibition in neurons. Also, it decreases the effects of corticotropin-releasing factor (CRF) on the production of c-Fos and FOS and the necrotic cell death associated with alkalosis (Trubiani et al., 2007, Tan et al., 2008, Tan et al., 2009, Tan et al., 2011, Ng et al., 2012, Chand et al., 2012). The upregulation of Tenm1 in 2-month hA30P mice supports our result of a reduction in c-Fos expression in the hA30P compared to WT mice at 2 months of age. Also, the current result of upregulation in Tenm1 is compatible with the trend of increased PV expression shown in the current thesis (Fig. 3.4) and previous work that demonstrated the hyperexcitability in the hippocampus of young hA30P mice (Tweedy et al., 2021). The upregulation of Tenm1 in the current study might be due to a compensatory action involving neuroprotection and neuroplasticity.

- **Heat shock 70 kDa protein 1-like (Hspa):** This molecular chaperone is involved in many different physiological functions, including the folding, and transporting of synthesized polypeptides, and protecting the proteome from stress. In addition, the Hspa protein plays an important role in the importation process of mitochondria, because it delivers protein to the TOMM70 mitochondrial import receptors (Egerton et al., 1996). Our findings of an increase of Hspa in hA30P mice were consistent with the previously reported findings showing that overexpression of α-syn leads to mitochondrial dysfunction in LBD patients and mice models of LBD (Thellung et al., 2019). The upregulation of Hspa in the current study might be due to a compensatory action aimed at repairing damaged mitochondria.

- **Ras-related protein (Rab-1A): a** regulator of intracellular membrane trafficking, formation of transport vesicles, and fusion with membranes (Wang et al., 2010, Ishida et al., 2012). IL-8 and growth hormones are secreted from the cell surface by Rab-1A, which regulates the transport of vesicular proteins from the endoplasmic reticulum to the Golgi compartment (Wang et al., 2010). I will expand on Rab-1A later due to its importance and because this protein belongs to the family of autophagy proteins identified in the first biological

functional term of the oncology report of DAVID, which has the highest fold enrichment upregulation change of 2.9 after the group of stress response proteins.

- **V-ral simian leukemia viral oncogene A (Rala):** Belongs to a hydrolase enzyme family that binds to nucleotide guanosine triphosphate (GTPase). GTPase has several functions involved in membrane trafficking, oncogenic transformation, gene expression, cell migration, and proliferation (Balasubramanian et al., 2010). It serves as a GTP sensor for dense-core vesicle exocytosis that is reliant on GTP (Balasubramanian et al., 2010). It also controls the fission of mitochondria (Kashatus et al., 2011, Balasubramanian et al., 2010). An increase of Rala in the young hA30P mice in the current results might be an indication of α-syn's role in cell trafficking and mitochondrial function.

- **Protein lin-7 homolog B (Lin7):** Assists in creating and maintaining the asymmetric distribution of receptors and channels at polarised cell's plasma membranes (Setou et al., 2000). Lin7 functions to localize synaptic vesicles at synapses where they are bound by β-catenin and cadherin, integral components of the adherens junctions, and may also couple synaptic vesicle exocytosis to cell adhesion in the brain. Lin 7 is also necessary for the GABA transporter and Kir2 (inward-rectifier potassium) localization, which contribute to the action potential repolarization and control of resting membrane potential (Setou et al., 2000, Bamji et al., 2003). The upregulation in Lin7 revealed in the current analysis might be attempted to regulate the hyperexcitability of the synapses in the hippocampus of young hA30P mice that was noticed previously (Tweedy et al., 2021).

- **40S ribosomal protein S7 (Rps7):** Protein synthesis in cells is carried out by the ribosome, a large ribonucleoprotein complex (Li et al., 2022). Rps7 is essential for the maturation of ribosomal ribonucleic acid (rRNA). A component of the small subunit (SSU) processome, which is the eukaryotic small ribosomal subunit's first progenitor (Li et al., 2022). Numerous ribosome biogenesis

factors, an RNA chaperone, and ribosomal proteins associate with the developing pre-rRNA during the assembly of the SSU processome in the nucleolus. These interactions result in RNA folding, modifications, rearrangements, and cleavage as well as the targeted degradation of pre-ribosomal RNA by the RNA exosome (Malygin and Karpova, 2010, Li et al., 2022, Konno et al., 2010). α-synucleinopathy in the hippocampus of 2-month hA30P mice resulted from a cascade of pathologic events related to overexpression of human mutant α-syn protein. The protein synthesis process occurs in ribosomes by the assessment of rRNA, and translated RNA (tRNA), in addition to pre- and post-translational processes such as splicing. So, the abnormal upregulation of Rps7 might reflect the increase of protein synthesis in the neurons of the hippocampus at this prodromal stage that ultimately leads to dysfunctional proteins at a symptomatic stage in the mice.

- **Mitochondrial import receptor subunit TOMM6 homolog (TOMM6)**: One of at least seven proteins that form the outer mitochondrial membrane (TOMM complex) pre-protein translocase complex (TOMM5, TOMM6, TOMM7, TOMM20, TOMM22, TOMM40 and TOMM70) (Dunn and Napier, 1975). The upregulation of this protein at this early prodromal stage in hA30P mice may indicate a compensatory change to enhance mitochondrial function because the mitochondria are under stress of overexpression of α-syn protein. I will expand on TOMM6 further below due to its importance, and because this protein/gene belongs to outer mitochondrial membrane proteins of the second biological functional term of the oncology report of DAVID that had the highest fold enrichment upregulation change of 2.3.

- **RNA binding motif protein, X chromosome (Rbmx):** Regulates the process of pre- and post-transcriptional modification of mRNA. It is involved in tumour suppression. It can either activate or repress exon inclusion, for instance acting to enhance exon 7 inclusion for survival motor neuron (SMN2) transcripts and suppressing the splicing of exon 10 for MAPT/Tau (Takemoto et al., 2007, Omura et al., 2009). An increase in Rbmx may indicate abnormalities in protein synthesis due to α-synucleinopathy in hA30P mice at this early age.

- **SNF-related serine/threonine-protein kinase (Snrk):** Snrk may contribute to the differentiation or proliferation of hematopoietic cells, and is also possibly an intermediate step in the apoptosis of neurons (Kertesz et al., 2002, Xie et al., 2023). Incorporation of the significant increase in Snrk in these proteomic results, combined with the significant reduction of % area of NeuN immunoreactivity we observed (Chapter 3) might indicate a greater possibility of neuron death in the hippocampus of 2 months hA30P mice, or at least it emphasizes a stress effect on neurons at this early age.

- **DDRGK domain-containing protein 1 (Ddrgk1)**: The endoplasmic reticulum that has a crucial role to play in autophagy. Ddrgk1 is responsible for the production of ubiquitin-fold modifier 1 (Ufm1), which covalently attaches to substrate proteins during vesicle trafficking of the protein degradation system (ufmylation) (Liu et al., 2017). The process of ufmylation is induced under conditions of endoplasmic stress and is required for processes such as hematopoiesis and inflammation when endoplasmic reticulum sheets are stressed (Egunsola et al., 2017). The upregulation of Ddrgk1 in the hippocampus of hA30P mice might result from stress induced by the α-synucleinopathy e.g., the neuroinflammation caused by the overexpression of α-syn, as the result in Chapters 3, and 4 showed.

The highest significantly downregulated protein:

- **Guanosine monophosphate reductase 2 (Gmpr2):** Curtails the conversion of the nucleobase, nucleoside, and nucleotide derivatives of Guanine to Adenine nucleotides that form the essential component of deoxyribonucleic acid (DNA). Gmpr2 also assists in controlling the differentiation of cells (Deng et al., 2002, Zhang et al., 2003, Li et al., 2006, Patton et al., 2011). Recent evidence showed that DNA damage is associated with α-synucleinopathy in post-mortem brain tissue of DLB patients and mouse models of DLB (Koss et al unpublished observations). The reduction of Gmpr2 expression in the hippocampus of hA30P compared to mice WT mice in the current study would

be consistent with DNA/RNA damage, even at this early age. I will expand on Gmpr2 later because this protein/gene belongs to purine metabolism proteins of the first biological functional term of the oncology report of DAVID that had the highest fold downregulation change of 131.2.

- **Active breakpoint cluster region-related protein (Abr):** A member of the Rho family of proteins that has a role in regulating dendritic spines and excitatory synapses. A peculiarly shaped protein with two conflicting regulatory functions towards tiny GTP-binding proteins. Defective Rho control causes mental retardation and Alzheimer's disease (Oh et al., 2010). Abr stimulates the transformation of the GTPase-activating protein domain from its GDP-bound form to its GTP-bound form. Serves as a significant inhibitor of RAC1, GTPase-activating protein domain, activity in neurons. Controls RAC1 activity, which in turn controls macrophage activities like phagocytosis and CSF-1-directed motility (Cho et al., 2007). A decrease in Abr may indicate phagocytosis dysfunction due to α-synucleinopathy in hA30P mice at this early age.

- **Synapsin (Syn):** Several neuropsychiatric disorders may be related to family members of Syn, all of whom have similar protein domains and are linked to synaptogenesis and neurotransmitter release regulation and development (Zaltieri et al., 2015). This gene may be a candidate gene for schizophrenia based on its location and potential locus of vulnerability to schizophrenia (Kao et al., 1998). In the current study, the decrease in Syn might mean there were fewer synapses because of α-synucleinopathy in the hippocampus of hA30P mice or reduced synaptic function. α-syn causes abnormalities in the SNARE-complex which is crucial for neurotransmitter release processes (Burré et al., 2010, Burré et al., 2014), which may lead to the downregulation of Syn. The current result of decreased Syn may indicate the effect of α-synucleinopathy in the CA3 region 2 months hA30P mice.

All the above proteins showed changes in expression because of overexpression of α-syn in the hA30P.

Interestingly many of the proteins with altered expression are related to autophagy, mitochondrial functions, and exocytosis. These are all pathways and processes we would expect to show changes due to abnormal α-syn.

Some of the most interesting changed proteins were included:

1- Rab1A is related to stress response as an upregulated protein.
2- TOMM6 is related to the MOM one of the upregulated proteins.
3- Gmpr2 is related to purine metabolism one of the down-regulated proteins.

5.5.1 Effect of Overexpression of Human α-syn on Oxidative Stress

The LF-MS found that Rab1A was significantly upregulated in the hippocampus tissue of 2-month hA30P mice compared to the control mice. Protein Coding gene RAB1A belongs to the Rab family of small GTPase, which are a family of proteins involved in the regulation of intracellular membrane trafficking, and the formation of transport vesicles (Wang et al., 2010, Ishida et al., 2012). IL-8 and growth hormone are secreted from the cell surface by Rab-1A, which regulates the transport of vesicular proteins from the endoplasmic reticulum to the Golgi apparatus and/or within Golgi compartments (Wang et al., 2010).

During the Rab cycle, GDP becomes inactive and GTP becomes active, allowing it to recruit downstream effectors directly involved in vesicle formation, movement, tethering, and fusion of vesicles to membranes (Wang et al., 2010). As one of the major functions of α-syn is vesicle fusion (Wang et al., 2010), this result suggests that abnormal α-syn may affect Rab function resulting in a compensatory increase in expression in the hippocampus to keep the Rab cycle balanced.

The additional interpretation for increasing Rab in hA30P mice might be because of its crucial role in autophagosomes and cellular defence reactions against the overexpressed α-syn, or result from cellular damage. By regulating protein trafficking, Rab1A is also involved in cell adhesion and migration (Wang et al., 2010). It contributes to the assembly of autophagosomes and cellular defence reactions

against pathogenic bacteria (Dong et al., 2012). It also activates early endosomes in the transport of microtubule-dependent proteins and melanosomes anterogradely (Dong et al., 2012). Wang et al., 2010, Wang et al. (2010) used an unbiased RNAi screen targeting GTPases to prove that Rab1a is a novel regulator of cell migration. Their results showed the role of Rab1a in the regulation of cell migration via controlling integrin β1 recycling and localization to lipid rafts through a specific downstream effector pathway. Recently, it has been shown that Rab 1 has a protective effect against α–syn toxicity and is an endogenous substrate of leucine-rich repeat kinase 2 (LRRK2), a common mutation that causes familial PD and sporadic disease (Nirujogi et al., 2021, Orenstein et al., 2013). The expression of PD-related LRRK2 mutation negatively affects autophagic activity (Alegre-Abarrategui et al., 2009). This mutation affects the maturation and transport of autophagosomes, which results in impaired autophagy (Boecker et al., 2021), leading to compromising the degradation of α-syn in PD (Orenstein et al., 2013). Numerous proteins in the Rabs family are LRRK2 substrates (Steger et al., 2016), ultimately an increase in Rabs has a protective effect against α–syn toxicity. Interestingly, the current result of the upregulation of Rab 1A in the hippocampus of 2-month hA30P mice agreed with previous research that found its upregulation in PD post-mortem human brain (Martínez-Menárguez et al., 2021). The surviving nigral neurons in PD cases showed overexpression of the small GTPase Rab1 by 50% in human PD samples (Tomás et al., 2021), and in a cellular model of PD (Rendón et al., 2013, Coune et al., 2011). The overexpression of wild-type or A53T mutant α-syn in mammalian cells caused inhibition of docking and fusion of vesicles with the Golgi apparatus by the disruption of the SNARE complex assembly (Thayanidhi et al., 2010). Due to the pathological accumulation of α-syn, hydrolase trafficking and lysosomal activity were affected, however, overexpression of Rab1 may improve this dysfunction (Mazzulli et al., 2016). The interaction of α-syn with Golgi-shaping matrix protein (GM130), an effector related to membrane traffic that disrupts Rab1-dependent endoplasmic reticulum–Golgi traffic, and the Golgi department causes this alteration (Martínez-Menárguez et al., 2021). Is this overexpression of Rab1 an attempt to rescue normal cell function in the hA30P mice or does it result from cellular damage? Currently, we do not know the answer but Rab1, as a substrate of LRRK2, and a regulator of α-syn toxicity, may be a good therapeutic target candidate for further PD research (Savitt and Jankovic, 2019).

5.5.2 Effect of Overexpression of Human α-syn on Mitochondrial Outer Membrane

The LF-MS results showed that TOMM6 was a significantly upregulated protein in the hippocampus in the 2-month hA30P mice compared to the control. Due to the abundance of mitochondria present in the fast-spiking PV interneurons, inflammatory stimuli that affect mitochondrial function and activity would be expected to negatively affect PV interneurons (Ruden et al., 2021).

Superoxide dismutase 2 (SOD2) is a genetic alteration that increases oxidative stress through a partial impairment of the rate-limiting enzyme in the antioxidant machinery of the mitochondria. Scudamore and Thomas Ciossek, 2018, generated a transgenic mouse model of PD with haplodeficiency of superoxide dismutase 2 (SOD2) in the (Thy-1)-hA30P α-synuclein transgenic line to oxidative to stress and α-synuclein aggregation in vivo (Scudamore and Ciossek, 2018). They found that the mice homozygous for the SOD2 mutation showed overexpression of α-syn and died a week after being born, and only wild-type or heterozygous mice survived after the weaning date. These results suggest that mitochondrial oxidative stress plays a significant role in α-syn pathology, where an increase in ROS-induced oxidative stress exacerbates α-syn aggregation and accumulation (Scudamore and Ciossek, 2018). Therefore, the increase in TOMM6 we found in the current study might be an indication of abnormalities in the MOM due to the α-synucleinopathy in the hippocampus of the hA30P mice at this early stage.

To perform their vital functions, more than 1500 proteins are found inside mitochondria, divided between two membranes and two aqueous compartments. The importation and sorting of nuclear-encoded proteins into mitochondrial compartments takes place through an extensive network of dedicated proteins. Various pathologies arise from defects in this fundamental system, including neurodegenerative diseases and cardiovascular disease (Bogorodskiy et al., 2021). Kato and Mihara (2008) showed, that the TOMM complex can be immuno-isolated from HeLa cells expressing human TOMM22-FLAG, identifying human TOMM5, TOMM6, and TOMM7 in the human TOMM complex. According to their results, human small TOMM proteins maintain TOMM's structural integrity.

The current result agreed with the previous finding that TOMM20 in PD is affected by aggregated α-syn. According to Di Maio et al. (2016), post-mortem brain

tissue from PD patients showed an abnormal interaction between α-syn and TOMM20 in nigrostriatal dopaminergic neurons. Furthermore, this interaction was associated with mitochondrial protein loss. That confirmed the pathogenic effect of α-syn in the mitochondrial membrane (Di Maio et al., 2016). A feasible interpretation of the significant increase in TOMM6 of hA30P compared to WT might be the interaction of accumulated hα-syn causing destruction of membrane structural integrity. This loss of MOM then leads to an upregulation of TOMM6 as a compensatory process aimed at mitigating the damage to MOM integrity.

5.5.3 Effect of Human α-syn on DNA damage

The result of the proteomics screen also showed that one of the most downregulated genes was Guanosine Monophosphate Reductase 2 (*Gmpr2*). *GMPR2* is a gene that codes for many proteins linked to a range of diseases including urethral cancer. It is associated with nucleotide salvage and nucleotide metabolism which retrieve bases and nucleosides from external sources, or the degradation of RNA and DNA and transform them back into nucleotides. Gmpr activity and oxidoreductase activity are gene ontology annotations related to the *Gmpr2* gene (Deng et al., 2002).

GMPR2 is responsible for converting nucleobases, nucleosides, and nucleotides of G to A, and it maintains the intracellular balance between A and G nucleotides (Deng et al., 2002). GMPR also plays a crucial role in the reutilization of free intracellular bases and purine nucleosides (Li et al., 2006). The decrease in Gmpr2 that we found in the current study may reveal degradation in the DNA in the hippocampus of 2-month hA30P mice due to the toxicity of overexpressed α-syn even at this early age.

Maintaining DNA integrity is crucial to preventing genomic instability, apoptosis, and senescence for cells to survive. Current research suggests that DNA damage can lead to neurodegeneration (Madabhushi et al., 2014). In recent years, studies have examined the functions of α-syn located in the nucleus to determine how DNA can be altered in its pathological form (Koss et al., 2022). In a study of hippocampal neurons, DNA damage was shown to rapidly relieve topological constraints on early-response gene expression (Madabhushi et al., 2014). DNA damage and neurodegenerative

diseases appear to have a bidirectional relationship (Yu et al., 2018, Suberbielle et al., 2015).

It has been found that α-syn alters DNA. Since α-syn is mainly associated with presynaptic proteins, it has been studied primarily in the cytoplasm. However, α-syn is also present in the nucleus, and its functions there are still being elucidated. The presence of nuclear α-syn in human post-mortem tissues was confirmed, in addition to alterations in nuclear α-syn of LBD patients (Koss et al., 2022). Additionally, a study looking at nuclear α-syn in hippocampal neurons suggests that abnormal DNA repair encourages synuclein aggregation, leading to Lewy pathology propagation and further DNA damage (Liu et al., 2021).

As mtDNA is more vulnerable to damage compared to nuclear DNA, I expect the reason behind our result of the downregulation of GMPR2 might be due to mtDNA damage. However, previous studies showed that DNA damage is causally related to α-syn pathology in the hippocampus of AD model transgenic mice APP/PSEN1 (Yu et al., 2018). Moreover, in transgenic mouse models of DLB, an analysis of *in vivo* α-syn function revealed that A53T mutant mice developed mitochondrial damage and neuronal cell death (Martin et al., 2006).

However, in the current study, there was no evidence that the downregulation of Gmpr2 indicated there were defects in nuclear DNA, mtDNA, or both. The mtDNA has a weak repair system and α-synucleinopathy affects neurons via mitochondrial dysfunction. PV interneurons require huge amounts of energy. Thus, they are highly susceptible to a decrease in mitochondrial function, and to metabolic stress and oxidative damage associated with the disease (Kann et al., 2014, Whittaker et al., 2011, Olkhova et al., 2024). Mitochondria are protected from Ca^{2+} overload by the parvalbumin protein. The PV protein buffers Ca^{2+} entering receptors and channels at physiological concentrations. By maintaining physiological Ca^{2+} levels in mitochondria, ATP production is promoted. A high level of Ca^{2+} disrupts mitochondrial membrane potential and a high level of means electron transport chain (ETC) releases ROS that trigger the apoptosis pathway (Ruden et al., 2021). Pro-apoptotic factors trigger MOM permeabilization. Upon widening of pores within the MOM, MIM folds, and releasing in mtDNA to the cytosol (Riley et al., 2018). So, the probability of mtDNA degradation is more expected at this early age of hA30P mice compared to nuclear DNA.

5.6 Conclusion

The results of LF-MS at 2 months in the hippocampus of male hA30P mice revealed that overexpressed human mutant alpha-synuclein caused significant changes in the proteome. There were 158 significantly upregulated proteins in the hippocampus of hA30P mice involved in neurotransmissions, neuropeptides, and neuronal activity, such as Tenm1, Wdfy3, Syn, and Lin7; mitochondrial dysfunction such as TOMM6 and Rala; oxidative stress such as Rab-1A; and apoptosis in neurons such as Snrk. There were 30 significantly downregulated proteins including those linked to DNA /RNA damage such as Gmpr2, Rps7, and Rbmx. Although there was no direct evidence for neuroinflammation or inflammatory protein upregulation that reflects microglial and astrocytic activation, there were still many proteins whose functions have been linked to inflammation such as Ddrgk1, Cadps, Syn2, Hspa1l; Hspa2; Hspa5; Hspa8, and Lin7a; Lin7b; Lin7c all showed upregulation in hA30P. Overall, this chapter's work has identified several key proteins that changed in the hippocampus of 2-month hA30P mice as a result of overexpression of human α-syn. Further work is needed to confirm these findings by western blot, and immunofluorescence staining for these changed proteins.

Chapter 6

General Discussion

6.1 The Main Findings in the Current Thesis

Our results confirmed detectable α-syn in the CA3 region of the hippocampus since 1-month hA30P mice, demonstrated that marked gliosis at 1-4 month hA30P mice compared to control, reduction in the % area of NeuN and PNN at 2-4 months, and the LF-MS revealed significant changes in protein content in 2-month hA30P compared to WT mice due to α- synucleinopathy long before the onset of any cognitive or motor deficits which occur at 12 and 14+ months respectively in the hA30P mouse line (Kahle et al., 2000, Freichel et al., 2007). In addition, we have shown a close association between early neuronal hyperexcitability and neuroinflammation. Chronic hyperexcitability, which we have previously observed (Tweedy et al., 2021), was proposed to account for the downregulation of c-Fos seen in hA30P mice aged 2–4 months. Changes in c-Fos were coupled to a marked increase in both reactive astrocytes and microglia. Evidence from human studies in patients with DLB also suggests that neuroinflammatory changes occur early (Loveland et al., 2023). The pilot study of intranasal metformin treatment showed no side effects and there was a significant effect on the iNOS inflammation marker in reactive microglia between metformin-treated and vehicle hA30P.

6.2 General Discussion

The current thesis found evidence of prodromal changes in neuronal excitability and neuroinflammation due to the overexpression of α-syn at 1-4 months in hA30P mice. Overexpression of human mutant α-syn in the hA30P mice is sufficient to trigger detectable neuroinflammation from 1 month of age. There was an increase in reactive astrocytes and reactive microglia. The increase in GFAP could be explained by the astrocytes' role in cleaning the parenchymal microenvironment. Lee et al., 2010, found that α-syn released from neuronal cells could be easily endocytosis by astrocytes, causing them to produce glial inclusions and release neuroinflammatory mediators. Upon exposure to neuronal α-syn, astrocytes undergo changes in gene expression that reflect a neuroinflammatory response, including the release of cytokines, chemokines, and adhesion molecules involved in cell migration (Lee et al., 2010). α-syn triggers neuroinflammation by interacting with TLR4 expressed on the astrocyte membrane leading to inflammatory responses (Fellner et al., 2013). The astrocyte

reactivity we found in the current study may have contributed to the hyperexcitable hippocampus network state seen in the hA30P mice (Tweedy et al., 2021). Alteration in reactive astrocytes' function caused changes in the regulation, release, and synthesis of GABA (Liddelow and Barres, 2017). Along with their homeostatic role, the astrocytes regulate inhibitory neurotransmission through GABA uptake and release (Kilb and Kirischuk, 2022, Andersen et al., 2023). The significant increase in the count Iba-1 within iNOS of reactive microglia in male hA30P compared to the control result was compatible with previous findings in cell culture of primary microglia (Scheiblich et al., 2021) that demonstrated an increase in microglia in response to aggregated α-syn and trigger signalling causes of neurodegeneration (Zhang et al., 2005). The correlation between aggregated α-syn and reactive gliosis has been documented increasingly (Çınar et al., 2022). Neurons and synaptic structures in the brain can be destroyed by prolonged inflammation caused by the activation of microglia (Du et al., 2022b). Sustained chronic microglia have been linked to neuronal cell dysfunction, excitability changes in neurons, and neuronal cell death (Vezzani and Viviani, 2015).

Interestingly although the IF data showed clear evidence for neuroinflammation the LF-MS proteomic data did not show direct evidence for neuroinflammation or inflammatory protein upregulation that reflects microglial and astrocytic activation, there were many proteins whose functions have been linked to inflammation such as Ddrgk1, Cadps, Syn2, Hspa1l; Hspa2; Hspa5; Hspa8, and Lin7a; Lin7b; Lin7c all showed upregulation in hA30P.

Our results showed hyperexcitability in the hippocampus of young hA30P mice reflects the stage of neuroinflammation. There was downregulation of c-Fos in 2-4 months hA30P mice consistent with chronic hyperexcitability. Other studies have shown that chronic activity leads to a decrease in c-Fos expression (Singh et al., 2019, Morris et al., 2015, Torres et al., 2021). Previous studies in α-syn transgenic mice showed cortical hyperexcitability due to the pathologic effects of overexpression of human α-syn occurred with decreased c-Fos expression (Singh et al., 2019, Morris et al., 2015, Torres et al., 2021). There is robust evidence demonstrating that c-Fos expression diversely influences the dynamics of networks associated with memory and learning (Gallo et al., 2018). IF results of the current thesis showed a reduction in c-Fos in 2 months hA30P mice observed, in addition to the upregulation of Tenm1 which decreases the effects of corticotropin-releasing factor (CRF) on the production of c-Fos (Tan et al., 2009) as LF-MS results showed were compatible. They might

reveal an early change that could contribute to the memory deficits of hA30P mice that occur at around 12 months (Kahle et al., 2000).

Interestingly, IF staining at 1 month revealed a contrasting result. There was an increase in c-Fos in the CA3 region of hA30P compared to control. c-Fos expression changes in the hA30P mice were therefore found to be biphasic, a transient initial increase in c-Fos in juvenile mice, which may be reflecting an early increase in neuronal excitability, followed by the later down-regulation following the chronic network hyperexcitability changes.

Interestingly IF results found a significant decrease in the NeuN IF in the CA3 region of males 2-4 months hA30P. However, many studies have reported that NeuN immunoreactivity in neurons is weakened or disappears as a result of various pathological cases (Lind et al., 2005, Kirik et al., 2009, Korzhevskii et al., 2009, Tippett et al., 2007), and in the CA3 region of the hippocampus in mice, brain injury was reported (Igarashi et al., 2001). The significant reduction in NeuN immunoreactivity might be due to the stress of overexpressed α-syn. LF-MS revealed a significant increase in Snrk protein which is possibly an intermediate step in the apoptosis of neurons (Kertesz et al., 2002, Xie et al., 2023). This result might indicate a greater possibility of neuron death in the hippocampus of 2-month hA30P mice.

The cohort of 2-4 months hA30P mice showed a trend of increase in PV interneurons in the CA3 region. This result was in line with previous research (Tweedy et al., 2021). Now, we know the PV interneurons upregulate PV expression in response to increased neuronal activity (Espinoza et al., 2018, Shi et al., 2019). At this stage, this might be a result of increased neuronal activity in PV interneurons as a compensatory attempt to enhance inhibition feedback of cortical activity (Espinoza et al., 2018, Shi et al., 2019). The increase in TOMM6 that we found in the current study might be an indication of abnormalities in the MOM due to the mitochondrial oxidative stress of abnormal α-syn aggregations (Scudamore and Ciossek, 2018) in the hippocampus of the hA30P mice at this early stage.

Interestingly, I found a decrease in PV interneuron that is surrounded by PNN in young 2-4 months hA30P mice compared to WT. The early decrease in the PNN we observed in this study might be a compensatory decrease to maintain normal levels of cognitive function and/or enhance memory. Research has disputed whether the digestion of PNNs in neurodegenerative diseases is a compensatory mechanism to increase neurons' plasticity and form new synapses, which would reduce cognitive

impairment (Yang et al., 2015). Also, studies in mouse models of AD pathologies demonstrate that removing PNNs enhances memory (Vegh et al., 2014).

In this thesis, I also looked at the potential role of metformin in reversing some of the above changes. To date we looked at the impact of metformin on hippocampal inflammatory changes using IF, however, in future work, it would be interesting to also repeat the proteomic experiments in mice treated with metformin versus vehicle.

To avoid the malabsorption of vitamin B12 that results from the interference of metformin with protein-bounds B12 in the gut (Guéant et al., 2022), the nasal delivery route offers an effective method for preventing and treating brain disorders invasively (Sun et al., 2018) especially metformin could penetrate the BBB (Cao et al., 2022, Sanz et al., 2021). Overall, the mice I used in this study were tolerant to the treatment of metformin dosage and route of delivery and did not exhibit weight loss in metformin-treated mice compared to the vehicle. This result agreed with previous findings (Golay, 2008). In a pilot experiment, metformin intranasal 11.5 mg/kg dosage treatment significantly reduced the proportion of activated microglia to total microglia per area in the CA3 hippocampal region in treated versus vehicle hA30P mice. The proportion of the number of microglia that co-expressed iNOS was significantly reduced in the metformin-treated hA30P mice compared to vehicle mice. This result suggested its ability to reduce reactive microglia in the CA3 region even in low dosages. This reduction in reactive microglia was compatible with many other studies' findings that used metformin as an anti-inflammatory drug (Liu et al., 2014, Ou et al., 2018, Tizazu et al., 2019, Ryu et al., 2020, Jing et al., 2018, Du et al., 2022a, Zhu et al., 2015). In addition to the neuroprotective effects of metformin (Roganovic et al., 2019, Yang et al., 2017), it has multifaceted features e.g., rapid ability to cross BBB to reach several brain regions through a safe pharmacokinetic pathway which may exert a therapeutic drug for cognitive decline and dementia of neurodegenerative disorders (Łabuzek et al., 2010a, Takata et al., 2013, Kazkayasi et al., 2022).

However, other c-Fos neuronal activity markers and reactive astrocytes showed no significant differences resulting from metformin treatment. A plethora of previous research reported the anti-inflammatory effects of metformin but in higher dosage, regime, duration, and different administration route (Rabieipoor et al., 2023, Fang et al., 2017). Further experiments are needed to explore the therapeutic potential of metformin.

6.3 Conclusion

Overall, the results of this thesis revealed obvious neuroinflammation and neuronal changes in the hippocampus of 1 and 2-4 months hA30P mice. The IF results showed detectable gliosis well in advance of any known motor or cognitive abnormalities even at this early age (Kahle et al., 2000, Freichel et al., 2007). The results suggested a close association between early neuronal hyperexcitability and neuroinflammation (Kilb and Kirischuk, 2022, Andersen et al., 2023, Kouli et al., 2020). The increase in reactive astrocytes and microglia was associated with an increase in c-Fos due to neuronal hyperexcitability in the CA3 region in 1-month hA30P mice. While the chronic hyperexcitability in 2-4 months hA30P mice causes the downregulation of c-Fos.

Intranasal metformin treatment was well tolerated by the mice and did not show observable side effects. Metformin-treated (11.5 mg/kg for five days weekly for 4 weeks) mice showed a significant reduction of iNOS expression in the microglia of the hippocampus compared to the vehicle. This result was compatible with many previous studies, which demonstrated the neuroprotective and anti-inflammatory role of metformin.

The LF-MS analysis showed proteomic content of the hippocampus of 2-month hA30P mice was affected. There were 188 significantly different proteins involved in neurotransmissions, neuropeptides, neuronal activity, mitochondrial dysfunction, oxidative stress, and apoptosis in neurons, inflammation, and DNA and/or RNA damage. α-synucleinopathy caused obvious and significant changes in the proteome of the hippocampus of young hA30P mice.

6.4 Limitations

The current project had a number of limitations. These included an absence of negative controls for the antibodies that were used in chapter 3, and 4. The statistical power for some samples was also low for some comparisons. For example the limited N=3 in the group of mice of 1 month age. However, a power calculation based on the variance of my data suggested that N=6 would be appropriate to give alpha=0.8 and in most of my analysis (apart from the pilot metformin study) I had sufficient mice included.

The pilot study of metformin also had some limitation factors, which were the dosage and duration of treatment. Using a small drop of 14 µl/day of metformin solution with a concentration of 100 mM (the maximum solubility) was suitable for the small nasal cavity of the juvenile mice, which resulted in a dosage of 11.5 mg/kg/day. However, this was a low dose compared to some studies in the literature. Not treating mice on the weekend days may also have affected the treatment regime as the drug could have reduce to a low concentration during these days. All these factors might negatively affect the results of this thesis.

6.5 Future Work

- It is worth trying to treat mice for continuous days, twice daily, using more specific antibodies and a larger group size of mice and keeping the same concentration of metformin and the same route of administration and treatment duration. Also, it will be beneficial to use more accurate detection methods like PCR, real-time PCR, Western blot consecutive, ELISA, and proteomic analysis to measure markers related to neuroinflammation and hyperexcitability at a molecular level difference such as enzymes, chemokines, and cytokines between metformin-treated and vehicle mice.
- It would be worth using more specific antibodies such as those to differentiate between microglia from other macrophages e.g. against trans-membrane protein 119 (Tmem119), and caspase 3 markers to detect apoptosis in young hA30P mice.
- To deepen our understanding of the relationship between early neuronal hyperexcitability and neuroinflammation, it would be interesting to co-label c-Fos antibody with markers for glial cells and/or neurons.
- It is worth to use a specific marker to detect the infiltered macrophage to recognise it from microglia in neuroinflammation.
- It would be interesting to stain human α-syn mRNA to determine if there are subregional differences in expression within the hippocampal pyramidal cell layer in the hippocampus of hA30P mice. Staining for phosphorylated human α-syn serine residue pS129 at young hA30P mice would be beneficial to study the progression pathology of α-syn that age-dependent.

- It would be worth studying the morphological changes of reactive astrocytes and reactive microglia in different age stages of male and female hA30P mice in the future by using suitable methodology such as stereology test. Also, it would be interesting to conduct differential quantification for the microglia in the different layers of the hippocampus.
- Determination of exact concentration of metformin in the hippocampus would be helpful to amend the dosage that I used intranasally.

Bibliography

AHMED, Z., SHAW, G., SHARMA, V. P., YANG, C., MCGOWAN, E. & DICKSON, D. W. 2007. Actin-binding proteins coronin-1a and IBA-1 are effective microglial markers for immunohistochemistry. *Journal of Histochemistry & Cytochemistry,* 55**,** 687-700.

AJMONE-CAT, M. A., BERNARDO, A., GRECO, A. & MINGHETTI, L. 2010. Non-steroidal anti-inflammatory drugs and brain inflammation: effects on microglial functions. *Pharmaceuticals,* 3**,** 1949-1965.

AL CHAWAF, A., XU, K., TAN, L., VACCARINO, F. J., LOVEJOY, D. A. & ROTZINGER, S. 2007. Corticotropin-releasing factor (CRF)-induced behaviors are modulated by intravenous administration of teneurin C-terminal associated peptide-1 (TCAP-1). *Peptides,* 28**,** 1406-15.

ALEGRE-ABARRATEGUI, J., CHRISTIAN, H., LUFINO, M. M., MUTIHAC, R., VENDA, L. L., ANSORGE, O. & WADE-MARTINS, R. 2009. LRRK2 regulates autophagic activity and localizes to specific membrane microdomains in a novel human genomic reporter cellular model. *Hum Mol Genet,* 18**,** 4022-34.

ALEYA, L. & UDDIN, M. S. 2020. Environmental pollutants and the risk of neurological disorders. *Environmental Science and Pollution Research,* 27**,** 44657-44658.

ALLEN, N. J. & LYONS, D. A. 2018. Glia as architects of central nervous system formation and function. *Science,* 362**,** 181-185.

ALLEN REISH, H. E. & STANDAERT, D. G. 2015. Role of α-synuclein in inducing innate and adaptive immunity in Parkinson disease. *J Parkinsons Dis,* 5**,** 1-19.

ALVAREZ-ERVITI, L., SEOW, Y., YIN, H., BETTS, C., LAKHAL, S. & WOOD, M. J. 2011. Delivery of siRNA to the mouse brain by systemic injection of targeted exosomes. *Nat Biotechnol,* 29**,** 341-5.

ANDERSEN, J. V., SCHOUSBOE, A. & WELLENDORPH, P. 2023. Astrocytes regulate inhibitory neurotransmission through GABA uptake, metabolism, and recycling. *Essays Biochem,* 67**,** 77-91.

ANDERSON, M. A., AO, Y. & SOFRONIEW, M. V. 2014. Heterogeneity of reactive astrocytes. *Neuroscience letters,* 565**,** 23-29.

ANDERSON, V. C., LENAR, D. P., QUINN, J. F. & ROONEY, W. D. 2011. The blood-brain barrier and microvascular water exchange in Alzheimer's disease. *Cardiovasc Psychiatry Neurol,* 2011**,** 615829.

ANDOH, M., IKEGAYA, Y. & KOYAMA, R. 2019. Synaptic pruning by microglia in epilepsy. *Journal of clinical medicine,* 8**,** 2170.

ANTONOUDIOU, P., TAN, Y. L., KONTOU, G., UPTON, A. L. & MANN, E. O. 2020. Parvalbumin and somatostatin interneurons contribute to the generation of hippocampal gamma oscillations. *Journal of Neuroscience,* 40**,** 7668-7687.

ARNAOUTOGLOU, N. A., O'BRIEN, J. T. & UNDERWOOD, B. R. 2019. Dementia with Lewy bodies - from scientific knowledge to clinical insights. *Nat Rev Neurol,* 15**,** 103-112.

AVERY, M. C. & KRICHMAR, J. L. 2017. Neuromodulatory Systems and Their Interactions: A Review of Models, Theories, and Experiments. *Front Neural Circuits,* 11**,** 108.

AZEVEDO, F. A., CARVALHO, L. R., GRINBERG, L. T., FARFEL, J. M., FERRETTI, R. E., LEITE, R. E., FILHO, W. J., LENT, R. & HERCULANO-HOUZEL, S. 2009. Equal numbers of neuronal and nonneuronal cells make the human brain an isometrically scaled-up primate brain. *Journal of Comparative Neurology,* 513**,** 532-541.

BAHADUR, S., PARDHI, D., RAUTIO, J., ROSENHOLM, J. & PATHAK, K. 2020. Intranasal nanoemulsions for direct nose-to-brain delivery of actives for cns disorders. Pharmaceutics, 2020, 12 (12), 1230.

BAILEY, C. J. & DAY, C. 2004. Metformin: its botanical background. *Practical diabetes international,* 21**,** 115-117.

BALASUBRAMANIAN, N., MEIER, J. A., SCOTT, D. W., NORAMBUENA, A., WHITE, M. A. & SCHWARTZ, M. A. 2010. RalA-exocyst complex regulates integrin-dependent membrane raft exocytosis and growth signaling. *Curr Biol,* 20**,** 75-9.

BALDUCCI, S., ZANUSO, S., NICOLUCCI, A., FERNANDO, F., CAVALLO, S., CARDELLI, P., FALLUCCA, S., ALESSI, E., LETIZIA, C. & JIMENEZ, A. 2010. Anti-inflammatory effect of exercise training in subjects with type 2 diabetes and the metabolic syndrome

is dependent on exercise modalities and independent of weight loss. *Nutrition, Metabolism and Cardiovascular Diseases,* 20**,** 608-617.
BAMJI, S. X., SHIMAZU, K., KIMES, N., HUELSKEN, J., BIRCHMEIER, W., LU, B. & REICHARDT, L. F. 2003. Role of beta-catenin in synaptic vesicle localization and presynaptic assembly. *Neuron,* 40**,** 719-31.
BANTLE, C. M., ROCHA, S. M., FRENCH, C. T., PHILLIPS, A. T., TRAN, K., OLSON, K. E., BASS, T. A., ABOELLAIL, T., SMEYNE, R. J. & TJALKENS, R. B. 2021. Astrocyte inflammatory signaling mediates α-synuclein aggregation and dopaminergic neuronal loss following viral encephalitis. *Exp Neurol,* 346**,** 113845.
BEAGLE, A. J., DARWISH, S. M., RANASINGHE, K. G., LA, A. L., KARAGEORGIOU, E. & VOSSEL, K. A. 2017. Relative Incidence of Seizures and Myoclonus in Alzheimer's Disease, Dementia with Lewy Bodies, and Frontotemporal Dementia. *J Alzheimers Dis,* 60**,** 211-223.
BEAR, M., CONNORS, B. & PARADISO, M. A. 2020. *Neuroscience: exploring the brain, enhanced edition: exploring the brain*, Jones & Bartlett Learning.
BEGGIATO, S., TOMASINI, M. C., CASSANO, T. & FERRARO, L. 2020. Chronic Oral Palmitoylethanolamide Administration Rescues Cognitive Deficit and Reduces Neuroinflammation, Oxidative Stress, and Glutamate Levels in A Transgenic Murine Model of Alzheimer's Disease. *J Clin Med,* 9.
BEHERE, A., THÖRNQVIST, P. O., WINBERG, S., INGELSSON, M., BERGSTRÖM, J. & EKMARK-LEWÉN, S. 2021. Visualization of early oligomeric α-synuclein pathology and its impact on the dopaminergic system in the (Thy-1)-h [A30P] α-syn transgenic mouse model. *Journal of Neuroscience Research,* 99**,** 2525-2539.
BELLUCCI, E., TERENZI, R., LA PAGLIA, G. M., GENTILESCHI, S., TRIPOLI, A., TANI, C. & ALUNNO, A. 2016. One year in review 2016: pathogenesis of rheumatoid arthritis. *Clin Exp Rheumatol,* 34**,** 793-801.
BENDER, A., DESPLATS, P., SPENCER, B., ROCKENSTEIN, E., ADAME, A., ELSTNER, M., LAUB, C., MUELLER, S., KOOB, A. O., MANTE, M., PHAM, E., KLOPSTOCK, T. & MASLIAH, E. 2013. TOM40 mediates mitochondrial dysfunction induced by α-synuclein accumulation in Parkinson's disease. *PLoS One,* 8**,** e62277.
BENNETT, M. L., BENNETT, F. C., LIDDELOW, S. A., AJAMI, B., ZAMANIAN, J. L., FERNHOFF, N. B., MULINYAWE, S. B., BOHLEN, C. J., ADIL, A. & TUCKER, A. 2016. New tools for studying microglia in the mouse and human CNS. *Proceedings of the National Academy of Sciences,* 113**,** E1738-E1746.
BERNAL-CONDE, L. D., RAMOS-ACEVEDO, R., REYES-HERNÁNDEZ, M. A., BALBUENA-OLVERA, A. J., MORALES-MORENO, I. D., ARGÜERO-SÁNCHEZ, R., SCHÜLE, B. & GUERRA-CRESPO, M. 2019. Alpha-Synuclein Physiology and Pathology: A Perspective on Cellular Structures and Organelles. *Front Neurosci,* 13**,** 1399.
BERNSTEIN, H. G., JOHNSON, M., PERRY, R. H., LEBEAU, F. E., DOBROWOLNY, H., BOGERTS, B. & PERRY, E. K. 2011. Partial loss of parvalbumin-containing hippocampal interneurons in dementia with Lewy bodies. *Neuropathology,* 31**,** 1-10.
BEYER, K., HUMBERT, J., FERRER, A., LAO, J. I., CARRATO, C., LÓPEZ, D., FERRER, I. & ARIZA, A. 2006. Low alpha-synuclein 126 mRNA levels in dementia with Lewy bodies and Alzheimer disease. *Neuroreport,* 17**,** 1327-30.
BEZZI, P., DOMERCQ, M., BRAMBILLA, L., GALLI, R., SCHOLS, D., DE CLERCQ, E., VESCOVI, A., BAGETTA, G., KOLLIAS, G., MELDOLESI, J. & VOLTERRA, A. 2001. CXCR4-activated astrocyte glutamate release via TNFalpha: amplification by microglia triggers neurotoxicity. *Nat Neurosci,* 4**,** 702-10.
BISAGLIA, M., MAMMI, S. & BUBACCO, L. 2009. Structural insights on physiological functions and pathological effects of alpha-synuclein. *Faseb j,* 23**,** 329-40.
BISULLI, F., MUCCIOLI, L., D'ORSI, G., CANAFOGLIA, L., FRERI, E., LICCHETTA, L., MOSTACCI, B., RIGUZZI, P., PONDRELLI, F. & AVOLIO, C. 2019. Treatment with metformin in twelve patients with Lafora disease. *Orphanet journal of rare diseases,* 14**,** 1-5.

BJERKE, I. E., YATES, S. C., LAJA, A., WITTER, M. P., PUCHADES, M. A., BJAALIE, J. G. & LEERGAARD, T. B. 2021. Densities and numbers of calbindin and parvalbumin positive neurons across the rat and mouse brain. *Iscience,* 24.

BLAGOSKLONNY, M. V. 2019. Rapamycin for longevity: opinion article. *Aging (Albany NY),* 11**,** 8048.

BOCCARDI, V., MURASECCO, I. & MECOCCI, P. 2019. Diabetes drugs in the fight against Alzheimer's disease. *Ageing Res Rev,* 54**,** 100936.

BOECKER, C. A., GOLDSMITH, J., DOU, D., CAJKA, G. G. & HOLZBAUR, E. L. F. 2021. Increased LRRK2 kinase activity alters neuronal autophagy by disrupting the axonal transport of autophagosomes. *Curr Biol,* 31**,** 2140-2154.e6.

BOGORODSKIY, A., OKHRIMENKO, I., BURKATOVSKII, D., JAKOBS, P., MASLOV, I., GORDELIY, V., DENCHER, N. A., GENSCH, T., VOOS, W., ALTSCHMIED, J., HAENDELER, J. & BORSHCHEVSKIY, V. 2021. Role of Mitochondrial Protein Import in Age-Related Neurodegenerative and Cardiovascular Diseases. *Cells,* 10.

BOHLKEN, J., JACOB, L. & KOSTEV, K. 2018. Association between the use of antihyperglycemic drugs and dementia risk: a case-control study. *Journal of Alzheimer's Disease,* 66**,** 725-732.

BOSE, A. & BEAL, M. F. 2016. Mitochondrial dysfunction in Parkinson's disease. *J Neurochem,* 139 Suppl 1**,** 216-231.

BROWN, A. M., TEKKÖK, S. B. & RANSOM, B. R. 2003. Glycogen regulation and functional role in mouse white matter. *J Physiol,* 549**,** 501-12.

BROWN, G. C. & NEHER, J. J. 2010. Inflammatory neurodegeneration and mechanisms of microglial killing of neurons. *Mol Neurobiol,* 41**,** 242-7.

BURRÉ, J., SHARMA, M. & SÜDHOF, T. C. 2014. α-Synuclein assembles into higher-order multimers upon membrane binding to promote SNARE complex formation. *Proc Natl Acad Sci U S A,* 111**,** E4274-83.

BURRÉ, J., SHARMA, M., TSETSENIS, T., BUCHMAN, V., ETHERTON, M. R. & SÜDHOF, T. C. 2010. Alpha-synuclein promotes SNARE-complex assembly in vivo and in vitro. *Science,* 329**,** 1663-7.

BUTLER, B., SAMBO, D. & KHOSHBOUEI, H. 2017. Alpha-synuclein modulates dopamine neurotransmission. *J Chem Neuroanat,* 83-84**,** 41-49.

BYERS, B., CORD, B., NGUYEN, H. N., SCHÜLE, B., FENNO, L., LEE, P. C., DEISSEROTH, K., LANGSTON, J. W., PERA, R. R. & PALMER, T. D. 2011. SNCA triplication Parkinson's patient's iPSC-derived DA neurons accumulate α-synuclein and are susceptible to oxidative stress. *PloS one,* 6**,** e26159.

CABUNGCAL, J.-H., STEULLET, P., MORISHITA, H., KRAFTSIK, R., CUENOD, M., HENSCH, T. K. & DO, K. Q. 2013a. Perineuronal nets protect fast-spiking interneurons against oxidative stress. *Proceedings of the National Academy of Sciences,* 110**,** 9130-9135.

CABUNGCAL, J. H., STEULLET, P., MORISHITA, H., KRAFTSIK, R., CUENOD, M., HENSCH, T. K. & DO, K. Q. 2013b. Perineuronal nets protect fast-spiking interneurons against oxidative stress. *Proc Natl Acad Sci U S A,* 110**,** 9130-5.

CACCAMO, A., MAJUMDER, S., RICHARDSON, A., STRONG, R. & ODDO, S. 2010. Molecular interplay between mammalian target of rapamycin (mTOR), amyloid-β, and Tau: effects on cognitive impairments. *Journal of Biological Chemistry,* 285**,** 13107-13120.

CALABRESI, P., MECHELLI, A., NATALE, G., VOLPICELLI-DALEY, L., DI LAZZARO, G. & GHIGLIERI, V. 2023. Alpha-synuclein in Parkinson's disease and other synucleinopathies: from overt neurodegeneration back to early synaptic dysfunction. *Cell Death Dis,* 14**,** 176.

CAMPEAU, S., DOLAN, D., AKIL, H. & WATSON, S. J. 2002. c-fos mRNA induction in acute and chronic audiogenic stress: possible role of the orbitofrontal cortex in habituation. *Stress,* 5**,** 121-130.

CAMPEAU, S., FALLS, W. A., CULLINAN, W. E., HELMREICH, D. L., DAVIS, M. & WATSON, S. J. 1997. Elicitation and reduction of fear: behavioural and neuroendocrine indices and brain induction of the immediate-early gene c-fos. *Neuroscience,* 78**,** 1087-104.

CAMPEAU, S. & WATSON, S. J. 1997. Neuroendocrine and behavioral responses and brain pattern of c-fos induction associated with audiogenic stress. *Journal of neuroendocrinology,* 9**,** 577-588.

CAO, G., GONG, T., DU, Y., WANG, Y., GE, T. & LIU, J. 2022. Mechanism of metformin regulation in central nervous system: Progression and future perspectives. *Biomed Pharmacother,* 156**,** 113686.

CAO, R., LI, L., YING, Z., CAO, Z., MA, Y., MAO, X., LI, J., QI, X., ZHANG, Z. & WANG, X. 2019. A small molecule protects mitochondrial integrity by inhibiting mTOR activity. *Proceedings of the National Academy of Sciences,* 116**,** 23332-23338.

CAO, Y., LIU, C., LI, G., GAO, W., TANG, H., FAN, S., TANG, X., ZHAO, L., WANG, H. & PENG, A. 2023. Metformin alleviates delayed hydrocephalus after intraventricular hemorrhage by inhibiting inflammation and fibrosis. *Translational stroke research,* 14**,** 364-382.

CARLSSON, C. M. 2010. Type 2 diabetes mellitus, dyslipidemia, and Alzheimer's disease. *Journal of Alzheimer's disease,* 20**,** 711-722.

CARRION, A. M., LINK, W. A., LEDO, F., MELLSTRÖM, B. & NARANJO, J. R. 1999. DREAM is a Ca2+-regulated transcriptional repressor. *Nature,* 398**,** 80-84.

CHAN, F., LAX, N. Z., VOSS, C. M., ALDANA, B. I., WHYTE, S., JENKINS, A., NICHOLSON, C., NICHOLS, S., TILLEY, E., POWELL, Z., WAAGEPETERSEN, H. S., DAVIES, C. H., TURNBULL, D. M. & CUNNINGHAM, M. O. 2019. The role of astrocytes in seizure generation: insights from a novel in vitro seizure model based on mitochondrial dysfunction. *Brain,* 142**,** 391-411.

CHAND, D., SONG, L., DELANNOY, L., BARSYTE-LOVEJOY, D., ACKLOO, S., BOUTROS, P. C., EVANS, K., BELSHAM, D. D. & LOVEJOY, D. A. 2012. C-Terminal region of teneurin-1 co-localizes with dystroglycan and modulates cytoskeletal organization through an extracellular signal-regulated kinase-dependent stathmin- and filamin A-mediated mechanism in hippocampal cells. *Neuroscience,* 219**,** 255-70.

CHARTIER-HARLIN, M.-C., KACHERGUS, J., ROUMIER, C., MOUROUX, V., DOUAY, X., LINCOLN, S., LEVECQUE, C., LARVOR, L., ANDRIEUX, J. & HULIHAN, M. 2004. α-synuclein locus duplication as a cause of familial Parkinson's disease. *The Lancet,* 364**,** 1167-1169.

CHAUNSALI, L., TEWARI, B. P. & SONTHEIMER, H. 2021. Perineuronal net dynamics in the pathophysiology of epilepsy. *Epilepsy Currents,* 21**,** 273-281.

CHEN, J., OU, Y., LI, Y., HU, S., SHAO, L.-W. & LIU, Y. 2017. Metformin extends C. elegans lifespan through lysosomal pathway. *Elife,* 6**,** e31268.

CHEN, W. B., CHEN, J., LIU, Z. Y., LUO, B., ZHOU, T. & FEI, E. K. 2020. Metformin Enhances Excitatory Synaptic Transmission onto Hippocampal CA1 Pyramidal Neurons. *Brain Sci,* 10.

CHEN, Y., ZHOU, K., WANG, R., LIU, Y., KWAK, Y.-D., MA, T., THOMPSON, R. C., ZHAO, Y., SMITH, L. & GASPARINI, L. 2009. Antidiabetic drug metformin (GlucophageR) increases biogenesis of Alzheimer's amyloid peptides via up-regulating BACE1 transcription. *Proceedings of the National Academy of Sciences,* 106**,** 3907-3912.

CHO, Y. J., CUNNICK, J. M., YI, S. J., KAARTINEN, V., GROFFEN, J. & HEISTERKAMP, N. 2007. Abr and Bcr, two homologous Rac GTPase-activating proteins, control multiple cellular functions of murine macrophages. *Mol Cell Biol,* 27**,** 899-911.

CHOI, I., ZHANG, Y., SEEGOBIN, S. P., PRUVOST, M., WANG, Q., PURTELL, K., ZHANG, B. & YUE, Z. 2020. Microglia clear neuron-released α-synuclein via selective autophagy and prevent neurodegeneration. *Nat Commun,* 11**,** 1386.

ÇıNAR, E., TEL, B. C. & ŞAHIN, G. 2022. Neuroinflammation in Parkinson's Disease and its Treatment Opportunities. *Balkan Med J,* 39**,** 318-333.

CLARKE, L. E., LIDDELOW, S. A., CHAKRABORTY, C., MUNCH, A. E., HEIMAN, M. & BARRES, B. A. 2018. Normal aging induces A1-like astrocyte reactivity. *Proc Natl Acad Sci U S A,* 115**,** E1896-e1905.

COLGIN, L. L. 2016. Rhythms of the hippocampal network. *Nat Rev Neurosci,* 17**,** 239-49.

COLONNA, M. & BUTOVSKY, O. 2017. Microglia function in the central nervous system during health and neurodegeneration. *Annual review of immunology,* 35**,** 441-468.

COUNE, P. G., BENSADOUN, J. C., AEBISCHER, P. & SCHNEIDER, B. L. 2011. Rab1A over-expression prevents Golgi apparatus fragmentation and partially corrects motor deficits in an alpha-synuclein based rat model of Parkinson's disease. *J Parkinsons Dis,* 1**,** 373-87.

CREWS, L., SPENCER, B., DESPLATS, P., PATRICK, C., PAULINO, A., ROCKENSTEIN, E., HANSEN, L., ADAME, A., GALASKO, D. & MASLIAH, E. 2010. Selective molecular alterations in the autophagy pathway in patients with Lewy body disease and in models of α-synucleinopathy. *PloS one,* 5**,** e9313.

CROTTI, A. & RANSOHOFF, R. M. 2016. Microglial physiology and pathophysiology: insights from genome-wide transcriptional profiling. *Immunity,* 44**,** 505-515.

CURRY, D. W., STUTZ, B., ANDREWS, Z. B. & ELSWORTH, J. D. 2018. Targeting AMPK signaling as a neuroprotective strategy in Parkinson's disease. *Journal of Parkinson's disease,* 8**,** 161-181.

DAI, J.-N., ZONG, Y., ZHONG, L.-M., LI, Y.-M., ZHANG, W., BIAN, L.-G., AI, Q.-L., LIU, Y.-D., SUN, J. & LU, D. 2011. Gastrodin inhibits expression of inducible NO synthase, cyclooxygenase-2 and proinflammatory cytokines in cultured LPS-stimulated microglia via MAPK pathways. *PloS one,* 6**,** e21891.

DALFÓ, E., GÓMEZ-ISLA, T., ROSA, J. L., NIETO BODELÓN, M., CUADRADO TEJEDOR, M., BARRACHINA, M., AMBROSIO, S. & FERRER, I. 2004. Abnormal alpha-synuclein interactions with Rab proteins in alpha-synuclein A30P transgenic mice. *J Neuropathol Exp Neurol,* 63**,** 302-13.

DAVIDSON, W. S., JONAS, A., CLAYTON, D. F. & GEORGE, J. M. 1998a. Stabilization of alpha-synuclein secondary structure upon binding to synthetic membranes. *J Biol Chem,* 273**,** 9443-9.

DAVIDSON, W. S., JONAS, A., CLAYTON, D. F. & GEORGE, J. M. 1998b. Stabilization of α-synuclein secondary structure upon binding to synthetic membranes. *Journal of Biological Chemistry,* 273**,** 9443-9449.

DAZERT, E. & HALL, M. N. 2011. mTOR signaling in disease. *Curr Opin Cell Biol,* 23**,** 744-55.

DENG, Y., WANG, Z., YING, K., GU, S., JI, C., HUANG, Y., GU, X., WANG, Y., XU, Y., LI, Y., XIE, Y. & MAO, Y. 2002. NADPH-dependent GMP reductase isoenzyme of human (GMPR2). Expression, purification, and kinetic properties. *Int J Biochem Cell Biol,* 34**,** 1035-50.

DENNIS, G., JR., SHERMAN, B. T., HOSACK, D. A., YANG, J., GAO, W., LANE, H. C. & LEMPICKI, R. A. 2003. DAVID: Database for Annotation, Visualization, and Integrated Discovery. *Genome Biol,* 4**,** P3.

DEYELL, J. S., SRIPARNA, M., YING, M. & MAO, X. 2023. The Interplay between α-Synuclein and Microglia in α-Synucleinopathies. *International journal of molecular sciences,* 24**,** 2477.

DI MAIO, R., BARRETT, P. J., HOFFMAN, E. K., BARRETT, C. W., ZHARIKOV, A., BORAH, A., HU, X., MCCOY, J., CHU, C. T., BURTON, E. A., HASTINGS, T. G. & GREENAMYRE, J. T. 2016. α-Synuclein binds to TOM20 and inhibits mitochondrial protein import in Parkinson's disease. *Sci Transl Med,* 8**,** 342ra78.

DI MARCO VIEIRA, B., RADFORD, R. A. W., HAYASHI, J., EATON, E. D., GREENAWAY, B., JAMBAS, M., PETCU, E. B., CHUNG, R. S. & POUNTNEY, D. L. 2020. Extracellular Alpha-Synuclein Promotes a Neuroinhibitory Secretory Phenotype in Astrocytes. *Life (Basel),* 10.

DISABATO, D. J., QUAN, N. & GODBOUT, J. P. 2016. Neuroinflammation: the devil is in the details. *Journal of neurochemistry,* 139**,** 136-153.

DITACCHIO, K. A., HEINEMANN, S. F. & DZIEWCZAPOLSKI, G. 2015. Metformin treatment alters memory function in a mouse model of Alzheimer's disease. *Journal of Alzheimer's Disease,* 44**,** 43-48.

DOBBINS, D. L., KLORIG, D. C., SMITH, T. & GODWIN, D. W. 2018. Expression of channelrhodopsin-2 localized within the deep CA1 hippocampal sublayer in the Thy1 line 18 mouse. *Brain research,* 1679**,** 179-184.

DOCRAT, T. F., NAGIAH, S. & CHUTURGOON, A. A. 2021. Metformin protects against neuroinflammation through integrated mechanisms of miR-141 and the NF-κB-mediated inflammasome pathway in a diabetic mouse model. *Eur J Pharmacol,* 903**,** 174146.

DONG, N., ZHU, Y., LU, Q., HU, L., ZHENG, Y. & SHAO, F. 2012. Structurally distinct bacterial TBC-like GAPs link Arf GTPase to Rab1 inactivation to counteract host defenses. *Cell,* 150**,** 1029-41.

DRAGICH, J. M., KUWAJIMA, T., HIROSE-IKEDA, M., YOON, M. S., EENJES, E., BOSCO, J. R., FOX, L. M., LYSTAD, A. H., OO, T. F., YARYGINA, O., MITA, T., WAGURI, S., ICHIMURA, Y., KOMATSU, M., SIMONSEN, A., BURKE, R. E., MASON, C. A. & YAMAMOTO, A. 2016. Autophagy linked FYVE (Alfy/WDFY3) is required for establishing neuronal connectivity in the mammalian brain. *Elife,* 5.

DRINGEN, R., GEBHARDT, R. & HAMPRECHT, B. 1993. Glycogen in astrocytes: possible function as lactate supply for neighboring cells. *Brain Res,* 623**,** 208-14.

DU, M.-R., GAO, Q.-Y., LIU, C.-L., BAI, L.-Y., LI, T. & WEI, F.-L. 2022a. Exploring the pharmacological potential of metformin for neurodegenerative diseases. *Frontiers in Aging Neuroscience,* 14**,** 838173.

DU, Y., BRENNAN, F. H., POPOVICH, P. G. & ZHOU, M. 2022b. Microglia maintain the normal structure and function of the hippocampal astrocyte network. *Glia,* 70**,** 1359-1379.

DUNN, C. D. & NAPIER, J. A. 1975. An evaluation of factors affecting the in vitro bioassay for erythropoietin. *Exp Hematol,* 3**,** 362-74.

DZAMKO, N., GYSBERS, A., PERERA, G., BAHAR, A., SHANKAR, A., GAO, J., FU, Y. & HALLIDAY, G. M. 2017. Toll-like receptor 2 is increased in neurons in Parkinson's disease brain and may contribute to alpha-synuclein pathology. *Acta Neuropathol,* 133**,** 303-319.

DZEJA, P. & TERZIC, A. 2009. Adenylate kinase and AMP signaling networks: metabolic monitoring, signal communication and body energy sensing. *International journal of molecular sciences,* 10**,** 1729-1772.

EDDLESTON, M. & MUCKE, L. 1993. Molecular profile of reactive astrocytes—implications for their role in neurologic disease. *Neuroscience,* 54**,** 15-36.

EDLER, M. K., SHERWOOD, C. C., MEINDL, R. S., MUNGER, E. L., HOPKINS, W. D., ELY, J. J., ERWIN, J. M., PERL, D. P., MUFSON, E. J. & HOF, P. R. 2018. Microglia changes associated to Alzheimer's disease pathology in aged chimpanzees. *Journal of Comparative Neurology,* 526**,** 2921-2936.

EGERTON, M., MORITZ, R. L., DRUKER, B., KELSO, A. & SIMPSON, R. J. 1996. Identification of the 70kD heat shock cognate protein (Hsc70) and alpha-actinin-1 as novel phosphotyrosine-containing proteins in T lymphocytes. *Biochem Biophys Res Commun,* 224**,** 666-74.

EGUNSOLA, A. T., BAE, Y., JIANG, M. M., LIU, D. S., CHEN-EVENSON, Y., BERTIN, T., CHEN, S., LU, J. T., NEVAREZ, L., MAGAL, N., RAAS-ROTHSCHILD, A., SWINDELL, E. C., COHN, D. H., GIBBS, R. A., CAMPEAU, P. M., SHOHAT, M. & LEE, B. H. 2017. Loss of DDRGK1 modulates SOX9 ubiquitination in spondyloepimetaphyseal dysplasia. *J Clin Invest,* 127**,** 1475-1484.

EKMARK-LEWÉN, S., LINDSTRÖM, V., GUMUCIO, A., IHSE, E., BEHERE, A., KAHLE, P. J., NORDSTRÖM, E., ERIKSSON, M., ERLANDSSON, A., BERGSTRÖM, J. & INGELSSON, M. 2018. Early fine motor impairment and behavioral dysfunction in (Thy-1)-h[A30P] alpha-synuclein mice. *Brain Behav,* 8**,** e00915.

EKMARK-LEWÉN, S., LINDSTRÖM, V., GUMUCIO, A., IHSE, E., BEHERE, A., KAHLE, P. J., NORDSTRÖM, E., ERIKSSON, M., ERLANDSSON, A. & BERGSTRÖM, J. 2018. Early fine motor impairment and behavioral dysfunction in (Thy-1)-h [A30P] alpha-synuclein mice. *Brain and behavior,* 8**,** e00915.

EL-AGNAF, O. M., JAKES, R., CURRAN, M. D. & WALLACE, A. 1998. Effects of the mutations Ala30 to Pro and Ala53 to Thr on the physical and morphological properties of α-synuclein protein implicated in Parkinson's disease. *FEBS letters,* 440**,** 67-70.

EMMANOUILIDOU, E., MELACHROINOU, K., ROUMELIOTIS, T., GARBIS, S. D., NTZOUNI, M., MARGARITIS, L. H., STEFANIS, L. & VEKRELLIS, K. 2010. Cell-produced alpha-synuclein is secreted in a calcium-dependent manner by exosomes and impacts neuronal survival. *J Neurosci,* 30**,** 6838-51.

EMMANOUILIDOU, E. & VEKRELLIS, K. 2016. Exocytosis and Spreading of Normal and Aberrant α-Synuclein. *Brain Pathol,* 26**,** 398-403.

ESPINOZA, C., GUZMAN, S. J., ZHANG, X. & JONAS, P. 2018. Parvalbumin+ interneurons obey unique connectivity rules and establish a powerful lateral-inhibition microcircuit in dentate gyrus. *Nature communications,* 9**,** 4605.

EXNER, N., LUTZ, A. K., HAASS, C. & WINKLHOFER, K. F. 2012. Mitochondrial dysfunction in Parkinson's disease: molecular mechanisms and pathophysiological consequences. *The EMBO Journal,* 31**,** 3038-3062.

FANG, M., JIANG, H., YE, L., CAI, C., HU, Y., PAN, S., LI, P., XIAO, J. & LIN, Z. 2017. Metformin treatment after the hypoxia-ischemia attenuates brain injury in newborn rats. *Oncotarget,* 8**,** 75308-75325.

FARR, S. A., ROESLER, E., NIEHOFF, M. L., ROBY, D. A., MCKEE, A. & MORLEY, J. E. 2019. Metformin improves learning and memory in the SAMP8 mouse model of Alzheimer's disease. *Journal of Alzheimer's Disease,* 68**,** 1699-1710.

FAVORETTO, C. A., PAGLIUSI JR, M. & MORAIS-SILVA, G. 2023. Involvement of brain cell phenotypes in stress-vulnerability and resilience. *Frontiers in Neuroscience,* 17**,** 1175514.

FAVUZZI, E., HUANG, S., SALDI, G. A., BINAN, L., IBRAHIM, L. A., FERNÁNDEZ-OTERO, M., CAO, Y., ZEINE, A., SEFAH, A. & ZHENG, K. 2021. GABA-receptive microglia selectively sculpt developing inhibitory circuits. *Cell,* 184**,** 4048-4063. e32.

FAWCETT, J. W., FYHN, M., JENDELOVA, P., KWOK, J. C., RUZICKA, J. & SORG, B. A. 2022. The extracellular matrix and perineuronal nets in memory. *Molecular Psychiatry,* 27**,** 3192-3203.

FAWCETT, J. W., OOHASHI, T. & PIZZORUSSO, T. 2019. The roles of perineuronal nets and the perinodal extracellular matrix in neuronal function. *Nature Reviews Neuroscience,* 20**,** 451-465.

FELLNER, L., IRSCHICK, R., SCHANDA, K., REINDL, M., KLIMASCHEWSKI, L., POEWE, W., WENNING, G. K. & STEFANOVA, N. 2013. Toll-like receptor 4 is required for α-synuclein dependent activation of microglia and astroglia. *Glia,* 61**,** 349-60.

FERNAGUT, P. O., HUTSON, C. B., FLEMING, S. M., TETREAUT, N. A., SALCEDO, J., MASLIAH, E. & CHESSELET, M. F. 2007. Behavioral and histopathological consequences of paraquat intoxication in mice: effects of alpha-synuclein over-expression. *Synapse,* 61**,** 991-1001.

FIXEMER, S., AMELI, C., HAMMER, G., SALAMANCA, L., URIARTE HUARTE, O., SCHWARTZ, C., GÉRARDY, J.-J., MECHAWAR, N., SKUPIN, A. & MITTELBRONN, M. 2022. Microglia phenotypes are associated with subregional patterns of concomitant tau, amyloid-β and α-synuclein pathologies in the hippocampus of patients with Alzheimer's disease and dementia with Lewy bodies. *Acta Neuropathologica Communications,* 10**,** 36.

FOO, M. Y., CHENG, Y.-S., SU, W.-C. & DONOVAN, M. D. 2007. The influence of spray properties on intranasal deposition. *Journal of Aerosol Medicine,* 20**,** 495-508.

FREICHEL, C., NEUMANN, M., BALLARD, T., MÜLLER, V., WOOLLEY, M., OZMEN, L., BORRONI, E., KRETZSCHMAR, H. A., HAASS, C. & SPOOREN, W. 2007. Age-

dependent cognitive decline and amygdala pathology in α-synuclein transgenic mice. *Neurobiology of aging,* 28**,** 1421-1435.
FREUND, T. F. & BUZSÁKI, G. 1996. Interneurons of the hippocampus. *Hippocampus,* 6**,** 347-470.
GALLO, F. T., KATCHE, C., MORICI, J. F., MEDINA, J. H. & WEISSTAUB, N. V. 2018. Immediate early genes, memory and psychiatric disorders: focus on c-Fos, Egr1 and Arc. *Frontiers in behavioral neuroscience,* 12**,** 79.
GANTOIS, I., POPIC, J., KHOUTORSKY, A. & SONENBERG, N. 2019. Metformin for Treatment of Fragile X Syndrome and Other Neurological Disorders. *Annu Rev Med,* 70**,** 167-181.
GASIOROWSKA, A., WYDRYCH, M., DRAPICH, P., ZADROZNY, M., STECZKOWSKA, M., NIEWIADOMSKI, W. & NIEWIADOMSKA, G. 2021. The Biology and Pathobiology of Glutamatergic, Cholinergic, and Dopaminergic Signaling in the Aging Brain. *Front Aging Neurosci,* 13**,** 654931.
GEORGE, S., REY, N. L., TYSON, T., ESQUIBEL, C., MEYERDIRK, L., SCHULZ, E., PIERCE, S., BURMEISTER, A. R., MADAJ, Z., STEINER, J. A., ESCOBAR GALVIS, M. L., BRUNDIN, L. & BRUNDIN, P. 2019. Microglia affect α-synuclein cell-to-cell transfer in a mouse model of Parkinson's disease. *Mol Neurodegener,* 14**,** 34.
GHADIRI, M., YOUNG, P. M. & TRAINI, D. 2019. Strategies to enhance drug absorption via nasal and pulmonary routes. *Pharmaceutics,* 11**,** 113.
GHATAK, S., DOLATABADI, N., TRUDLER, D., ZHANG, X., WU, Y., MOHATA, M., AMBASUDHAN, R., TALANTOVA, M. & LIPTON, S. A. 2019. Mechanisms of hyperexcitability in Alzheimer's disease hiPSC-derived neurons and cerebral organoids vs isogenic controls. *Elife,* 8.
GHIGLIERI, V., CALABRESE, V. & CALABRESI, P. 2018. Alpha-Synuclein: From Early Synaptic Dysfunction to Neurodegeneration. *Front Neurol,* 9**,** 295.
GHOSH, D., SAHAY, S., RANJAN, P., SALOT, S., MOHITE, G. M., SINGH, P. K., DWIVEDI, S., CARVALHO, E., BANERJEE, R. & KUMAR, A. 2014. The newly discovered Parkinson's disease associated Finnish mutation (A53E) attenuates α-synuclein aggregation and membrane binding. *Biochemistry,* 53**,** 6419-6421.
GIUSTI, V., KAUR, G., GIUSTO, E. & CIVIERO, L. 2024. Brain clearance of protein aggregates: a close-up on astrocytes. *Mol Neurodegener,* 19**,** 5.
GOLAY, A. 2008. Metformin and body weight. *Int J Obes (Lond),* 32**,** 61-72.
GOPAR-CUEVAS, Y., SAUCEDO-CARDENAS, O., LOERA-ARIAS, M. J., MONTES-DE-OCA-LUNA, R., RODRIGUEZ-ROCHA, H. & GARCIA-GARCIA, A. 2023. Metformin and Trehalose-Modulated Autophagy Exerts a Neurotherapeutic Effect on Parkinson's Disease. *Molecular Neurobiology,* 60**,** 7253-7273.
GOTTLIEB, B. & AULD, W. 1962. Metformin in treatment of diabetes mellitus. *British Medical Journal,* 1**,** 680.
GRAZIOTTO, J. J., CAO, K., COLLINS, F. S. & KRAINC, D. 2012. Rapamycin activates autophagy in Hutchinson-Gilford progeria syndrome: implications for normal aging and age-dependent neurodegenerative disorders. *Autophagy,* 8**,** 147-51.
GROZDANOV, V. & DANZER, K. M. 2018. Release and uptake of pathologic alpha-synuclein. *Cell Tissue Res,* 373**,** 175-182.
GUÉANT, J. L., GUÉANT-RODRIGUEZ, R. M. & ALPERS, D. H. 2022. Vitamin B12 absorption and malabsorption. *Vitam Horm,* 119**,** 241-274.
GUNN, A., SINGH, A., DIAO, A. & CHEN, R. 2018. Pharmacological modulation of autophagy for neuroprotection in ischaemic stroke. *J. Exp. Stroke Trans. Med,* 11**,** 1-10.
GUSEL'NIKOVA, V. & KORZHEVSKIY, D. 2015. NeuN as a neuronal nuclear antigen and neuron differentiation marker. *Acta Naturae (англоязычная версия),* 7**,** 42-47.
GUZMAN-MARTINEZ, L., MACCIONI, R. B., ANDRADE, V., NAVARRETE, L. P., PASTOR, M. G. & RAMOS-ESCOBAR, N. 2019. Neuroinflammation as a common feature of neurodegenerative disorders. *Frontiers in pharmacology,* 10**,** 1008.
HAIM, L. B. & ROWITCH, D. H. 2017. Functional diversity of astrocytes in neural circuit regulation. *Nature Reviews Neuroscience,* 18**,** 31-41.

HAN, J., PLUHACKOVA, K. & BÖCKMANN, R. A. 2017. The Multifaceted Role of SNARE Proteins in Membrane Fusion. *Front Physiol,* 8**,** 5.
HAN, T., QIN, Y., MOU, C., WANG, M., JIANG, M. & LIU, B. 2016. Seizure induced synaptic plasticity alteration in hippocampus is mediated by IL-1β receptor through PI3K/Akt pathway. *American journal of translational research,* 8**,** 4499.
HANSON, L. R., FINE, J. M., SVITAK, A. L. & FALTESEK, K. A. 2013. Intranasal administration of CNS therapeutics to awake mice. *J Vis Exp*.
HARDY, J., LEE, S. & WILSON, C. 1985. Intranasal drug delivery by spray and drops. *Journal of pharmacy and pharmacology,* 37**,** 294-297.
HARRIS, J. J. & ATTWELL, D. 2012. The energetics of CNS white matter. *J Neurosci,* 32**,** 356-71.
HAWLEY, S. A., GADALLA, A. E., OLSEN, G. S. & HARDIE, D. G. 2002. The antidiabetic drug metformin activates the AMP-activated protein kinase cascade via an adenine nucleotide-independent mechanism. *Diabetes,* 51**,** 2420-2425.
HENEKA, M. T., CARSON, M. J., EL KHOURY, J., LANDRETH, G. E., BROSSERON, F., FEINSTEIN, D. L., JACOBS, A. H., WYSS-CORAY, T., VITORICA, J. & RANSOHOFF, R. M. 2015. Neuroinflammation in Alzheimer's disease. *The Lancet Neurology,* 14**,** 388-405.
HERAS-SANDOVAL, D., PÉREZ-ROJAS, J. M. & PEDRAZA-CHAVERRI, J. 2020. Novel compounds for the modulation of mTOR and autophagy to treat neurodegenerative diseases. *Cellular signalling,* 65**,** 109442.
HERVÁS, D., FORNÉS-FERRER, V., GÓMEZ-ESCRIBANO, A. P., SEQUEDO, M. D., PEIRÓ, C., MILLÁN, J. M. & VÁZQUEZ-MANRIQUE, R. P. 2017. Metformin intake associates with better cognitive function in patients with Huntington's disease. *PLoS One,* 12**,** e0179283.
HIJAZ, B. A. & VOLPICELLI-DALEY, L. A. 2020. Initiation and propagation of α-synuclein aggregation in the nervous system. *Mol Neurodegener,* 15**,** 19.
HINKLE, J. T., PATEL, J., PANICKER, N., KARUPPAGOUNDER, S. S., BISWAS, D., BELINGON, B., CHEN, R., BRAHMACHARI, S., PLETNIKOVA, O., TRONCOSO, J. C., DAWSON, V. L. & DAWSON, T. M. 2022. STING mediates neurodegeneration and neuroinflammation in nigrostriatal α-synucleinopathy. *Proc Natl Acad Sci U S A,* 119**,** e2118819119.
HIRAGI, T., IKEGAYA, Y. & KOYAMA, R. 2018. Microglia after seizures and in epilepsy. *Cells,* 7**,** 26.
HOGAN, R. E., GIDAL, B. E., KOPLOWITZ, B., KOPLOWITZ, L. P., LOWENTHAL, R. E. & CARRAZANA, E. 2020. Bioavailability and safety of diazepam intranasal solution compared to oral and rectal diazepam in healthy volunteers. *Epilepsia,* 61**,** 455-464.
HSU, C.-C., WAHLQVIST, M. L., LEE, M.-S. & TSAI, H.-N. 2011. Incidence of dementia is increased in type 2 diabetes and reduced by the use of sulfonylureas and metformin. *Journal of Alzheimer's Disease,* 24**,** 485-493.
HSU, L. J., SAGARA, Y., ARROYO, A., ROCKENSTEIN, E., SISK, A., MALLORY, M., WONG, J., TAKENOUCHI, T., HASHIMOTO, M. & MASLIAH, E. 2000. alpha-synuclein promotes mitochondrial deficit and oxidative stress. *Am J Pathol,* 157**,** 401-10.
HUANG, D. W., SHERMAN, B. T., TAN, Q., COLLINS, J. R., ALVORD, W. G., ROAYAEI, J., STEPHENS, R., BASELER, M. W., LANE, H. C. & LEMPICKI, R. A. 2007. The DAVID Gene Functional Classification Tool: a novel biological module-centric algorithm to functionally analyze large gene lists. *Genome Biol,* 8**,** R183.
HUR, K. Y. & LEE, M. S. 2015. New mechanisms of metformin action: Focusing on mitochondria and the gut. *Journal of diabetes investigation,* 6**,** 600-609.
HUSSEIN, A. M., ELDOSOKY, M., EL-SHAFEY, M., EL-MESERY, M., ALI, A. N., ABBAS, K. M. & ABULSEOUD, O. A. 2019. Effects of metformin on apoptosis and α-synuclein in a rat model of pentylenetetrazole-induced epilepsy. *Canadian Journal of Physiology and Pharmacology,* 97**,** 37-46.
IBA, M., KIM, C., KWON, S., SZABO, M., HORAN-PORTELANCE, L., PEER, C. J., FIGG, W. D., REED, X., DING, J. & LEE, S.-J. 2023. Inhibition of p38α MAPK restores neuronal

p38γ MAPK and ameliorates synaptic degeneration in a mouse model of DLB/PD. *Science translational medicine,* 15**,** eabq6089.
IBA, M., KIM, C., SALLIN, M., KWON, S., VERMA, A., OVERK, C., RISSMAN, R. A., SEN, R., SEN, J. M. & MASLIAH, E. 2020. Neuroinflammation is associated with infiltration of T cells in Lewy body disease and α-synuclein transgenic models. *Journal of Neuroinflammation,* 17**,** 1-14.
IGARASHI, T., HUANG, T.-T. & NOBLE, L. J. 2001. Regional vulnerability after traumatic brain injury: gender differences in mice that overexpress human copper, zinc superoxide dismutase. *Experimental neurology,* 172**,** 332-341.
IMFELD, P., BODMER, M., JICK, S. S. & MEIER, C. R. 2012. Metformin, other antidiabetic drugs, and risk of Alzheimer's disease: a population-based case–control study. *Journal of the American Geriatrics Society,* 60**,** 916-921.
INOUE, Y., AYAKI, T., ISHIMOTO, T., YAMAKADO, H., MAKI, T., MATSUZAWA, S., SAWAMOTO, N. & TAKAHASHI, R. 2021. The stimulator of interferon genes (STING) pathway is upregulated in striatal astrocytes of patients with multiple system atrophy. *Neurosci Lett,* 757**,** 135972.
INZUCCHI, S. E., BERGENSTAL, R. M., BUSE, J. B., DIAMANT, M., FERRANNINI, E., NAUCK, M., PETERS, A. L., TSAPAS, A., WENDER, R. & MATTHEWS, D. R. 2015. Management of hyperglycemia in type 2 diabetes, 2015: a patient-centered approach: update to a position statement of the American Diabetes Association and the European Association for the Study of Diabetes. *Diabetes care,* 38**,** 140-149.
IRWIN, D. J., LEE, V. M. & TROJANOWSKI, J. Q. 2013. Parkinson's disease dementia: convergence of α-synuclein, tau and amyloid-β pathologies. *Nat Rev Neurosci,* 14**,** 626-36.
ISHIDA, M., OHBAYASHI, N., MARUTA, Y., EBATA, Y. & FUKUDA, M. 2012. Functional involvement of Rab1A in microtubule-dependent anterograde melanosome transport in melanocytes. *J Cell Sci,* 125**,** 5177-87.
ISOP, L. M., NECULAU, A. E., NECULA, R. D., KAKUCS, C., MOGA, M. A. & DIMA, L. 2023. Metformin: The Winding Path from Understanding Its Molecular Mechanisms to Proving Therapeutic Benefits in Neurodegenerative Disorders. *Pharmaceuticals,* 16**,** 1714.
JANSEN, I. E., YE, H., HEETVELD, S., LECHLER, M. C., MICHELS, H., SEINSTRA, R. I., LUBBE, S. J., DROUET, V., LESAGE, S. & MAJOUNIE, E. 2017. Discovery and functional prioritization of Parkinson's disease candidate genes from large-scale whole exome sequencing. *Genome biology,* 18**,** 1-26.
JENCO, J. M., RAWLINGSON, A., DANIELS, B. & MORRIS, A. J. 1998. Regulation of phospholipase D2: selective inhibition of mammalian phospholipase D isoenzymes by alpha- and beta-synucleins. *Biochemistry,* 37**,** 4901-9.
JENSEN, D. E., PROCTOR, M., MARQUIS, S. T., GARDNER, H. P., HA, S. I., CHODOSH, L. A., ISHOV, A. M., TOMMERUP, N., VISSING, H., SEKIDO, Y., MINNA, J., BORODOVSKY, A., SCHULTZ, D. C., WILKINSON, K. D., MAUL, G. G., BARLEV, N., BERGER, S. L., PRENDERGAST, G. C. & RAUSCHER, F. J., 3RD 1998a. BAP1: a novel ubiquitin hydrolase which binds to the BRCA1 RING finger and enhances BRCA1-mediated cell growth suppression. *Oncogene,* 16**,** 1097-112.
JENSEN, P. H., NIELSEN, M. S., JAKES, R., DOTTI, C. G. & GOEDERT, M. 1998b. Binding of α-synuclein to brain vesicles is abolished by familial Parkinson's disease mutation. *Journal of Biological Chemistry,* 273**,** 26292-26294.
JEONG, S.-H., JANG, J.-H. & LEE, Y.-B. 2023. Drug delivery to the brain via the nasal route of administration: exploration of key targets and major consideration factors. *Journal of pharmaceutical investigation,* 53**,** 119-152.
JETHVA, P. N., KARDANI, J. R. & ROY, I. 2011. Modulation of α-synuclein aggregation by dopamine in the presence of MPTP and its metabolite. *The FEBS journal,* 278**,** 1688-1698.
JIANG, X., LACHANCE, M. & ROSSIGNOL, E. 2016. Involvement of cortical fast-spiking parvalbumin-positive basket cells in epilepsy. *Prog Brain Res,* 226**,** 81-126.

JIN, Q., CHENG, J., LIU, Y., WU, J., WANG, X., WEI, S., ZHOU, X., QIN, Z., JIA, J. & ZHEN, X. 2014. Improvement of functional recovery by chronic metformin treatment is associated with enhanced alternative activation of microglia/macrophages and increased angiogenesis and neurogenesis following experimental stroke. *Brain Behav Immun,* 40**,** 131-42.

JING, Y., WU, F., LI, D., YANG, L., LI, Q. & LI, R. 2018. Metformin improves obesity-associated inflammation by altering macrophages polarization. *Mol Cell Endocrinol,* 461**,** 256-264.

JO, E., FULLER, N., RAND, R. P., ST GEORGE-HYSLOP, P. & FRASER, P. E. 2002. Defective membrane interactions of familial Parkinson's disease mutant A30P α-synuclein. *Journal of molecular biology,* 315**,** 799-807.

KAHLE, P. J., NEUMANN, M., OZMEN, L., MÜLLER, V., JACOBSEN, H., SCHINDZIELORZ, A., OKOCHI, M., LEIMER, U., VAN DER PUTTEN, H. & PROBST, A. 2000. Subcellular localization of wild-type and Parkinson's disease-associated mutant α-synuclein in human and transgenic mouse brain. *Journal of Neuroscience,* 20**,** 6365-6373.

KAHLE, P. J., NEUMANN, M., OZMEN, L., MÜLLER, V., ODOY, S., OKAMOTO, N., JACOBSEN, H., IWATSUBO, T., TROJANOWSKI, J. Q. & TAKAHASHI, H. 2001. Selective insolubility of α-synuclein in human Lewy body diseases is recapitulated in a transgenic mouse model. *The American journal of pathology,* 159**,** 2215-2225.

KAMAT, P. K. 2015. Streptozotocin induced Alzheimer's disease like changes and the underlying neural degeneration and regeneration mechanism. *Neural Regeneration Research,* 10**,** 1050-1052.

KANDA, S., BISHOP, J., EGLITIS, M., YANG, Y. & MOURADIAN, M. 2000. Enhanced vulnerability to oxidative stress by α-synuclein mutations and C-terminal truncation. *Neuroscience,* 97**,** 279-284.

KANN, O., PAPAGEORGIOU, I. E. & DRAGUHN, A. 2014. Highly energized inhibitory interneurons are a central element for information processing in cortical networks. *J Cereb Blood Flow Metab,* 34**,** 1270-82.

KAO, H. T., PORTON, B., CZERNIK, A. J., FENG, J., YIU, G., HÄRING, M., BENFENATI, F. & GREENGARD, P. 1998. A third member of the synapsin gene family. *Proc Natl Acad Sci U S A,* 95**,** 4667-72.

KARKI, R. & HOFMANN-APITIUS, M. 2017. Comorbidity analysis between Alzheimer's disease and type 2 diabetes mellitus (T2DM) based on shared pathways and the role of T2DM drugs. *Journal of Alzheimer's Disease,* 60**,** 721-731.

KASHATUS, D. F., LIM, K. H., BRADY, D. C., PERSHING, N. L., COX, A. D. & COUNTER, C. M. 2011. RALA and RALBP1 regulate mitochondrial fission at mitosis. *Nat Cell Biol,* 13**,** 1108-15.

KATO, H. & MIHARA, K. 2008. Identification of Tom5 and Tom6 in the preprotein translocase complex of human mitochondrial outer membrane. *Biochem Biophys Res Commun,* 369**,** 958-63.

KAZKAYASI, I., TELLI, G., NEMUTLU, E. & UMA, S. 2022. Intranasal metformin treatment ameliorates cognitive functions via insulin signaling pathway in ICV-STZ-induced mice model of Alzheimer's disease. *Life Sciences,* 299**,** 120538.

KEMSHEAD, J. T., RITTER, M. A., COTMORE, S. F. & GREAVES, M. F. 1982. Human Thy-1: Expression on the cell surface of neuronal and and glial cells. *Brain research,* 236**,** 451-461.

KERTESZ, N., SAMSON, J., DEBACKER, C., WU, H. & LABASTIE, M. C. 2002. Cloning and characterization of human and mouse SNRK sucrose non-fermenting protein (SNF-1)-related kinases. *Gene,* 294**,** 13-24.

KETTENMANN, H., KIRCHHOFF, F. & VERKHRATSKY, A. 2013. Microglia: new roles for the synaptic stripper. *Neuron,* 77**,** 10-18.

KHALAF, O., FAUVET, B., OUESLATI, A., DIKIY, I., MAHUL-MELLIER, A.-L., RUGGERI, F. S., MBEFO, M. K., VERCRUYSSE, F., DIETLER, G. & LEE, S.-J. 2014. The H50Q mutation enhances α-synuclein aggregation, secretion, and toxicity. *Journal of Biological Chemistry,* 289**,** 21856-21876.

KILB, W. & KIRISCHUK, S. 2022. GABA Release from Astrocytes in Health and Disease. *Int J Mol Sci,* 23.

KIM, W. J., NOH, J. H., HAN, K. & PARK, C.-Y. 2021. The association between second-line oral antihyperglycemic medication on types of dementia in type 2 diabetes: a nationwide real-world longitudinal study. *Journal of Alzheimer's Disease,* 81**,** 1263-1272.

KIRIK, O. V., SUKHORUKOVA, E. G., VLASOV, T. D. & KORZHEVSKIĬ, D. E. 2009. [Selective death of the striatum neurons in rats after the transient occlusion of the middle cerebral artery]. *Morfologiia,* 135**,** 80-2.

KLEGERIS, A., PELECH, S., GIASSON, B. I., MAGUIRE, J., ZHANG, H., MCGEER, E. G. & MCGEER, P. L. 2008. Alpha-synuclein activates stress signaling protein kinases in THP-1 cells and microglia. *Neurobiol Aging,* 29**,** 739-52.

KOENIG, A. M., MECHANIC-HAMILTON, D., XIE, S. X., COMBS, M. F., CAPPOLA, A. R., XIE, L., DETRE, J. A., WOLK, D. A. & ARNOLD, S. E. 2017. Effects of the insulin sensitizer metformin in Alzheimer disease: pilot data from a randomized placebo-controlled crossover study. *Alzheimer Disease & Associated Disorders,* 31**,** 107-113.

KONNO, Y., TOKI, T., TANDAI, S., XU, G., WANG, R., TERUI, K., OHGA, S., HARA, T., HAMA, A., KOJIMA, S., HASEGAWA, D., KOSAKA, Y., YANAGISAWA, R., KOIKE, K., KANAI, R., IMAI, T., HONGO, T., PARK, M. J., SUGITA, K. & ITO, E. 2010. Mutations in the ribosomal protein genes in Japanese patients with Diamond-Blackfan anemia. *Haematologica,* 95**,** 1293-9.

KOOPMAN, W. J., NIJTMANS, L. G., DIETEREN, C. E., ROESTENBERG, P., VALSECCHI, F., SMEITINK, J. A. & WILLEMS, P. H. 2010. Mammalian mitochondrial complex I: biogenesis, regulation, and reactive oxygen species generation. *Antioxid Redox Signal,* 12**,** 1431-70.

KORDOWER, J. H., CHU, Y., HAUSER, R. A., FREEMAN, T. B. & OLANOW, C. W. 2008. Lewy body-like pathology in long-term embryonic nigral transplants in Parkinson's disease. *Nat Med,* 14**,** 504-6.

KORZHEVSKII, D. E., PETROVA, E. S., KIRIK, O. V. & OTELLIN, V. A. 2009. Assessment of neuron differentiation during embryogenesis in rats using immunocytochemical detection of doublecortin. *Neurosci Behav Physiol,* 39**,** 513-6.

KOSAKA, T., KATSUMARU, H., HAMA, K., WU, J.-Y. & HEIZMANN, C. W. 1987. GABAergic neurons containing the Ca2+-binding protein parvalbumin in the rat hippocampus and dentate gyrus. *Brain research,* 419**,** 119-130.

KOSS, D. J., ERSKINE, D., PORTER, A., PALMOSKI, P., MENON, H., TODD, O. G. J., LEITE, M., ATTEMS, J. & OUTEIRO, T. F. 2022. Nuclear alpha-synuclein is present in the human brain and is modified in dementia with Lewy bodies. *Acta Neuropathol Commun,* 10**,** 98.

KOULI, A., CAMACHO, M., ALLINSON, K. & WILLIAMS-GRAY, C. H. 2020. Neuroinflammation and protein pathology in Parkinson's disease dementia. *Acta neuropathologica communications,* 8**,** 1-19.

KREZYMON, A., RICHETIN, K., HALLEY, H., ROYBON, L., LASSALLE, J.-M., FRANCÈS, B., VERRET, L. & RAMPON, C. 2013. Modifications of hippocampal circuits and early disruption of adult neurogenesis in the tg2576 mouse model of Alzheimer's disease. *PloS one,* 8**,** e76497.

KRÜGER, R., KUHN, W., MÜLLER, T., WOITALLA, D., GRAEBER, M., KÖSEL, S., PRZUNTEK, H., EPPLEN, J. T., SCHÖLS, L. & RIESS, O. 1998. Ala30Pro mutation in the gene encoding alpha-synuclein in Parkinson's disease. *Nat Genet,* 18**,** 106-8.

KUMAR, S. S. & BUCKMASTER, P. S. 2007. Neuron-specific nuclear antigen NeuN is not detectable in gerbil subtantia nigra pars reticulata. *Brain research,* 1142**,** 54-60.

KWON, H. S. & KOH, S.-H. 2020. Neuroinflammation in neurodegenerative disorders: the roles of microglia and astrocytes. *Translational neurodegeneration,* 9**,** 42.

ŁABUZEK, K., SUCHY, D., GABRYEL, B., BIELECKA, A., LIBER, S. & OKOPIEŃ, B. 2010a. Quantification of metformin by the HPLC method in brain regions, cerebrospinal fluid and plasma of rats treated with lipopolysaccharide. *Pharmacol Rep,* 62**,** 956-65.

ŁABUZEK, K., SUCHY, D., GABRYEL, B., BIELECKA, A., LIBER, S. & OKOPIEŃ, B. 2010b. Quantification of metformin by the HPLC method in brain regions, cerebrospinal fluid and plasma of rats treated with lipopolysaccharide. *Pharmacological Reports,* 62**,** 956-965.

LAMONTAGNE-PROULX, J., COULOMBE, K., MORISSETTE, M., RIEUX, M., CALON, F., DI PAOLO, T. & SOULET, D. 2023. Sex and Age Differences in a Progressive Synucleinopathy Mouse Model. *Biomolecules,* 13**,** 977.

LARSEN, N. B., RASMUSSEN, M. & RASMUSSEN, L. J. 2005. Nuclear and mitochondrial DNA repair: similar pathways? *Mitochondrion,* 5**,** 89-108.

LARSON, M. E., SHERMAN, M. A., GREIMEL, S., KUSKOWSKI, M., SCHNEIDER, J. A., BENNETT, D. A. & LESNÉ, S. E. 2012. Soluble α-synuclein is a novel modulator of Alzheimer's disease pathophysiology. *J Neurosci,* 32**,** 10253-66.

LAURENT, C., DOROTHÉE, G., HUNOT, S., MARTIN, E., MONNET, Y., DUCHAMP, M., DONG, Y., LÉGERON, F. P., LEBOUCHER, A., BURNOUF, S., FAIVRE, E., CARVALHO, K., CAILLIEREZ, R., ZOMMER, N., DEMEYER, D., JOUY, N., SAZDOVITCH, V., SCHRAEN-MASCHKE, S., DELARASSE, C., BUÉE, L. & BLUM, D. 2017. Hippocampal T cell infiltration promotes neuroinflammation and cognitive decline in a mouse model of tauopathy. *Brain,* 140**,** 184-200.

LE DUIGOU, C., SIMONNET, J., TELEÑCZUK, M. T., FRICKER, D. & MILES, R. 2014. Recurrent synapses and circuits in the CA3 region of the hippocampus: an associative network. *Frontiers in cellular neuroscience,* 7**,** 262.

LEE, C., LEE, K. & PENNINGS, J. M. 2001. Internal capabilities, external networks, and performance: a study on technology-based ventures. *Strategic management journal,* 22**,** 615-640.

LEE, H. J., SUK, J. E., PATRICK, C., BAE, E. J., CHO, J. H., RHO, S., HWANG, D., MASLIAH, E. & LEE, S. J. 2010. Direct transfer of alpha-synuclein from neuron to astroglia causes inflammatory responses in synucleinopathies. *J Biol Chem,* 285**,** 9262-72.

LEE, S.-J., DESPLATS, P., LEE, H.-J., SPENCER, B. & MASLIAH, E. 2012. Cell-to-cell transmission of α-synuclein aggregates. *Amyloid Proteins: Methods and Protocols***,** 347-359.

LI, H., HUO, Y., HE, X., YAO, L., ZHANG, H., CUI, Y., XIAO, H., XIE, W., ZHANG, D., WANG, Y., ZHANG, S., TU, H., CHENG, Y., GUO, Y., CAO, X., ZHU, Y., JIANG, T., GUO, X., QIN, Y. & SHA, J. 2022. A male germ-cell-specific ribosome controls male fertility. *Nature,* 612**,** 725-731.

LI, H., ZHANG, X., CHEN, M., CHEN, J., GAO, T. & YAO, S. 2018. Dexmedetomidine inhibits inflammation in microglia cells under stimulation of LPS and ATP by c-Fos/NLRP3/caspase-1 cascades. *EXCLI journal,* 17**,** 302.

LI, J., DENG, J., SHENG, W. & ZUO, Z. 2012. Metformin attenuates Alzheimer's disease-like neuropathology in obese, leptin-resistant mice. *Pharmacology biochemistry and behavior,* 101**,** 564-574.

LI, J., WEI, Z., ZHENG, M., GU, X., DENG, Y., QIU, R., CHEN, F., JI, C., GONG, W., XIE, Y. & MAO, Y. 2006. Crystal structure of human guanosine monophosphate reductase 2 (GMPR2) in complex with GMP. *J Mol Biol,* 355**,** 980-8.

LIAO, W., XU, J., LI, B., RUAN, Y., LI, T. & LIU, J. 2021. Deciphering the Roles of Metformin in Alzheimer's Disease: A Snapshot. *Front Pharmacol,* 12**,** 728315.

LIDDELOW, S. A. & BARRES, B. A. 2017. Reactive Astrocytes: Production, Function, and Therapeutic Potential. *Immunity,* 46**,** 957-967.

LIND, D., FRANKEN, S., KAPPLER, J., JANKOWSKI, J. & SCHILLING, K. 2005. Characterization of the neuronal marker NeuN as a multiply phosphorylated antigen with discrete subcellular localization. *J Neurosci Res,* 79**,** 295-302.

LINDSTRÖM, V., FAGERQVIST, T., NORDSTRÖM, E., ERIKSSON, F., LORD, A., TUCKER, S., ANDERSSON, J., JOHANNESSON, M., SCHELL, H. & KAHLE, P. J. 2014. Immunotherapy targeting α-synuclein protofibrils reduced pathology in (Thy-1)-h [A30P] α-synuclein mice. *Neurobiology of Disease,* 69**,** 134-143.

LIU, J., WANG, Y., SONG, L., ZENG, L., YI, W., LIU, T., CHEN, H., WANG, M., JU, Z. & CONG, Y. S. 2017. A critical role of DDRGK1 in endoplasmic reticulum homoeostasis via regulation of IRE1α stability. *Nat Commun,* 8**,** 14186.
LIU, N., PANG, X., ZHANG, H. & JI, P. 2021. The cGAS-STING Pathway in Bacterial Infection and Bacterial Immunity. *Front Immunol,* 12**,** 814709.
LIU, Y., TANG, G., LI, Y., WANG, Y., CHEN, X., GU, X., ZHANG, Z., WANG, Y. & YANG, G. Y. 2014. Metformin attenuates blood-brain barrier disruption in mice following middle cerebral artery occlusion. *J Neuroinflammation,* 11**,** 177.
LOBSIGER, C. S. & CLEVELAND, D. W. 2007. Glial cells as intrinsic components of non-cell-autonomous neurodegenerative disease. *Nat Neurosci,* 10**,** 1355-60.
LOCHHEAD, J. J. & THORNE, R. G. 2012. Intranasal delivery of biologics to the central nervous system. *Advanced drug delivery reviews,* 64**,** 614-628.
LOCHHEAD, J. J., WOLAK, D. J., PIZZO, M. E. & THORNE, R. G. 2015. Rapid transport within cerebral perivascular spaces underlies widespread tracer distribution in the brain after intranasal administration. *Journal of Cerebral Blood Flow & Metabolism,* 35**,** 371-381.
LOTHARIUS, J. & BRUNDIN, P. 2002. Impaired dopamine storage resulting from α-synuclein mutations may contribute to the pathogenesis of Parkinson's disease. *Human molecular genetics,* 11**,** 2395-2407.
LOU, N., TAKANO, T., PEI, Y., XAVIER, A. L., GOLDMAN, S. A. & NEDERGAARD, M. 2016. Purinergic receptor P2RY12-dependent microglial closure of the injured blood-brain barrier. *Proc Natl Acad Sci U S A,* 113**,** 1074-9.
LOVELAND, P. M., YU, J. J., CHURILOV, L., YASSI, N. & WATSON, R. 2023. Investigation of inflammation in Lewy body dementia: a systematic scoping review. *International Journal of Molecular Sciences,* 24**,** 12116.
LU, M., CHEN, H., NIE, F., WEI, X., TAO, Z. & MA, J. 2020a. The potential role of metformin in the treatment of Parkinson's disease. *Journal of Bio-X Research,* 3**,** 27-35.
LU, X.-Y., HUANG, S., CHEN, Q.-B., ZHANG, D., LI, W., AO, R., LEUNG, F. C.-Y., ZHANG, Z., HUANG, J. & TANG, Y. 2020b. Metformin Ameliorates Aβ Pathology by Insulin-Degrading Enzyme in a Transgenic Mouse Model of Alzheimer's Disease. *Oxidative medicine and cellular longevity,* 2020**,** 2315106.
LYONS, M. R. & WEST, A. E. 2011. Mechanisms of specificity in neuronal activity-regulated gene transcription. *Progress in neurobiology,* 94**,** 259-295.
MA, J., YU, H., LIU, J., CHEN, Y., WANG, Q. & XIANG, L. 2015. Metformin attenuates hyperalgesia and allodynia in rats with painful diabetic neuropathy induced by streptozotocin. *Eur J Pharmacol,* 764**,** 599-606.
MA, T. C., BUESCHER, J. L., OATIS, B., FUNK, J. A., NASH, A. J., CARRIER, R. L. & HOYT, K. R. 2007. Metformin therapy in a transgenic mouse model of Huntington's disease. *Neuroscience letters,* 411**,** 98-103.
MA, W., JIN, Q., GUO, H., HAN, X., XU, L., LU, S. & WU, C. 2022. Metformin ameliorates inflammation and airway remodeling of experimental allergic asthma in mice by restoring AMPK α activity. *Frontiers in Pharmacology,* 13**,** 780148.
MACVICAR, B. A. & NEWMAN, E. A. 2015. Astrocyte regulation of blood flow in the brain. *Cold Spring Harbor perspectives in biology,* 7**,** a020388.
MADABHUSHI, R., PAN, L. & TSAI, L. H. 2014. DNA damage and its links to neurodegeneration. *Neuron,* 83**,** 266-282.
MALYGIN, A. A. & KARPOVA, G. G. 2010. Site-specific cleavage of the 40S ribosomal subunit reveals eukaryote-specific ribosomal protein S28 in the subunit head. *FEBS Lett,* 584**,** 4396-400.
MARTIN, L. J., PAN, Y., PRICE, A. C., STERLING, W., COPELAND, N. G., JENKINS, N. A., PRICE, D. L. & LEE, M. K. 2006. Parkinson's disease alpha-synuclein transgenic mice develop neuronal mitochondrial degeneration and cell death. *J Neurosci,* 26**,** 41-50.
MARTÍNEZ-MENÁRGUEZ, J., MARTÍNEZ-ALONSO, E., CARA-ESTEBAN, M. & TOMÁS, M. 2021. Focus on the Small GTPase Rab1: A Key Player in the Pathogenesis of Parkinson's Disease. *Int J Mol Sci,* 22.

MAVROEIDI, P. & XILOURI, M. 2021. Neurons and glia interplay in α-synucleinopathies. *International journal of molecular sciences,* 22**,** 4994.
MAZUMDER, A. G., JULÉ, A. M., CULLEN, P. F. & SUN, D. 2022. Astrocyte heterogeneity within white matter tracts and a unique subpopulation of optic nerve head astrocytes. *iScience,* 25**,** 105568.
MAZZULLI, J. R., ZUNKE, F., ISACSON, O., STUDER, L. & KRAINC, D. 2016. α-Synuclein-induced lysosomal dysfunction occurs through disruptions in protein trafficking in human midbrain synucleinopathy models. *Proc Natl Acad Sci U S A,* 113**,** 1931-6.
MCCREIGHT, L. J., BAILEY, C. J. & PEARSON, E. R. 2016. Metformin and the gastrointestinal tract. *Diabetologia,* 59**,** 426-435.
MCKEITH, I., MINTZER, J., AARSLAND, D., BURN, D., CHIU, H., COHEN-MANSFIELD, J., DICKSON, D., DUBOIS, B., DUDA, J. E., FELDMAN, H., GAUTHIER, S., HALLIDAY, G., LAWLOR, B., LIPPA, C., LOPEZ, O. L., CARLOS MACHADO, J., O'BRIEN, J., PLAYFER, J. & REID, W. 2004. Dementia with Lewy bodies. *Lancet Neurol,* 3**,** 19-28.
MCKEITH, I. G., BOEVE, B. F., DICKSON, D. W., HALLIDAY, G., TAYLOR, J. P., WEINTRAUB, D., AARSLAND, D., GALVIN, J., ATTEMS, J., BALLARD, C. G., BAYSTON, A., BEACH, T. G., BLANC, F., BOHNEN, N., BONANNI, L., BRAS, J., BRUNDIN, P., BURN, D., CHEN-PLOTKIN, A., DUDA, J. E., EL-AGNAF, O., FELDMAN, H., FERMAN, T. J., FFYTCHE, D., FUJISHIRO, H., GALASKO, D., GOLDMAN, J. G., GOMPERTS, S. N., GRAFF-RADFORD, N. R., HONIG, L. S., IRANZO, A., KANTARCI, K., KAUFER, D., KUKULL, W., LEE, V. M. Y., LEVERENZ, J. B., LEWIS, S., LIPPA, C., LUNDE, A., MASELLIS, M., MASLIAH, E., MCLEAN, P., MOLLENHAUER, B., MONTINE, T. J., MORENO, E., MORI, E., MURRAY, M., O'BRIEN, J. T., ORIMO, S., POSTUMA, R. B., RAMASWAMY, S., ROSS, O. A., SALMON, D. P., SINGLETON, A., TAYLOR, A., THOMAS, A., TIRABOSCHI, P., TOLEDO, J. B., TROJANOWSKI, J. Q., TSUANG, D., WALKER, Z., YAMADA, M. & KOSAKA, K. 2017. Diagnosis and management of dementia with Lewy bodies: Fourth consensus report of the DLB Consortium. *Neurology,* 89**,** 88-100.
MEADE, R. M., FAIRLIE, D. P. & MASON, J. M. 2019. Alpha-synuclein structure and Parkinson's disease - lessons and emerging principles. *Mol Neurodegener,* 14**,** 29.
MERLINI, M., RAFALSKI, V. A., MA, K., KIM, K.-Y., BUSHONG, E. A., RIOS CORONADO, P. E., YAN, Z., MENDIOLA, A. S., SOZMEN, E. G. & RYU, J. K. 2021. Microglial Gi-dependent dynamics regulate brain network hyperexcitability. *Nature neuroscience,* 24**,** 19-23.
MILLER, S. J., CAMPBELL, C. E., JIMENEZ-COREA, H. A., WU, G. H. & LOGAN, R. 2022. Neuroglial Senescence, α-Synucleinopathy, and the Therapeutic Potential of Senolytics in Parkinson's Disease. *Front Neurosci,* 16**,** 824191.
MIYATA, S. & KITAGAWA, H. 2017. Formation and remodeling of the brain extracellular matrix in neural plasticity: Roles of chondroitin sulfate and hyaluronan. *Biochimica et Biophysica Acta (BBA)-General Subjects,* 1861**,** 2420-2434.
MIYATA, S., NISHIMURA, Y. & NAKASHIMA, T. 2007. Perineuronal nets protect against amyloid β-protein neurotoxicity in cultured cortical neurons. *Brain research,* 1150**,** 200-206.
MOCHIZUKI, H., CHOONG, C. J. & MASLIAH, E. 2018. A refined concept: α-synuclein dysregulation disease. *Neurochem Int,* 119**,** 84-96.
MOISSAN, H. 2016. *Sur les volumes d'oxygène absorbé et d'acide carbonique émis dans la respiration végétale: thèse présentée et soutenue à l'Ecole supérieure de pharmacie de Paris le [] mai 1879 pour obtenir le diplôme de pharmacien de première classe.* BIU Santé.
MOODY, D. M., BELL, M. A. & CHALLA, V. R. 1990. Features of the cerebral vascular pattern that predict vulnerability to perfusion or oxygenation deficiency: an anatomic study. *AJNR Am J Neuroradiol,* 11**,** 431-9.
MOR, D. E., SOHRABI, S., KALETSKY, R., KEYES, W., TARTICI, A., KALIA, V., MILLER, G. W. & MURPHY, C. T. 2020. Metformin rescues Parkinson's disease phenotypes

caused by hyperactive mitochondria. *Proceedings of the National Academy of Sciences,* 117**,** 26438-26447.
MORALES, I., GUZMÁN-MARTÍNEZ, L., CERDA-TRONCOSO, C., FARÍAS, G. A. & MACCIONI, R. B. 2014. Neuroinflammation in the pathogenesis of Alzheimer's disease. A rational framework for the search of novel therapeutic approaches. *Frontiers in cellular neuroscience,* 8**,** 112.
MORRIS, M., SANCHEZ, P. E., VERRET, L., BEAGLE, A. J., GUO, W., DUBAL, D., RANASINGHE, K. G., KOYAMA, A., HO, K., YU, G. Q., VOSSEL, K. A. & MUCKE, L. 2015. Network dysfunction in α-synuclein transgenic mice and human Lewy body dementia. *Ann Clin Transl Neurol,* 2**,** 1012-28.
MOSER, M. B., ROWLAND, D. C. & MOSER, E. I. 2015. Place cells, grid cells, and memory. *Cold Spring Harb Perspect Biol,* 7**,** a021808.
MOTYL, K. & MCCABE, L. R. 2009. Streptozotocin, type I diabetes severity and bone. *Biol Proced Online,* 11**,** 296-315.
MUTREJA, Y. & GAMBLIN, T. C. 2017. Optimization of in vitro conditions to study the arachidonic acid induction of 4R isoforms of the microtubule-associated protein tau. *Methods Cell Biol,* 141**,** 65-88.
NAGATSU, T., MOGI, M., ICHINOSE, H. & TOGARI, A. 2000. Changes in cytokines and neurotrophins in Parkinson's disease. *J Neural Transm Suppl***,** 277-90.
NANDINI, H., PAUDEL, Y. N. & KRISHNA, K. 2019. Envisioning the neuroprotective effect of Metformin in experimental epilepsy: A portrait of molecular crosstalk. *Life sciences,* 233**,** 116686.
NARHI, L., WOOD, S. J., STEAVENSON, S., JIANG, Y., WU, G. M., ANAFI, D., KAUFMAN, S. A., MARTIN, F., SITNEY, K. & DENIS, P. 1999. Both familial Parkinson's disease mutations accelerate α-synuclein aggregation. *Journal of Biological Chemistry,* 274**,** 9843-9846.
NEMANI, V. M., LU, W., BERGE, V., NAKAMURA, K., ONOA, B., LEE, M. K., CHAUDHRY, F. A., NICOLL, R. A. & EDWARDS, R. H. 2010. Increased expression of α-synuclein reduces neurotransmitter release by inhibiting synaptic vesicle reclustering after endocytosis. *Neuron,* 65**,** 66-79.
NEUMANN, M., KAHLE, P. J., GIASSON, B. I., OZMEN, L., BORRONI, E., SPOOREN, W., MÜLLER, V., ODOY, S., FUJIWARA, H. & HASEGAWA, M. 2002. Misfolded proteinase K–resistant hyperphosphorylated α-synuclein in aged transgenic mice with locomotor deterioration and in human α-synucleinopathies. *The Journal of clinical investigation,* 110**,** 1429-1439.
NG, T., CHAND, D., SONG, L., AL CHAWAF, A., WATSON, J. D., BOUTROS, P. C., BELSHAM, D. D. & LOVEJOY, D. A. 2012. Identification of a novel brain derived neurotrophic factor (BDNF)-inhibitory factor: regulation of BDNF by teneurin C-terminal associated peptide (TCAP)-1 in immortalized embryonic mouse hypothalamic cells. *Regul Pept,* 174**,** 79-89.
NIJBOER, C. H., HEIJNEN, C. J., GROENENDAAL, F., VAN BEL, F. & KAVELAARS, A. 2009. Alternate Pathways Preserve Tumor Necrosis Factor-α Production After Nuclear Factor-κB Inhibition in Neonatal Cerebral Hypoxia–Ischemia. *Stroke,* 40**,** 3362-3368.
NIRUJOGI, R. S., TONELLI, F., TAYLOR, M., LIS, P., ZIMPRICH, A., SAMMLER, E. & ALESSI, D. R. 2021. Development of a multiplexed targeted mass spectrometry assay for LRRK2-phosphorylated Rabs and Ser910/Ser935 biomarker sites. *Biochem J,* 478**,** 299-326.
NORRIS, E. H., GIASSON, B. I. & LEE, V. M.-Y. 2004. α-Synuclein: normal function and role in neurodegenerative diseases. *Current topics in developmental biology,* 60**,** 17-54.
NORWITZ, N. G. & QUERFURTH, H. 2020. mTOR mysteries: Nuances and questions about the mechanistic target of rapamycin in neurodegeneration. *Frontiers in Neuroscience,* 14**,** 565468.
OH, D., HAN, S., SEO, J., LEE, J. R., CHOI, J., GROFFEN, J., KIM, K., CHO, Y. S., CHOI, H. S., SHIN, H., WOO, J., WON, H., PARK, S. K., KIM, S. Y., JO, J., WHITCOMB, D. J., CHO, K., KIM, H., BAE, Y. C., HEISTERKAMP, N., CHOI, S. Y. & KIM, E. 2010.

Regulation of synaptic Rac1 activity, long-term potentiation maintenance, and learning and memory by BCR and ABR Rac GTPase-activating proteins. *J Neurosci,* 30**,** 14134-44.

OLKHOVA, E. A., SMITH, L. A., DENNIS, B. H., NG, Y. S., LEBEAU, F. E. & GORMAN, G. S. 2024. Delineating mechanisms underlying parvalbumin neuron impairment in different neurological and neurodegenerative disorders: the emerging role of mitochondrial dysfunction. *Biochemical Society Transactions,* 52**,** 553-565.

OLTRA, J., HABICH, A., SCHWARZ, C. G., NEDELSKA, Z., PRZYBELSKI, S. A., INGUANZO, A., DIAZ-GALVAN, P., LOWE, V. J., OPPEDAL, K., BLANC, F., LEMSTRA, A. W., HORT, J., PADOVANI, A., REKTOROVA, I., BONANNI, L., MASSA, F., KRAMBERGE, M. G., TAYLOR, J. P., SNÆDAL, J., WALKER, Z., ANTONINI, A., SEGURA, B., JUNQUE, C., WESTMAN, E., BOEVE, B. F., AARSLAND, D., KANTARCI, K. & FERREIRA, D. 2023. Sex differences in brain atrophy in dementia with Lewy bodies. *Res Sq*.

OMURA, Y., NISHIO, Y., TAKEMOTO, T., IKEUCHI, C., SEKINE, O., MORINO, K., MAENO, Y., OBATA, T., UGI, S., MAEGAWA, H., KIMURA, H. & KASHIWAGI, A. 2009. SAFB1, an RBMX-binding protein, is a newly identified regulator of hepatic SREBP-1c gene. *BMB Rep,* 42**,** 232-7.

ONKEN, B. & DRISCOLL, M. 2010. Metformin induces a dietary restriction–like state and the oxidative stress response to extend C. elegans healthspan via AMPK, LKB1, and SKN-1. *PloS one,* 5**,** e8758.

ORENSTEIN, S. J., KUO, S. H., TASSET, I., ARIAS, E., KOGA, H., FERNANDEZ-CARASA, I., CORTES, E., HONIG, L. S., DAUER, W., CONSIGLIO, A., RAYA, A., SULZER, D. & CUERVO, A. M. 2013. Interplay of LRRK2 with chaperone-mediated autophagy. *Nat Neurosci,* 16**,** 394-406.

OROSCO, L. A., ROSS, A. P., CATES, S. L., SCOTT, S. E., WU, D., SOHN, J., PLEASURE, D., PLEASURE, S. J., ADAMOPOULOS, I. E. & ZARBALIS, K. S. 2014. Loss of Wdfy3 in mice alters cerebral cortical neurogenesis reflecting aspects of the autism pathology. *Nat Commun,* 5**,** 4692.

OSMANOVIC BARILAR, J., KNEZOVIC, A., GRÜNBLATT, E., RIEDERER, P. & SALKOVIC-PETRISIC, M. 2015. Nine-month follow-up of the insulin receptor signalling cascade in the brain of streptozotocin rat model of sporadic Alzheimer's disease. *Journal of neural transmission,* 122**,** 565-576.

OU, Y., ZHANG, W., CHEN, S. & DENG, H. 2021. Baicalin improves podocyte injury in rats with diabetic nephropathy by inhibiting PI3K/Akt/mTOR signaling pathway. *Open Medicine,* 16**,** 1286-1298.

OU, Z., KONG, X., SUN, X., HE, X., ZHANG, L., GONG, Z., HUANG, J., XU, B., LONG, D. & LI, J. 2018. Metformin treatment prevents amyloid plaque deposition and memory impairment in APP/PS1 mice. *Brain, behavior, and immunity,* 69**,** 351-363.

OUTEIRO, T. F., KOSS, D. J., ERSKINE, D., WALKER, L., KURZAWA-AKANBI, M., BURN, D., DONAGHY, P., MORRIS, C., TAYLOR, J. P., THOMAS, A., ATTEMS, J. & MCKEITH, I. 2019. Dementia with Lewy bodies: an update and outlook. *Mol Neurodegener,* 14**,** 5.

PACHER, P., BECKMAN, J. S. & LIAUDET, L. 2007. Nitric oxide and peroxynitrite in health and disease. *Physiol Rev,* 87**,** 315-424.

PALIT, P., FURMAN, B. & GRAY, A. 1999. Novel weight-reducing activity of Galega officinalis in mice. *Journal of pharmacy and pharmacology,* 51**,** 1313-1319.

PARDRIDGE, W. 2019. Blood-brain barrier and delivery of protein and gene therapeutics to brain. Front Aging Neurosci 11: 373.

PARDRIDGE, W. M. 2020. Treatment of Alzheimer's disease and blood–brain barrier drug delivery. *Pharmaceuticals,* 13**,** 394.

PATADE, G. & MARITA, A. 2014. Metformin: A Journey from countryside to the bedside. *Journal of Obesity and Metabolic research,* 1**,** 127-127.

PATTON, G. C., STENMARK, P., GOLLAPALLI, D. R., SEVASTIK, R., KURSULA, P., FLODIN, S., SCHULER, H., SWALES, C. T., EKLUND, H., HIMO, F., NORDLUND, P.

& HEDSTROM, L. 2011. Cofactor mobility determines reaction outcome in the IMPDH and GMPR (β-α)8 barrel enzymes. *Nat Chem Biol,* 7**,** 950-8.
PELLERIN, L., PELLEGRI, G., BITTAR, P. G., CHARNAY, Y., BOURAS, C., MARTIN, J. L., STELLA, N. & MAGISTRETTI, P. J. 1998. Evidence supporting the existence of an activity-dependent astrocyte-neuron lactate shuttle. *Dev Neurosci,* 20**,** 291-9.
PEÑA-BAUTISTA, C., BAQUERO, M., VENTO, M. & CHÁFER-PERICÁS, C. 2019. Omics-based Biomarkers for the Early Alzheimer Disease Diagnosis and Reliable Therapeutic Targets Development. *Curr Neuropharmacol,* 17**,** 630-647.
PERALTA, S., PINTO, M., ARGUELLO, T., GARCIA, S., DIAZ, F. & MORAES, C. T. 2020. Metformin delays neurological symptom onset in a mouse model of neuronal complex I deficiency. *JCI insight,* 5.
PÉREZ-REVUELTA, B., HETTICH, M., CIOCIARO, A., ROTERMUND, C., KAHLE, P., KRAUSS, S. & DI MONTE, D. 2014. Metformin lowers Ser-129 phosphorylated α-synuclein levels via mTOR-dependent protein phosphatase 2A activation. *Cell death & disease,* 5**,** e1209-e1209.
PERLUIGI, M., DI DOMENICO, F. & BUTTERFIELD, D. A. 2022. Oxidative stress and mTOR in Down syndrome brain: Link to Alzheimer's dysmetabolism, neuropathology, and possible therapies. *The Neurobiology of Aging and Alzheimer Disease in Down Syndrome.* Elsevier.
PERNICOVA, I., KELLY, S., AJODHA, S., SAHDEV, A., BESTWICK, J. P., GABROVSKA, P., AKANLE, O., AJJAN, R., KOLA, B. & STADLER, M. 2020. Metformin to reduce metabolic complications and inflammation in patients on systemic glucocorticoid therapy: a randomised, double-blind, placebo-controlled, proof-of-concept, phase 2 trial. *The lancet Diabetes & endocrinology,* 8**,** 278-291.
PESTANA, F., EDWARDS-FARET, G., BELGARD, T. G., MARTIROSYAN, A. & HOLT, M. G. 2020. No longer underappreciated: the emerging concept of astrocyte heterogeneity in neuroscience. *Brain Sciences,* 10**,** 168.
PETERS, S. T., FAHRENKOPF, A., CHOQUETTE, J. M., VERMILYEA, S. C., LEE, M. K. & VOSSEL, K. 2020. Ablating Tau Reduces Hyperexcitability and Moderates Electroencephalographic Slowing in Transgenic Mice Expressing A53T Human α-Synuclein. *Front Neurol,* 11**,** 563.
PICCIONI, G., MANGO, D., SAIDI, A., CORBO, M. & NISTICÒ, R. 2021. Targeting microglia-synapse interactions in Alzheimer's disease. *International journal of molecular sciences,* 22**,** 2342.
PINEDA, A. & BURRÉ, J. 2017. Modulating membrane binding of α-synuclein as a therapeutic strategy. *Proc Natl Acad Sci U S A,* 114**,** 1223-1225.
POLYMEROPOULOS, M. H., LAVEDAN, C., LEROY, E., IDE, S. E., DEHEJIA, A., DUTRA, A., PIKE, B., ROOT, H., RUBENSTEIN, J. & BOYER, R. 1997a. Mutation in the α-synuclein gene identified in families with Parkinson's disease. *science,* 276**,** 2045-2047.
POLYMEROPOULOS, M. H., LAVEDAN, C., LEROY, E., IDE, S. E., DEHEJIA, A., DUTRA, A., PIKE, B., ROOT, H., RUBENSTEIN, J., BOYER, R., STENROOS, E. S., CHANDRASEKHARAPPA, S., ATHANASSIADOU, A., PAPAPETROPOULOS, T., JOHNSON, W. G., LAZZARINI, A. M., DUVOISIN, R. C., DI IORIO, G., GOLBE, L. I. & NUSSBAUM, R. L. 1997b. Mutation in the alpha-synuclein gene identified in families with Parkinson's disease. *Science,* 276**,** 2045-7.
PUIG, M. V., USHIMARU, M. & KAWAGUCHI, Y. 2008. Two distinct activity patterns of fast-spiking interneurons during neocortical UP states. *Proceedings of the National Academy of Sciences,* 105**,** 8428-8433.
RABIEI POOR, S., ETTCHETO ARRIOLA, M., CANO FERNÁNDEZ, A., SÁNCHEZ-LÓPEZ, E., MANZINE, P. R., OLLOQUEQUI, J., CAMINS ESPUNY, A. & JAVAN, M. 2021. Promising application of metformin in Alzheimer's disease. *Pharmaceuticals, 2021, vol. 14, num. 9*.

RABIEIPOOR, S., ZARE, M., ETTCHETO, M., CAMINS, A. & JAVAN, M. 2023. Metformin restores cognitive dysfunction and histopathological deficits in an animal model of sporadic Alzheimer's disease. *Heliyon,* 9**,** e17873.
RAJKUMAR, A. P., BIDKHORI, G., SHOAIE, S., CLARKE, E., MORRIN, H., HYE, A., WILLIAMS, G., BALLARD, C., FRANCIS, P. & AARSLAND, D. 2020. Postmortem Cortical Transcriptomics of Lewy Body Dementia Reveal Mitochondrial Dysfunction and Lack of Neuroinflammation. *Am J Geriatr Psychiatry,* 28**,** 75-86.
RAMANAN, V. K. & SAYKIN, A. J. 2013. Pathways to neurodegeneration: mechanistic insights from GWAS in Alzheimer's disease, Parkinson's disease, and related disorders. *American journal of neurodegenerative disease,* 2**,** 145.
RANA, A. & MUSTO, A. E. 2018. The role of inflammation in the development of epilepsy. *J Neuroinflammation,* 15**,** 144.
RANNIKKO, E. H., WEBER, S. S. & KAHLE, P. J. 2015. Exogenous α-synuclein induces toll-like receptor 4 dependent inflammatory responses in astrocytes. *BMC neuroscience,* 16**,** 1-11.
RANSOM, B. R. & ORKAND, R. K. 1996. Glial-neuronal interactions in non-synaptic areas of the brain: studies in the optic nerve. *Trends Neurosci,* 19**,** 352-8.
REICHELT, A. C. 2020. Is loss of perineuronal nets a critical pathological event in Alzheimer's disease? *EBioMedicine,* 59.
REICHELT, A. C., HARE, D. J., BUSSEY, T. J. & SAKSIDA, L. M. 2019. Perineuronal nets: plasticity, protection, and therapeutic potential. *Trends in neurosciences,* 42**,** 458-470.
REJMAN, J., OBERLE, V., ZUHORN, I. S. & HOEKSTRA, D. 2004. Size-dependent internalization of particles via the pathways of clathrin-and caveolae-mediated endocytosis. *Biochemical journal,* 377**,** 159-169.
RENA, G., PEARSON, E. R. & SAKAMOTO, K. 2013. Molecular mechanism of action of metformin: old or new insights? *Diabetologia,* 56**,** 1898-1906.
RENDÓN, W. O., MARTÍNEZ-ALONSO, E., TOMÁS, M., MARTÍNEZ-MARTÍNEZ, N. & MARTÍNEZ-MENÁRGUEZ, J. A. 2013. Golgi fragmentation is Rab and SNARE dependent in cellular models of Parkinson's disease. *Histochem Cell Biol,* 139**,** 671-84.
RIETDIJK, C. D., PEREZ-PARDO, P., GARSSEN, J., VAN WEZEL, R. J. & KRANEVELD, A. D. 2017. Exploring Braak's Hypothesis of Parkinson's Disease. *Front Neurol,* 8**,** 37.
RILEY, J. S., QUARATO, G., CLOIX, C., LOPEZ, J., O'PREY, J., PEARSON, M., CHAPMAN, J., SESAKI, H., CARLIN, L. M., PASSOS, J. F., WHEELER, A. P., OBERST, A., RYAN, K. M. & TAIT, S. W. 2018. Mitochondrial inner membrane permeabilisation enables mtDNA release during apoptosis. *Embo j,* 37.
ROBSON, A. G., NILSSON, J., LI, S., JALALI, S., FULTON, A. B., TORMENE, A. P., HOLDER, G. E. & BRODIE, S. E. 2018. ISCEV guide to visual electrodiagnostic procedures. *Documenta Ophthalmologica,* 136**,** 1-26.
ROGANOVIC, M., PANTOVIC, S. & DIZDAREVIC, S. 2019. Role of the oxidative stress in the pathogenesis of epilepsy. *brain,* 1**,** 1-10.
ROSS, T., MARTINEZ, P., RENNER, J., THORNE, R., HANSON, L. & FREY II, W. 2004. Intranasal administration of interferon beta bypasses the blood–brain barrier to target the central nervous system and cervical lymph nodes: a non-invasive treatment strategy for multiple sclerosis. *Journal of neuroimmunology,* 151**,** 66-77.
RÜBER, T., DAVID, B., LÜCHTERS, G., NASS, R. D., FRIEDMAN, A., SURGES, R., STÖCKER, T., WEBER, B., DEICHMANN, R., SCHLAUG, G., HATTINGEN, E. & ELGER, C. E. 2018. Evidence for peri-ictal blood-brain barrier dysfunction in patients with epilepsy. *Brain,* 141**,** 2952-2965.
RUDEN, J. B., DUGAN, L. L. & KONRADI, C. 2021. Parvalbumin interneuron vulnerability and brain disorders. *Neuropsychopharmacology,* 46**,** 279-287.
RUDY, B., FISHELL, G., LEE, S. & HJERLING-LEFFLER, J. 2011. Three groups of interneurons account for nearly 100% of neocortical GABAergic neurons. *Developmental neurobiology,* 71**,** 45-61.

RUGGIERO-LOPEZ, D., LECOMTE, M., MOINET, G., PATEREAU, G., LAGARDE, M. & WIERNSPERGER, N. 1999. Reaction of metformin with dicarbonyl compounds. Possible implication in the inhibition of advanced glycation end product formation. *Biochemical pharmacology,* 58**,** 1765-1773.

RUTHERFORD, N. J., MOORE, B. D., GOLDE, T. E. & GIASSON, B. I. 2014. Divergent effects of the H50Q and G51D SNCA mutations on the aggregation of α-synuclein. *Journal of neurochemistry,* 131**,** 859-867.

RYU, Y. K., GO, J., PARK, H. Y., CHOI, Y. K., SEO, Y. J., CHOI, J. H., RHEE, M., LEE, T. G., LEE, C. H. & KIM, K. S. 2020. Metformin regulates astrocyte reactivity in Parkinson's disease and normal aging. *Neuropharmacology,* 175**,** 108173.

SAHAY, S., GHOSH, D., DWIVEDI, S., ANOOP, A., MOHITE, G. M., KOMBRABAIL, M., KRISHNAMOORTHY, G. & MAJI, S. K. 2015. Familial Parkinson disease-associated mutations alter the site-specific microenvironment and dynamics of α-synuclein. *Journal of Biological Chemistry,* 290**,** 7804-7822.

SALEH, H., SALEH, A., YAO, H., CUI, J., SHEN, Y. & LI, R. 2015. Mini review: linkage between α-Synuclein protein and cognition. *Transl Neurodegener,* 4**,** 5.

SALPETER, S. R., GREYBER, E., PASTERNAK, G. A. & SALPETER, E. E. 2010. Risk of fatal and nonfatal lactic acidosis with metformin use in type 2 diabetes mellitus. *Cochrane database of systematic reviews*.

SANCHEZ, P. E., ZHU, L., VERRET, L., VOSSEL, K. A., ORR, A. G., CIRRITO, J. R., DEVIDZE, N., HO, K., YU, G.-Q. & PALOP, J. J. 2012. Levetiracetam suppresses neuronal network dysfunction and reverses synaptic and cognitive deficits in an Alzheimer's disease model. *Proceedings of the National Academy of Sciences,* 109**,** E2895-E2903.

SANCHIS, A., GARCÍA-GIMENO, M. A., CAÑADA-MARTÍNEZ, A. J., SEQUEDO, M. D., MILLÁN, J. M., SANZ, P. & VAZQUEZ-MANRIQUE, R. P. 2019. Metformin treatment reduces motor and neuropsychiatric phenotypes in the zQ175 mouse model of Huntington disease. *Experimental & molecular medicine,* 51**,** 1-16.

SANG, J. C., HIDARI, E., MEISL, G., RANASINGHE, R. T., SPILLANTINI, M. G. & KLENERMAN, D. 2021. Super-resolution imaging reveals α-synuclein seeded aggregation in SH-SY5Y cells. *Commun Biol,* 4**,** 613.

SANZ, P., RUBIO, T. & GARCIA-GIMENO, M. A. 2024. Neuroinflammation and Epilepsy: From Pathophysiology to Therapies Based on Repurposing Drugs. *International Journal of Molecular Sciences,* 25**,** 4161.

SANZ, P., SERRATOSA, J. M. & SÁNCHEZ, M. P. 2021. Beneficial Effects of Metformin on the Central Nervous System, with a Focus on Epilepsy and Lafora Disease. *Int J Mol Sci,* 22.

SARNAT, H. B., NOCHLIN, D. & BORN, D. E. 1998. Neuronal nuclear antigen (NeuN): a marker of neuronal maturation in the early human fetal nervous system. *Brain and Development,* 20**,** 88-94.

SASAKI, A., KAWARABAYASHI, T., MURAKAMI, T., MATSUBARA, E., IKEDA, M., HAGIWARA, H., WESTAWAY, D., GEORGE-HYSLOP, P. S., SHOJI, M. & NAKAZATO, Y. 2008. Microglial activation in brain lesions with tau deposits: comparison of human tauopathies and tau transgenic mice TgTauP301L. *Brain research,* 1214**,** 159-168.

SATAKE, W., NAKABAYASHI, Y., MIZUTA, I., HIROTA, Y., ITO, C., KUBO, M., KAWAGUCHI, T., TSUNODA, T., WATANABE, M. & TAKEDA, A. 2009. Genome-wide association study identifies common variants at four loci as genetic risk factors for Parkinson's disease. *Nature genetics,* 41**,** 1303-1307.

SAVITT, D. & JANKOVIC, J. 2019. Targeting α-Synuclein in Parkinson's Disease: Progress Towards the Development of Disease-Modifying Therapeutics. *Drugs,* 79**,** 797-810.

SAYEDALI, E., YALIN, A. E. & YALIN, S. 2023. Association between metformin and vitamin B12 deficiency in patients with type 2 diabetes. *World J Diabetes,* 14**,** 585-593.

SCHEIBLICH, H., DANSOKHO, C., MERCAN, D., SCHMIDT, S. V., BOUSSET, L., WISCHHOF, L., EIKENS, F., ODAINIC, A., SPITZER, J., GRIEP, A., SCHWARTZ, S.,

BANO, D., LATZ, E., MELKI, R. & HENEKA, M. T. 2021. Microglia jointly degrade fibrillar alpha-synuclein cargo by distribution through tunneling nanotubes. *Cell,* 184**,** 5089-5106.e21.
SCHELL, H., HASEGAWA, T., NEUMANN, M. & KAHLE, P. 2009. Nuclear and neuritic distribution of serine-129 phosphorylated α-synuclein in transgenic mice. *Neuroscience,* 160**,** 796-804.
SCHRÖDER, H., MOSER, N., HUGGENBERGER, S., SCHRÖDER, H., MOSER, N. & HUGGENBERGER, S. 2020. The mouse hippocampus. *Neuroanatomy of the Mouse: An Introduction***,** 267-288.
SCHULZ-SCHAEFFER, W. J. 2010. The synaptic pathology of alpha-synuclein aggregation in dementia with Lewy bodies, Parkinson's disease and Parkinson's disease dementia. *Acta Neuropathol,* 120**,** 131-43.
SCOTT, D. A., TABAREAN, I., TANG, Y., CARTIER, A., MASLIAH, E. & ROY, S. 2010. A pathologic cascade leading to synaptic dysfunction in alpha-synuclein-induced neurodegeneration. *J Neurosci,* 30**,** 8083-95.
SCUDAMORE, O. & CIOSSEK, T. 2018. Increased Oxidative Stress Exacerbates α-Synuclein Aggregation In Vivo. *J Neuropathol Exp Neurol,* 77**,** 443-453.
SCUDERI, C., BRONZUOLI, M. R., FACCHINETTI, R., PACE, L., FERRARO, L., BROAD, K. D., SERVIDDIO, G., BELLANTI, F., PALOMBELLI, G., CARPINELLI, G., CANESE, R., GAETANI, S., STEARDO, L., JR., STEARDO, L. & CASSANO, T. 2018. Ultramicronized palmitoylethanolamide rescues learning and memory impairments in a triple transgenic mouse model of Alzheimer's disease by exerting anti-inflammatory and neuroprotective effects. *Transl Psychiatry,* 8**,** 32.
SELKOE, D. J. 2001. Alzheimer's disease: genes, proteins, and therapy. *Physiol Rev,* 81**,** 741-66.
SERLIN, Y., LEVY, J. & SHALEV, H. 2011. Vascular pathology and blood-brain barrier disruption in cognitive and psychiatric complications of type 2 diabetes mellitus. *Cardiovasc Psychiatry Neurol,* 2011**,** 609202.
SERRANO-POZO, A., MUZIKANSKY, A., GÓMEZ-ISLA, T., GROWDON, J. H., BETENSKY, R. A., FROSCH, M. P. & HYMAN, B. T. 2013. Differential relationships of reactive astrocytes and microglia to fibrillar amyloid deposits in Alzheimer disease. *Journal of Neuropathology & Experimental Neurology,* 72**,** 462-471.
SETOU, M., NAKAGAWA, T., SEOG, D. H. & HIROKAWA, N. 2000. Kinesin superfamily motor protein KIF17 and mLin-10 in NMDA receptor-containing vesicle transport. *Science,* 288**,** 1796-802.
SHARMA, M., NAZARETH, I. & PETERSEN, I. 2016. Trends in incidence, prevalence and prescribing in type 2 diabetes mellitus between 2000 and 2013 in primary care: a retrospective cohort study. *BMJ open,* 6**,** e010210.
SHI, W., WEI, X., WANG, X., DU, S., LIU, W., SONG, J. & WANG, Y. 2019. Perineuronal nets protect long-term memory by limiting activity-dependent inhibition from parvalbumin interneurons. *Proceedings of the National Academy of Sciences,* 116**,** 27063-27073.
SHIELD, P. C. 2021. 9 Bionanotechnology Meets Medicine.
SIERRA, A., NAVASCUÉS, J., CUADROS, M. A., CALVENTE, R., MARTÍN-OLIVA, D., FERRER-MARTÍN, R. M., MARTÍN-ESTEBANÉ, M., CARRASCO, M.-C. & MARÍN-TEVA, J. L. 2014. Expression of inducible nitric oxide synthase (iNOS) in microglia of the developing quail retina. *PLoS One,* 9**,** e106048.
SINGH, B., COVELO, A., MARTELL-MARTÍNEZ, H., NANCLARES, C., SHERMAN, M. A., OKEMATTI, E., MEINTS, J., TERAVSKIS, P. J., GALLARDO, C., SAVONENKO, A. V., BENNEYWORTH, M. A., LESNÉ, S. E., LIAO, D., ARAQUE, A. & LEE, M. K. 2019. Tau is required for progressive synaptic and memory deficits in a transgenic mouse model of α-synucleinopathy. *Acta Neuropathol,* 138**,** 551-574.
SLOMIANKA, L., AMREIN, I., KNUESEL, I., SØRENSEN, J. C. & WOLFER, D. P. 2011a. Hippocampal pyramidal cells: the reemergence of cortical lamination. *Brain Structure and Function,* 216**,** 301-317.

SLOMIANKA, L., AMREIN, I., KNUESEL, I., SØRENSEN, J. C. & WOLFER, D. P. 2011b. Hippocampal pyramidal cells: the reemergence of cortical lamination. *Brain Struct Funct,* 216**,** 301-17.
SNEAD, D. & ELIEZER, D. 2014. Alpha-synuclein function and dysfunction on cellular membranes. *Exp Neurobiol,* 23**,** 292-313.
SOFRONIEW, M. V. & VINTERS, H. V. 2010. Astrocytes: biology and pathology. *Acta neuropathologica,* 119**,** 7-35.
SOMMER, B., BARBIERI, S., HOFELE, K., WIEDERHOLD, K.-H., PROBST, A., MISTL, C., DANNER, S., KAUFFMANN, S., SPOOREN, W. & TOLNAY, M. 2000. Mouse models of α-synucleinopathy and Lewy pathology. *Experimental Gerontology,* 35**,** 1389-1403.
SON, S. M., SHIN, H.-J., BYUN, J., KOOK, S. Y., MOON, M., CHANG, Y. J. & MOOK-JUNG, I. 2016. Metformin facilitates amyloid-β generation by β-and γ-secretases via autophagy activation. *Journal of Alzheimer's Disease,* 51**,** 1197-1208.
SPILMAN, P., PODLUTSKAYA, N., HART, M., DEBNATH, J. & GOROSTIZA, O. 2010. Inhibition of mTOR by Rapamycin Abolishes Cognitive Deficits and Reduces.
STARGARDT, A., SWAAB, D. F. & BOSSERS, K. 2015. The storm before the quiet: neuronal hyperactivity and Aβ in the presymptomatic stages of Alzheimer's disease. *Neurobiology of aging,* 36**,** 1-11.
STEGER, M., TONELLI, F., ITO, G., DAVIES, P., TROST, M., VETTER, M., WACHTER, S., LORENTZEN, E., DUDDY, G., WILSON, S., BAPTISTA, M. A., FISKE, B. K., FELL, M. J., MORROW, J. A., REITH, A. D., ALESSI, D. R. & MANN, M. 2016. Phosphoproteomics reveals that Parkinson's disease kinase LRRK2 regulates a subset of Rab GTPases. *Elife,* 5.
STYKEL, M. G. & RYAN, S. D. 2022. Nitrosative stress in Parkinson's disease. *npj Parkinson's Disease,* 8**,** 104.
STYLIANOU, M., ZAAIMI, B., THOMAS, A., TAYLOR, J.-P. & LEBEAU, F. E. 2020. Early disruption of cortical sleep-related oscillations in a mouse model of dementia with Lewy bodies (DLB) expressing human mutant (A30P) alpha-synuclein. *Frontiers in Neuroscience,* 14**,** 579867.
SUBERBIELLE, E., DJUKIC, B., EVANS, M., KIM, D. H., TANEJA, P., WANG, X., FINUCANE, M., KNOX, J., HO, K., DEVIDZE, N., MASLIAH, E. & MUCKE, L. 2015. DNA repair factor BRCA1 depletion occurs in Alzheimer brains and impairs cognitive function in mice. *Nat Commun,* 6**,** 8897.
SUN, B.-L., WANG, L.-H., YANG, T., SUN, J.-Y., MAO, L.-L., YANG, M.-F., YUAN, H., COLVIN, R. A. & YANG, X.-Y. 2018. Lymphatic drainage system of the brain: a novel target for intervention of neurological diseases. *Progress in neurobiology,* 163**,** 118-143.
SUN, Q., SOTAYO, A., CAZZULINO, A. S., SNYDER, A. M., DENNY, C. A. & SIEGELBAUM, S. A. 2017. Proximodistal Heterogeneity of Hippocampal CA3 Pyramidal Neuron Intrinsic Properties, Connectivity, and Reactivation during Memory Recall. *Neuron,* 95**,** 656-672.e3.
SURENDRANATHAN, A., ROWE, J. B. & O'BRIEN, J. T. 2015. Neuroinflammation in Lewy body dementia. *Parkinsonism & related disorders,* 21**,** 1398-1406.
TAKATA, F., DOHGU, S., MATSUMOTO, J., MACHIDA, T., KANESHIMA, S., MATSUO, M., SAKAGUCHI, S., TAKESHIGE, Y., YAMAUCHI, A. & KATAOKA, Y. 2013. Metformin induces up-regulation of blood–brain barrier functions by activating AMP-activated protein kinase in rat brain microvascular endothelial cells. *Biochemical and biophysical research communications,* 433**,** 586-590.
TAKEMOTO, T., NISHIO, Y., SEKINE, O., IKEUCHI, C., NAGAI, Y., MAENO, Y., MAEGAWA, H., KIMURA, H. & KASHIWAGI, A. 2007. RBMX is a novel hepatic transcriptional regulator of SREBP-1c gene response to high-fructose diet. *FEBS Lett,* 581**,** 218-22.
TAN, L. A., AL CHAWAF, A., VACCARINO, F. J., BOUTROS, P. C. & LOVEJOY, D. A. 2011. Teneurin C-terminal associated peptide (TCAP)-1 modulates dendritic morphology in hippocampal neurons and decreases anxiety-like behaviors in rats. *Physiol Behav,* 104**,** 199-204.

TAN, L. A., XU, K., VACCARINO, F. J., LOVEJOY, D. A. & ROTZINGER, S. 2008. Repeated intracerebral teneurin C-terminal associated peptide (TCAP)-1 injections produce enduring changes in behavioral responses to corticotropin-releasing factor (CRF) in rat models of anxiety. *Behav Brain Res,* 188**,** 195-200.

TAN, L. A., XU, K., VACCARINO, F. J., LOVEJOY, D. A. & ROTZINGER, S. 2009. Teneurin C-terminal associated peptide (TCAP)-1 attenuates corticotropin-releasing factor (CRF)-induced c-Fos expression in the limbic system and modulates anxiety behavior in male Wistar rats. *Behav Brain Res,* 201**,** 198-206.

TANRIÖVER, G., BACIOGLU, M., SCHWEIGHAUSER, M., MAHLER, J., WEGENAST-BRAUN, B. M., SKODRAS, A., OBERMÜLLER, U., BARTH, M., KRONENBERG-VERSTEEG, D., NILSSON, K. P. R., SHIMSHEK, D. R., KAHLE, P. J., EISELE, Y. S. & JUCKER, M. 2020. Prominent microglial inclusions in transgenic mouse models of α-synucleinopathy that are distinct from neuronal lesions. *Acta Neuropathol Commun,* 8**,** 133.

TAYARA, K., ESPINOSA-OLIVA, A. M., GARCÍA-DOMÍNGUEZ, I., ISMAIEL, A. A., BOZA-SERRANO, A., DEIERBORG, T., MACHADO, A., HERRERA, A. J., VENERO, J. L. & DE PABLOS, R. M. 2018. Divergent effects of metformin on an inflammatory model of Parkinson's disease. *Frontiers in cellular neuroscience,* 12**,** 440.

TAYMANS, J.-M. & BAEKELANDT, V. 2014. Phosphatases of α-synuclein, LRRK2, and tau: important players in the phosphorylation-dependent pathology of Parkinsonism. *Frontiers in genetics,* 5**,** 105973.

TEKKÖK, S. B., BROWN, A. M., WESTENBROEK, R., PELLERIN, L. & RANSOM, B. R. 2005. Transfer of glycogen-derived lactate from astrocytes to axons via specific monocarboxylate transporters supports mouse optic nerve activity. *J Neurosci Res,* 81**,** 644-52.

THAYANIDHI, N., HELM, J. R., NYCZ, D. C., BENTLEY, M., LIANG, Y. & HAY, J. C. 2010. Alpha-synuclein delays endoplasmic reticulum (ER)-to-Golgi transport in mammalian cells by antagonizing ER/Golgi SNAREs. *Mol Biol Cell,* 21**,** 1850-63.

THELLUNG, S., CORSARO, A., NIZZARI, M., BARBIERI, F. & FLORIO, T. 2019. Autophagy activator drugs: a new opportunity in neuroprotection from misfolded protein toxicity. *International Journal of Molecular Sciences,* 20**,** 901.

THORNE, R., PRONK, G., PADMANABHAN, V. & FREY II, W. 2004. Delivery of insulin-like growth factor-I to the rat brain and spinal cord along olfactory and trigeminal pathways following intranasal administration. *Neuroscience,* 127**,** 481-496.

TIPPETT, L. J., WALDVOGEL, H. J., THOMAS, S. J., HOGG, V. M., VAN ROON-MOM, W., SYNEK, B. J., GRAYBIEL, A. M. & FAULL, R. L. 2007. Striosomes and mood dysfunction in Huntington's disease. *Brain,* 130**,** 206-21.

TIZAZU, A. M., NYUNT, M. S. Z., CEXUS, O., SUKU, K., MOK, E., XIAN, C. H., CHONG, J., TAN, C., HOW, W. & HUBERT, S. 2019. Metformin monotherapy downregulates diabetes-associated inflammatory status and impacts on mortality. *Frontiers in physiology,* 10**,** 572.

TOMÁS, M., MARTÍNEZ-ALONSO, E., MARTÍNEZ-MARTÍNEZ, N., CARA-ESTEBAN, M. & MARTÍNEZ-MENÁRGUEZ, J. A. 2021. Fragmentation of the Golgi complex of dopaminergic neurons in human substantia nigra: New cytopathological findings in Parkinson's disease. *Histol Histopathol,* 36**,** 47-60.

TOMKINS, O., FEINTUCH, A., BENIFLA, M., COHEN, A., FRIEDMAN, A. & SHELEF, I. 2011. Blood-brain barrier breakdown following traumatic brain injury: a possible role in posttraumatic epilepsy. *Cardiovasc Psychiatry Neurol,* 2011**,** 765923.

TORRES, E. R. S., STANOJLOVIC, M., ZELIKOWSKY, M., BONSBERGER, J., HEAN, S., MULLIGAN, C., BALDAUF, L., FLEMING, S., MASLIAH, E., CHESSELET, M. F., FANSELOW, M. S. & RICHTER, F. 2021. Alpha-synuclein pathology, microgliosis, and parvalbumin neuron loss in the amygdala associated with enhanced fear in the Thy1-aSyn model of Parkinson's disease. *Neurobiol Dis,* 158**,** 105478.

TOTH, K. & FREUND, T. 1992. Calbindin D28k-containing nonpyramidal cells in the rat hippocampus: their immunoreactivity for GABA and projection to the medial septum. *Neuroscience,* 49**,** 793-805.
TREMBLAY, R., LEE, S. & RUDY, B. 2016. GABAergic Interneurons in the Neocortex: From Cellular Properties to Circuits. *Neuron,* 91**,** 260-92.
TREVIÑO, M., VIVAR, C. & GUTIÉRREZ, R. 2007. β/γ oscillatory activity in the CA3 hippocampal area is depressed by aberrant GABAergic transmission from the dentate gyrus after seizures. *Journal of Neuroscience,* 27**,** 251-259.
TRUBIANI, G., AL CHAWAF, A., BELSHAM, D. D., BARSYTE-LOVEJOY, D. & LOVEJOY, D. A. 2007. Teneurin carboxy (C)-terminal associated peptide-1 inhibits alkalosis-associated necrotic neuronal death by stimulating superoxide dismutase and catalase activity in immortalized mouse hypothalamic cells. *Brain Res,* 1176**,** 27-36.
TURRENS, J. F. & BOVERIS, A. 1980. Generation of superoxide anion by the NADH dehydrogenase of bovine heart mitochondria. *Biochem J,* 191**,** 421-7.
TWEEDY, C., KINDRED, N., CURRY, J., WILLIAMS, C., TAYLOR, J.-P., ATKINSON, P., RANDALL, F., ERSKINE, D., MORRIS, C. M. & REEVE, A. K. 2021. Hippocampal network hyperexcitability in young transgenic mice expressing human mutant alpha-synuclein. *Neurobiology of disease,* 149**,** 105226.
TYANOVA, S., TEMU, T., SINITCYN, P., CARLSON, A., HEIN, M. Y., GEIGER, T., MANN, M. & COX, J. 2016. The Perseus computational platform for comprehensive analysis of (prote)omics data. *Nat Methods,* 13**,** 731-40.
TZOUR, A., LEIBOVICH, H., BARKAI, O., BIALA, Y., LEV, S., YAARI, Y. & BINSHTOK, A. M. 2017. KV7/M channels as targets for lipopolysaccharide-induced inflammatory neuronal hyperexcitability. *The Journal of physiology,* 595**,** 713-738.
UGWOKE, M. I., VERBEKE, N. & KINGET, R. 2001. The biopharmaceutical aspects of nasal mucoadhesive drug delivery. *Journal of pharmacy and pharmacology,* 53**,** 3-22.
UNAL-CEVIK, I., KILINÇ, M., CAN, A., GÜRSOY-OZDEMIR, Y. & DALKARA, T. 2004. Apoptotic and necrotic death mechanisms are concomitantly activated in the same cell after cerebral ischemia. *Stroke,* 35**,** 2189-94.
VALERO, M. & DE LA PRIDA, L. M. 2018. The hippocampus in depth: a sublayer-specific perspective of entorhinal-hippocampal function. *Curr Opin Neurobiol,* 52**,** 107-114.
VAN SKIKE, C. E., JAHRLING, J. B., OLSON, A. B., SAYRE, N. L., HUSSONG, S. A., UNGVARI, Z., LECHLEITER, J. D. & GALVAN, V. 2018. Inhibition of mTOR protects the blood-brain barrier in models of Alzheimer's disease and vascular cognitive impairment. *American Journal of Physiology-Heart and Circulatory Physiology*.
VARGAS, J. Y., GRUDINA, C. & ZURZOLO, C. 2019. The prion-like spreading of α-synuclein: From in vitro to in vivo models of Parkinson's disease. *Ageing Res Rev,* 50**,** 89-101.
VEGH, M. J., RAUSELL, A., LOOS, M., HELDRING, C. M., JURKOWSKI, W., VAN NIEROP, P., PALIUKHOVICH, I., LI, K. W., DEL SOL, A. & SMIT, A. B. 2014. Hippocampal extracellular matrix levels and stochasticity in synaptic protein expression increase with age and are associated with age-dependent cognitive decline. *Molecular & Cellular Proteomics,* 13**,** 2975-2985.
VERHOOG, Q. P., HOLTMAN, L., ARONICA, E. & VAN VLIET, E. A. 2020. Astrocytes as guardians of neuronal excitability: mechanisms underlying epileptogenesis. *Frontiers in neurology,* 11**,** 591690.
VEZZANI, A. & VIVIANI, B. 2015. Neuromodulatory properties of inflammatory cytokines and their impact on neuronal excitability. *Neuropharmacology,* 96**,** 70-82.
VICENTE, M., ADDO-OSAFO, K. & VOSSEL, K. 2024. Latest advances in mechanisms of epileptic activity in Alzheimer's disease and dementia with Lewy Bodies. *Frontiers in Neurology,* 15**,** 1277613.
VICO VARELA, E., ETTER, G. & WILLIAMS, S. 2019. Excitatory-inhibitory imbalance in Alzheimer's disease and therapeutic significance. *Neurobiol Dis,* 127**,** 605-615.
VIDAL-ITRIAGO, A., RADFORD, R. A., ARAMIDEH, J. A., MAUREL, C., SCHERER, N. M., DON, E. K., LEE, A., CHUNG, R. S., GRAEBER, M. B. & MORSCH, M. 2022. Microglia

morphophysiological diversity and its implications for the CNS. *Frontiers in immunology,* 13**,** 997786.
VOLLES, M. J. & LANSBURY, P. T., JR. 2002. Vesicle permeabilization by protofibrillar alpha-synuclein is sensitive to Parkinson's disease-linked mutations and occurs by a pore-like mechanism. *Biochemistry,* 41**,** 4595-602.
WALKER, M. C., RUIZ, A. & KULLMANN, D. M. 2002. Do mossy fibers release GABA? *Epilepsia,* 43 Suppl 5**,** 196-202.
WANG, C., YOO, Y., FAN, H., KIM, E., GUAN, K. L. & GUAN, J. L. 2010. Regulation of Integrin β 1 recycling to lipid rafts by Rab1a to promote cell migration. *J Biol Chem,* 285**,** 29398-405.
WANG, G., CUI, W., CHEN, S., SHAO, Z., LI, Y., WANG, W., MAO, L., LI, J. & MEI, X. 2021. Metformin alleviates high glucose-induced ER stress and inflammation by inhibiting the interaction between caveolin1 and AMPKα in rat astrocytes. *Biochem Biophys Res Commun,* 534**,** 908-913.
WANG, L., DAS, U., SCOTT, D. A., TANG, Y., MCLEAN, P. J. & ROY, S. 2014. α-synuclein multimers cluster synaptic vesicles and attenuate recycling. *Curr Biol,* 24**,** 2319-26.
WANG, L., ROTZINGER, S., AL CHAWAF, A., ELIAS, C. F., BARSYTE-LOVEJOY, D., QIAN, X., WANG, N. C., DE CRISTOFARO, A., BELSHAM, D., BITTENCOURT, J. C., VACCARINO, F. & LOVEJOY, D. A. 2005. Teneurin proteins possess a carboxy terminal sequence with neuromodulatory activity. *Brain Res Mol Brain Res,* 133**,** 253-65.
WANG, T., QIN, L., LIU, B., LIU, Y., WILSON, B., ELING, T. E., LANGENBACH, R., TANIURA, S. & HONG, J. S. 2004. Role of reactive oxygen species in LPS-induced production of prostaglandin E2 in microglia. *J Neurochem,* 88**,** 939-47.
WANG, W. Y., TAN, M. S., YU, J. T. & TAN, L. 2015. Role of pro-inflammatory cytokines released from microglia in Alzheimer's disease. *Ann Transl Med,* 3**,** 136.
WANG, X., LUO, C., MAO, X.-Y., LI, X., YIN, J.-Y., ZHANG, W., ZHOU, H.-H. & LIU, Z.-Q. 2019. Metformin reverses the schizophrenia-like behaviors induced by MK-801 in rats. *Brain Research,* 1719**,** 30-39.
WATSON, M. B., RICHTER, F., LEE, S. K., GABBY, L., WU, J., MASLIAH, E., EFFROS, R. B. & CHESSELET, M.-F. 2012. Regionally-specific microglial activation in young mice over-expressing human wildtype alpha-synuclein. *Experimental neurology,* 237**,** 318-334.
WEN, T. H., BINDER, D. K., ETHELL, I. M. & RAZAK, K. A. 2018. The Perineuronal 'Safety' Net? Perineuronal Net Abnormalities in Neurological Disorders. *Front Mol Neurosci,* 11**,** 270.
WENDER, R., BROWN, A. M., FERN, R., SWANSON, R. A., FARRELL, K. & RANSOM, B. R. 2000. Astrocytic glycogen influences axon function and survival during glucose deprivation in central white matter. *J Neurosci,* 20**,** 6804-10.
WERSINGER, C. & SIDHU, A. 2006. An inflammatory pathomechanism for Parkinson's disease? *Curr Med Chem,* 13**,** 591-602.
WEYER, A. & SCHILLING, K. 2003. Developmental and cell type-specific expression of the neuronal marker NeuN in the murine cerebellum. *Journal of neuroscience research,* 73**,** 400-409.
WHITTAKER, R. G., TURNBULL, D. M., WHITTINGTON, M. A. & CUNNINGHAM, M. O. 2011. Impaired mitochondrial function abolishes gamma oscillations in the hippocampus through an effect on fast-spiking interneurons. *Brain,* 134**,** e180-e180.
WIRTH, C., BRANDT, U., HUNTE, C. & ZICKERMANN, V. 2016. Structure and function of mitochondrial complex I. *Biochimica et Biophysica Acta (BBA) - Bioenergetics,* 1857**,** 902-914.
WOLF, H. K., BUSLEI, R., SCHMIDT-KASTNER, R., SCHMIDT-KASTNER, P. K., PIETSCH, T., WIESTLER, O. D. & BLÜMCKE, I. 1996. NeuN: a useful neuronal marker for diagnostic histopathology. *Journal of Histochemistry & Cytochemistry,* 44**,** 1167-1171.
WULLSCHLEGER, S., LOEWITH, R. & HALL, M. N. 2006. TOR signaling in growth and metabolism. *Cell,* 124**,** 471-484.

XIE, Z., TANG, J., CHEN, Z., WEI, L., CHEN, J. & LIU, Q. 2023. Human bone marrow mesenchymal stem cell-derived extracellular vesicles reduce inflammation and pyroptosis in acute kidney injury via miR-223-3p/HDAC2/SNRK. *Inflamm Res,* 72**,** 553-576.
XU, S. & CHAN, P. 2015. Interaction between neuromelanin and alpha-synuclein in Parkinson's disease. *Biomolecules,* 5**,** 1122-1142.
XU, Y., ZHAO, M., HAN, Y. & ZHANG, H. 2020. GABAergic Inhibitory Interneuron Deficits in Alzheimer's Disease: Implications for Treatment. *Front Neurosci,* 14**,** 660.
YAN, J.-Q., YUAN, Y.-H., GAO, Y.-N., HUANG, J.-Y., MA, K.-L., GAO, Y., ZHANG, W.-Q., GUO, X.-F. & CHEN, N.-H. 2014. Overexpression of human E46K mutant α-synuclein impairs macroautophagy via inactivation of JNK1-Bcl-2 pathway. *Molecular neurobiology,* 50**,** 685-701.
YANG, A. J., FRENDO-CUMBO, S. & MACPHERSON, R. E. 2019. Resveratrol and metformin recover prefrontal cortex AMPK activation in diet-induced obese mice but reduce BDNF and synaptophysin protein content. *Journal of Alzheimer's Disease,* 71**,** 945-956.
YANG, S., CACQUEVEL, M., SAKSIDA, L. M., BUSSEY, T. J., SCHNEIDER, B. L., AEBISCHER, P., MELANI, R., PIZZORUSSO, T., FAWCETT, J. W. & SPILLANTINI, M. G. 2015. Perineuronal net digestion with chondroitinase restores memory in mice with tau pathology. *Exp Neurol,* 265**,** 48-58.
YANG, S., GIGOUT, S., MOLINARO, A., NAITO-MATSUI, Y., HILTON, S., FOSCARIN, S., NIEUWENHUIS, B., TAN, C. L., VERHAAGEN, J. & PIZZORUSSO, T. 2021. Chondroitin 6-sulphate is required for neuroplasticity and memory in ageing. *Molecular psychiatry,* 26**,** 5658-5668.
YANG, Y., ZHU, B., ZHENG, F., LI, Y., ZHANG, Y., HU, Y. & WANG, X. 2017. Chronic metformin treatment facilitates seizure termination. *Biochemical and biophysical research communications,* 484**,** 450-455.
YATES, R., NAIRN, K., DIXON, R. & SEABER, E. 2002. Preliminary studies of the pharmacokinetics and tolerability of zolmitriptan nasal spray in healthy volunteers. *The Journal of Clinical Pharmacology,* 42**,** 1237-1243.
YAVICH, L., TANILA, H., VEPSÄLÄINEN, S. & JÄKÄLÄ, P. 2004. Role of alpha-synuclein in presynaptic dopamine recruitment. *J Neurosci,* 24**,** 11165-70.
YEREVANIAN, A. & SOUKAS, A. A. 2019. Metformin: Mechanisms in Human Obesity and Weight Loss. *Curr Obes Rep,* 8**,** 156-164.
YU, H., HARRISON, F. E. & XIA, F. 2018. Altered DNA repair; an early pathogenic pathway in Alzheimer's disease and obesity. *Sci Rep,* 8**,** 5600.
YU, Z., UENO, K., FUNAYAMA, R., SAKAI, M., NARIAI, N., KOJIMA, K., KIKUCHI, Y., LI, X., ONO, C., KANATANI, J., ONO, J., IWAMOTO, K., HASHIMOTO, K., KINOSHITA, K., NAKAYAMA, K., NAGASAKI, M. & TOMITA, H. 2023. Sex-Specific Differences in the Transcriptome of the Human Dorsolateral Prefrontal Cortex in Schizophrenia. *Mol Neurobiol,* 60**,** 1083-1098.
ZAJDA, A., HUTTUNEN, K. M., SIKORA, J., PODSIEDLIK, M. & MARKOWICZ-PIASECKA, M. 2020. Is metformin a geroprotector? A peek into the current clinical and experimental data. *Mech Ageing Dev,* 191**,** 111350.
ZALTIERI, M., GRIGOLETTO, J., LONGHENA, F., NAVARRIA, L., FAVERO, G., CASTREZZATI, S., COLIVICCHI, M. A., DELLA CORTE, L., REZZANI, R., PIZZI, M., BENFENATI, F., SPILLANTINI, M. G., MISSALE, C., SPANO, P. & BELLUCCI, A. 2015. α-synuclein and synapsin III cooperatively regulate synaptic function in dopamine neurons. *J Cell Sci,* 128**,** 2231-43.
ZHANG, J., ZHANG, W., ZOU, D., CHEN, G., WAN, T., ZHANG, M. & CAO, X. 2003. Cloning and functional characterization of GMPR2, a novel human guanosine monophosphate reductase, which promotes the monocytic differentiation of HL-60 leukemia cells. *J Cancer Res Clin Oncol,* 129**,** 76-83.
ZHANG, W., WANG, T., PEI, Z., MILLER, D. S., WU, X., BLOCK, M. L., WILSON, B., ZHANG, W., ZHOU, Y. & HONG, J.-S. 2005. Aggregated α-synuclein activates microglia: a

process leading to disease progression in Parkinson's disease. *The FASEB Journal,* 19**,** 533-542.
ZHAO, J., BI, W., ZHANG, J., XIAO, S., ZHOU, R., TSANG, C. K., LU, D. & ZHU, L. 2020. USP8 protects against lipopolysaccharide-induced cognitive and motor deficits by modulating microglia phenotypes through TLR4/MyD88/NF-κB signaling pathway in mice. *Brain, behavior, and immunity,* 88**,** 582-596.
ZHOU, G., MYERS, R., LI, Y., CHEN, Y., SHEN, X., FENYK-MELODY, J., WU, M., VENTRE, J., DOEBBER, T. & FUJII, N. 2001. Role of AMP-activated protein kinase in mechanism of metformin action. *The Journal of clinical investigation,* 108**,** 1167-1174.
ZHU, J., VINOTHKUMAR, K. R. & HIRST, J. 2016. Structure of mammalian respiratory complex I. *Nature,* 536**,** 354-358.
ZHU, X. C., JIANG, T., ZHANG, Q. Q., CAO, L., TAN, M. S., WANG, H. F., DING, Z. Z., TAN, L. & YU, J. T. 2015. Chronic Metformin Preconditioning Provides Neuroprotection via Suppression of NF-κB-Mediated Inflammatory Pathway in Rats with Permanent Cerebral Ischemia. *Mol Neurobiol,* 52**,** 375-85.